Vertical susceptibility profiles: its use in magnetic pollution screening

Dissertation
zur Erlangung des Grades eines Doktors der Naturwissenschaften

der Geowissenschaftlichen Fakultät
der Eberhard Karls Universität Tübingen

vorgelegt von
Ulrich Blaha
aus Owen

2010

Tag der mündlichen Prüfung: 28.03.2008

Dekan: Prof. Dr. Grathwohl

1. Berichterstatter: Prof. Dr. Erwin Appel

2. Berichterstatter: Prof. Dr. Helge Stanjek

Publications

[1] **Blaha U.**, Appel E., Stanjek H., **2008a**: Determination of anthropogenic boundary depth in soil profiles and semi-quantification of heavy metal loads using magnetic susceptibility. **Environmental Pollution** 156 (2), 278-289 ……...… **27**

[2] **Blaha U.**, Sapkota B., Appel E., Stanjek H., Rösler W., **2008b**: Micro-scale grain-size analysis and magnetic properties of coal-fired power plant fly ash and its relevance for environmental magnetic pollution studies. **Atmospheric Environment** 42, 8359-8370 ……..…… **41**

[3] Gautam P., **Blaha U.**, Appel E., **2008**: Assessment of vehicular pollution in Kathmandu: magnetic properties and heavy metal chemistry of dust from streets and leaves. **Journal of Nepal Geological Society** 37, 67-76 ……..…..……...… **55**

[4] Hu S., Duan X., Shen M., **Blaha U.**, Rösler W., Yan H., Appel E., Hoffmann V., **2008**: Magnetic response to atmospheric heavy metal pollution recorded by dust-loaded leaves in Shougang industrial area, western Beijing. **Chinese Science Bulletin** 53 (10), 1555-1564 ……..…….. **67**

[5] Shen M., Hu S., **Blaha U.**, Yan H., Rösler W., Hoffmann V., **2006**: A magnetic study of a polluted soil profile at the Shijingshan industrial area, western Beijing, China. **Chinese Journal of Geophysics** 49 (6), 1524-1532 ……..…...… **79**

[6] Gautam P., **Blaha U.**, Appel E., **2005a**: Magnetic susceptibility of dust loaded leaves as a proxy of traffic related heavy metal pollution in Kathmandu city, Nepal. **Atmospheric Environment** 39, 2201-2211 ...……...….... **91**

[7] Gautam P., **Blaha U.**, Appel E., **2005b**: Integration of magnetism and heavy metal chemistry of soils to quantify the environmental pollution in Kathmandu, Nepal. **The Island Arc** 14, 424-435 …...……..…...… **105**

[8] Gautam P., **Blaha U.**, Appel E., and Neupane G., **2004**: Environmental magnetic approach towards the quantification of pollution in Kathmandu urban area, Nepal. **Physics and Chemistry of the Earth** 29, 973-984 ……....… **119**

Own contribution to the joint publications

[1] **Blaha U.**, Appel E., Stanjek H., **2008a**: Determination of anthropogenic boundary depth in soil profiles and semi-quantification of heavy metal loads using magnetic susceptibility. **Environmental Pollution** 156, 278-289.

Ideas:	Blaha/Appel
Data:	90%
Analyses:	100%
Elaboration:	100%

[2] **Blaha U.**, Sapkota B., Appel E., Stanjek H., Rösler W., **2008b**: Micro-scale grain-size analysis and magnetic properties of coal-fired power plant fly ash and its relevance for environmental magnetic pollution studies. **Atmospheric Environment** 42, 8359-8370.

Ideas:	Blaha
Data:	80%
Analyses:	90%
Elaboration:	100%

[3] Gautam P., **Blaha U.**, Appel E., **2008**: Assessment of vehicular pollution in Kathmandu: magnetic properties and heavy metal chemistry of dust from streets and leaves. **Journal of Nepal Geological Society**

Ideas:	Gautam/ Blaha
Data:	50%
Analyses:	20%
Elaboration:	20%

[4] Hu S., Duan X., Shen M., **Blaha U.**, Rösler W., Yan H., Appel E., Hoffmann V., **2008**: Magnetic response to atmospheric heavy metal pollution recorded by dust-loaded leaves in Shougang industrial area, western Beijing. **Chinese Science Bulletin**

Ideas:	Appel/Rösler/Hu/Blaha
Data:	20%
Analyses:	10%
Elaboration:	10%

[5] Shen M., Hu S., **Blaha U.**, Yan H., Rösler W., Hoffmann V., **2006**: A magnetic study of a polluted soil profile at the Shijingshan industrial area, western Beijing, China. **Chinese Journal of Geophysics** 49 (6), 1524-1532.

Ideas: Blaha/Shen
Data: 40%
Analyses: 20%
Elaboration: 10%

[6] Gautam P., **Blaha U.**, Appel E., **2005a**: Magnetic susceptibility of dust loaded leaves as a proxy of traffic related heavy metal pollution in Kathmandu city, Nepal. **Atmospheric Environment** 39, 2201-2211.

Ideas: Gautam/Blaha/Appel
Data: 50%
Analyses: 30%
Elaboration: 30%

[7] Gautam P., **Blaha U.**, Appel E., **2005b**: Integration of magnetism and heavy metal chemistry of soils to quantify the environmental pollution in Kathmandu, Nepal. **The Island Arc** 14, 424-435.

Ideas: Gautam/Blaha/Appel
Data: 50%
Analyses: 30%
Elaboration: 30%

[8] Gautam P., **Blaha U.**, Appel E., and Neupane G., **2004**: Environmental magnetic approach towards the quantification of pollution in Kathmandu urban area, Nepal. **Physics and Chemistry of the Earth** 29, 973-984.

Ideas: Blaha/Gautam/Appel
Data: 50%
Analyses: 30%
Elaboration: 30%

Summary

In this work magnetic methods were used for systematic and high-resolution investigation of industrially polluted soils, where soil pollution is caused by heavy metal bearing air-borne particulate matter. The focus of the study is on the characteristic magnetic signals determined from ultra-shallow (~0.5 m) vertical profiles acquired in areas of <10 m² ("site scale"). The development of measuring techniques for efficient (fast and high-quality) acquisition of the magnetic susceptibility (MS) is based on the specific properties of these vertical profiles. Optimization of the MS proxy potential for semi-quantitative assessment of heavy metal (HM) loads from anthropogenic and geogenic origin in soils is a central part of this work.

For evaluation of the potential of different sampling and measuring techniques plus the impact of soil types on anthropogenic MS distribution in soils, investigations were conducted at three different industrial sites with different soil types.

An experiment with artificially applied magnetic tracer (fly ash) for investigation of the time-dependent spatial behavior (migration/accumulation) of magnetic particles was performed in forest soil. Comparison of the results from the "artificial" tracer test (surface MS and vertical profile MS) and data from soils contaminated by atmospheric deposition contributes for better assessment of the influence of soils on the development of the MS signal.

Within this framework new sampling and measuring strategies for best possible high-resolution and efficient (time-saving) MS data acquisition in soil profiles collected from "site scale" sized areas are presented. Sampling and measuring techniques in areas of a few m² are systematically compared and innovative analysis and assessment methods are developed.

The potential of an integrative measuring strategy for an individual investigation site ("site scale") comprising MS surface measurements, vertical MS profiles plus important soil parameters is systematically investigated in four soil types. It is demonstrated that only the combination of different measuring techniques, taking into account specific soil properties and individual soil development, enhances data quality for reliable assessment of HM loads when conducting applied MS screening. In this context the proof for correlation of MS and HM was performed independently from the modern and fast measuring methods. Differently contaminated soil profiles are exemplarily and representatively (bigger sample volumes of ~200 cm³) investigated for their MS and HM concentration at high-resolution (0.5 cm vertical spacing). The methodologically independent, precise results are utilized for assessment of the potential of rapidly measured vertical MS profiles.

It is shown that a larger number of vertical MS profiles enables numerical determination of a "boundary depth". This magnetically defined depth separates the upper, polluted soil zone

with anthropogenically enhanced MS (pollution MS) from the lower, unpolluted zone, which represents the geogenic signal. Only this important, systematic MS acquisition strategy, which directly includes soil type specific properties into the MS data, provides the opportunity for reliable, numerical determination of the "boundary depth". This forms the boundary conditions for standardized quantification of pollution MS by signal integration.

Possible sources for errors, which might occur from rapid data acquisition and the impact on the results are investigated from comprising data sets. Results show the high importance of systematic and accurate data acquisition, assessment, processing and interpretation, while already small systematic discrepancies in the data sets might lead to considerable false estimation. In this context a universal processing strategy is presented [1]. This is a milestone concerning information generation and quality, which is not provided yet by simple vertical MS profile assessment.

Soils are only one type of pollution sinks, respectively pollution accumulators in the environment. Therefore, besides the central part of this work [1] publications about magnetic screening are contained. The framework of the entire discipline is outlined, especially by including atmospheric deposition collected on tree leaves [4, 6]. This work is not only unique to industrial pollution sources, but it also includes traffic-generated and common urban immissions. The impact of such sources on urban soils is investigated [7, 8], and important magnetic, chemical and physical parameters are tested for their typical distribution patterns. These systematic analyses provide the basis for further optimization of magnetic proxy methods.

Furthermore, fly ash samples from coal-fired power plants were investigated for their magnetic and chemical properties [2]. Fly ashes are one of the most important industrially generated pollutants world-wide, and investigations about their behavior in soils are important for magnetic soil pollution screening.

Zusammenfassung

In dieser Arbeit werden mit magnetischen Methoden durch atmosphärische Deposition von schwermetallhaltigen Industriestäuben unterschiedlich stark verschmutzte Oberböden systematisch und hochauflösend untersucht. Der Schwerpunkt der Untersuchung liegt dabei auf der charakteristischen Ausbildung des magnetischen Signals in ultraflachen (~0,5 m) Vertikalprofilen auf kleinen Flächen (<10 m²) sowie der methodischen Entwicklung von Messtechniken für eine ökonomisch-effiziente (schnelle und qualitativ hochwertige) Erfassung der magnetischen Suszeptibilität (MS). Das optimierte Proxy- (Stellvertreter) Potential der MS zur semi-quantitativen Abschätzung der anthropogen und geogen bedingten Schwermetallbelastung (HM) in Böden ist zentraler Bestandteil der Arbeit.

Zur Bewertung des Potentials verschiedener Beprobungs- und Messtechniken sowie des Einflusses der Bodenart auf das Verteilungsmuster anthropogen erzeugter MS im Bodenprofil werden drei verschiedene Industriestandorte mit unterschiedlichen Böden präsentiert. Zusätzlich wird in einem Experiment mit künstlich ausgebrachtem magnetischen Tracer (Flugasche) das räumlich-zeitliche Verhalten (Migration/Akkumulation) von magnetischen Partikeln in einer weiteren Bodenart untersucht. Der Vergleich von “synthetischen“ Tracer-Daten (Oberflächen-MS, Vertikalprofil-MS) mit Daten aus “diffus anthropogen kontaminierten“ Böden (atmosphärische Deposition) trägt dazu bei, den Einfluss des Bodens auf die Ausbildung des MS-Signals besser bewerten zu können.

Im Rahmen dieser Untersuchungen, werden neue Beprobungs- und Messstrategien zur hochauflösenden/bestmöglichen sowie zur effizienten (zeitsparenden) Erfassung der MS in Bodenprofilen und auf Flächen von wenigen Quadratmetern vorgestellt, Beprobungs- und Messtechniken systematisch verglichen sowie innovative Analyse- und Bewertungsmethoden entwickelt.

Das Potential einer integrierten Messstrategie für einzelne Untersuchungsstellen, bestehend aus MS-Oberfächenmessungen, MS-Vertikalprofilen sowie wichtiger Bodenparameter wird systematisch an allen vier Bodentypen untersucht. Es wird gezeigt, dass nur die Kombination verschiedener Messtechniken unter Berücksichtigung des spezifischen Bodentyps und dessen individueller Ausbildung die Datenqualität für eine zuverlässige Abschätzung der Schwermetallbelastung im angewandten Screening (schnelle Messmethoden) steigert. In diesem Zusammenhang wird der Nachweis der Korrelation von MS und Schwermetallen unabhängig von den modernen und schnellen Messmethoden geführt. Unterschiedlich stark verschmutzte Bodenarten werden exemplarisch hochauflösend und repäsentativ (größere Volumina – 200 cm³) auf ihre MS und Schwermetallkonzentrationen hin untersucht, und die

methodisch unabhängigen, genauen Resultate zur Bewertung des Potentials schnell gemessener MS-Vertikalprofile eingesetzt.

Es wird gezeigt, dass eine größere Anzahl an MS-Vertikalprofilen die Abgrenzung ("Grenztiefe") der oberen Bodenschichten mit anthropogen erhöhter MS (Verschmutzungs-MS) vom darunterliegenden Bereich mit geogener MS signifikant erleichtert und numerisch fassbar macht. Erst diese entscheidende systematische, den Bodentyp bzw. die Bodeneigenschaften direkt einschließende Signalerfassungsstrategie liefert MS-Daten für eine eindeutige rechnerische Bestimmung der 'Grenztiefe' zwischen anthropogener und geogener MS an einer Untersuchungsstelle. Damit sind die Randbedingungen für eine standardisierte Quantifizierung der Verschmutzungs-MS über den Weg der Signalintegration (MS-Tiefenfunktion) gegeben.

Mögliche Fehlerquellen bei der schnellen MS-Erfassung, ihre Auswirkungen auf die Messergebnisse sowie deren Interpretation im Zusammenhang mit der Schwermetalldetektion werden anhand umfangreicher Datensätze untersucht. Die Ergebnisse zeigen die herausragende Bedeutung systematischer und sorgfältiger Datenerfassung, Bewertung, Aufbereitung und Interpretation, wobei schon geringe systematische Diskrepanzen im Datensatz zu erheblichen Fehleinschätzungen führen können. In diesem Zusammenhang wird eine universelle Processing-Strategie vorgestellt, die verglichen mit bisherigen, einfachen MS-Vertikalprofil-Bewertungen einen Meilenstein an Informationsgewinn und Qualität darstellt [1].

Da Böden nur einen Teil von Schadstoffsenken bzw. Schadstoffakkumulatoren in der Umwelt darstellen, sind neben dem zentralen Teil dieser Arbeit [1] Publikationen über magnetisches Screening enthalten, die den Gesamtrahmen der Disziplin umreißen, v.a. durch Einbeziehung atmosphärischer Deposition auf Blättern [4, 6]. Diese Arbeiten bleiben nicht nur auf industrielle Schadstoffquellen beschränkt, sondern schließen auch straßenverkehrsbedingte und allgemeine urbane Immissionen [3, 7, 8] mit ein. Auch wird der Einfluss dieser Schadstoffquellen auf urbane Böden untersucht [7, 8], wobei wichtige magnetische, chemische und physikalische Parameter untersucht und typische Verteilungsmuster herausgearbeitet werden. Diese systematischen Analysen bilden eine solide Basis für die weitere Optimierung magnetischer Proxy-Methoden.

Darüberhinaus werden Flugaschen aus Kohlekraftwerken, die weltweit eine der wichtigsten industriellen Verschmutzungskomponenten darstellen auf ihre magnetischen und chemischen Eigenschaften, sowie auf ihr Verhalten im Boden hin untersucht [2].

Acknowledgements

This doctoral thesis was completed at the Faculty of Geoscience (IFG), Center of Applied Geoscience (ZAG), Geophysics working group (University of Tübingen).

First of all I would like to thank all family members very much for their continuous support during preparation of this PhD thesis. Without their great help it would not have been possible to finish this work in time.

For providing this interesting research topic and for the continuous support during preparation of this work I am very grateful to my academic supervisor Prof. Dr. Erwin Appel. Without the good working conditions and the opportunity for independent research this work could have not been done.

For good cooperation and helpful discussions on many aspects of this work I am grateful to Prof. Dr. Helge Stanjek (RWTH Aachen). Discussions provided big help and stimulated this research work.

Dr. Wolfgang Rösler I want to thank a lot for perfect field work cooperation in Beijing and Nanjing/China. Without his help it would have not been possible to conduct these studies in such an efficient way. Also thanks for the numerous discussions on various aspects of magnetic pollution screening.

Dr. Pitambar Gautam is thanked for the successful cooperation in the Kathmandu magnetic pollution screening project, which contributed a lot for the development of our field of research. My special thanks goes to Prof. Dr. Nathani Basavaiah who invited me for conducting environmental magnetic studies in Bombay/India. This work, done in my spare-time, enabled for entering an entirely new level of magnetic pollution screening, proving that magnetic proxy methods can be successfully applied in magnetically very difficult areas. Moreover, confirming that the method has truly an enormous potential for universal application.

Big thanks to the supervised master students M.L. Rijal, M. Hoppe, V. Soares da Cruz, B. Sapkota, and all the student workers who contributed to the success of this work. Thanks also to all cooperation partners within the various projects. And last but not least, my cordial thanks to all the members of IFG and the Geophysics working group who supported my work in various ways.

This work was financially supported by the German Research Foundation (DFG) under the grant of AP 34/21-1,2.

Environmental Magnetism: an overview

Within the last two decades Environmental Magnetism applied to anthropogenic pollution has become a steadily and fastly growing field of research. This fact has been significantly driven by the fascination of magnetism and the broad applicability of magnetic methods regarding environmental pollution issues. Starting with pioneering studies on magnetic properties of dust particles and using magnetic parameters as a proxy for the detection of anthropogenic pollutants such as heavy metals (HM) and Polycyclic Aromatic Hydrocarbons (PAH) (e.g., Flanders 1994; Hanesch and Scholger, 2002; Hunt et al. 1984; Oldfield et al. 1985; Scholger 1998; Strzyszcz and Magiera, 1998) the potential of magnetic methods has been widely recognized, leading to numerous studies at various scales and in nearly every environment. Targets for magnetic investigations were soils, sediments, tree leaves, fly ashes from coal-fired power plants, industrial dusts, dusts from road-traffic, road dusts, etc.

All these studies on apparently different and wide spread topics contributed significantly to the fast development of magnetic methods for environmental magnetic pollution studies. They are key elements for a holistic approach in soil pollution assessment, as anthropogenic pollution sources and pollution sinks form one unit. Therefore, magnetic investigations of polluted soils are always the investigation of anthropogenic dust particles derived from high temperature combustion processes or other magnetic dust emissions from technical processes.

Accounted challenges of environmental magnetic pollution assessment in soils are the natural magnetic background signal, originating from geological sources and/or pedogenic processes. These natural magnetic signals can interfere with the anthropogenic signal and make it difficult for estimation of anthropogenic contributions. Therefore, adequate strategies and analytical methods are required to solve this problem.

Milestones towards applied, standardized and optimized magnetic susceptibility screening utilizing vertical susceptibility profiles were reached and are presented in the central paper of this PhD thesis [1].

Introduction

Soils are the “Earth skin” and “natural interface” between both the atmosphere and geosphere. More precise, soils are the pedosphere which has developed from geologic material under specific weathering and soil forming conditions. The pedosphere is the basis for any kind of agriculture and forestry, and thus of highest importance for man. Soils provide food, allow plants and forests to grow, and function as water filters and regulators.

Steel mills and coal-fired power plants as pollution sources plus soils, functioning as sinks and accumulators for anthropogenic magnetic particulate matter.

Due to exposure to the atmosphere soils are affected by any kind of air pollution. This is especially the case in the vicinity of industrial centers with heavy industries such as steel mills and coal-fired power plants. But not only there, also in areas with lower anthropogenic emissions soils function as sinks or accumulators for airborne particulate matter. Consequences are the enrichment of soils with e.g., heavy metals (HM) and Polycyclic Aromatic Hydrocarbons (PAH) derived from anthropogenic sources. Such accumulation processes are of long-term nature and can lead to significant soil deterioration.
Vertical susceptibility profiles are the central elements for efficient magnetic soil pollution screening. They enable for depth delineation of anthropogenic particulate matter accumulation

in soils. The central part of this work was the implementation of an efficient and standardized methodological approach for applied environmental magnetic pollution screening. This includes vertical soil profile analysis plus MS data processing for semi-quantification of heavy metal loads in soils. Magnetic investigation was performed at different industrially polluted sites and in different soil types. The systematics of pollution particle distribution has been worked out and implemented into the analytical scheme. Thus, the outcome of this work mainly results from detailed investigation of industrially polluted soils plus former and case studies concerning anthropogenic environmental pollution.

Currently, the method of MS pollution screening in soils is at the stage of entering the standardized application level, making the method uniformly applicable and results comparable. The presented work is a central part towards such highly efficient and standardized data acquisition addressing both MS as well as HM.

1. Vertical magnetic susceptibility profiles and its use

1.1 Soils and magnetic susceptibility (MS)

Magnetic investigations conducted in anthropgenically polluted soils revealed typical enhancement of MS in the upper soil horizons ([1]; Magiera et al. 2006; Petrovsky et al. 2004). Many studies showed that these MS anomalies were associated with HM or PAH. Good correlations of magnetic parameters with HM were found (e.g., Blaha, unpublished data; Gautam et al., 2005; Hanesch and Scholger 2002; Spiteri et al. 2005)

Therefore, magnetic susceptibility can be employed as a useful proxy for the detection of HM in soils. The enormous advantages of MS measurements are the rapidity of data acquisition, non-destructive measurements and the opportunity to collect large data sets for statistical analysis within a short time. This results in economically gathered MS data which can be efficiently processed for sophisticated pollution assessment in soils.

In contrast to MS measurements, the determination of pollutants i.e. HM is time-consuming and expensive.

Nevertheless, for assessment of soil pollution a certain number of HM analyses is always required. Therefore, the key aspect for efficient magnetic proxy screening is an optimized combination of MS measurements with HM analyses. Combination of the strength of both methods is the integrated analytical approach, which makes MS the first choice for data acquisition providing rapidity and accuracy, plus HM analyses at an absolutely reduced number for calibration purposes.

In this context, our special interest regarding magnetic soil pollution screening is on vertical magnetic susceptibility profiles. MS profiles enable easily spatial analysis of anthropogenically polluted soils and provide the basis for sophisticated and efficient pollution assessment.

1.2 Vertical magnetic susceptibility (MS) profiles

High-quality magnetic soil pollution screening requires comprising vertical MS profile analysis. Surface MS screening is the fastest way of magnetic data acquisition, but these comparatively comfortable measurements only provide 2D data. Additionally acquired vertical MS profiles provide 3D data, significantly increasing the efficiency of MS soil pollution screening methods.

For magnetic studies on vertical soil profiles normally individual samples are collected. Sampling volumes are ~10 cm^3 (fitting measuring equipment standards – AGICO KLY-Kappabridge, Bartington MS2B) and commonly only one vertical profile is sampled per investigated site. Such single profiles allow more for the qualitative detection of magnetic anomalies caused by anthropogenic particulate matter input. Airborne magnetic particulate matter usually accumulates in the upper soil horizons in undisturbed soils (forest soils) forming typical MS peaks. Studying soil profiles in this conventional way using individual samples provides important, but more qualitative magnetic information. However, for the implementation of the existing knowledge into efficient soil pollution screening and assessment methods solitary soil profiles are insufficient as shown in [1].

Correlations between MS and HM originating from anthropogenic sources are well studied and commonly accepted [1, 3-8]. This is indeed the most central key factor that environmental magnetic proxy screening for HM detection is possible at all.

In soil profiles the central problem of magnetic analyses is the interaction between the anthropogenic magnetic contribution caused by particulate matter input and the geogenic/pedogenic signal. Magnetic studies employing additional parameters such as isothermal remanent magnetization (IRM) or frequency dependence of MS (χfd%) strongly support and extend the information obtained from magnetic susceptibility analysis. Soil zones with anthropogenically enhanced MS are better defined and e.g., low χfd% values known from pollution particle analysis are found in the anthropogenically affected upper soil layers (Blaha et al., in preparation).

Such information from detailed soil profile analysis is the basis towards further improvement and efficiency enhancement of practically applicable magnetic proxy screening methods using vertical MS profiles.

Studies, compiled in this PhD thesis, provide results comprising information about magnetic properties of airborne environmental pollutants, physical soil properties determining particulate matter accumulation in soils plus a practically applicable method for vertical MS soil profile sampling. Moreover, efficient processing strategies of MS data obtained from vertical soil profiles for systematic and standardized semi-quantification of HM loads in forest soil are presented.

2. Magnetic measuring and sampling equipment

For many MS measurements the Bartington MS2 system was used. The MS2 susceptibility meter provides a measuring range of 1-9999 × 10^{-5} [SI] (volume specific). The resolution is 2 × 10^{-6} SI on the × 0.1 measuring range (www.bartington.com).

2.1 Bartington MS2 susceptibility meter and field sensors

The system comprises a portable MS2 susceptibility meter (Fig. 1 a), which can be connected to a variety of specific sensors. For surface MS measurements the MS2D-sensor (Fig. 1 b) was used. It is the most suitable sensor for soil surface screening. For measurements on vertical sections the MS2F-sensors (Fig. 1 c) was employed, providing high-resolution information. The MS2D and MS2F-sensors are operated in conjunction with the probe handle (shown with the MS2F-sensor in Fig. 1 d).

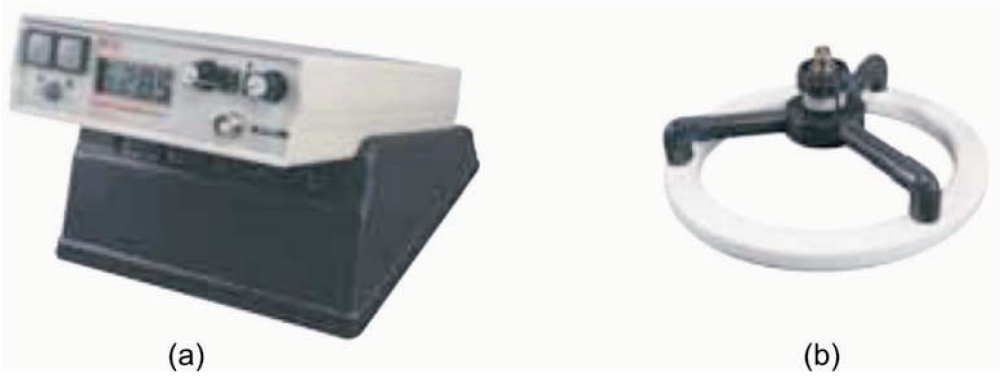

Fig. 1 Bartington MS2 susceptibility meter (a), MS2D-sensor (b), MS2F-sensor (c) and probe handle for MS2D and MS2F sensors.

2.2 Bartington laboratory sensors

MS measurements of soil cores were performed with a MS2C-sensor with 40 mm internal diameter (Fig. 1 e). For determination of frequency dependence of MS on individual samples the MS2B-sensor (Fig. 1 f) was employed (specifications of the sensors are provided in www.bartington.com).

Figs. 1 e-f MS2C core sensor (e) and MS2B dual frequency sensor (f).

2.3 Soil core sampling and in-situ MS profile data acquisition

Soil cores analyzed in this work were collected with a 30 or 50 cm long stainless-steel coring device. The outer diameter of 40 mm corresponds with the diameter of the SM400 down-hole susceptibility meter, ensuring compatibility of both sampling methods.

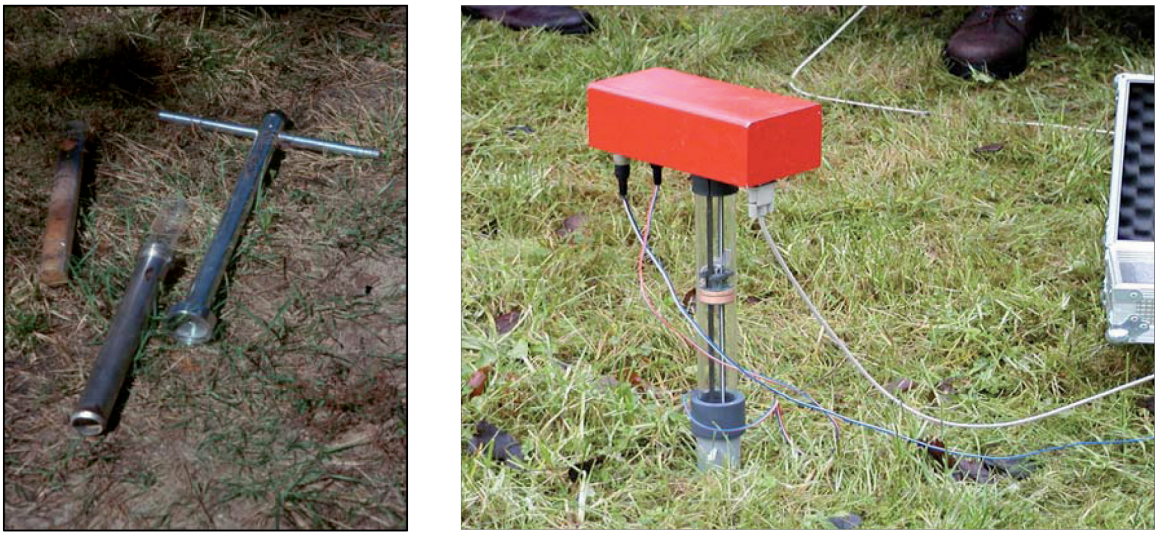

Fig. 2 Stainless-steel soil corer (40 mm outer diameter) plus a soil core sample are shown in (a). In (b) the MS400 down-hole susceptibility meter (ZH instruments) is presented.

2.4 Magnetic laboratory equipment

An AGICO, KLY-3 Kappabridge was used for MS measurements of individual samples. The instrument is operating at 875 Hz with a sensitivity of 3×10^{-8} [SI]. High and low temperature measurements of MS were also performed with this instrument attached to a CS-3 heating unit and a CS-L cryostat, respectively.

A pulse magnetizer MMPM9 (Magnetic Measurements Ltd) was employed for isothermal remanent magnetization (IRM). For measurement of the acquired magnetic moment a Molspin spinner magnetometer was used.

A 2G enterprises cryogenic magnetometer was used for measuring weakly magnetic samples.

3. Methodological requirements for applied vertical MS profile screening

3.1 Boundary conditions for applied vertical MS profile soil pollution screening

Limitations of magnetic soil pollution screening are the naturally given soil conditions plus the currently available MS screening equipment. Natural soil conditions are and will remain the same now and in future. In contrast to the soils, the employed sampling and measuring equipment can undergo technical improvement and provide better output in future (e.g. higher sensitivity). However, currently both of these crucial considerations have to be regarded as constants.

Due to these limiting circumstances only sophisticated soil profile sampling strategies plus adequate MS data processing schemes provide the opportunity for further methodological development towards standardized semi-quantification of anthropogenic pollution loads in soils.

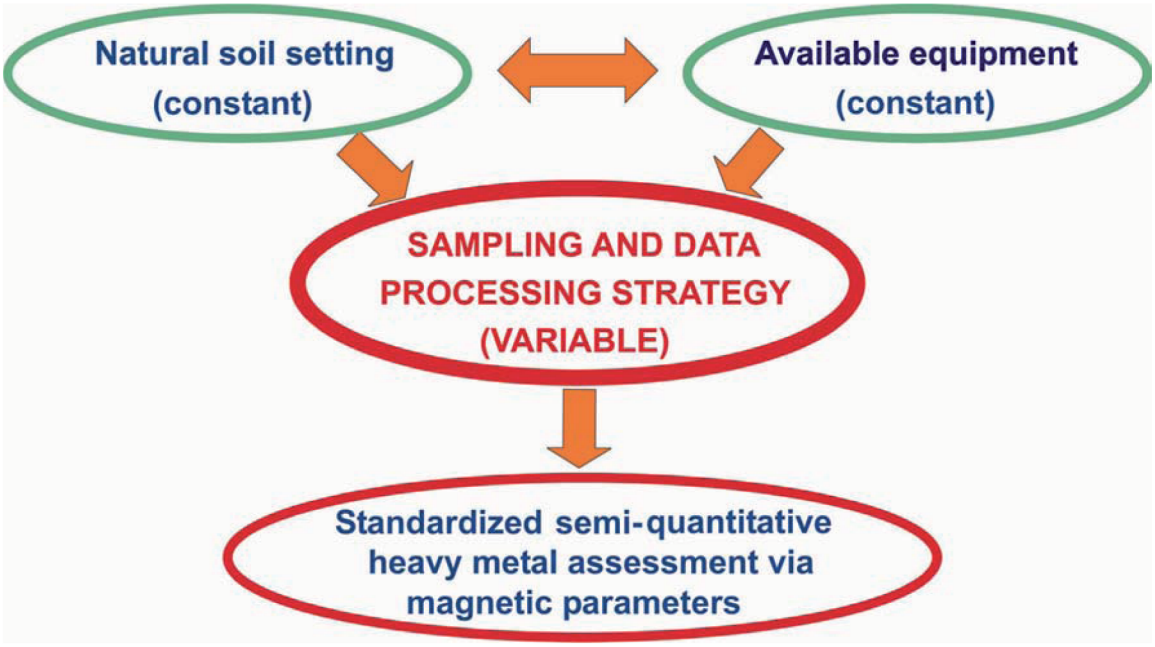

Fig. 3 Interaction of soil and magnetic measuring equipment as constants with respect of sampling and data processing strategies is presented. The final result of an optimized methodological approach is a standardized scheme for semi-quantitative anthropogenic pollution assessment.

The definition of fundamental groups (Fig. 3) are: (1) natural soil setting, (2) available equipment and (3) sampling and data processing strategies are the supporting pillars for standardized magnetic pollution assessment in soils. Separation into constant parameters and variable parameters is a crucial step for the setup of a sophisticated assessment procedure.
All aspects for efficient methodological approaches, comprising soil core sampling, magnetic equipment, measuring schemes, MS data analysis and HM analysis have to be adjusted forming one integrative system. These multiple aspects are forming the boundary conditions for establishing an efficient and applicable MS soil pollution scheme.

3.2 Modular approach for applied vertical MS profile acquisition and analysis

The defined goal for applied magnetic pollution screening is high-grade applicability and reliability of the introduced assessment procedure. At the same time, fast and cost-efficient semi-quantitative pollution screening in soils is the main aspect. This goal is reached by combination of suitable elements, being evaluated prior to definition of the final assessment procedure. Factors essential for such evaluation are arranged in Figure 4.

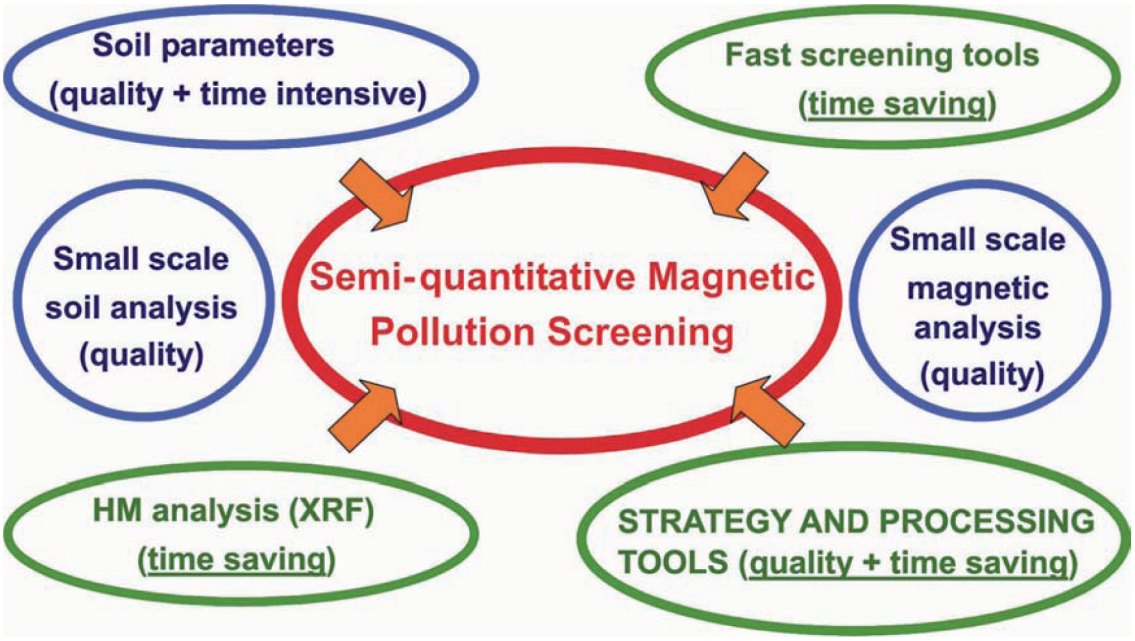

Fig. 4 Implementation model for the setup of an efficient semi-quantitative magnetic pollution screening procedure. Blue outlined parts represent analyses done one-time for the acquisition of fundamentals and calibration purposes. Green parts indicate elements being employed for applied MS pollution screening. Most cost-efficient and time-saving semi-quantitative HM content determination in soils (red) is the final goal.

For the setup of an efficient semi-quantitative magnetic pollution screening procedure two test stages were defined.

The first stage provided high resolution data based on detailed and time-intensive small scale analysis of magnetic and soil properties. These analyses comprised in-situ MS measurements, magnetic analysis of small volume soil samples (10 cm^3) and samples collected at 0.5 cm

vertical spacing. Additionally, soil density analysis was performed on small volume soil samples, providing indispensable information for setup of the final analytical scheme.
The second stage comprised the application level utilizing fast MS screening tools for measurement of entire soil cores of up to 50 cm length in the laboratory plus soil profiles in-situ. Additionally, HM data which were rapidly acquired by XRF technique were integrated into the analytical procedure of MS data, resulting in an efficient strategy for pollution assessment at applied scale [1].
However, the central part of this multiple approach was the systematic implementation of the specific results obtained from both stages into an efficient pollution assessment procedure.

4. Soil characteristics, MS distribution and their importance for MS pollution screening

4.1 Physical characteristics of natural (forest) soil and its impact on MS

Natural soils are typically layered structures consisting of horizons with different porous structures and properties. These porous structures and properties are determining factors for anthropogenic magnetic particulate matter transport and accumulation as they form a trap and filtering system.
In soil science the interest is more on established parameters such as, pH-values, soil mineralogy, grain-size, clay content or color related to soil horizons and soil types, rather than on small volume analysis of soil density, controlled by porosity. However, approaches for magnetic screening of anthropogenic particulate matter input require different strategies, also considering the properties of pollution particles and their interaction with the soil material.
Airborne dusts consist of solid particles of sub-µm to some 100 µm in size, which accumulate in interaction with soil material properties (Blaha et al., in preparation). Information about particle sizes of environmentally relevant magnetic particulate matter are also provided by e.g., Veneva et al. and 2004, Jordanova et al., 2006. The uppermost, loose soil zone allows particle movement due to their porous structure, whereas more compact layers with less pore space, less connectivity and adhering surfaces accumulate infiltrating particles. These basic, but dominating soil characteristics for dust particle input were systematically brought into conjunction with the magnetic observations made and were used for the setup of an efficient vertical MS profile screening scheme [1].

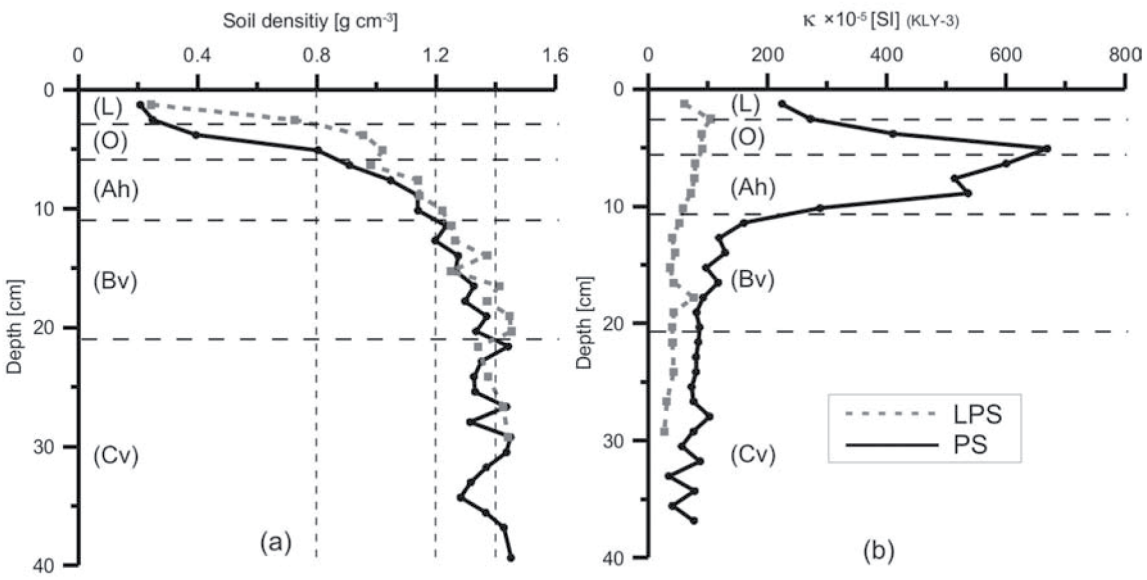

Fig. 5 (a) Density distribution from two brown-earth profiles from the Donawitz steel mill study area is presented. The continuous increase of density (controlled by porosity) with depth is the main controlling factor for dust particle accumulation. In (b) the MS peaks directly represent the anthropogenic magnetic particulate matter accumulation mainly controlled by soil density [1]. PS stands for the "polluted site", while LPS indicates the "less polluted site".

For vertical MS profile screening the dominating factor is soil density, controlled by porosity, as this is obviously typical for any kind of natural soils. Density profiles as shown in Fig. 5 a were also observed in other investigated soils (Blaha, unpublished data).

4.2 Spatial magnetic susceptibility distribution in polluted natural soil

High-resolution MS analysis on soil sections revealed significant spatial variability of MS values in the upper zone of a polluted soil. Figure 6 shows the MS pattern of a 40 cm wide soil section polluted through airborne magnetic particulate matter. This soil pollution originated from steel mill and coal-fired power plant emissions of the Shijingshan industrial area, western Beijing [5].

Observations, revealing highly variable MS values in the upper soil zone were also made in other high-resolution studies comprising different soil types (Blaha, unpublished data).

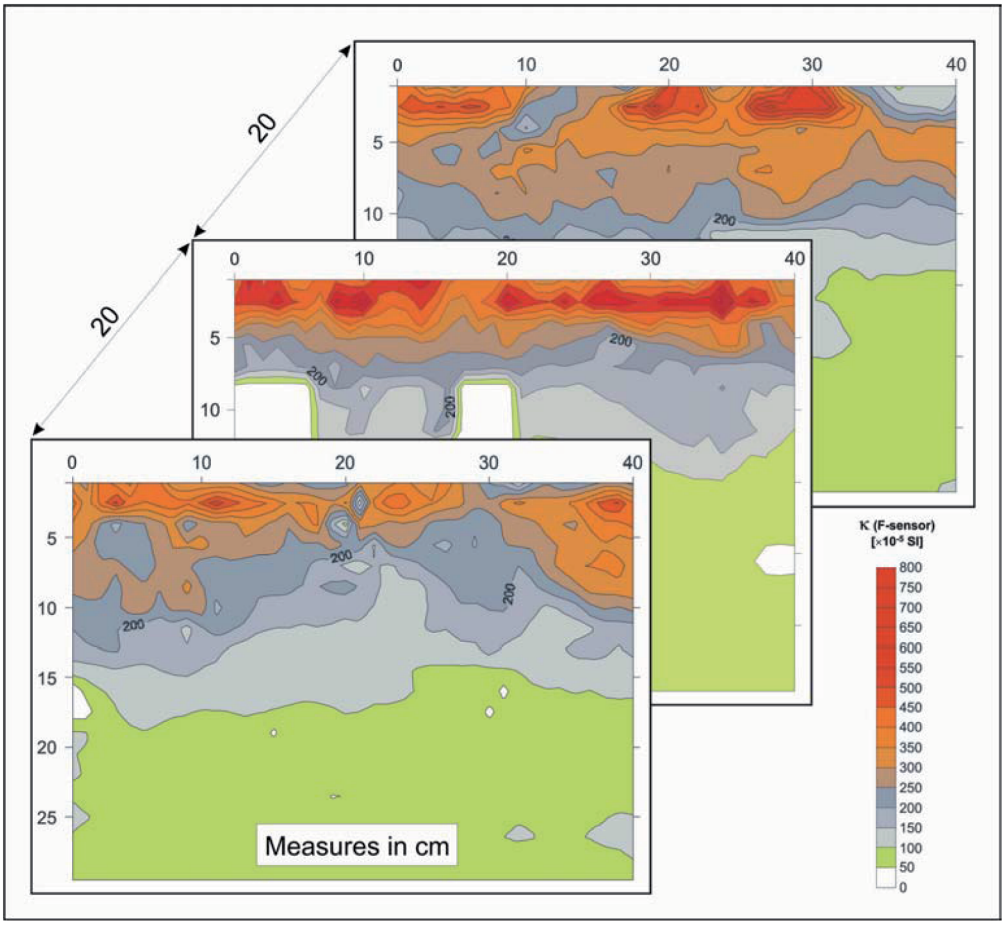

Fig. 6 MS distribution patterns of vertical soil sections from the Shijingshan industrial area, western Beijing. Anthropogenic MS enhancement in the upper 10 to 15 cm of the vertical sections and its spatial variability is shown.

In-situ MS data acquisition with the Bartington MS2F-senor at measuring intervals of 1 cm revealed detailed distribution patterns of the deposited and accumulated magnetic particulate matter input. Anthropogenic MS is represented by red to gray color (Fig. 6). Areas with green and white color in the lower part represent the natural background signal.

Such highly heterogeneous MS distribution in the upper soil zone is caused by soil properties, vegetation (roots), wet and dry cycles or/and bioturbation through soil organisms. All these processes may contribute to extremely irregular accumulation of airborne magnetic particulate matter.

Up to now there have been no studies about small-scale MS distribution in polluted soils in such detail. However, detailed knowledge about MS distribution in soil profiles is the basis for sophisticated MS soil pollution screening using vertical MS profiles.

There are quite a lot of magnetic studies on vertical soil sections investigating the pure vertical MS distribution, revealing anthropogenic magnetic enhancement in the upper soil horizons (e.g., Gautam et al., 2004; Kapicka et al., 2001; Magiera et al., 2007; Petrovsky et al., 2004; Spiteri et al., 2005). These studies show the importance of the upper soil horizons for accumulation of anthropogenic magnetic particulate matter. Furthermore, many of them reveal correlations between anthropogenic MS and HM elements originating from anthropogenic sources.

However, up to now no satisfying approach for systematic implementation of the established knowledge towards efficient employment of MS soil profile analysis has been published. Thus, in this work requirements for such an applied approach are formulated on the basis of the main determining factors concerning soil structure, pollution characteristics, measuring equipment plus data analysis. Furthermore, an applicable model for semi-quantification of HM pollution in soils is presented being the consequential step towards efficient application of vertical MS soil profile screening.

4.3 Basic principles for sampling strategies in polluted natural soil

Prospects for a straightforward approach in soil profile analysis are significantly reduced through MS heterogeneities as shown in Fig. 6. Requirements for efficient and representative soil profile analysis are therefore methodological approaches finally leveling out such natural heterogeneities.

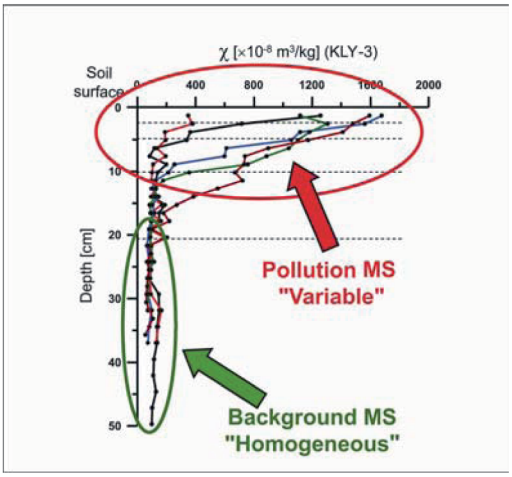

Fig. 7 Five MS profiles collected from the "polluted sampling site" at Leoben, Austria. Lateral distance between the profiles was ~10 cm, and vertical spacing was ~2.5 cm. The sampling volumes are 8.6 cm³. Curves are highly variable in the upper soil zone, but stable in the lower part.

Highly variable MS values in the polluted soil zone directly influence sampling of vertical MS profiles (Fig. 7). It is obvious that sampling without adequate strategies will not provide satisfying results when going beyond standard MS soil profile sampling and analysis.

Therefore, the knowledge derived from the soil section case study in western Beijing (Fig. 6) and other case studies (Blaha, unpublished data) is of high importance for vertical MS pollution screening. It explicitly shows that spatial variability of anthropogenic MS is a determining parameter which cannot be neglected. Furthermore, systematic MS differences between the upper and lower soil zones, showing highly variable, respectively stable values are one key factor for further methodological development towards applied MS pollution screening.

However, for holistic approaches in applied vertical MS soil profile screening multiple factors, ranging from soil properties, magnetic particulate matter properties and measuring equipment to MS data processing must be integrated into the model.

In Fig. 8 vertical MS and χfd% profiles originating from the "polluted site" in Leoben are shown [1].

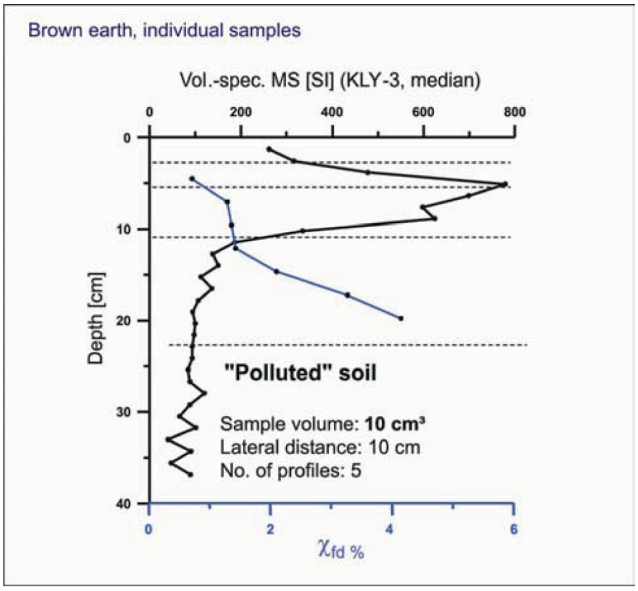

Fig. 8 MS and χfd% profiles from a polluted brown-earth profile are presented. The MS peak depicts magnetic particulate matter accumulation in the O and Ah horizons. The χfd% curve reveals values between 1 and 2 in the polluted zone, reflecting specific magnetic properties of anthropogenic magnetic particles originating from the nearby steel mill. Systematically

increasing values of χfd% in the lower soil zone, depending on pedogenic and geogenic magnetic mineral contents (magnetically fine grained) are shown.

MS is the most important parameter applied in magnetic screening. This central parameter is the only one which can be currently measured at minimum time effort, in the laboratory and in the field. In Fig. 8 MS reveals the accumulation of anthropogenic magnetic particulate matter in the O and Ah horizons. The MS signal directly depicts accumulated magnetic particulate matter originating from the steel mill exhaust gases. Complementary to MS, frequency dependence of MS provides information about magnetic pollution particle accumulation through low χfd% values. However, χfd% analysis requires more time and a larger measuring effort. Therefore, such measurements can provide additional information for research and calibration purposes, rather than being employed for applied magnetic screening on a big scale. Thus, MS is the only magnetic key parameter for fast measurements, and data have to be currently acquired only utilizing this parameter.

4.4 Soil horizons, MS and HM in polluted natural soil

For adequate analysis concerning correlation between MS and HM the role of soil horizons, respectively the layered structure of soils with its different physical properties is a crucial factor. In Fig. 9 the correlation between MS and Pb determined from distinct soil horizons in polluted brown-earth is shown.

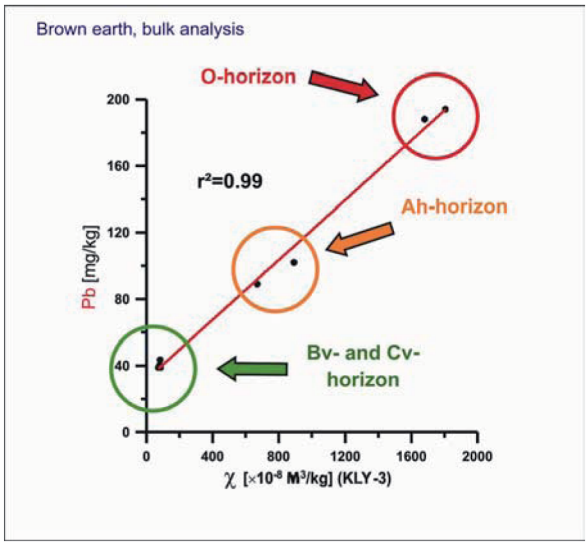

Fig. 9 Correlation between MS and Pb from defined soil horizons is shown. Analysis was done on bulk soil material, and two samples per selected horizon are plotted.

Excellent correlation between anthropogenic MS and certain HM in the upper soil horizons indicate the close relationship between both parameters (see also Blaha et al., 2008a [1]). Such relationship explicitly confirms the anthropogenic origin of magnetic particulate matter plus HM, similar way of transport and similar fate of deposition. Moreover, it clearly shows that possible pedogenic enhancement of MS in polluted soils is low compared to anthropogenic MS. Therefore, pedogenic MS has hardly any influence on the results and can be neglected. Confirmation of this fact is another key factor for the development of more sophisticated pollution screening methods. It is clearly shown that only the upper soil zone, which is mostly affected by magnetic particulate matter input reveals such correlation. The O and Ah horizons are identified as the main accumulation zone. In contrast, data from Bv and Cv horizons plot already quite close to each other with low values of MS and HM content. Therefore, putting the focus on systematic analysis including soil horizons and depth enhances the outcome of soil pollution studies significantly.

5. Properties of magnetic particulate matter

Regarding results from vertical soil profile analysis, investigation on magnetic particulate matter is inseparable from the development of sophisticated methods for magnetic screening of anthropogenically polluted soils. Soil structure plus mainly physical properties of magnetic particulate matter interact and determine typical accumulation patterns (see Fig. 6).

Therefore, grain-size distribution, surface structure of particles, internal structures plus magnetic and chemical properties of fly ash from a coal-fired power plant were exemplarily studied. There are studies on various types of fly ash particles (e.g., Fisher et al., 1978; Hansen et al., 1981 and Del Monte and Sabbioni, 1984), investigating preferably physical and chemical properties. However, these studies do not include magnetic investigations. Magnetic investigations on fly ash or fly ash particles were conducted by e.g., Kapicka et al. (2003), Veneva et al. (2004) and Jordanova et al. (2006). These studies showed that magnetic particulate matter is highly diverse regarding magnetic properties and its physical structures. For putting more emphasis on quantity of certain particles, their structures and their magnetic properties, investigation on fly ash was performed [2]. Fly ash is ideal for such studies, as it can be a main pollutant, and as it is collected in precipitator systems under controlled conditions. It is shown that only the combination of different parameters leads to better assessment of potential pollution particles and their interaction with natural collectors such as soils, sediments or tree leaves.

In Figure 10 cumulative grain-size distribution of fly ash samples collected from a two-stage electrostatic precipitator system of a black-coal fired power plant in Bexbach, Saarland is shown [2].

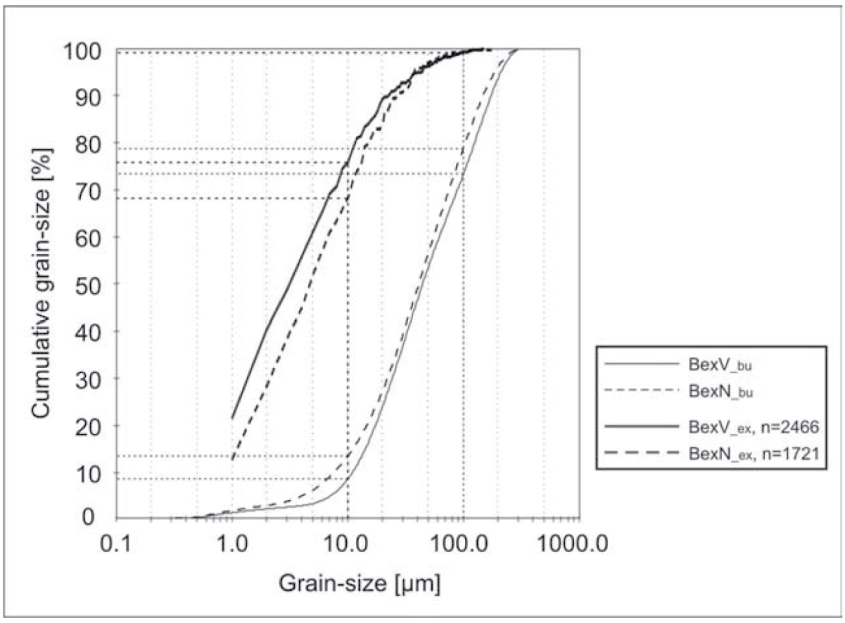

Fig. 10 Cumulative grain-size distribution of bulk fly ash samples and magnetic extracts from Bexbach coal-fired power plant (Blaha et al., 2008b [2]). Curves show results from two flue gas purification steps ("Vor- und Nachreinigung", samples termed BexV, respectively BexN).

Differences between grain-size distribution of bulk fly ash samples and extracted magnetic particles are obvious. Comparatively small bulk grain-sizes of <10 µm comprise ~75% of highly magnetic fly ash spherules. This also means that smaller magnetic fly ash spherules contain relatively higher amounts of magnetic phases (mostly magnetite) compared to bigger spherules. Such differentiation might have consequences for magnetic investigation methods when fly ash material is distributed and fractionized. This could comprise airborne transport and specific accumulation in certain soil layers or distribution in aquatic systems with subsequent sedimentation.

However, at the current level of development regarding measuring technology and at the scale of applied vertical soil profile screening, these effects might be of minor relevance. In contrast to this, there might be high interest for the investigation of details on the links between MS and HM contents in individual magnetic particles or grain-size fractions. Such knowledge might lead for better assessment of potential environmental risks.

Investigation on the MS contribution of fly ash grain-size fractions including their relative amount, revealed that the small fraction (<63 µm) significantly contributes to MS of the bulk sample [2].

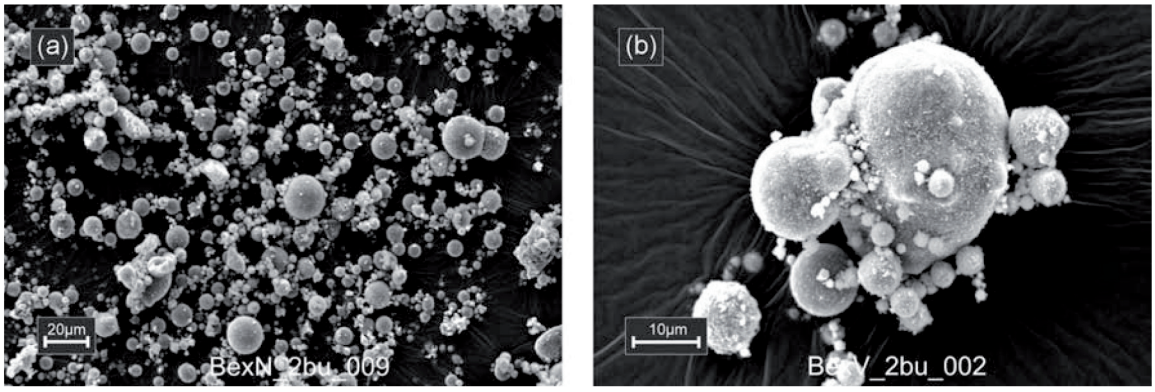

Fig. 11 SEM images of bulk fly ash samples from a black coal-fired power plant (Bexbach), [2].

Fly ash particles show typically spherical shape. This is the case for highly magnetic and non-magnetic particles, while any intermediate stages might occur. SEM investigation on polished fly ash particles as shown in Fig. 12 provide insight into the diverse structures of strongly magnetic spherules originating from Bexbach coal-fired power plant.

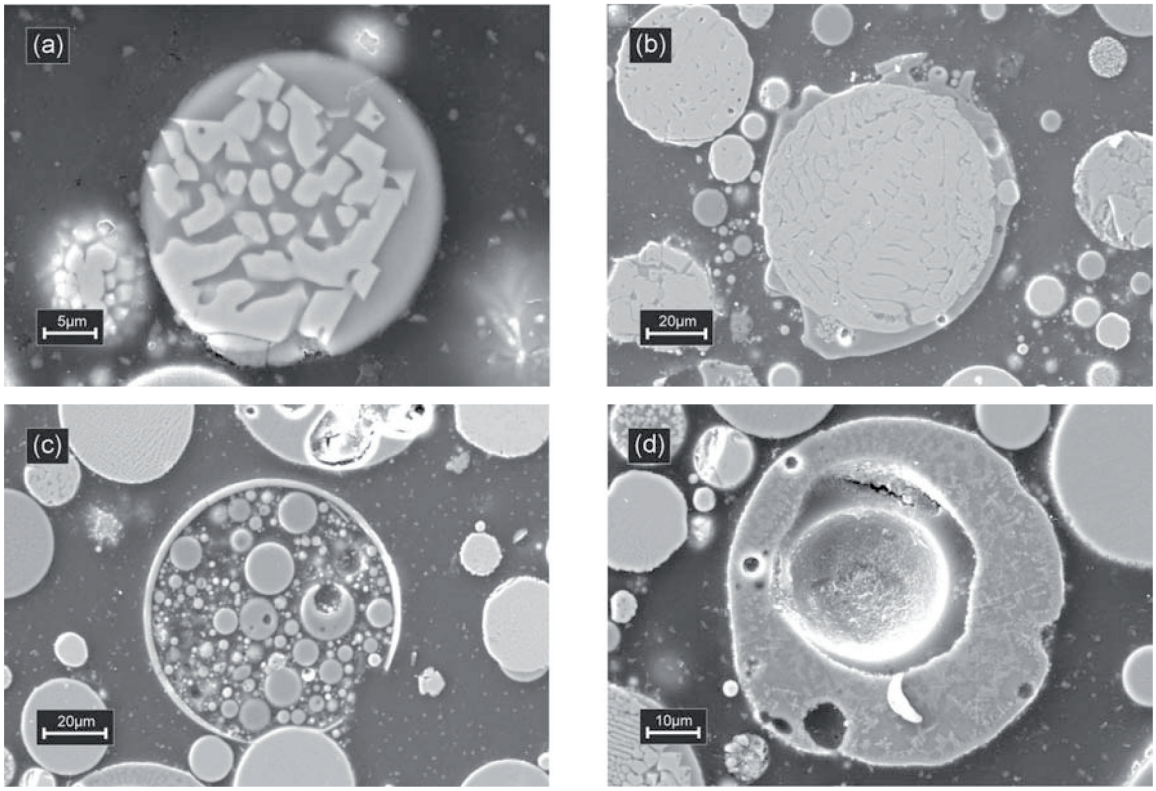

Figs. 12 (a-d) Selection of SEM images from polished sections showing highly varied internal structures of fly ash particles (Blaha, unpublished).

Under favorable conditions SEM/EDX analysis on polished fly ash particles reveals in general two, more or less clearly distinguishable internal zones. Separation into magnetic phases bearing areas indicated by brighter color, and glassy areas indicated by dark grayish color (Fig. 12 a, b) is possible. Bright areas with clear boundaries towards the matrix consist of sub- to anhedral magnetic crystals (Fig. 12 a). EDX analysis determined on crystals and matrix material in Fig. 12 a show high Fe content of ~28 atom-% in the crystals, respectively ~7 atom-% in the matrix. Data for element contents are presented in Table 1.

Table 1 Element contents determined by EDX analysis are presented. In the crystal structures 25, and in the matrix 20 analyses were performed. Mean values and standard deviations are given.

	Fe	Ti	Si	Al	Ca	Mg	Oxygen
Crystals	27.84	-	3.15	2.76	1.02	1.16	65.76
Stddev	3.46	-	1.77	0.53	0.58	0.21	0.75
Matrix	7.11	0.28	12.62	5.28	5.88	0.59	68.95
Stddev	3.17	0.09	1.06	0.31	0.83	-	1.74

SEM/EDX analysis on internal particle structures shows that main element contents can be reliably determined (Table 1 and [2]). It also shows that best possible data quality is ensured by conducting EDX analysis on polished structures, as target areas can be clearly identified. In contrast, EDX analysis on particle surfaces must be regarded to be of lower quality, as contributions from internal heterogeneous microstructures cannot be sufficiently controlled. However, EDX analysis is mostly suitable for confirmation of SEM observations on individual particle structures (e.g., determination of Fe contents). Therefore, it is an essential tool for supporting interpretation of magnetic data obtained from fly ash analysis [2]. For bulk fly ash analysis it is certainly not an appropriate method, since heterogeneities are manifold and obtained data scatter widely.

6. Magnetic particulate matter behavior in forest soil

Magnetic particulate matter migration and accumulation in forest soil was tested with artificially distributed fly ash (Blaha et al., in preparation). A test site in an unpolluted forest soil (coniferous forest) was prepared and the migration behavior of magnetic particles was monitored. This experiment provided extended knowledge about the role of the uppermost soil horizons for particle accumulation, revealing retardation of particles by sticking to undecayed organic matter (litter layer) plus fast vertical translocation of particles into the O horizon at the same time. Accumulation of particles on leaves or pine needles is shown by e.g., Hanesch et al., 2003 and Urbat et al., 2004. This process still seems to take place in the litter horizon. In the beginning of the experiment particle migration occurred at an unexpectedly high rate, caused by the porous structure of the uppermost soil zone. Median values of the MS surface signal declined rapidly by 40 % between day 1 and 17 (Fig. 13 a).

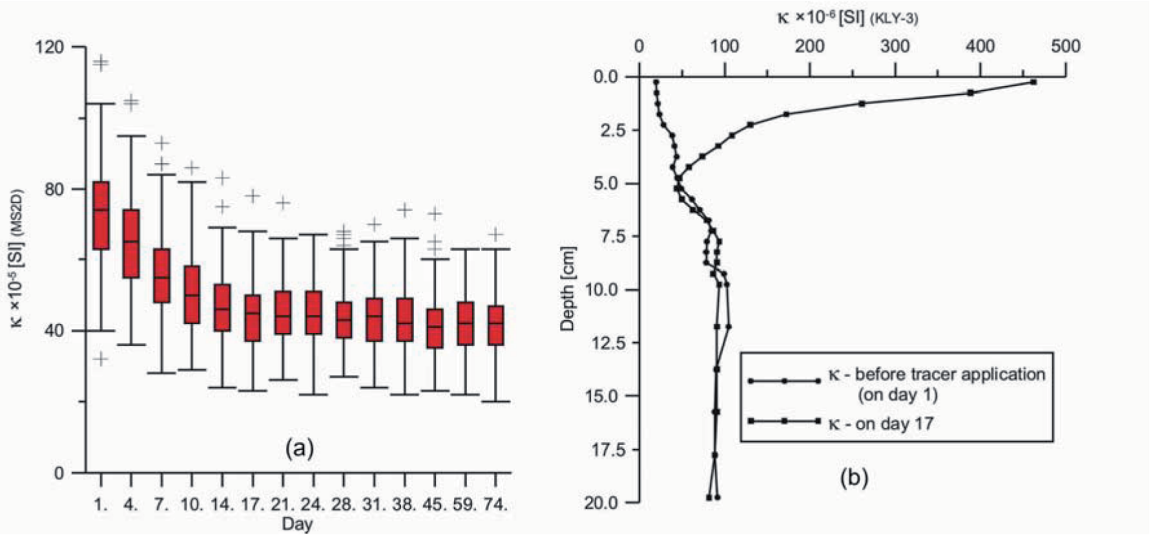

Fig. 13 In (a) surface MS data (MS2D) from test site monitoring are shown. Each set consists of 160 individual readings. Box-plots show median (Q2) and quartile (Q1, Q3) values. Outliers are marked with crosses and are defined as Q1 (Q3) + 1.5* IQR. In (b) MS curves before tracer application and on the 17 day after application are shown.

Box-plots are suitable tools for assessing data sets obtained from MS measurements. Variations of the data sets in Fig. 13 a show clearly that statistical assessment is required, and that a sufficient number of data has to be acquired for representative analysis (Blaha et al., in preparation). In Fig. 13 b two vertical MS profiles are presented, reflecting MS in unpolluted stage and after 17 days of tracer application. Magnetic particle migration down to ~5 cm is

observed. At the same time MS values near the soil surface are still comparatively high, which means that retardation by sticking of particulate matter to litter occurs. Therefore, two processes, migration plus retardation determine the vertical MS distribution pattern. As such accumulation processes cannot be studied with normal particulate matter input from industrial sources, migration experiments can provide answers how particle accumulation works.
In Fig. 14 a, b soil density, controlled by porosity and the according soil profiles from the tracer test site are shown.

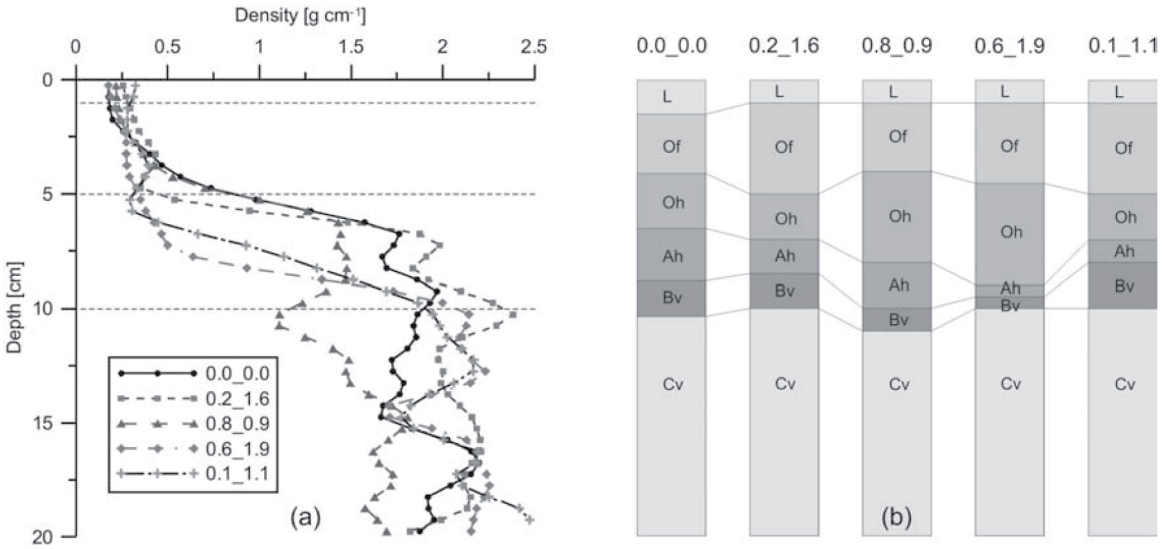

Fig. 14 Five soil density curves (a) from the monitoring site and the according soil profiles (b) are presented. L and O horizons show lowest density and determine particulate matter distribution.

The soil-fly ash interaction experiment, shown with Figs. 13 a, b and 14 a, b provides systematic insight into particle migration/accumulation processes for the short-time case. Long-time tests are on the way and will reveal both MS changes in the vertical profile and on the soil surface. MS surface data (Fig. 13) revealed that there are significant lateral variations between the individual measurements. Surface MS structures at different times of the experiment are shown in Fig. 15.

.

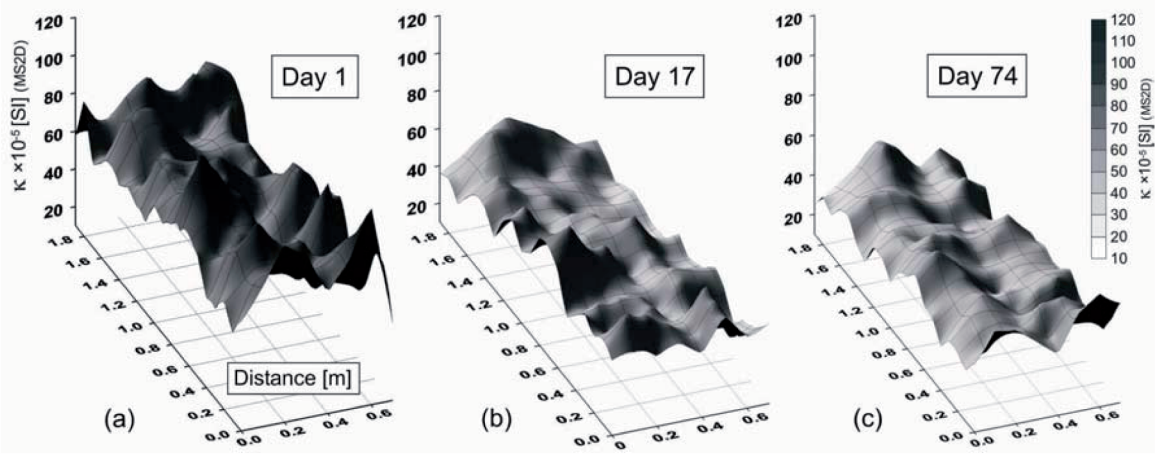

Figs. 15 (a-c) MS surface patterns at different times after tracer application (Blaha et al., in preparation)

Anthropogenic magnetic particulate matter distribution and the resulting MS surface data variability (Figs. 15) are significantly determined by physical soil properties, respectively the natural heterogeneities of the upper soil zone. It is shown that loose soil layers, such as the litter layer in forest soils enable trapping and fast vertical migration of dust particles.

So far, studies investigating the role of physical soil properties and spatial variability of MS for systematic screening purposes do not exist. Therefore, information from such systematic tests is of high importance for further improvement of measuring procedures as introduced in [1].

Furthermore, the experiments revealed close similarities with measurements made in industrially polluted soils (Fig. 16). The results from both types of investigation strongly point at the dominating role of the upper soil structure being responsible for the typical, anthropogenic MS distribution patterns. As the variations are always high, screening methods have to be adapted to these conditions.

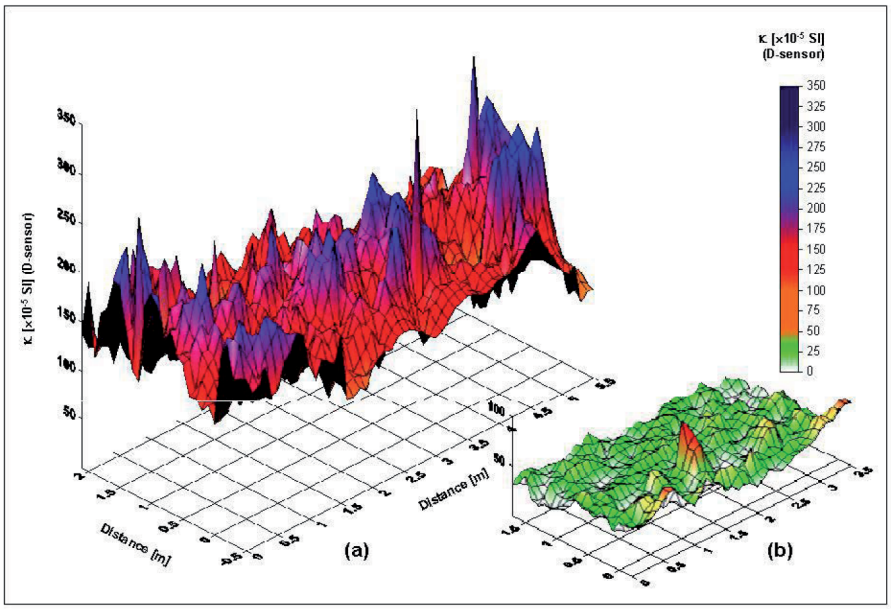

Fig. 16 MS data from sites which were differently intense affected by airborne magnetic particulate matter input are shown. The sites are located at different distances to a steel mill.

Statistically evaluated surface MS data from the three different, industrially polluted soils are presented in Fig. 17.

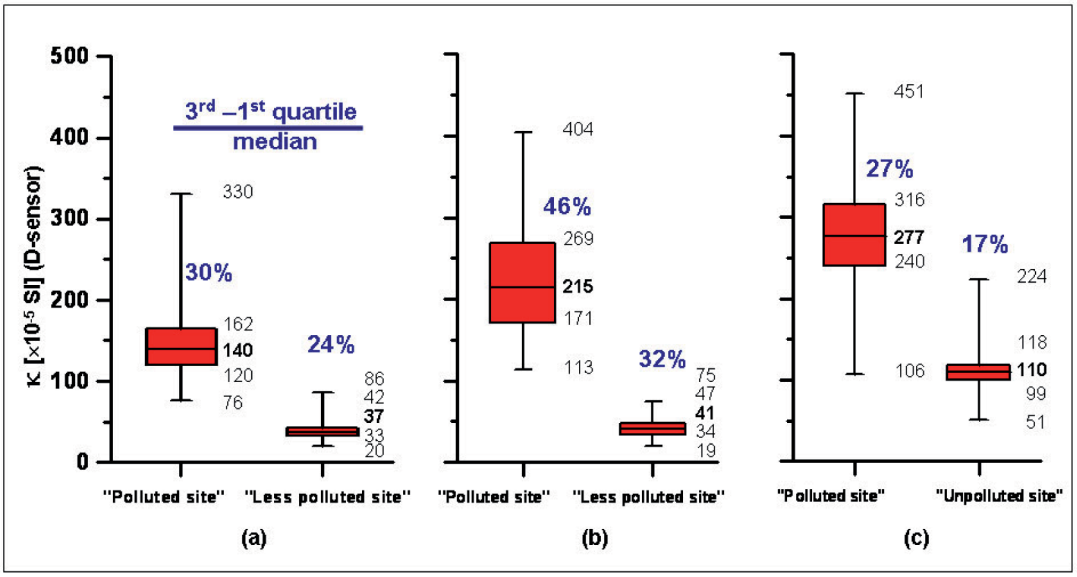

Fig. 17 MS surface data from the three investigated, industrially affected locations are presented. Two "site scale" sized test sites revealing more or less intense pollution were investigated at each location. Soil types are: (a) brown-earth, (b) Podzol and (c) aeolic deposition (Blaha et al., in preparation).

MS values showing higher variability are always observed in the more polluted sites (Fig. 17). This indicates that higher magnetic particulate matter input leads to wider scattered MS data. For MS screening purposes this might be a further criterion to be implemented into methodological improvements.

Variable MS surface data seem to reflect irregular deposition of dust-loaded tree leaves, unsteady direct magnetic particle input in the soil, and the interaction of particulate matter with soil heterogeneities in the Ah and Bv horizons. Fresh tree leaves or needles collect in the litter horizon (L) before they decay and the organic matter plus adhering pollution particles accumulate in the O horizon. Thus, results from surface MS measurements strongly depend on the thickness and spatial heterogeneities of these upper soil layers. As 60 % (90 %) of the recorded MS signal of the Bartington MS2D sensor come from the uppermost 2 cm (6 cm) (Lecoanet et al., 1999), MS variations observed in this zone are of high importance for the development of accurate and efficient surface MS measuring strategies.

In this work an applicable method for HM semi-quantification utilizing vertical MS profile assessment is provided [1]. For surface MS data acquisition and assessment, which is in applied MS screening closely linked with vertical profiles, the development of an optimized screening methodology on the basis of the presented data sets (Figs. 13 a and 17) is suggested. These MS data reflect site specific variability, which is definitely one aspect that can be used for further development of efficient measuring and assessment schemes. However, as this is not the topic of this work, only fundamentals for the solution of this problem are provided. Since different ways of particulate matter input are regarded to influence MS distribution patterns in soils, dust collectors as tree leaves were included into investigations [4, 6].

Dust-loaded leaves are intermediate collectors, retarding particulate matter input according to leave fall cycles of the according tree types. Therefore, tree leaves can be efficiently used for pollution screening and monitoring, as the accumulation rate of magnetic particles per time interval can be assessed. Finally, leaves and magnetic particulate matter get accumulated in the soil, enhancing anthropogenic MS and pollution loads. Thereby, irregular accumulation of dust-loaded leaves in soil, and especially their magnetic particle load might significantly contribute to scattered surface MS data, as well as to variable MS values in vertical profiles.

Investigations on soils and leaves presented in this work include industrial pollution sources [1, 3-5], urban sources [7] plus road traffic [3, 6-8] and show the broad range, where magnetic screening methods can be usefully applied.

7. Standardized, semi-quantitative in-situ MS profile assessment

Merged results from this multi-aspect study on polluted soils and potential pollutants resulted in the assessment procedure described in [1]. This assessment procedure for MS profile acquisition and data analysis was worked out basing on the established fundamentals, the procedure itself being already designed for fitting demands for further optimization and extension.

Such extension includes the implementation of the presented assessment procedure into computerized, software supported on site MS soil profile assessment. MS profile data acquired in-situ with a SM400 down-hole susceptibility meter, as described by Petrovsky et al. (2004) can be processed following the principles for soil cores [1]. The crucial advantage of such vertical MS profile on site analysis is the selection of an optimized number of profiles adapted to the actual situation at the according test site. This will significantly reduce cost and time-effort for sampling plus further assessment. Soils can be even directly and efficiently assessed concerning their general suitability for sampling. Furthermore, boundary depth determination, separating the upper polluted soil zone from the lower unpolluted one can be done software supported on site. In addition, the most suitable soil core(s) for laboratory analysis can be selected fitting the defined requirements of the introduced assessment scheme [1]. As any magnetic soil pollution survey is actually undertaken in areas which can be termed as “Terra incognita”, the application of fast data acquisition methodologies is able to provide immediate results and has far-ranging consequences for applied environmental magnetic pollution screening.

However, as the final implementation steps for semi-automatized on site MS processing go far beyond this PhD thesis, only the fundamental structures for this technology are introduced.

References

Del Monte M., Sabbioni C., 1984. Morphology and mineralogy of fly ash from a coal fueled power plant. *Archives for Meteorology, Geophysics, and Bioclimatology* **Ser. B 35**, 93-104.

Flanders P., 1994. Collection, measurement, and analysis of airborne magnetic particulates from pollution in the environment. Journal of Applied Physics **75**, 5931-5936.

Fisher G.L., Prentice B.A., Silberman D., Onodov J.M., Biermann A.H., Ragaini R.C., and McFarland A.R., 1978: Physical and morphological studies of size-classified coal fly ash. *Environmental Science & Technology* **12,** 447-451.

Gautam P., Blaha U. and Appel E., 2005. Integration of magnetism and heavy metal chemistry of soils to quantify the environmental pollution in Kathmandu, Nepal. *The Island Arc* **14**, 424−435.

Gautam P., Blaha U., Appel E., and Neupane G., 2004. Environmental magnetic approach towards the quantification of pollution in Kathmandu urban area, Nepal. *Physics and Chemistry of the Earth* **29**, 973-984.

Hanesch M., Scholger R., Rey D., 2003. Mapping dust distribution around an industrial site by measuring magnetic parameters of tree leaves. *Atmospheric Environment* **37**, 5125-5133.

Hanesch M. and Scholger R., 2002. Mapping of heavy metal loadings in soils by means of magnetic susceptibility measurements. *Environmental Geology* **42**, 857-870.

Hansen L.D., Silberman D., and Fisher G.L., 1981: Crystalline components of stack-collected, size-fractioned coal fly ash. *Environmental Science & Technology* **15,** 1057-1062.

Jordanova D., Jordanova N., and Hoffmann V., 2006: Magnetic mineralogy and grain-size dependence of hysteresis parameters of single spherules from industrial waste products. *Physics of the Earth and Planetary Interiors* **154,** 255-265.

Kapicka A., Petrovsky E., Jordanova N., Podrazsky V., 2001. Magnetic parameters of forest top soils in Krkonose Mountains, Czech Republic. *Physics and Chemistry of the Earth* **26,** 11-12, 917-922.

Kapicka A., Jordanova N., Petrovsky E., Podrazsky V., 2003. Magnetic study of weakly contaminated forest soils. *Water, Air and Soil Pollution* **148,** 31-44.

Lecoanet H., Leveque F., Segura S., 1999. Magnetic susceptibility in environmental applications: comparison of field probes. *Physics of the Earth and Planetary Interiors* **115**, 191-204.

Magiera T., Strzyszcz Z., Kapicka A., Petrovyky E., and Magprox team, 2006. Discrimination of lithogenic and anthropogenic influences on topsoil magnetic susceptibility in Central Europe. *Geoderma* **130,** 299-311.

Magiera T., Strzyszcz Z., Rachwal M., 2007. Mapping particulate pollution loads using soil magnetimetry in urban forests in the Upper Silesia Industrial Region, Poland. *Forest Ecology and Management* **248**, 36-42.

Oldfield F., Hunt A., Jones M.D.H., Chester R., Dearing J.A., Olsson L., Prospero J.M., 1985. Magnetic differentiation of atmospheric dusts. Nature 317, 516-518.

Petrovsky E., Hulka Z., and Kapicka A., 2004. A new tool for in situ measurements of the vertical distribution of magnetic susceptibility in soils as basis for mapping deposited dust. *Environmental Technology* **25,** 1021-1029.

Scholger R., 1998. Heavy metal pollution monitoring by magnetic susceptibility measurements applied to sediments of the river Mur (Styria, Austria). *European Journal of Environmental and Engineering Geophysics* **3**, 25-37.

Spiteri C., Kalinski V., Rösler W., Hoffmann V., Appel E., and Magprox team, 2005. Magnetic screening of a pollution hotspot in the Lausitz area, Eastern Germany: correlation analysis between magnetic proxies and heavy metal contamination in soils. *Environmental Geology* **49**, 1−9.

Strzyszcz Z. and Magiera T., 1998. Magnetic susceptibility and heavy metal contamination in soils of Southern Poland. *Physics and Chemistry of the Earth* **23,** 9-10, 1127-1131.

Urbat M., Lehndorff E., Schwark L., 2004. Biomonitoring of air quality in the Cologne conurbation using pine needles as a passive sampler-Part I: magnetic properties. *Atmospheric Environment* **38,** 3781-3792.

Veneva L., Hoffmann V., Jordanova D., Jordanova N., and Fehr Th., 2004: Rock magnetic, mineralogical and microstructural characterization of fly ashes from Bulgarian power plants and the nearby anthropogenic soils. *Physics and Chemistry of the Earth* **29,** 1011-1023.

www.bartington.com

1

Determination of anthropogenic boundary depth in industrially polluted soil and semi-quantification of heavy metal loads using magnetic susceptibility

Available online at www.sciencedirect.com
ScienceDirect
Environmental Pollution 156 (2008) 278–289
ENVIRONMENTAL POLLUTION
www.elsevier.com/locate/envpol

Determination of anthropogenic boundary depth in industrially polluted soil and semi-quantification of heavy metal loads using magnetic susceptibility

U. Blaha [a,*], E. Appel [a], H. Stanjek [b]

[a] Institute for Geoscience, University of Tübingen, Sigwartstrasse 10, 72076 Tübingen, Germany
[b] Clay and Interface Mineralogy, RWTH Aachen, 52056 Aachen, Germany

Received 29 August 2007; received in revised form 11 December 2007; accepted 17 February 2008

Our method allows standardized semi-quantification of anthropogenic heavy metal loads in soils by magnetic susceptibility processing plus only two heavy metal analyses

Abstract

This study focuses on magnetic susceptibility processing and analysis towards fast and cost-efficient discrimination and semi-quantification of anthropogenic heavy metal loads in soil. Spatial variability of magnetic susceptibility was investigated on sets of soil cores from both "polluted" and "less polluted" forest soil close to a steel mill near Leoben, Austria. Test sites of $\sim 10\ m^2$ represent "site scale" dimensions. Statistical analysis of magnetic data provides a boundary depth indicating the transition from the "polluted" to the deeper, "unpolluted" zone in contaminated natural soil. Introduction of a block master curve simplifies the complex variations of individual curves, and represents magnetic susceptibility at "site scale". For linking the block master curve to heavy metals we only require magnetic susceptibility data from one soil core and heavy metal data from two sub-samples from the same core. Our optimized magnetic susceptibility data processing scheme provides an applicable tool to semi-quantify anthropogenic heavy metal loads in soil.

Keywords: Magnetic susceptibility; Soil; Contamination; Pollution; Heavy metals; Boundary depth

1. Introduction

In recent years many studies (e.g., Strzyszcz and Magiera, 1998; Petrovský and Ellwood, 1999; Kapička et al., 2001; Maier and Scholger, 2004; Gautam et al., 2005; Spiteri et al., 2005) have shown the suitability and the benefits of magnetic susceptibility proxy screening towards detecting and spatially outlining anthropogenic heavy metal (HM) contamination in soils. Magnetic susceptibility (MS) measurement for applied magnetic pollution screening is commonly accepted, and is the first choice, as well as the most important parameter when conducting surveys. Advantages of MS are: non-destructive measurements, the potential to even measure traces of highly magnetic anthropogenic phases and rapid data acquisition. MS screening is a fast and cost-efficient tool for pre-screening campaigns towards better sampling site selection for conventional chemical analysis.

Nevertheless, there is almost always the problem of the natural MS background contribution to the measured signal. MS background signals depend strongly on the soil type, and can vary significantly as shown by Hanesch and Scholger (2005). Fialová et al. (2006) applied magnetic methods in soils to discriminate between anthropogenic and lithogenic contributions in different geological and environmental settings. Magiera et al. (2006) measured the vertical MS distribution in soil profiles to distinguish between lithogenic and anthropogenic contributions to topsoil MS values. On a regional scale they could separate seven different types of MS profiles from forest areas where the maximum MS values were mostly observed at

* Corresponding author. Fax: +49 7071 29 5842.
E-mail address: ulrich.blaha@uni-tuebingen.de (U. Blaha).

0269-7491/$ - see front matter © 2008 Elsevier Ltd. All rights reserved.
doi:10.1016/j.envpol.2008.02.013

depths of 3–4 cm. Their results additionally proved that soils which were affected by atmospherically deposited anthropogenic dusts were characterized by a magnetically enhanced humus layer, which also contained the highest HM concentrations.

Since environmental MS proxy screening is a scale dependent method, and can cover size ranges from individual fly ash spherules of <1 μm in diameter up to potential regional scale maps, it is important to evaluate different sampling scales. On the centimeter scale, where soil-forming factors such as lithology, climate, biota and topography are virtually constant, correlations between parameters show up more clearly (Göttlein and Stanjek, 1996). Moreover, as MS maps basically consist of data from individual sites, the focus of this study is on spatial variability of MS at "site scale" (a few m^2). Our strategy was the integration of vertical soil profile (soil core) sampling and MS data processing into an analysis procedure. The final goal was data quality improvement and method reliability to semi-quantify anthropogenic HM loads in contaminated natural soil.

The study focuses on the investigation of vertical and lateral MS distribution patterns in soil caused by natural and anthropogenic influences in areas of $\sim 10\ m^2$. As there are no such studies yet, we systematically analyzed spatial heterogeneity and physical properties of soil to reveal their impact on MS distribution. The entire suite of soil horizons was included in the analysis scheme. Efficient generation of MS data sets for spatial analysis was done with the rapid and standardized soil core sampling technique as used by Spiteri et al. (2005). Additionally, soil samples of $8.6\ cm^3$ were collected at high spatial resolution to study the impact of site-specific soil density distribution on magnetic particle migration and accumulation. Also, HM analysis was conducted on soil samples originating from high-resolution sampling (5 mm vertical spacing), which ensured that HM values could be clearly related to the distinct soil horizons.

Module combination of MS data, HM content and physical soil properties enabled us to semi-quantitatively assess anthropogenic HM content in soil. Investigations were carried out at two test sites close to a steel mill complex.

The proposed methodology is the principle approach towards the application of MS for semi-quantitative environmental magnetic soil pollution screening.

2. Sampling and data acquisition

2.1. Site specifications and sampling methodologies

The investigated sites are near the Donawitz steel mill, situated in Styria, Austria (Fig. 1a). The steel mill facilities are located west of Leoben (Fig. 1b), which lies on the bottom (550 m a.s.l.) of a V-shaped, NW–SE striking valley. The sampling sites of $\sim 10\ m^2$ in size, showing different degrees of airborne particulate matter deposition, are situated on the valley slope southwest of the pollution source. Both test sites are located in the same geological unit comprising Carboniferous shale and sandstone. The soil is undisturbed brown earth. According to the impact of airborne particulate matter, the site closer to the steel mill has been termed the "polluted" site (PS), while the more remote location is the "less polluted" site (LPS). The PS and LPS are located at a distance of ~ 1.5 km and ~ 3 km away from the steel mill, at altitudes of 775 m and 920 m, respectively (Fig. 1b,c). The relative

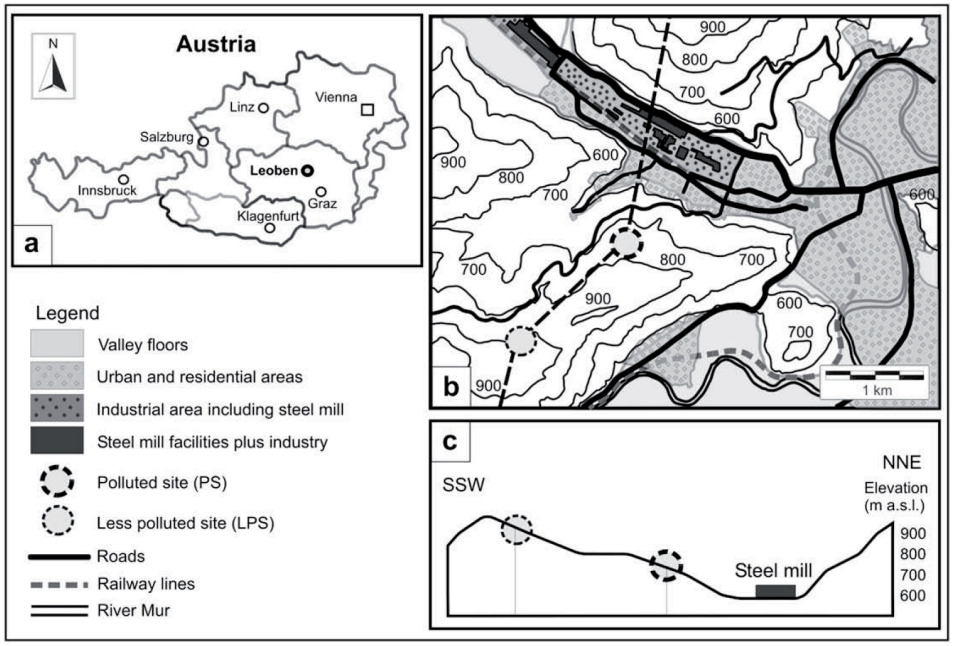

Fig. 1. (a) Map of Austria. (b) Leoben map with steel mill and test sites. (c) Valley cross section.

height differences above the pollution source were 225 m and 370 m. Surface MS test measurements for site selection using a Bartington MS2D system provide median values of 140×10^{-5} $[SI]_{(MS2D)}$ ($n = 1350$) for the PS and 37×10^{-5} $[SI]_{(MS2D)}$ ($n = 706$) for the LPS.

The slope at the sampling sites dips by $\sim 5^{\circ}$. Therefore, the soils were regarded as being little influenced by gravity-driven processes. Disturbances to the soil by natural processes such as fallen trees, rotten roots or human impact were not observed.

Sampling was carried out at three scale levels (mm to m) applying three different sampling techniques, comprising soil coring, collection of individual samples (8.6 cm^3) and sampling of soil layers 5 mm in thickness. The same sampling strategies were applied at both sites.

2.1.1. Soil core sampling

Soil sampling using a plastic casing-fitted corer provided cores of 3.3 cm in diameter. This fast and economic sampling method covered the dm to m range of the study.

Soil cores of up to 50 cm length were collected by vertically inserting the corer into the ground. Sampling depth was either limited by the length of the corer or hard objects such as stones or roots. Special care was taken to keep disturbances of the soil cores as small as possible, e.g., compression of the upper softer soil parts. According to the individual core lengths, casings were trimmed and closed to prevent any possible disturbances of the soil material during transport and storage.

A total of 26 and 30 soil cores were sampled at the LPS and PS, respectively. A coordinate system was defined (Fig. 2a,b) and sampling was carried out in the most systematic way possible. Limiting factors for regular sampling were adjoining trees and their roots. To avoid interfering effects of trees, a minimum distance of 1 m from the trunk was systematically maintained.

On average, the resulting sampling density is ~ 3 cores m^{-2} for the LPS and PS. It should be noted that such sampling patterns cannot be termed "homogeneously" distributed. Nevertheless, all samples originate from roughly equal sized areas, and it is accepted that practical sampling problems at forest sites can influence the geometric configuration of a set of samples.

2.1.2. Small-volume (8.6 cm^3) soil sampling

In situ collection of discrete 8.6 cm^3 samples was applied to cover the cm to dm scale range. Fresh samples were collected from the walls of newly dug pits. Seven and five individual vertical profiles with a lateral distance of 10 cm between them, respectively, were collected at the LPS and PS. Cylindrical plastic containers were horizontally inserted into cleaned soil profiles comprising all soil horizons (including the litter-layer L). For soil density analysis we ensured that all the containers were completely filled, and that no disturbance of the natural density occurred by excessively applied pressure when inserting containers into the soil section.

High vertical resolution was achieved by sampling of two adjacent rows of containers with a vertical offset of the second row measuring half a container in diameter, resulting in a zig-zag sampling scheme. Using this strategy, a vertical resolution of 1.27 cm (1/2 inch) was achieved revealing both continuous MS and soil density changes throughout the vertical soil profiles, as well as within the individual soil horizons. Maximum

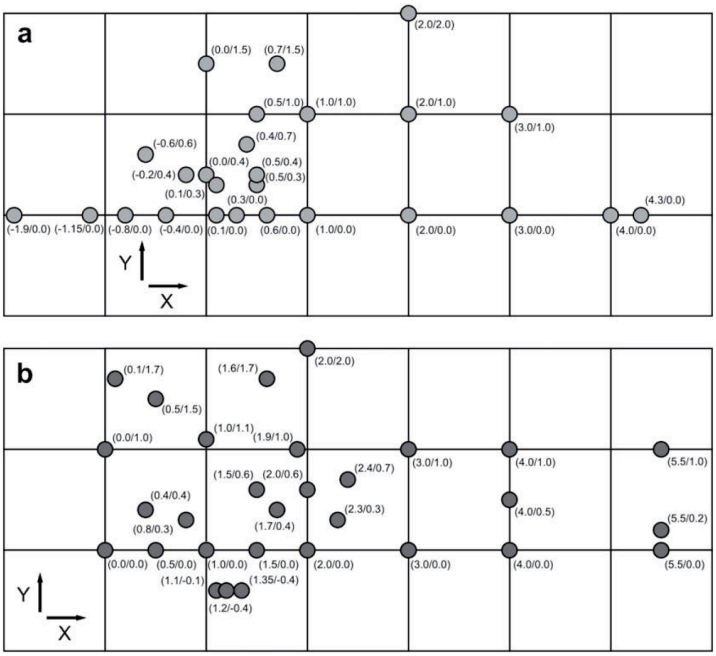

Fig. 2. Soil core sampling patterns at the LPS (a) and PS (b) with coordinates (X/Y) in m. Node distance is 1 m. Note: only squares containing two cores or more are counted towards the ~ 10 m^2 size specification.

sampling depth was 50 cm, and since the upper soil part was expected to bear most spatial variations, it was sampled at the higher resolution of 1.27 cm. The zone below 30 cm was covered with a single row resulting in a 2.54 cm vertical resolution.

2.1.3. High-resolution (5 mm) soil layer sampling

Layer sampling covered the vertical resolution of 5 mm in a lateral range of $\sim 20 \times 20$ cm, comprising all soil horizons. At both sites, one soil column of 40 cm vertical extent was collected. Columns were separated from the adjacent soil by trenches to avoid contamination with soil material from upper levels. Stainless steel tools were used for digging and slicing to prevent magnetic contamination. The 5 mm scale represents the highest vertical resolution and the samples were used for magnetic and HM analyses.

2.2. Data acquisition and analytical techniques

2.2.1. Magnetic analysis

All soil cores were systematically labeled and measured for volume-specific MS at 0.5 cm spacing in the laboratory. A Bartington MS2 susceptibility meter attached to a MS2C core sensor (diameter = 40 mm) was used, and measurements were carried out in the 10^{-5} [SI] range. Analysis was done shortly after sampling (within a few days), when the cores still had their natural moisture content.

Subsequently, the cores were air-dried until constant weight was reached; then some of them were re-measured to check for possible volume-specific MS changes. Comparison with the initially determined volume-specific MS values revealed no disparity between both measurements.

Also, the discrete samples collected in situ (8.6 cm^3) and the "sliced soil material" ($20 \times 20 \times 0.5$ cm volume) were air-dried until constant weight. The "sliced soil material" was stored in aluminium trays, and after drying, parts were put in plastic containers (also 8.6 cm^3) for MS measurement. Nearly all samples were free of stones and had grain sizes of <2 mm.

Low field MS measurement on both types of samples was conducted with an AGICO KLY-3 Kappabridge having a sensitivity of 3×10^{-8} [SI].

2.2.2. Non-magnetic analysis

For high-resolution soil density analysis, using the samples collected in situ (8.6 cm^3), the mass of moist and air-dried samples was determined using a laboratory balance with an accuracy of 10 mg.

HM analysis was performed on selected samples from "sliced soil material". The selection was done with respect to typical MS values from the peak and background areas of the vertical MS curves. Additionally, it was ensured that the samples were selected from the center parts of the individual soil horizons.

X-ray fluorescence (XRF) technique was used to conduct HM analysis. The air-dried soil material of <2 mm grain-size was ground with a ball mill in zircon-oxide mortars for 20 min. Eight grams of the powdered material was taken to prepare glass beads. The measurements were made with an X-LAB 2000 spectrometer fitted with a 400 W/54 kV palladium anode X-ray tube controlled by Spectro XLABPro software.

Bulk soil samples were separated into grain-size fractions by wet sieving. Parts of the fractions were suspended in acetone and the magnetic components extracted using a hand magnet. Scanning electron microscopy (SEM) analysis was done with a LEO 1450VP on carbon-sputtered samples. For this paper, magnetic particles from the grain-size fraction <63 μm were investigated.

3. Results and discussion

3.1. Small-scale soil density and MS distribution analysis

Small-scale soil density and MS analysis were conducted to better understand magnetic particle migration and accumulation processes in soil. Among others, soil density, controlled by porosity, is a determining factor for airborne particulate matter accumulation and the development of typical MS peaks in the upper soil zone.

Fig. 3a,b shows soil density and κ profiles at both sites. The data originated from 8.6 cm^3 samples collected in situ.

The "main contribution" to MS peaks in the soil sections is due to accumulation of industrially generated airborne magnetic particles. Infiltration into the soil either takes place through fallen tree needles covered with collected airborne particulate matter or direct settlement of dust particles onto the ground, with subsequent migration and preferential accumulation in the O- and Ah-horizons.

To visualize the "source" of anthropogenic MS in industrially polluted soils, we used scanning electron microscopy (SEM) images of typical magnetic spherules (Fig. 4a,b) extracted from the central peak area at the PS. Such spherules are typical for industrial emissions and have been shown in various publications (e.g., Hanesch et al., 2003; Kapička et al., 2003; Spiteri et al., 2005).

Magnetic spherules of grain sizes ranging from <1 μm up to several 10 μm in diameter were observed. Also a small number of larger spherules were present. The spherules revealed various surface structures ranging from smooth types to those with rough surfaces. These features are generated by the conditions of formation, for example, chemical composition, temperature or cooling time.

3.2. High-resolution soil profile analysis (5 mm) for MS and HM correlation

Bulk soil samples (grain size <2 mm) from layered samplings were analyzed for their HM contents. Homogenized soil volumes of $20 \times 20 \times 0.5$ cm were regarded as sufficiently large to average out lateral small-scale variations of MS and HM. However, since the focus of this study is on the optimization of MS processing schemes, rather than conducting extensive HM analysis, we have only shown data for Pb and Zn. The HM data presented in this section are intended to better visualize

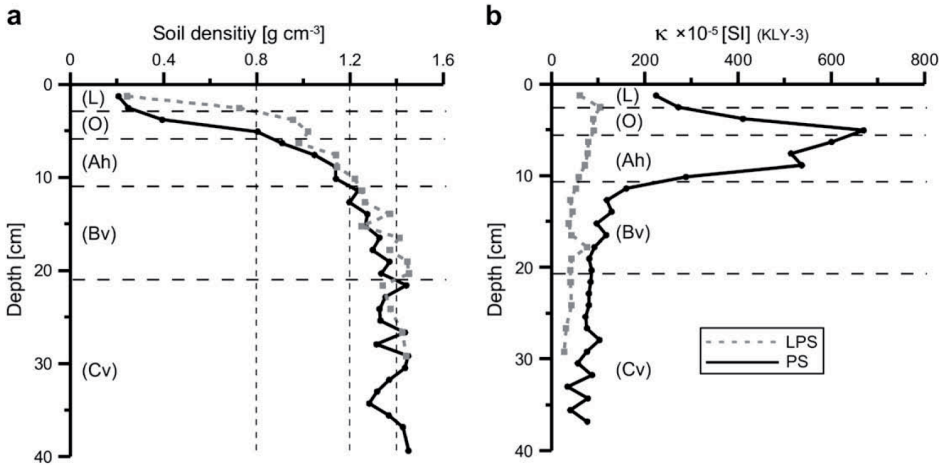

Fig. 3. Soil density (a) and volume-specific MS (b) profiles at both the LPS and PS. Median values of seven (LPS) and five (PS) individual profiles at 10 cm lateral spacing are shown. The soil surface is the top of the litter-layer and marked with zero. (Soil horizon boundaries may vary up to 1 cm; MS axes of diagrams are specified by the type of measuring equipment used).

the links between mass-specific MS (χ) and HM in a systematically analyzed soil profile (comprising all soil horizons).

Fig. 5a,c shows the vertical distribution of χ and HM contents at the LPS and PS, indicating clear enhancement of the parameters in the upper soil layers. The samples from the O- and Ah-horizons reveal the highest values and continuously decrease with increasing depth. The Bv-horizons still show some small enhancement compared to the lower Cv-horizons, but the values are significantly lower than the ones observed in the uppermost soil layers.

The relatively constant MS and HM values in the Cv-horizon are used as a measure of natural background values. Background MS originates from magnetic material of the parent rocks and magnetic minerals formed during pedogenesis. HM contents in the Cv-horizon also originate from the parent rocks. Therefore, background MS depends on site-specific, i.e., geogenic and partly soil type specific pedogenic contents; whereas background HM contents only depend on the geogenic source. MS and HM of anthropogenic origin we call anthropogenic MS and anthropogenic HM pollution.

Fig. 5b,d shows the correlation of χ and HM (Pb and Zn). At both sites, correlations between χ and HM are significant. At the LPS, the coefficients of determination are $R^2 = 0.97$ (χ and Pb) and 0.95 (χ and Zn). Similar values obtained for the PS, are $R^2 = 0.99$ (χ and Pb) and 0.98 (χ and Zn).

The decrease of MS and HM values with increasing depth and the coefficients of determination reflect the filtering or accumulation function of the upper soil parts for magnetic and HM loaded particulate matter. The close link between χ and HM (Pb and Zn) suggests the same origin, shared pathways and similar fate upon deposition of the highly magnetic phase and the HM. Additionally, the absolute values of both MS and HM in the upper soil parts reflect the airborne particulate matter input into the soil at the LPS and PS as a function of both the distance from and height above the steel mill.

Therefore, this high-resolution study provides important information about the vertical distribution of MS and HM in the soil profiles. This knowledge allows approaches to reliably distinguish between anthropogenic MS and HM and their geogenic background values.

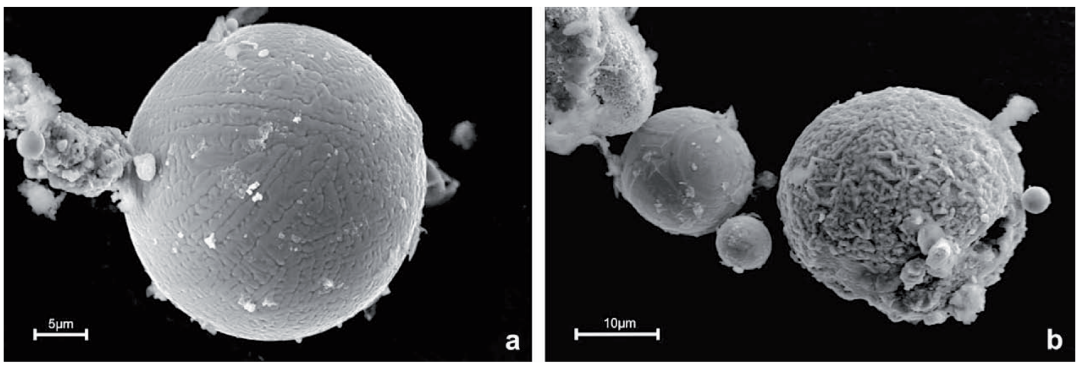

Fig. 4. a,b. Scanning electron microscopy images of typical anthropogenic magnetic spherules originating from the Ah-horizon at the PS.

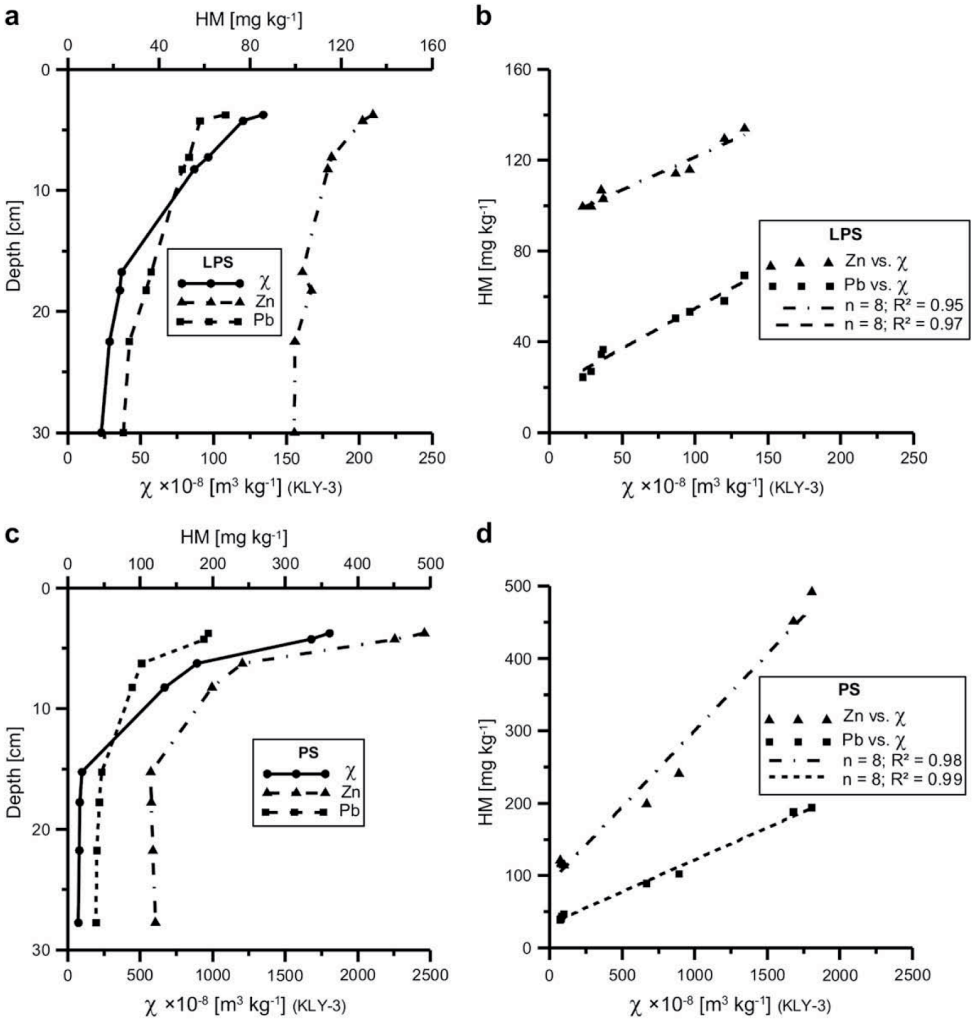

Fig. 5. Vertical distribution of χ, Pb- and Zn-concentrations at the LPS (a) and PS (c) (note the different scales for χ and HM) and correlation of Pb and Zn with χ on the basis of two samples from each soil horizon (O, Ah, Bv and Cv) (b, d).

3.3. Soil cores and numerical models for standardized vertical MS profile analysis

In order to streamline sampling and data processing for efficient semi-quantification of HM loads, standardized and easily applicable numerical analysis of vertical MS profiles is required. Typical features in contaminated natural soils are spatially variable MS values in the upper ''polluted'' horizons, whereas the lower zone represents constant background MS values (Fig. 6a,b). These features are utilized in a standardized numerical model for the separation of ''polluted'' and ''unpolluted'' soil zones by analyzing a sufficiently large number of vertical MS profiles. The numerical result is the boundary depth (BD) representative of a ''site scale'' area, which provides the lower limit of the ''polluted'' soil zone. Knowledge of both the vertical boundary of the ''polluted'' part and an established correlation as shown in Section 3.2, enables one to calculate the anthropogenically enhanced MS and the determination of the corresponding HM loads.

3.3.1. Soil core end MS data correction

MS2C sensor readings are comparable when the whole measuring volume of the sensor is filled with core material. This is not the case at the core ends. There, the system provides raw data which must be corrected before further data processing. Following the fact that at the core end the measuring volume of the sensor is only half-filled with material, the MS reading is 50% compared to that of the completely filled measuring volume. This implies that the first reading at the core end ($l = 0$ cm) has to be multiplied by two to obtain the ''true'' MS. For calibration of the end section, a calibration core has been measured at steps of 5 mm. With the obtained percentage values, the correction factors have been determined and are listed in Table 1.

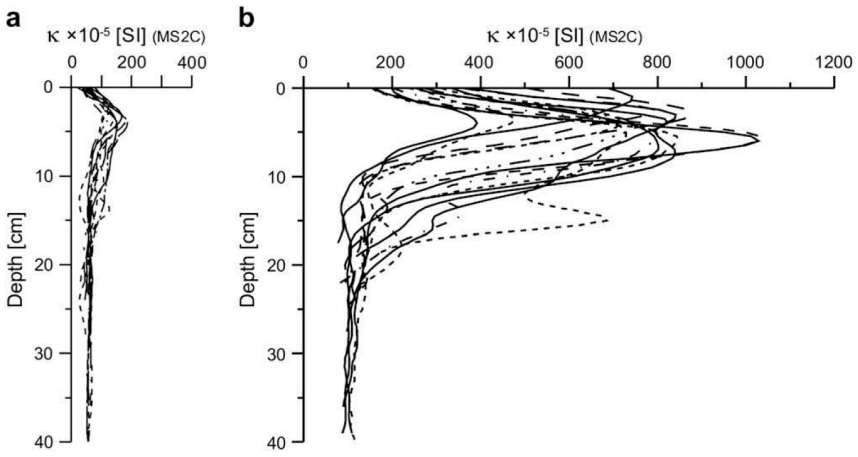

Fig. 6. Selected MS2C curves (corrected data) at the LPS (a) and PS (b) representing the spatial MS variations in soil at ''site scale''.

We are aware that core end correction in a ''layered'' core produces systematic errors. Since the layering is most evident in the upper level of the core, this is consequentially the zone with the ''largest error''. Nevertheless, for practical application we think it is acceptable to correct the ''core end measurement error'' by applying the correction factors as shown in Table 1.

3.3.2. Separation of ''polluted'' and ''unpolluted'' soil layers by MS boundary depth determination

MS curve sets from both the LPS and PS (Fig. 6a,b) show the variability of MS in soil at ''site scale''. The variability within a few m^2 depends on soil type, soil development, varying soil horizon thickness as well as possible disturbances. Also the amount of anthropogenically enhanced magnetic dust input through the air-path has a significant influence on the development of the magnetic signal and superposes with the specific soil properties. The density of soil layers as well as cracks, root channels, biological activities and direct disturbances on the soil surface determine the properties of the upper layers.

High MS variability among the individual soil cores does not allow direct or straightforward curve evaluation for pollution assessment at ''site scale'', even when it is known that any individual MS curve represents a specific HM load as shown by Spiteri et al. (2005). Instead, a statistical approach with a sufficient number of individual MS curves is required.

Median (Q2) curves of the original MS curve sets of 26 and 30 soil cores, respectively, were determined (Fig. 7a,b). The MS values of the median curves are calculated from data gathered from the same depth levels at both the LPS and PS. The vertical spacing measured 5 mm.

Median curves are considered as ''master curves'' (MC) of the investigated ''site scale'' areas, systematically simplifying the various individual curves. Additional standard parameters such as inter-quartile range (IQR) or min-max-values can be used to demonstrate the lateral variability of the MS curve sets. These standard parameters can therefore, be regarded as quality assessment factors.

Moreover, such additional parameters have the potential to differentiate individual curve parts as they reflect specific properties of layered soils and the impact of magnetic particulate matter. Typically, this is expressed in lateral soil samples, by strongly varied MS values in the upper, ''polluted'' soil zone, resulting in large IQR-values. In the lower curve part the IQR-values are small. Analysis of these values can help to distinguish between the ''polluted'' and ''unpolluted'' zones, resulting in the introduction of a boundary depth (BD).

Our approach to determining the BD is based on the statistical parameters, median (Q2), inter-quartile range (IQR) and IQR/Q2, which have been normalized for easy evaluation (Fig. 8a,b).

The normalized master curve in Fig. 8a,b shows the representative vertical MS distribution with continuous transition from the ''polluted'' to the ''unpolluted'' zone. Definition of the BD requires information provided by the IQR-curve. As an additional parameter for confirmation the IQR/Q2-curve is employed. The significant gradient changes and the sharp bend of the IQR and IQR/Q2-curves after the steady decrease in the upper curve section indicate the BD, which separates the ''polluted'' and ''unpolluted'' soil zones.

Table 1
Correction factors for core end MS correction based on the MS2C sensor characteristics (diameter = 40 mm) determined on a magnetically homogeneous core

Length (mm)	% MS signal	Correction factor
(Core end) 0	0.50	2.00
5	0.67	1.48
10	0.81	1.23
15	0.91	1.10
20	0.96	1.04
25	0.99	1.01
30	1.00	1.00

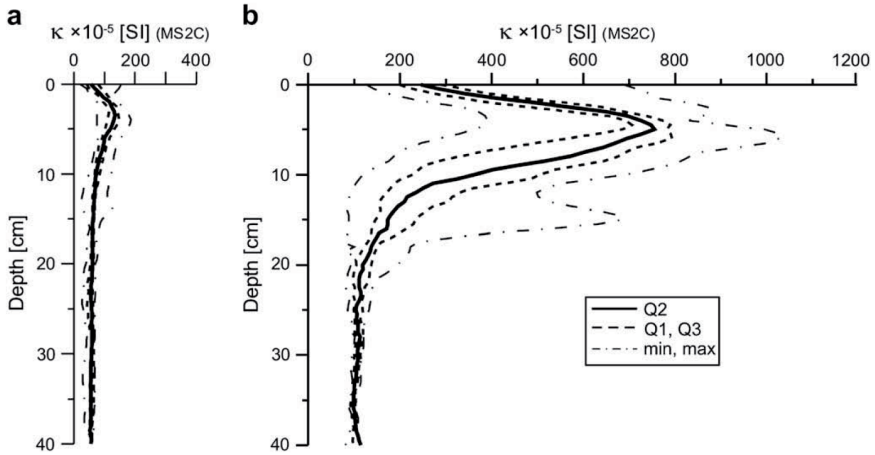

Fig. 7. MS2C median (Q2), 1st quartile (Q1), 3rd quartile (Q3) and min- and max-value curves of the 26 and 30 soil cores from the LPS (a) and PS (b), respectively, are shown.

The minimum values represent the lower limit (BD) of larger IQR and IQR/Q2-values and low gradients both expressing the heterogeneity of MS in the "polluted" zone with respect to magnetic particulate matter accumulation. In principle, the IQR-curve would be sufficient to separate both zones, but as MS values might also fluctuate more in some cases than in others it is useful to introduce an additional ratio that depends on one more parameter.

Moreover, the additional IQR/Q2-curve allows for much easier graphic determination of the transition point, respectively the BD, by parallelizing both minima.

Gradients and fluctuations in the lower curve section mainly reflect natural MS background variations, which might be superposed by the contribution of single curves with higher variations closer to the BD. Nevertheless, being able to numerically determine the BD at "site scale" with a standardized procedure, allows for the neglect of such minor variations. Moreover, depth uncertainties of probably <1 cm in soils which are complex, "heterogeneous" natural structures can be accepted as sufficiently accurate regarding this new methodological approach.

At the LPS (PS) the BD was found to be at 16 cm (18 cm), which has been used for further MS curve assessment.

3.3.3. Principles of pollution MS peak integration and MS data processing

Pollution MS analysis using vertical soil profiles is based on two typical characteristics of the MS curves. Firstly, the natural background MS measured below the BD, which we termed vertical background (VBG) and secondly, the anthropogenically enhanced pollution MS represented by the peak area. Principally, natural background MS is regarded as the site-specific background MS which depends on the soil type and on the geologic background. This background MS is "superposed" by the pollution MS signal that has to be appropriately separated.

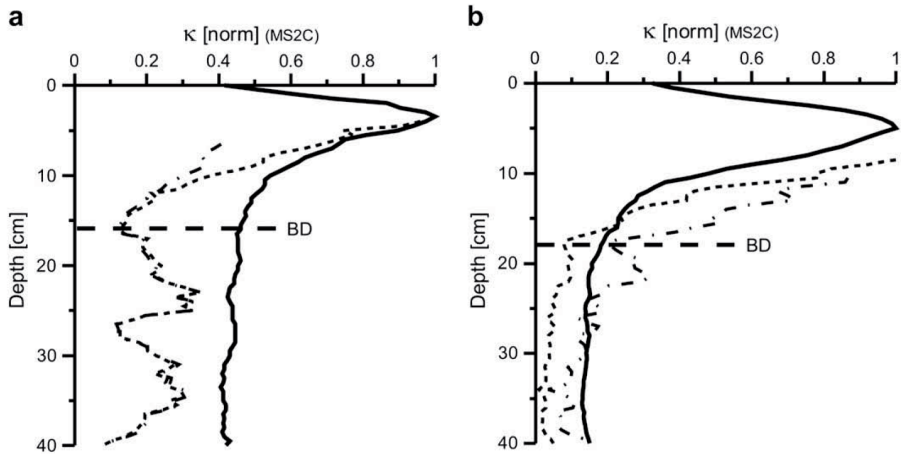

Fig. 8. Normalized MS median curve ("master curve", full line), inter-quartile range (IQR, dashed line) and IQR/Q2 (dot and dash line) of the "less polluted" site (a) and the "polluted" site (b) are shown. All soil cores, in (a) $n = 26$ and (b) $n = 30$ are included. The horizontal line marks the boundary depth.

In the following we present a methodology for separating the natural and anthropogenic MS contribution in soil for practical application. To achieve this goal, the individual areas of a MS curve have to be defined and integrated into an appropriate processing scheme. In this context, the already introduced site-specific BD determined from a sufficiently large number of individual MS profiles (Fig. 8a,b) plays a major role.

In Fig. 9 four characteristic areas are introduced; the MS peak area (1), the VBG area (2), and a mixed part consisting of areas (3) and (4).

Area (1) exclusively represents anthropogenic MS (''pollution''), whereas the area below the BD (2) depicts the site-specific VBG MS. The triangular shaped areas (3) and (4) represent a simplified model taking into consideration soil genetic factors, i.e., horizon dependent MS distribution of the upper soil section. According to its contribution, area (1) is called pollution peak area (PPA), and area (3) pollution correction triangle (PCT). Area (4), reflecting the natural background above the BD, is termed lateral background (LBG).

The double-triangle model is regarded as sufficiently accurate for an approximation of the origin of MS and is suitable for further processing. This approach is based on the assumption of a ''linear relationship'' between anthropogenic and natural MS in the upper soil zone. The mean background contribution above the determined BD is lower than that below the BD. In the L- and O-horizons only anthropogenic magnetic particulate matter is accumulated, whereas in the Ah- and Bv-horizons a mixture of anthropogenic and natural magnetic particles occurs. Therefore, an increased contribution of background MS is assumed in the lower Bv-horizon (approaching the background value at the BD), ''compensating'' for the contribution of the pure anthropogenic MS in the L- and O-horizons.

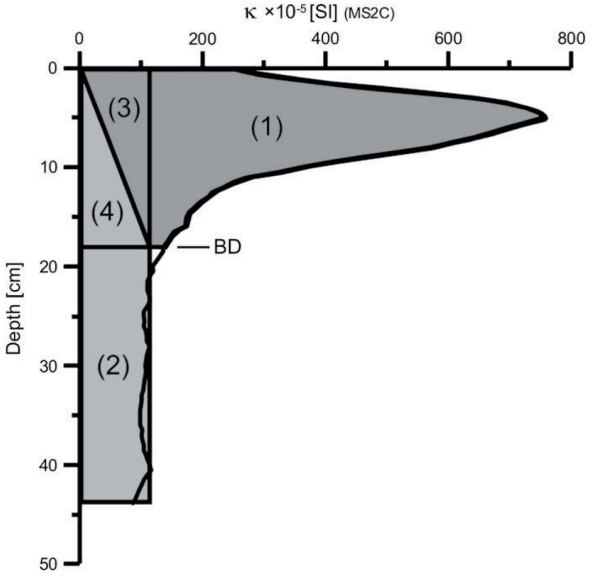

Fig. 9. Subdivision of the MS curve into a pollution related part (areas 1 and 3) and natural background (areas 2 and 4). See text for further explanation.

For practical use, the simple triangular shape is ideal. The area of the LBG-triangle can be directly determined from the mean MS in the VBG area, and easily transformed into a rectangle with the same area at half the base of the triangle.

Summarizing, areas (2) (VBG) and (4) (LBG), are genetically of natural origin, while areas (1) (PPA) and (3) (PCT) are of anthropogenic nature. As anthropogenic MS co-exists with anthropogenic HM loads, MS curve data have to be divided into the anthropogenic and natural parts before establishing linkage of both anthropogenic MS and HM.

Simplifications, considering basic geometric relationships, result in a model to semi-quantify anthropogenic HM loads. Detailed steps of HM analysis and linkage of MS data to HM contents for ''site scale'' assessment are presented in Section 3.3.4.

Based on the newly introduced parameters, i.e., master curve (MC), boundary depth (BD), pollution peak area (PPA), vertical background (VBG), pollution correction triangle (PCT), and lateral background (LBG), the necessary steps for an optimized and standardized MS data processing scheme towards anthropogenic HM load determination are made. The processing scheme tests for Pb using the curve sets and selected individual curves from the LPS and PS.

The MS master curve (Fig. 9) is the central element for further analysis since it quantitatively represents the ''polluted'' and the ''unpolluted'' layers based on the individual MS curve set at ''site scale''. In order to minimize analytical problems due to complex individual and variable vertical MS curves, the introduction of MS block curves (Fig. 10b), i.e., a two-layer model, is the consequential step. The BD marks the lower limit of enhanced anthropogenic MS for successive data processing, being the depth marker to determine the arithmetic mean of MS for the ''polluted'' and ''unpolluted'' parts, respectively above and below the BD. The boundary, in reality a narrow fuzzy zone, depends on the enrichment of anthropogenic magnetic particles and the comparatively porous structure of the upper soil horizons, i.e., on the heterogeneous internal structure and varying thickness of the upper soil layers. Due to the simplicity of the MS block master curve, each of the individual MS curves can easily be connected to this condensed, yet central curve, still keeping all crucial information. This procedure allows, for the first time, both systematic and numerical MS curve analysis that is practically independent of the soil type and soil development. Therefore, vertical MS distribution directly reflects the magnetic particulate matter input depending on the soil properties without placing emphasis on them.

The analytical steps of our approach are shown in Fig. 10a–c. We utilize the MS master curve (MC), a suitable individual curve (IC) and the BD to calculate the pure anthropogenic MS in a standardized, time-saving and practically applicable way.

In order to simplify both the MC and IC (Fig. 10a) we introduce the block curves (BMC and BIC, Fig. 10b), which fit the two-layer model. Block curves show the arithmetic mean of MS above and below the BD. To obtain the best results from IC processing and subsequent HM analysis, an IC shape which comes close to that of the MC, as well as

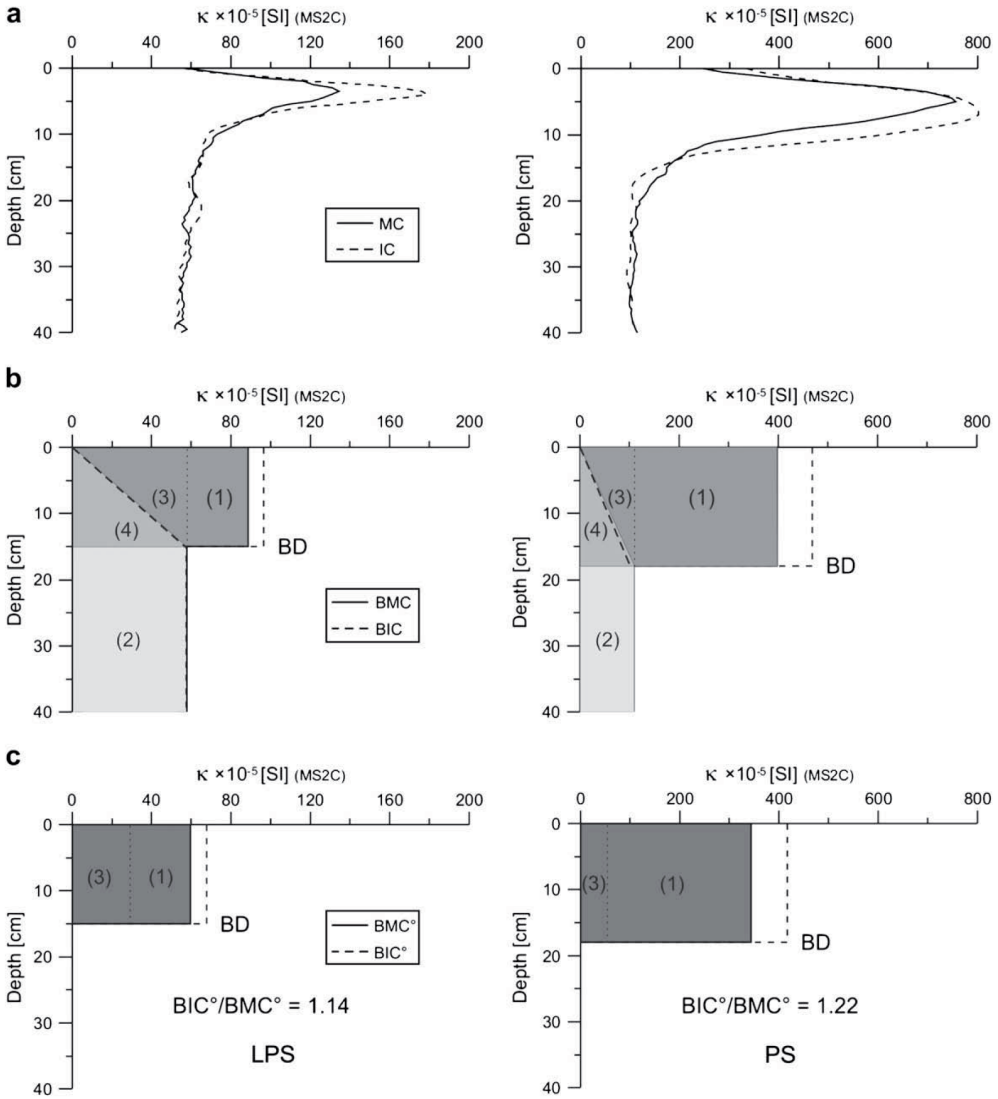

Fig. 10. (a) Master curves (MC, full line) and selected individual curves (IC, dashed line). (b) Block master curves (BMC) and block individual curves (BIC) representing a two-layer model; note that shaded areas belong to the BMC; for the BIC, only the curve shape is presented (dashed lines). (c) BMC and BIC have been corrected for background MS (as described in Fig. 9) representing the anthropogenic MS contribution.

a BIC°/BMC°-ratio of >1 (Fig. 10c) are most suitable to minimize analytical errors. BIC° and BMC° are the curves exclusively representing the anthropogenic MS.

Staying with this concept, the BMC is the statistically representative reference curve, containing all spatial information of the investigated area, respectively from all the individual MS curves. In contrast, the BIC contains only the information from a selected individual curve.

In Fig. 10b, both MS block curves show the according size of the areas (1–4). The principle is the same for both, only the size of the areas is different. This systematic curve analysis makes it possible to correct both curve types for the natural background MS, resulting in block curves BMC° and BIC° (Fig. 10c). Finally, determination of the BIC°/BMC° ratio links the statistically representative MS values (BMC°) to the MS from BIC. In the cases presented, the MS value of the BIC° is 14% (22%) higher than BMC° (BIC°/BMC° = 1.14 (1.22)).

3.3.4. Principles and results of anthropogenic HM semi-quantification

Fast and cost-efficient MS measurements provide the basis for minimizing the number of HM analyses required for "site scale" assessment. In this context, it is necessary to efficiently include HM data of only one soil core into the MS data processing scheme. The selected individual soil core is separated into two sub-samples at the BD, providing mean HM data of

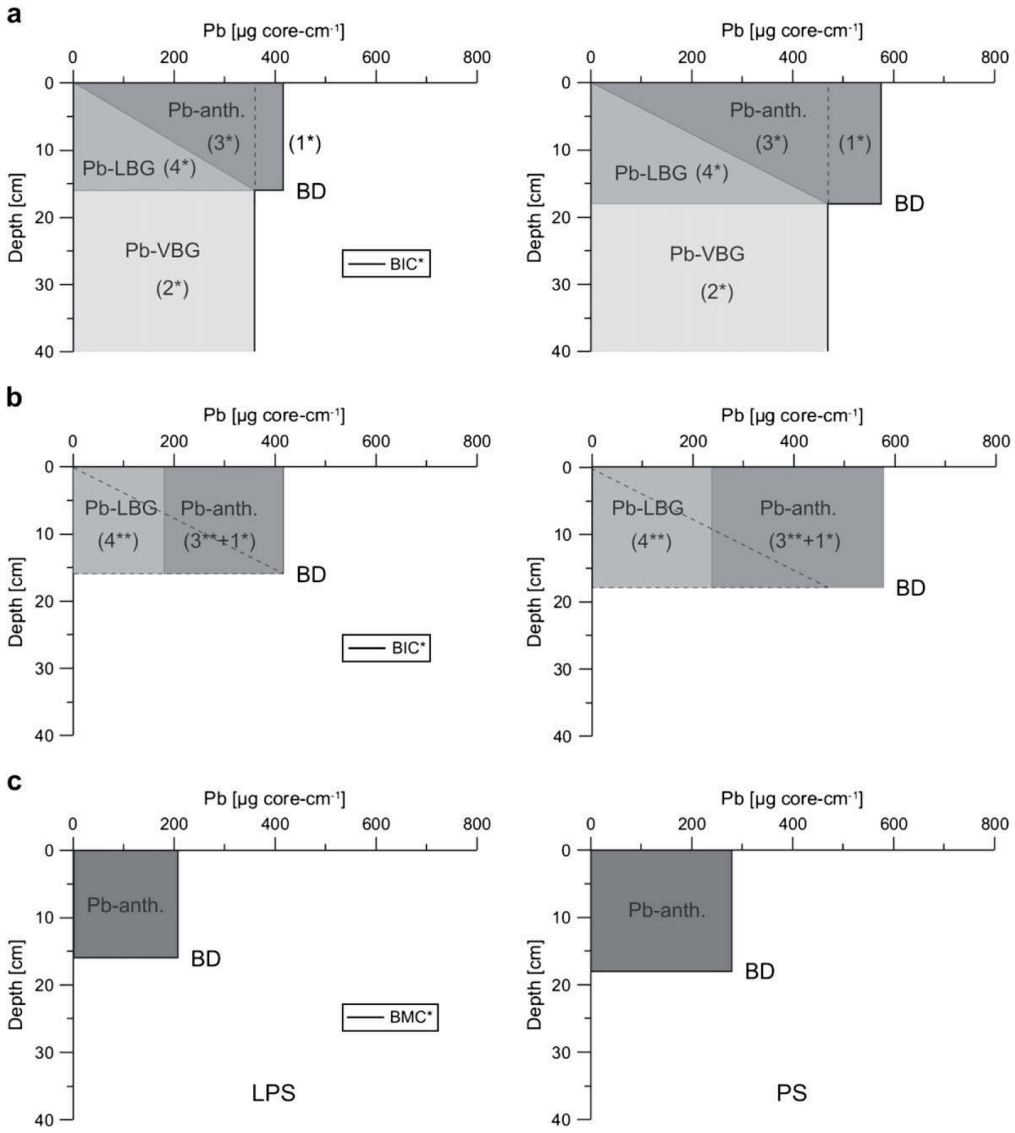

Fig. 11. (a) The four characteristic areas (1*, 2*, 3* and 4*) representing the according Pb-content. (b) The pollution correction triangle (PCT*, 3*) and the lateral background triangle (LBG*, 4*) of (a) are transformed into the rectangles (3**) and (4**) of the same size. Areas (3** + 1*) represent the average anthropogenic Pb-load of the individual core. In (c) the anthropogenic Pb-contents are presented as final result after correction using $BIC^{\circ}/BMC^{\circ} = 1.14$ (LPS) and 1.22 (PS).

both the "polluted" as well as of the "unpolluted" soil parts. These HM data fit into the introduced MS data processing scheme and can be efficiently processed similarly to MS.

In Fig. 11a the four characteristic areas introduced for MS analysis are presented for HM semi-quantification, in this case determining the levels of Pb present. The important aspect as defined by the approach is using the BD and consequentially the "polluted" and "unpolluted" soil areas. HM separation uses in principle the same steps applied to MS. Fig. 11b shows the transformation of the LBG* triangle (4*) into the LBG* rectangle (4**) and the resulting anthropogenic HM content (3** + 1*) for the individual core. At this point, the results from both MS curve and HM data processing are merged by applying the correction factor $BIC^{\circ}/BMC^{\circ} = 1.14$ (1.22) (Fig. 11c). This step transfers the anthropogenic HM content of the individual core to the statistically determined median value (block master curve), which is representative of the "site scale" area. Results for Zn are 281 µg core-cm^{-1} for the LPS and 517 µg core-cm^{-1} for the PS.

Usually, there are also HM elements in the analyzed vertical soil profiles, which do not show correlation with MS (Blaha, unpublished data). This will be revealed by our HM

data processing when the resulting area (3** + 1*; Fig. 11b) is approximately zero. Such HM elements might be of natural origin.

In Fig. 11c the shaded areas represent the total anthropogenic HM content above the BD for the "site scale" areas. The unit given as μg core-cm^{-1} can be converted into μg cm^{-3} by dividing this value through the cross section area of the cylindrical core or, alternatively, into mg kg^{-1} by further dividing by the mean density (g cm^{-3}) of the soil layer above the BD.

4. Conclusions

The influence of soil density, controlled by porosity on the accumulation of airborne anthropogenic magnetic particulate matter in the upper soil horizons is revealed by high resolution analysis of vertical soil sections. Differentiation between the upper, "polluted" zone and the lower natural or background zone is possible with a sufficiently large set of MS curves, systematically revealing spatial distribution of MS. Statistical analysis of the higher, variable MS peak values in the upper zone and lower, but constant MS values in the background area is the basis for separation. Implementation of the MS master curve is a central element, containing condensed site-specific information that can be easily processed. The statistically determined boundary depth is a universally applicable parameter in "polluted" natural soil. On the basis of the two-layer model ("polluted" and background zone) complex MS curves are reduced to easily processable MS block curves, still containing all important site-specific information. MS block master curve processing systematically integrates the two-layer model into the analysis scheme, providing "site scale" representative MS values of the anthropogenic magnetic particle input or "pollution" MS. Transformation of one selected, individual MS curve into an individual block curve, enables application of the block master curve processing scheme, and the easy linkage of the individual curve to the "site scale" representative result from MS block master curve analysis. The MS processing model provides the framework to reduce HM analysis into only two sub-samples from the individual core (one from the "polluted" zone, and one from the natural background). Determination of the anthropogenic HM content from the "site scale" area is based on the same principles as MS processing. Only, instead of handling MS, HM data are calculated with the block curve model. Processed HM values from the individual core (anthropogenic HM contents) are connected back to the "site scale" by a site-specific correlation factor determined from MS analysis. The result is the HM load representative for the "site scale" area.

The presented model transfers most of the required data acquisition and processing procedures to fast and economically applicable MS, reducing costly HM analysis to a minimum. Therefore, this methodological approach is an appropriate tool for practical application.

It should be noted that we are applying magnetic proxy screening to outline and semi-quantify anthropogenic HM pollution in soil with emphasis on quick measurements and the most accurate procedures possible. This consequentially means that we accept minor uncertainties resulting from simplifications made when introducing our new approach. Considering the fact that there is currently no comparatively efficient process of MS pollution screening in soil, this approach is an important step towards improving magnetic proxy methods for practical pollution assessment. Further optimization will be the next step of our work. This will include adaptation to other soil types and evaluating the applicability and accuracy of the method through more detailed analysis of the spatial variation of MS and HM data.

Acknowledgements

The authors gratefully acknowledge the fieldwork support of Prof. Dr R. Scholger and Dr G. Maier (University of Leoben). We thank Moti Lal Rijal and Valentina Soares da Cruz for their help in sampling, sample preparation and measurements. This research has been funded by DFG (AP 34/21-1,2).

References

Fialová, H., Maier, G., Petrovský, E., Kapička, A., Boyko, T., Scholger, R., Magprox team, 2006. Magnetic properties of soils from sites with different geological and environmental settings. Journal of Applied Geophysics 59, 273–283.

Gautam, P., Blaha, U., Appel, E., 2005. Integration of magnetism and heavy metal chemistry of soils to quantify the environmental pollution in Kathmandu, Nepal. The Island Arc 14, 424–435.

Göttlein, A., Stanjek, H., 1996. Micro-scale variation of solid-phase properties and soil solution chemistry in a forest podzol and its relation to soil horizons. European Journal of Soil Science 47, 627–636.

Hanesch, M., Scholger, R., Rey, D., 2003. Mapping dust distribution around an industrial site by measuring parameters of tree leaves. Atmospheric Environment 37, 5125–5133.

Hanesch, M., Scholger, R., 2005. The influence of soil type on the magnetic susceptibility measured throughout soil profiles. Geophysical Journal International 161, 50–56.

Kapička, A., Petrovský, E., Jordanova, N., Podrázský, V., 2001. Magnetic parameters of forest top soils in Krkonose Mountains, Czech Republic. Physics and Chemistry of the Earth 26 (11–12), 917–922.

Kapička, A., Jordanova, N., Petrovský, E., Podrázský, V., 2003. Magnetic study of weakly contaminated forest soils. Water, Air, & Soil Pollution 148, 31–44.

Magiera, T., Strzyszcz, Z., Kapička, A., Petrovský, E., Magprox team, 2006. Discrimination of lithogenic and anthropogenic influences on topsoil magnetic susceptibility in Central Europe. Geoderma 130, 299–311.

Maier, G., Scholger, R., 2004. Demonstration of connection between pollutant dispersal and atmospheric boundary layers by use of magnetic susceptibility mapping, St. Jacob (Austria). Physics and Chemistry of the Earth 29, 997–1009.

Petrovský, E., Ellwood, B.B., 1999. Magnetic monitoring of air-, land- and water-pollution. In: Maher, B., Thompson, R. (Eds.), Quaternary Climates, Environments and Magnetism. Cambridge University Press, pp. 279–322.

Spiteri, C., Kalinski, V., Rösler, W., Hoffmann, V., Appel, E., Magprox team, 2005. Magnetic screening of a pollution hotspot in the Lausitz area, Eastern Germany: correlation analysis between magnetic proxies and heavy metal contamination in soils. Environmental Geology 49, 1–9.

Strzyszcz, Z., Magiera, T., 1998. Magnetic susceptibility and heavy metal contamination in soils of southern Poland. Physics and Chemistry of the Earth 23 (9–10), 1127–1131.

2

Micro-scale grain-size analysis and magnetic properties of coal-fired power plant fly ash and its relevance for environmental magnetic pollution studies

Atmospheric Environment 42 (2008) 8359–8370

Contents lists available at ScienceDirect

Atmospheric Environment

journal homepage: www.elsevier.com/locate/atmosenv

Review

Micro-scale grain-size analysis and magnetic properties of coal-fired power plant fly ash and its relevance for environmental magnetic pollution studies

U. Blaha [a,*], B. Sapkota [a], E. Appel [a], H. Stanjek [b], W. Rösler [a]

[a] Institute for Geoscience, University of Tübingen, 72076 Tübingen, Germany
[b] Clay and Interface Mineralogy, RWTH Aachen, 52062 Aachen, Germany

ARTICLE INFO

Article history:
Received 25 March 2008
Received in revised form 31 July 2008
Accepted 31 July 2008

Keywords:
Magnetic susceptibility
Fly ash
Coal-fired power plant
Magnetic spherules
Grain-size
Environmental pollution

ABSTRACT

Two fly ash samples from a black coal-fired power plant (Bexbach, Germany) were investigated for their magnetic properties, particle structure, grain-size distribution and chemical composition. Grain-size distribution was determined on bulk samples and on magnetic extracts. Magnetic susceptibility of different grain-size fractions was analyzed with respect to the according amount of fractions. High- and low-temperature dependence of magnetic susceptibility and thermal demagnetization of IRM identified magnetite and hematite as magnetic phases. Magnetic spherules were quantitatively extracted from bulk fly ash samples and examined using SEM/EDX analysis. Particle morphology and grain-size analysis on the magnetically extracted material were studied. Individual spherule types were identified and internal structures of selected polished particles were investigated by SEM and EDX analyses. Main element contents of the internal structures which consist of "magnetite" crystals and "glassy" matrix were systematically determined and statistically assessed. The chemical data of the micro-scale structures in the magnetic spherules were compared with XRF data from bulk material, revealing the relative element distribution in composed magnetic spherules. Comparison of the bulk sample grain-size (0.5–300 μm) and grain-size spectra from magnetic extracts (1–186.5 μm) shows that strongly magnetic particles mainly occur in the fine fractions of <63 μm.
This study comprises a comprehensive characterization of coal-fired power plant fly ash, using magnetic, chemical, and microscopic methods. The results can serve as reference data for a variety of environmental magnetic studies.

1. Introduction

Anthropogenic air, soil and water pollution caused by fly ash from coal-fired power plants can be a significant environmental problem. Fly ashes can be either harmful to human health because of their small sized particles or by carrying pollutants such as heavy metals (HM) or polycyclic aromatic hydrocarbons (PAH). Modern filtering technologies preventing the environment from serious hazards are not yet standard in all power plants. Increased environmental pollution caused by fly ash and various other pollutants is a typical problem in newly industrializing countries with fast growing economies e.g., China or India. For example, the Panki power plant in Kanpur, India, uses 3000 tons of coal and churns out 40 tons of fly ash every day. Five super thermal power plants in the Singrauli area supply 10% of India's power. These power plants release about six million tons of fly ash a year, making land unfit for cultivation (www.blacksmithinstitute.org). Sharma and Tripathi (2007) conducted environmental magnetic studies around one of the power plants in the Singrauli area. They

* Corresponding author. Fax: +49 7071 29 5842.
E-mail address: ulrich.blaha@uni-tuebingen.de (U. Blaha).

1352-2310/$ – see front matter © 2008 Published by Elsevier Ltd.
doi:10.1016/j.atmosenv.2008.07.051

showed that fly ash contributes significantly to soil pollution in the vicinity of the plant.

Large amounts of fly ash produced in coal-fired power plants can create severe environmental threats. Malfunction, operating errors, or even missing filtering systems lead directly to air and subsequently to soil, sediment and water pollution. Inappropriate deposition and disposal of collected fly ash bears the risk of direct soil contamination and dissemination of fly ash particles to the environment by resuspension in air or water.

Comprehensive target-oriented approaches, combining magnetic, physical, and chemical properties of filter fly ash could help to address current environmental problems concerning fly ash production and disposal.

Until a few decades ago, environmental protection standards in many industrialized countries all over the world have been still comparatively low. Technologies for efficient flue gas purification of coal-fired power plants have been developed and improved since then. Therefore, quite a number of areas with polluted soils and sediments can be found also in industrialized countries, nowadays having established efficiently working flue gas purification systems in their facilities.

In particular, soil pollution is caused by atmospherically transported and distributed particulate matter. Thus, soils are sinks or accumulators for any kind of atmospherically deposited pollutants. Rose et al. (1999) studied the spatial and temporal distribution of spheroidal carbonaceous fly ash particles in sediments of European mountain lakes, demonstrating that virtually any environment is affected by airborne particulate matter distribution. Environmental magnetic pollution studies on soils affected by coal-fired power plants and other pollution sources were conducted by e.g., Strzyszcz et al. (1996), Hay et al. (1997), Kapicka et al. (1999), Veneva et al. (2004), Spiteri et al. (2005) and Magiera et al. (2006). For semi-quantitative magnetic pollution screening in soils as introduced by Blaha et al. (in press) information on particulate matter is helpful, since particle sizes determine specific accumulation patterns. Moreover, grain-size specific magnetic properties e.g., different contents of magnetic phases and consequentially different MS impact on the results of magnetic soil pollution screening. Fly ash collected from the source can serve as reference material for anthropogenic particulate matter.

Different key aspects such as chemical, morphological and magnetic properties of fly ash and its components have been investigated by a number of studies. Magnetic properties of fly ash, respectively, fly ash particles, were studied by e.g., Chaddha and Seehra (1983), Strzyszcz et al. (1996), Veneva et al. (2004) and Jordanova et al. (2006). Kapicka et al. (2000) investigated the magnetic stability of fly ash in different soil solutions. Fisher et al. (1978) worked on physical and morphological properties of size-classified coal fly ash. Hansen et al. (1981) and Del Monte and Sabbioni (1984) conducted morphological and mineralogical studies on fly ash from coal-fired power plants. More recently, surface properties of various fly ashes were characterized by Sarbak et al. (2004).

Spherules, magnetically extracted from pollution sinks such as soils, were studied by Kapicka et al. (2003) and Spiteri et al. (2005). Fly ash properties differ depending on the chemical composition of the fired coal types, power plant technologies and other factors (see e.g., Jordanova et al., 2006).

Our work comprises the investigation of fly ash samples from a two-stage electrostatic precipitator system of a black coal-fired power plant in Bexbach, Saarland, Germany. The focus is set on an integrated approach comprising magnetic properties, chemical composition, grain-size analysis, morphological features and typical structures of magnetic particles and their relative distribution in fly ash. As magnetic spherules from combustion processes can be found in nearly any pollution sink, e.g., Gautam et al. (2004, 2005), Hanesch et al. (2003), Maier and Scholger (2004) and Urbat et al. (2004), more information on fly ash particles in common will be helpful towards improving magnetic screening and assessment methods.

This study on fly ash and its magnetic fractions tries to interlink the benefits of various analytical methods towards a more comprehensive understanding of pollution particles and their properties.

2. Materials and methods

2.1. Sample material

The investigated fly ash samples originate from the two-stage filter system of a black coal-fired power plant in Bexbach, Germany. A two-stage electrostatic precipitator system is used to extract fly ash particles from flue gas. The filter system collects 99.8% of the fly ash particles generated through combustion of fossil fuel (www.steag-saarenergie.de). The two precipitation steps are termed "Vorreinigung" (1st flue gas purification step) and "Nachreinigumg" (2nd flue gas purification step), accordingly the samples were named BexV and BexN. In order to avoid misunderstandings when handling fractions and extracts from the samples, the bulk samples were further specified terming them BexV_bu and BexN_bu.

2.2. Sample preparation

2.2.1. Sieve analysis

Sieve analysis was carried out on BexV_bu and BexN_bu samples using stainless steel sieves of 63 μm, 125 μm and 200 μm mesh size. One kilogram of dry fly ash from each filtering step was analyzed in eight portions of 125 g employing a sieving machine. Each analysis was performed at a sieving time of 20 min. The material loss during sieving and handling was determined with 0.51% and 0.45% for BexV_bu and BexN_bu, respectively. For mass determination a laboratory balance with an accuracy of 10 mg was used.

2.2.2. Magnetic extraction

The magnetic extracts from bulk samples were prepared from the dry state in order to avoid the employment of additional tools, e.g., wet extraction or ultrasonic treatment. Four grams of bulk fly ash were filled in a cylindrical 15 cm^3 plastic container with an inner diameter of 22.8 mm (outer $\varnothing = 24.8$ mm) and 36 mm height, closed with

a non-static lid. Prior to each extraction step, the sample material was homogenised by manually shaking the container. The extraction was carried out by moving a tip-fitted hand magnet along the outer cylinder wall. The magnetic force from outside accumulated and trapped the extracted magnetic particles at the inner cylinder wall. The rotation of the container along its cylinder axis during extraction assured both material mixing and proper exposure of the fly ash surface to the magnetic field. The distance between the magnet and the sample material was maintained constant for all extraction steps, given by the cylinder geometry. For removing the collected extract from the container, the magnetic material was carefully transferred to the center of the non-static lid, still being kept by the magnetic force. Then the lid was taken off and the magnetic particles were released into a cone-shaped small volume plastic container by removing the magnet from the top of the lid. In order to ensure the collection of particles with the highest contents of magnetic phases, 10 extraction steps were performed. The same procedure was applied on both samples. The separated mass of magnetic particles decreased from ~22 mg to ~9 mg from the first to the last extraction step for both samples.

2.3. Magnetic measurements

Magnetic susceptibility (MS) measurements were conducted using a KLY-3 Kappabridge (AGICO) operating at 875 Hz with a sensitivity of 3×10^{-8} [SI]. The samples were measured in 8.6 cm^3 cylindrical plastic containers. High- and low-temperature curves of MS were also measured with a KLY-3 attached to a CS-3 heating unit and a CS-L cryostat, respectively. Heating experiments were conducted in air.

Isothermal remanent magnetization (IRM) was imposed at room temperature using a pulse magnetizer MMPM9 (Magnetic Measurements Ltd) and the acquired magnetic moment was measured using a Molspin spinner magnetometer. IRM acquisition curves were analyzed using cumulative log normal Gaussian decomposition technique to discriminate the contribution of magnetic phases with different coercivity spectra as introduced by Kruiver et al. (2001).

Thermal demagnetization of the IRM of bulk fly ash samples was carried out using an ASC Scientific thermal demagnetizer model TD-48SC. An amount of 1.5 g of sample material was put in cylindrical 2 cm^3 quartz glass containers ($d = 12$ mm, $h = 18$ mm) and magnetized in a 2.5 T pulsed magnetic field. Stepwise thermal demagnetization was performed in steps of 25 °C from 100 °C to 700 °C. The remanence measurements were carried out using a Molspin spinner magnetometer.

2.4. Non-magnetic analysis techniques

2.4.1. SEM/EDX investigation

Scanning electron microscopy (SEM) and energy dispersive X-ray (EDX) analysis were performed using a LEO 1450VP connected with an Oxford INCA system. The volume analyzed by EDX is ~1 μm^3, and the detection limit of the instrument is 0.1–0.5% depending on the respective element. Analysis was carried out on carbon sputtered magnetic extracts from BexV_bu and BexN_bu samples. For "quantitative" analysis, a mass of 1.5 mg of magnetic extract was put on the sample holder. To ensure statistical reproducibility, the spherules contained in 10 pre-defined patches (areas of ~0.04 mm^2 on the SEM sample holder) were measured and counted. For efficiency and feasibility reasons particle sizes of <1 μm were excluded from analysis. The surface structures of the magnetic spherules were visually analyzed and the frequency of certain types was estimated. EDX analysis focusing on internal structures was performed on polished samples.

2.4.2. XRF analysis

X-ray fluorescence (XRF) technique was used to conduct chemical element analysis. Element contents were determined on BexV_bu and BexN_bu fly ash samples. Dry bulk fly ash was ground with a ball mill in zircon-oxide mortars for 15 min. Eight grams of the powdered material were taken to prepare glass beads. The XRF measurements were performed at the RWTH Aachen with an X-LAB 2000 spectrometer fitted with a 400 W/54 kV palladium anode X-ray tube controlled by Spectro XLABPro software.

2.4.3. Laser-granulometry

Detailed grain-size analysis was performed using a Malvern Mastersizer Micro laser-granulometer with a detection range from 0.3 μm to 300 μm and an accuracy of

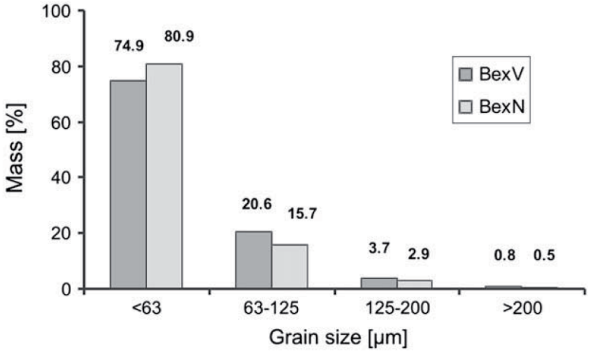

Fig. 1. Mass distribution of the grain-size fractions of BexV_bu and BexN_bu.

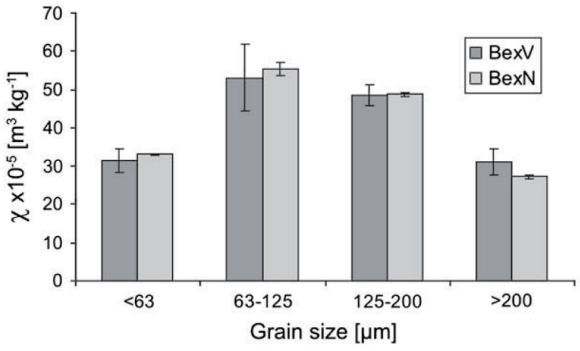

Fig. 2. Magnetic susceptibility (χ) of the grain-size fractions of BexV and BexN samples.

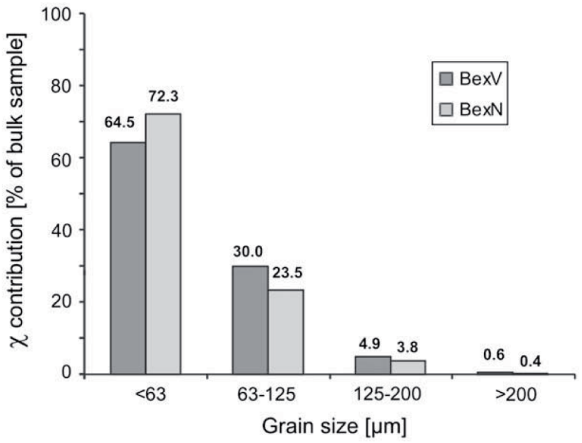

Fig. 3. Relative χ contribution of the grain-size fractions (mass by χ) to the bulk magnetic signal of the fly ash samples.

±3%. BexV_bu and BexN_bu samples were analyzed for their detailed grain-size spectra with three individual runs per sample.

3. Results and discussion

3.1. Grain-size distribution of BexV_bu and BexN_bu samples

The sieve analysis of the BexV_bu and BexN_bu samples (Fig. 1a) reveals that the grain-size fractions of <63 µm have the highest contribution to the bulk sample mass with 74.9 mass-% and 80.9 mass-%, respectively. The fractions of 63–125 µm contribute with 20.6 mass-% and 15.7 mass-%, respectively. The mass contribution of the grain-size fractions of >125 µm represents only comparatively low rates of 4.5% and 3.4%, respectively. The particulate matter of <125 µm, comprising ~95% of the total fly ash mass, is the dominating fly ash fraction in this study and must be regarded as a main contributor to environmental pollution.

The comparison of the finest grain-size fractions of <63 µm from BexV and BexN (Fig. 1) reveals a relatively higher amount for BexN. In the 63–125 µm fractions, an inverse behavior is observed. The observed relative grain-size distributions in both bulk samples are linked to flue gas dust collection characteristics, including the technical set-up of electrostatic precipitators, flue gas stream rate, and other factors. Since the electrostatic precipitator operates at an efficiency rate of 99.8% (www.steag-saarenergie.de), the fly ash particle investigation is representative for comparable coal-fired power plant emissions. Only 0.2% of the originally produced fly ash particles pass the electrostatic filter system, getting finally removed from flue gas together with sulphur compounds in the desulfurization step. With respect to environmental protection issues, virtually none of the originally produced fly ash particles pass the filter system and get emitted into the atmosphere. For coal-fired power plants without efficient filtering technologies, emissions with grain-size distribution, dominated by smaller particles, can be expected.

3.2. Magnetic investigations

3.2.1. Magnetic susceptibility of grain-size fractions

The MS measurements of the different grain-size fractions (Fig. 2) reveal varied contributions to χ. The highest χ values are observed in the grain-size spectra of 63–125 µm and 125–200 µm. The fractions of <63 µm and >200 µm show 40–50% lower χ values compared to those with the higher χ values. No significant χ variation between the BexV and BexN samples is observed. The results reveal that the content of ferri(o)magnetic mineral phases in the 63–125 µm and 125–200 µm fractions is significantly enhanced compared to the finest (<63 µm) and the coarsest fractions (>200 µm).

The MS of the fly ash fractions depend on the concentrations of the ferri(o)magnetic phases in the samples. For the estimation of the total magnetic contribution of a grain-size fraction to the bulk fly ash sample (BexV_bu or BexN_bu) χ is multiplied by the respective fraction mass determined by sieve analysis.

In Fig. 3 the relative % contributions of the grain-size fractions to χ of the bulk samples are presented. The

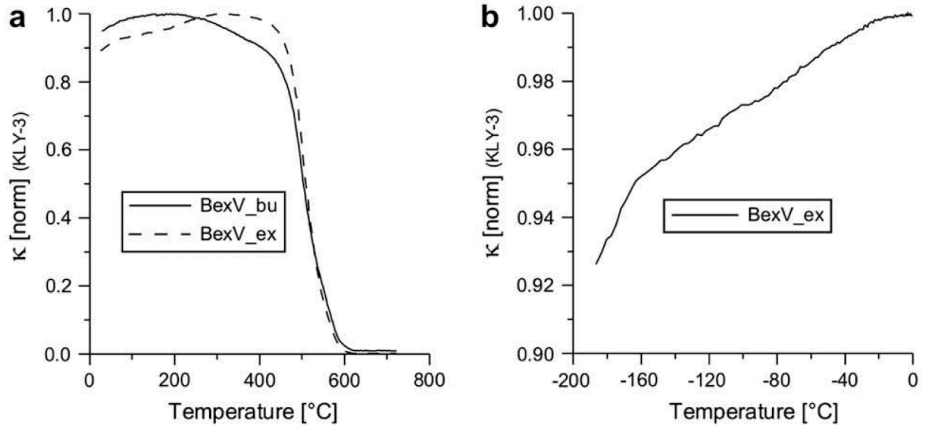

Fig. 4. (a) Thermo-magnetic heating curves from BexV_bu and BexV_ex. In (b) the low-temperature behavior of MS from BexV_ex is shown.

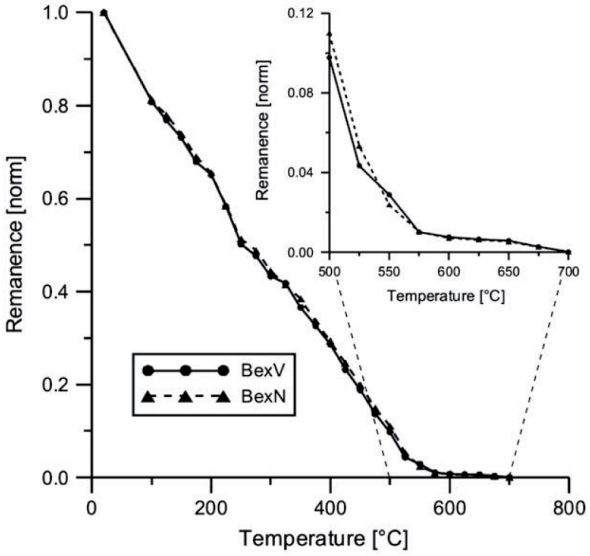

Fig. 5. Thermal demagnetization of a magnetic remanence acquired at 2.5 T from BexV_bu and BexN_bu samples. The enlarged view into the higher temperature range shows that hematite is contained.

contributions of the smaller sized fractions (<63 μm and 63–125 μm) to the total particulate matter emission account for ~95%. Hence, studies dealing with power plant fly ash found in the environment should focus on these small grain-size fractions.

3.2.2. Temperature dependent MS measurements

Thermo-magnetic analysis was conducted on both BexV and BexN samples (only data for BexV are presented, as results from BexN are almost identical).

Fig. 4a,b show the results from heating runs on bulk material and magnetic extract from BexV_bu. Both thermo-magnetic curves show a dominating magnetic phase with Curie temperatures at ~575 °C, indicating magnetite. The shapes of the thermo-magnetic curves and the different positions of the MS maxima reflect slightly

Table 1
Coercivity values determined from bulk fly ash samples and grain-size fractions of <63 μm (determined after Kruiver et al., 2001)

Sample	Soft (mT)	Hard (mT)
BexV_bu	71	647
BexN_bu	74	664
BexV_63	81	778
BexN_63	79	929

different magneto-mineralogical contents in both samples. A hematite phase (T_c ~ 680 °C) cannot be identified.

In Fig. 4b the Vervey-transition (T_v) of magnetite is observed at ~110 K by low-temperature measurement of the magnetic extract. A significant content of SD particles is indicated by increasing χ above T_v.

Thermal demagnetization curves of IRM from BexV_bu and BexN_bu samples (Fig. 5) reveal a continuous decrease of the remanence until the Curie temperature of magnetite at ~575 °C, with slight variations from 200 °C to 250 °C. At demagnetization temperatures from 650 °C to 700 °C a further magnetic phase, interpreted as hematite, can be identified (inset of Fig. 5).

3.2.3. IRM acquisition characteristics and analysis

Samples BexV_bu and BexN_bu show a nearly identical IRM acquisition behavior (Fig. 6a). In general, the presence of a low and a high coercivity phase is obvious from the slopes of the curves. IRM acquisition data analysis for BexV_bu after Kruiver et al. (2001) provides coercivity values of 71 mT (soft magnetic phase) and 647 mT (hard magnetic phase). The results for BexN_bu are similar showing values of 74 mT and 664 mT, respectively.

Besides the bulk samples, the grain-size fractions of <0.63 μm were analyzed. BexV_63 show values of 81 mT for the soft magnetic component and 778 mT for the hard magnetic component. For BexN_63, 79 mT and 929 mT were obtained.

The determination of the coercivity values of the soft magnetic phase is reliably represented by a good fit of the modelled curve (Fig. 6b). The presence of a hard magnetic phase is evident, but the limited range of applicable IRM

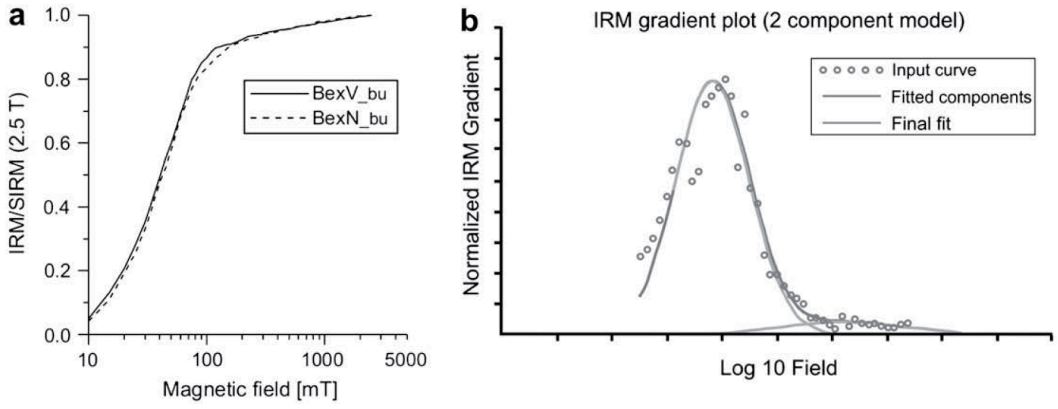

Fig. 6. (a) IRM acquisition curves of BexV_bu and BexN_bu. The contribution of low and high coercivity phases is obvious. (b) IRM gradient plot of BexV_bu for a two component model analyzed after Kruiver et al., 2001.

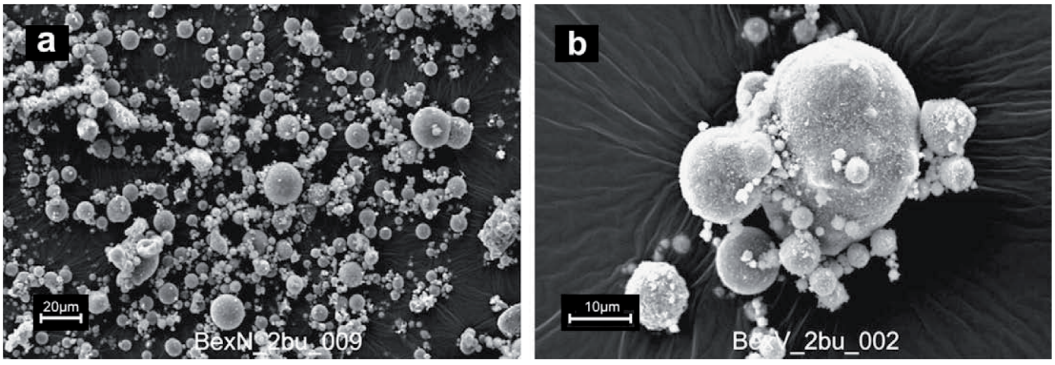

Fig. 7. (a) and (b) show SEM images of spherules from fly ash bulk samples (BexV_bu and BexN_bu).

fields, together with low absolute values of the IRM gradient inhibit a precise determination of the coercivity value of this hard magnetic phase. Higher coercivity values in the sieved fractions of <63 μm suggest that domain states in the fine grained and bulk material are different, and the magnetic phases in larger particles are in average magnetically "softer" than in smaller particles (Table 1).

The presence of magnetite and hematite is proven by thermal demagnetization of IRM. The obtained coercivity values can be attributed to a low coercive magnetite phase (~70–80 mT) and a high coercive hematite phase (>600 mT), which is incompletely resolved by this approach.

3.3. SEM/EDX and XRF investigation

3.3.1. SEM analysis

SEM investigation of bulk fly ash provides an overview of the most prominent and frequent particle sizes and structures. A representative depiction of particles (magnetic and non-magnetic) in bulk fly ash is shown in Fig. 7a. Nearly all particles are of spherical shape. Only a small amount of "loosely attached" agglomerates as shown in Fig. 7b is observed.

Detailed SEM investigations, including EDX and grain-size analyses, were performed on magnetic extracts. The

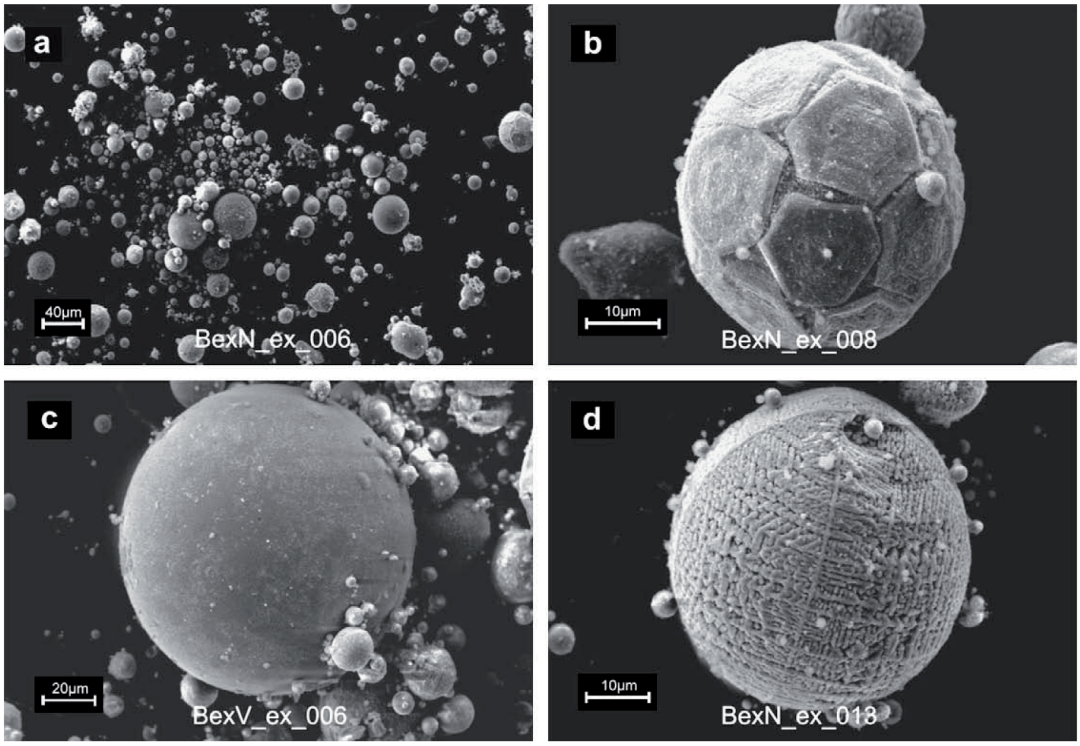

Fig. 8. (a) Overview of particles from the magnetic extract of fly ash (BexN_ex sample). (b) Magnetic spherule with hexagonal-pattern surface structure (rarely observed). (c) Spherule with smooth orange-peel surface structure (frequently occurring). (d) Spherule with thread-like surface structure (frequently observed).

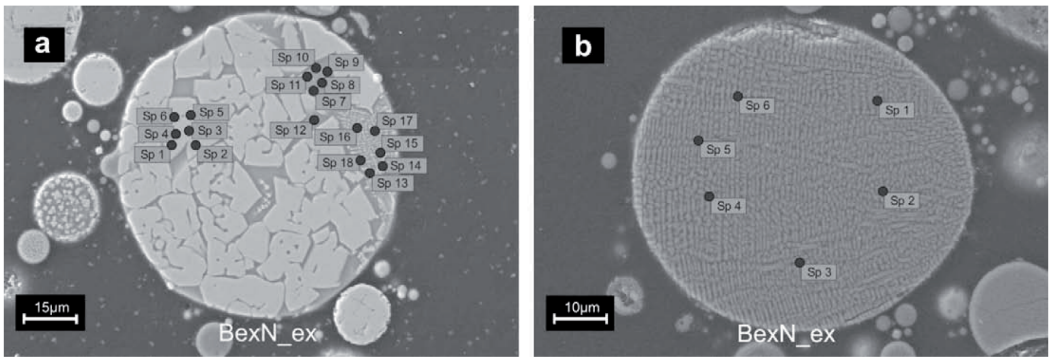

Fig. 9. SEM micrographs from polished specimens of BexN_ex. (a) Spherule with "blocky" internal structure. (b) Spherule with "regular" pattern. Dots indicate the spots of EDX analysis. Six EDX spectra were analyzed in each "homogeneous" area.

magnetic material enabled the relative quantification of grain-size ranges and the observation of typical surface structures of individual spherules.

The overview of extracted magnetic particles (Fig. 8a) reveals varied particle sizes and surface structures. Surface structures range from smooth types to those showing "crystalline patterns". A typical example for a rare "crystalline structure" is seen in Fig. 8b, showing hexagonal-patterns on the spherule surface. In both samples under investigation <0.1% of this spherule type (3 out of ~4000) are observed. Most frequently appearing spherule types are such with variably intense orange-peel surface structures (Fig. 8c), and thread-like surfaces as shown in (Fig. 8d) or intermediate types. Very rough and irregular surfaces are also observed. Surface and internal structures are results from the formation conditions including furnace design, chemical composition of the fired coal, formation temperature or cooling procedures.

3.3.2. EDX analysis

SEM/EDX analysis was performed on polished specimens from magnetic extracts, embedded in epoxy resin. Internal structures of typical magnetic spherules can be observed in detail and suitable areas for representative EDX analyses can be selected.

A spherule with large "magnetite" crystals in blocky fabric (Fig. 9a, bright color), embedded in a "glassy" matrix, reflects the internal structure of spherules as shown in Fig. 8b. A spherule with uniform structure consisting of fine "magnetite" crystals in a "glassy" matrix (Fig. 9b) represents the internal structure of the thread-like surface type (Fig. 8d).

EDX analysis reveals characteristic element distribution patterns for the investigated spherule types (Table 2a,b). Areas with high iron contents (~65%) represent zones with "magnetite" crystals, respectively, high concentrations of magnetic phases. In the "glassy" matrix, lower iron contents (~15%), together with high contents of Si, Al and Ca are observed. Data from EDX analyses on the spherules in Fig. 9a,b are presented in Table 2a,b.

3.3.3. Chemical analysis (XRF) on bulk fly ash samples

The chemical composition of BexV_bu and BexN_bu fly ash samples was determined using XRF analysis. The results (oxides) and the calculated element contents are given in Table 3 a and b, respectively.

In addition to the main elements (Fe, Si, Al, Ca, Mg, Mn), which were observed by EDX analysis on single grain structures (see Table 2a,b) of the magnetic extract, XRF analyses on the bulk material reveal a number of additional elements (Ti, Na, K, P, S), either in low concentrations or in particles of the "non-magnetic" fraction.

3.4. Grain-size distribution analysis on magnetic extracts using SEM

3.4.1. Micro-scale particle quantification

For relative quantification of magnetic spherules and their grain-size distributions, SEM measuring techniques were applied using amounts of ~1.5 mg of magnetic extracts from BexV_ex and BexN_ex.

Individual particle counting and diameter determination revealed grain-sizes of up to 186.5 µm, while particle sizes of <1 µm were excluded from the analysis. For ensuring statistical reproducibility, the spherules contained in 10 pre-defined patches (areas of ~0.04 mm^2 on the SEM sample holder) were measured and counted. In total 2466 spherules from BexV_ex and 1721 spherules from BexN_ex were analyzed in BexV_ex and BexN_ex, respectively (Figs. 10 and 11, Table 4a,b).

The variability of individual grain-size distributions of magnetic spherules is represented in Fig. 10. The underlying data and statistical parameters are listed in Table 4a,b.

Statistical data from individual patch analyses show consistency when comparing values across the sets. As data were gathered from randomly distributed particles in randomly distributed patches, variations in the results are comparatively small. The results from the total particle number assessment are presented in Fig. 11.

The grain-size median values of magnetic spherules determined through SEM assessment are 4.3 µm and 5.3 µm, respectively, for the BexV_ex and BexN_ex samples. The median spherule diameter of the 2nd flue gas purification step is ~23% larger than that from the 1st purification step. Comparison of IQR values (representing 50% of the counted spherules) reveals an increase in spherule diameters of ~24%. As median and IQR values increase at similar rates, the particle size distribution must be very similar in both samples. Furthermore, these nearly

Table 2
(a) EDX data for the typical areas of the spherule in Fig. 9a ("blocky" structure): 1–6, large iron-bearing crystals; 7–12, "glassy" matrix; 13–18, "glassy" matrix with small iron-bearing crystals; (b) EDX data for the "uniform" structure of the spherule in Fig. 9b (thread-like structure)

(a)	Fe	Mn	Si	Al	Ca	Mg	Oxygen
Spectrum 1–18							
1	67.14	–	–	–	–	–	32.86
2	58.34	–	2.13	–	2.52	–	37.01
3	66.26	–	–	–	–	–	33.74
4	64.10	–	–	2.59	–	1.14	32.17
5	63.38	–	–	2.58	–	1.19	32.85
6	64.86	–	–	1.80	–	–	33.35
7	14.36	–	21.71	4.51	14.34	–	45.08
8	14.82	–	21.58	4.49	13.76	–	45.35
9	13.95	–	21.40	4.20	14.65	–	45.80
10	15.23	–	20.29	4.62	14.42	–	45.44
11	31.64	–	17.50	4.29	8.61	–	37.96
12	15.86	–	20.87	4.64	14.34	–	44.29
13	31.48	–	14.67	2.65	9.18	0.70	41.32
14	42.24	–	9.42	2.99	5.56	–	39.79
15	32.55	–	13.83	3.41	8.95	–	41.27
16	29.29	–	16.01	3.47	10.83	–	40.38
17	31.82	–	15.48	3.30	9.64	0.88	38.88
18	33.17	–	15.18	3.48	9.38	–	38.79
Spectrum 1–6							
Median	64.48	–	–	2.58	–	1.16	33.11
Mean	64.01	–	–	2.32	–	1.16	33.66
Stddev	3.10	–	–	0.45	–	0.03	1.72
Spectrum 7–12							
Median	15.02	–	21.13	4.50	14.34	–	45.22
Mean	17.64	–	20.56	0.46	13.35	–	43.99
Stddev	6.89	–	1.59	0.18	2.34	–	3.00
Spectrum 13–18							
Median	32.18	–	14.92	3.35	9.28	0.79	40.09
Mean	33.43	–	14.10	3.22	8.92	0.79	40.07
Stddev	4.52	–	2.41	0.33	1.78	0.12	1.12
(b)	Fe	Mn	Si	Al	Ca	Mg	Oxygen
Spectrum 1–18							
1	37.64	1.02	11.76	7.65	1.77	–	40.15
2	37.66	1.28	11.14	7.61	1.65	0.88	39.78
3	41.45	1.43	8.32	7.43	1.11	0.90	39.37
4	36.33	1.42	12.12	8.01	1.50	0.88	39.74
5	42.33	1.31	8.32	7.61	1.30	0.90	38.40
6	40.40	1.32	8.68	8.14	1.17	1.09	39.20
Spectrum 1–6							
Median	39.03	1.31	9.91	7.63	1.33	0.90	39.56
Mean	39.30	1.30	10.06	7.74	1.39	0.93	39.44
Stddev	2.42	0.15	1.80	0.27	0.29	0.09	0.61

All values are given in mass-%.

identical values support the efficiency of the applied SEM particle assessment method, applicable for small amounts of sample material (a few micrograms).

The increase of particle diameters can be attributed to technical specifications of the flue gas filtering system.

3.4.2. Grain-size distribution of bulk fly ash samples and magnetic extracts

The grain-size analysis on bulk fly ash samples (Fig. 12) reveals particle sizes ranging from 0.5 μm to 300 μm. Comparison of bulk samples from both filtering steps shows slightly higher amounts of larger particles in BexN_bu (2nd flue gas purification step). Grain-size sum curves from magnetic extracts investigated and quantified using SEM techniques reveal higher amounts of smaller spherules. While in BexV_bu (BexN_bu) the fraction of <10 μm makes up ~9.5% (~14%), the BexV_ex (BexN_ex) sample reveals ~76% (~68%) for the same grain-size spectrum. In contrast, larger grain-sizes of magnetic particles, i.e., >100 μm are very rare, while ~25% of the bulk samples comprises this fraction. The largest magnetic spherule diameter found in BexV_ex (BexN_ex) is 143.9 μm (186.5 μm). The grain-size fraction of >100 μm (125 μm) constitutes only 0.65% (0.12%) of the total number of magnetic spherules in BexV_ex and 0.58% (0.06%) in BexN_ex, respectively.

The relative grain-size distributions of magnetic particles of <60 μm are presented in Fig. 13. Spherule sizes of >60 μm are not shown, as they comprise only 2.6% of the totally analyzed particles in BexV_ex, respectively, 2% in BexN_ex.

Table 3
XRF data from bulk fly ash samples; (a) oxides; (b) element contents calculated from (a)

(a)													
Sample	Fe_2O_3 (T)	TiO_2	SiO_2	Al_2O_3	MnO	MgO	CaO	Na_2O	K_2O	P_2O_5	SO_3	LOI	Total
BexV	16.64	0.82	39.28	21.41	0.25	3.13	11.66	1.23	2.20	0.11	1.94	1.48	100.16
BexN	16.12	0.82	38.94	21.16	0.25	3.12	11.42	1.22	2.19	0.26	2.34	1.38	99.23
(b)													
Sample	Fe	Ti	Si	Al	Mn	Mg	Ca	Na	K	P	S	Oxygen	LOI	Total
BexV	11.64	0.49	18.36	11.33	0.19	1.88	8.34	0.91	1.83	0.05	0.78	42.87	1.48	100.16
BexN	11.28	0.49	18.20	11.20	0.19	1.88	8.16	0.91	1.82	0.11	0.94	42.66	1.38	99.23

All values are given in mass-%.

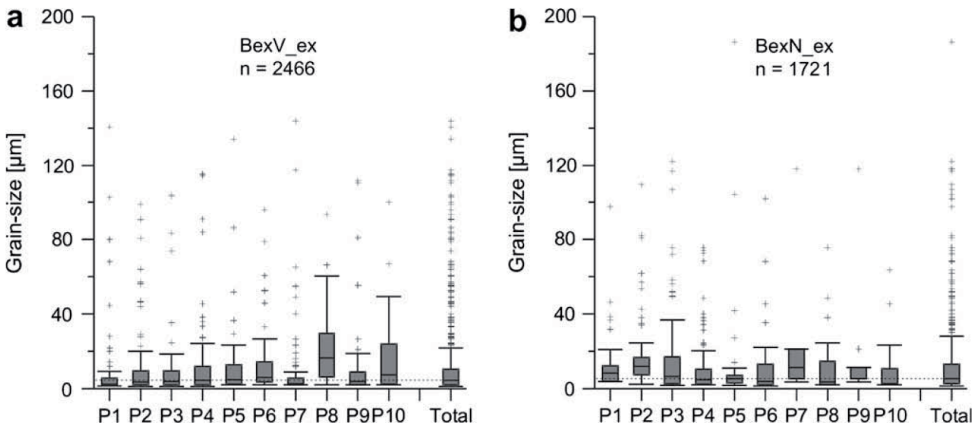

Fig. 10. Grain-size distribution of magnetic spherules in extracts from BexV_ex (a) and BexN_ex (b) determined by SEM counting. P1–P10 denote the individual patches; "Total" represents all patches ($n = 2466$ and $n = 1721$, respectively). For further explanation see text.

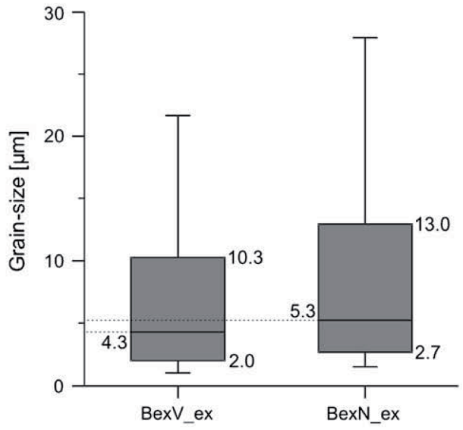

[µm]	BexV_ex [n=2266]	BexN_ex [n=1721]
Median	4.3	5.3
1. Quartile	2.0	2.7
3. Quartile	10.3	13.0
IQR	8.3	10.3
Minimum	1.0	1.5
Maximum	143.9	186.5

Fig. 11. Statistically relevant grain-size distribution from SEM magnetic spherule assessment of BexV_ex and BexN_ex. "Outliers", defined by >Q3 + 1.5*IQR are not considered in the diagram.

"Particles of <10 µm in diameter (PM_{10}) pose a health concern because they can be inhaled into and accumulate in the respiratory system. Particles of <2.5 µm in diameter ($PM_{2.5}$) are referred to as "fine" particles and are believed to post the largest health risks. Because of their small size, fine particles can lodge deeply into the lungs. Sources of fine particles include all types of combustion (motor vehicles, power plants, wood burning, etc.) and some industrial processes. Particles with diameters between 2.5 µm and 10 µm are referred to as "coarse"" (www.epa.gov).

Even if magnetic spherules make up only a small fraction of fly ash, they can accumulate with other particles in the respiratory system. Efficient filtering technologies as applied in modern coal-fired power plants protect the

Table 4
Grain-size data statistics from SEM particle counting; (a) BexV_ex; (b) BexN_ex

(a)											
BexV_ex: Fig 10a	P1	P2	P3	P4	P5	P6	P7	P8	P9	P10	Total
Number of spherules [*n*]	280	401	265	379	336	153	199	133	237	84	2466
Minimum	1.5	1	1	1	1.9	1.9	1.9	1.9	1.9	1.9	1
Maximum	140.7	99	104	115.3	134	96.04	143.9	93.55	111.8	100	143.9
Range	139.2	98	103	114.3	132.1	94.14	142	91.65	109.9	98.1	142.9
Mean	7.9	9.5	8.5	11.1	9.6	12.3	7.5	20.0	8.3	14.9	10.0
Median	2.4	3.4	3.8	4.4	4.8	5.9	2.6	16.4	3.7	7.3	4.3
1. Quartile	1.9	1.9	2.0	2.0	2.3	3.4	1.9	6.0	1.9	2.3	2.0
3. Quartile	5.4	8.2	9.4	11.9	12.6	14.2	5.5	29.6	8.7	238	10.3
(b)											
BexN_ex: Fig 10b	P1	P2	P3	P4	P5	P6	P7	P8	P9	P10	Total
Number of spherules [*n*]	78	150	403	451	126	194	69	102	65	83	1721
Minimum	3.8	2.3	1.7	1.9	1.8	1.5	3.4	1.9	3.4	1.9	1.5
Maximum	97.7	109.6	122.1	75.7	186.5	102.0	118.1	75.7	118.1	63.6	186.5
Range	93.9	107.3	120.4	73.8	184.7	100.5	114.7	73.8	114.7	61.7	185.0
Mean	11.2	17.7	13.2	9.3	10.5	10.0	12.3	9.6	11.5	7.9	11.4
Median	8.3	11.8	6.6	4.7	5.3	3.8	11.3	3.5	5.2	2.6	5.3
1. Quartile	3.8	7.2	2.5	2.3	2.8	1.9	5.2	2.0	5.2	2.1	2.7
3. Quartile	12.1	16.7	17.0	10.2	7.0	13.0	21.2	14.5	11.3	10.6	13.0

environment and human beings from harmful particulate matter exposition.

4. Conclusions

Fly ashes from filtering systems are ideal study materials, as they represent main air and soil pollutants when technical standards of coal-fired power plant precipitator systems are low.

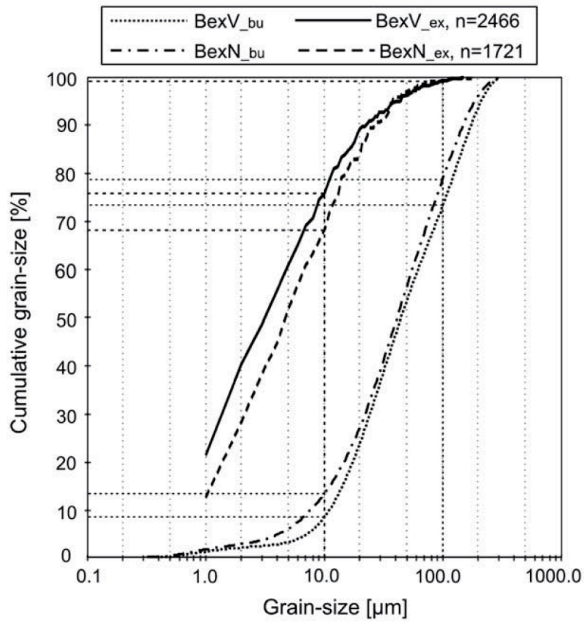

Fig. 12. Grain-size sum curves from BexV_bu and BexN_bu samples analyzed by laser-granulometry and curves from SEM analysis of magnetically extracted spherules (BexV_ex and BexN_ex).

Grain-size fractions prepared by sieve analysis provide the basis for focused magnetic, physical or chemical analyses of fly ash. The amount of individual grain-size fractions can be easily and precisely determined. The finest fraction of <63 μm accounts for the dominating amount of the total mass of the fly ash. Magnetic susceptibility values of the different grain-size fractions reveal the highest values for the fractions of 63–125 μm and 125–200 μm. The relative contribution of individual grain-size fractions to the bulk magnetic signal can be determined by multiplication of the mass of the respective grain-size fraction by χ. Similar to the mass contribution, the small fractions of <63 μm and 63–125 μm account for a large portion of the bulk magnetic signal.

Thermo-magnetic analyses prove magnetite as the dominating magnetic phase. Stepwise thermal demagnetization of IRM proves magnetite and small amounts of hematite as magnetic phases. Two magnetic phases are observed by stepwise IRM acquisition. The softer magnetic phase with coercivities of ~70–80 mT can be attributed to magnetite, whereas the harder magnetic phase with coercivities of >600 mT, attributed to hematite, cannot be satisfyingly determined.

SEM screening of bulk fly ash samples reveals a vast majority of spherical particles, which is also observed in the magnetic extracts. In the magnetic extracts, spherules with different surface morphology and different frequency of occurrence can be found. Internal structures and element distributions of individual magnetic spherules can be examined on polished specimens using SEM/EDX. The relative quantification of the sizes of magnetic spherules can be performed by visual observation and diameter determination of individual spherules within patches of equal areas. Median spherule sizes were determined with 4.3 μm and 5.3 μm for BexV_ex and BexN_ex, respectively. Cumulative grain-sizes of bulk fly ash samples, ranging from 0.5 μm to 300 μm, and magnetic extracts, ranging from 1 μm to 186.5 μm, reveal different grain-size

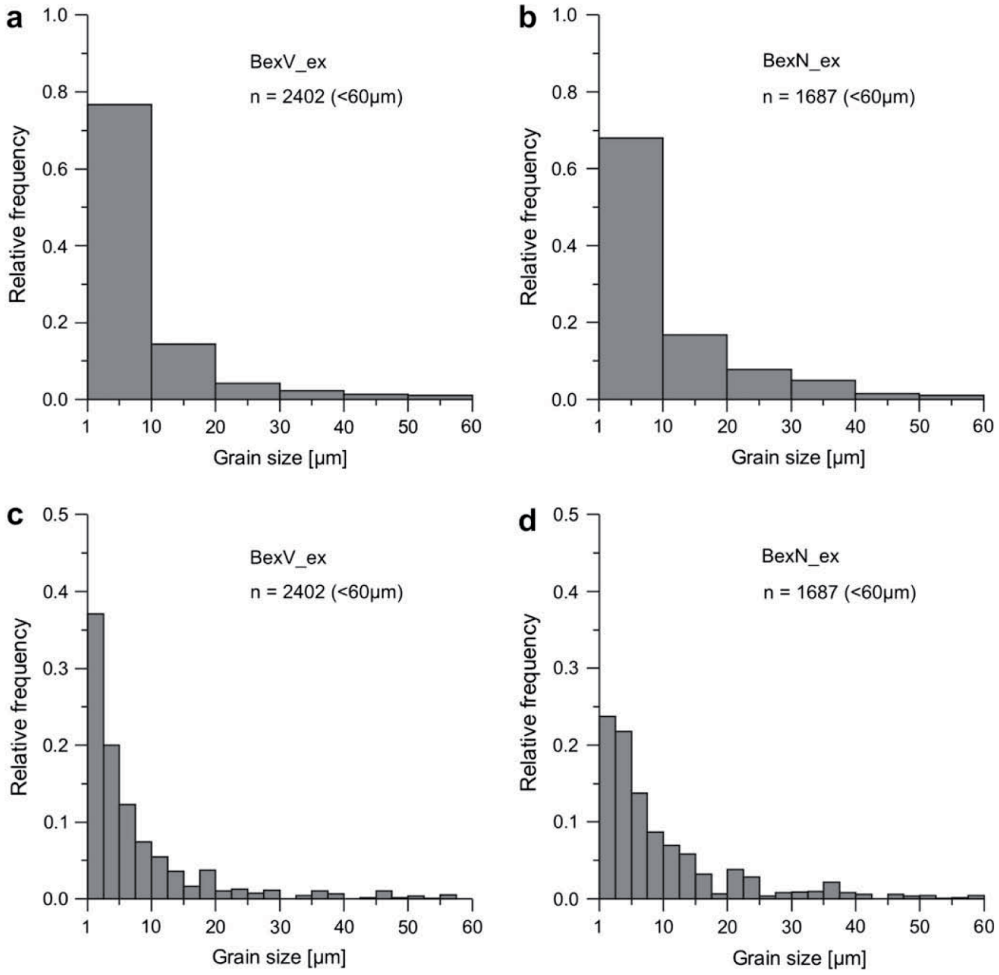

Fig. 13. Relative frequency of magnetic spherules with respect to their grain-sizes determined from SEM particle counting; (a) and (b) for BexV_ex in 10 µm, respectively, 2.5 µm grain-size ranges; (c) and (d) for BexN_ex in 10 µm, respectively, 2.5 µm grain-size ranges.

distributions for bulk and magnetic materials. A high portion of magnetic spherules is found in the grain-size range of 1–10 µm, representing respirable, potentially hazardous, particles.

Magnetic methods are powerful tools to be used for investigation of fly ash specimens. Identification of magnetic phases is possible by performing temperature dependent MS measurements and thermal demagnetization of IRM.

Relative quantification of magnetic spherules from extracts using SEM techniques shows that even low amounts (a few milligrams) of magnetic material are suitable for detailed and representative grain-size analysis, and at the same time, for morphological studies. Moreover, it is demonstrated that systematic and precise handling of micro-scale magnetic particles down to 1 µm in size (with more effort even below) is possible, and can be efficiently implemented following defined strategies. It is also proven that adequate fly ash sample preparation plus systematic combination of SEM and EDX analyses provides valuable additional information on internal particle structures, and enables for small scale element analysis on individual particles. In combination with XRF analysis a more complete characterization of the sample material is facilitated. Quantitative assessment of the main chemical element contents, especially iron and its distribution is possible with basic investigation steps.

Altogether, the methodology tested in this study can help for better qualitative and quantitative assessment of magnetic particles and particle structures in fly ashes and magnetic dusts. The integrative application of magnetic and non-magnetic methods, supporting each other, leads to a better characterization of environmentally hazardous materials.

Acknowledgements

We gratefully acknowledge the support of Hartmut Schulz during SEM/EDX analysis, Christoph Berthold and Daniel Russ for their help with grain-size analysis, and Indra Gill-Kopp for the preparation of the polished sections (all from University of Tübingen). For the reviews and

constructive comments for improvement of the paper we are thankful to Leonardo Sagnotti and an anonymous reviewer. This research was funded by DFG (AP 34/21–1,2).

References

Blaha U., Appel E., Stanjek H. Determination of anthropogenic boundary depth in soil profiles and semi-quantification of heavy metal loads using magnetic susceptibility. Environmental Pollution, in press. doi:10.1016/j.envpol.2008.02.013

Chaddha, G., Seehra, M.S., 1983. Magnetic components and particle size distribution of coal fly ash. Journal of Physics D Applied Physics 16, 1767–1776.

Del Monte, M., Sabbioni, C., 1984. Morphology and mineralogy of fly ash from a coal fueled power plant. Archives for Meteorology Geophysics and Bioclimatology Series B 35, 93–104.

Fisher, G.L., Prentice, B.A., Silberman, D., Onodov, J.M., Biermann, A.H., Ragaini, R.C., McFarland, A.R., 1978. Physical and morphological studies of size-classified coal fly ash. Environmental Science & Technology 12, 447–451.

Gautam, P., Blaha, U., Appel, E., Neupane, G., 2004. Environmental magnetic approach towards the quantification of pollution in Kathmandu urban area, Nepal. Physics and Chemistry of the Earth 29, 973–984.

Gautam, P., Blaha, U., Appel, E., 2005. Magnetic susceptibility of dust loaded leaves as a proxy of traffic related heavy metal pollution in Kathmandu city, Nepal. Atmospheric Environment 39, 2201–2211.

Hanesch, M., Scholger, R., Rey, D., 2003. Mapping dust distribution around an industrial site by measuring magnetic parameters of tree leaves. Atmospheric Environment 37, 5125–5133.

Hansen, L.D., Silberman, D., Fisher, G.L., 1981. Crystalline components of stack-collected, size-fractionated coal fly-ash. Environmental Science & Technology 15, 1057–1062.

Hay, K.L., Dearing, J.A., Baban, S.M.J., Loveland, P., 1997. A preliminary attempt to identify atmospherically-derived pollution particles in English topsoils from magnetic susceptibility measurements. Physics and Chemistry of the Earth 22, 207–210.

Jordanova, D., Jordanova, N., Hoffmann, V., 2006. Magnetic mineralogy and grain-size dependence of hysteresis parameters of single spherules from industrial waste products. Physics of the Earth and Planetary Interiors 154, 255–265.

Kapicka, A., Petrovsky, E., Ustjak, S., Machackova, K., 1999. Proxy mapping of fly-ash pollution of soils around a coal-burning power-plant: a case study in the Czech Republic. Journal of Geochemical Exploration 66, 291–297.

Kapicka, A., Jordanova, N., Petrovsky, E., Ustjak, S., 2000. Magnetic stability of power-plant fly ash in different soil solutions. Physics and Chemistry of the Earth 25, 431–436.

Kapicka, A., Jordanova, N., Petrovsky, E., Podrazsky, V., 2003. Magnetic study of weakly contaminated forest soils. Water Air and Soil Pollution 148, 31–44.

Kruiver, P.K., Dekkers, M.J., Heslop, D., 2001. Quantification of magnetic coercivity components by the analysis of acquisition curves of isothermal remanent magnetization. Earth and Planetary Science Letters 189, 269–276.

Magiera, T., Strzyszcz, Z., Kapicka, A., Petrovsky, E., Magprox team, 2006. Discrimination of lithogenic and anthropogenic influences on topsoil magnetic susceptibility in central Europe. Geoderma 130, 299–311.

Maier, G., Scholger, R., 2004. Demonstration of connection between pollutant dispersal and atmospheric boundary layers by use of magnetic susceptibility mapping, St. Jacob (Austria). Physics and Chemistry of the Earth 29, 997–1009.

Rose, N.L., Harlock, S., Appleby, P.G., 1999. The spatial and temporal distributions of spheroidal carbonaceous fly ash particles (scp) in the sediment records of European mountain lakes. Water Air and Soil Pollution 113, 1–32.

Sarbak, Z., Stanczyk, A., Kramer-Wachowiak, M., 2004. Characterization of surface properties of various fly ashes. Powder Technology 145, 82–87.

Sharma, A.P., Tripathi, B.D., 2007. Magnetic mapping of fly-ash pollution and heavy metals from soil samples around a point source in a dry tropical environment. Environmental Monitoring and Assessment. doi:10.1007/s10661-007-9788-x.

Spiteri, C., Kalinski, V., Rösler, W., Hoffmann, V., Appel, E., Magprox team, 2005. Magnetic screening of a pollution hotspot in the Lausitz area, Eastern Germany: correlation analysis between magnetic proxies and heavy metal contamination in soils. Environmental Geology 49, 1–9.

Strzyszcz, Z., Magiera, T., Heller, F., 1996. The influence of industrial immissions on the magnetic susceptibility of soils in Upper Silesia. Studia Geophysica et Geodaetica 40, 276–286.

Urbat, M., Lehndorff, E., Schwark, L., 2004. Biomonitoring of air quality in the cologne conurbation using pine needles as a passive sampler—part I: magnetic properties. Atmospheric Environment 38, 3781–3792.

Veneva, L., Hoffmann, V., Jordanova, D., Jordanova, N., Fehr, T., 2004. Rock magnetic, mineralogical and microstructural characterization of fly ashes from Bulgarian power plants and the nearby anthropogenic soils. Physics and Chemistry of the Earth 29, 1011–1023.

3

Assessment of vehicular pollution in Kathmandu: magnetic properties and heavy metal chemistry of dust from streets and leaves

Journal of Nepal Geological Society, 2008, Vol. 37, pp. 67–76

Assessment of vehicular pollution in Kathmandu: magnetic properties and heavy metal chemistry of dust from streets and leaves

***Pitambar Gautam[1], Ulrich Blaha[2], and Erwin Appel[2]**
[1]*Creative Research Initiative "Sousei", Hokkaido University, N21 W10, Sapporo 001-0021, Japan*
[2]*Institute of Geosciences, University of Tübingen, Sigwartstrasse 10, D-72076 Tübingen, Germany*
*(*Email: pgautam2000@yahoo.com, pgautam@cris.hokudai.ac.jp)*

ABSTRACT

Road sediment (solid inorganic material accumulated on the road surface) and leaf-dust (dust deposited on leaves of short, <1 m in height, roadside rubber plants) samples collected from the roads of Kathmandu were studied for magnetism (magnetic susceptibility χ, isothermal remanence IRM, anhysteretic remanence ARM, and microscopy) and contents of heavy metals (HM: Cd, Co, Cr, Cu, Fe, Mn, Ni, Pb, Zn), to judge their suitability to assess the traffic-related urban environment pollution. Bulk samples (grain diameter: <0.63 mm) of road sediment samples at 10 sites, from both major and minor roads, had χ within (0.6–3.5) × 10^{-6} m^3/kg. Both χ and IRM showed strong inverse relationship with size fractions. Magnetite-like phase, of both geogenic and anthropogenic origin, is the dominant magnetic material. In general, the finer the grain size fraction the higher the HM content; compared to the coarse fraction, the fine fraction was enriched 1.5 times in Ni and 4 times in Pb. For a particular size fraction, however, χ had no clear relationship with HM content implying its limited use as a universal proxy of the HM enrichment in non-regulated urban roads.

For bulk samples of leaf dust from 14 sites, χ had a range of (0.9–2.6) × 10^{-6} m^3/kg, with notably lower values for those along secondary roads or largely off the road margin even in the case of major roads. Based on X-ray assisted microscopy, magnetite or magnetite-like phase having soft-coercivity, in magnetic terms, contributes to ca. 88% of saturation IRM. The magnetic susceptibility of leaf dust correlates well with the contents of urban elements (Zn, Cu, and Pb) and thus serves as a good proxy of the vehicular metallic pollution.

Keywords: environmental pollution, road sediments, heavy metals, isothermal remanence, Kathmandu, magnetic susceptibility, magnetic spherules

Received: 28 July 2007; **revision accepted:** 16 April 2008

INTRODUCTION

Environmental pollution, such as the degradation of air, water, vegetation and land systems, as a result of increased vehicular movement, industrial activities (e.g., emissions from cement and brick kilns), and biomass burning in Kathmandu has been of public concern in recent years and necessitated introducing new measures by the traffic authorities (Sharma et al. 2002; Gautam et al. 2004). Emission tests data for CO, HC, CO_2 and O_2 prove the motor vehicles to be the major source of air pollutant emissions, contributing to urban air quality deterioration in the Kathmandu valley (Faiz et al. 2006). The statistical data for the Fiscal Year 2003–04 show a concentration of 58% (about 4,32,000) of the total national vehicle fleet in Kathmandu. Out of them, 70% of the vehicles in Kathmandu were 2-wheelers; of which 25% had two-stroke engines that utilise fuel mixed with engine oil and emit a relatively high amount of pollutants.

This study was carried out in urban and suburban areas of Kathmandu to evaluate the suitability of magnetic methods, using a number of parameters as heavy metal (HM) pollution proxies (Gautam et al. 2005b). Environmental pollution can be effectively studied by: (i) in situ susceptibility mapping of urban or suburban parks, profiling across roads, conducting soil susceptibility traverses, and preparing vertical logs (Gautam et al. 2004); (ii) laboratory measurements of mass-specific magnetic susceptibility (χ) on dust-laden leaves of trees (commonly >2 m high) and determination of HM contents on them (Gautam et al. 2005a); and (iii) zonation of vertical soil profiles based on the degree of metal enrichment revealed from the combined interpretation of χ, saturation isothermal remanence (SIRM), and HM contents (Gautam et al. 2005b).

Studies on HM chemistry carried out globally from 1980s show that the street dust may serve as a trap of toxic metals and organic contaminants derived from both natural (e.g., weathering, pedogenesis) and anthropogenic (e.g., road construction, vehicular movement, industrial emission) as well as mixed (atmospheric deposition by sedimentation, impaction, and interception) processes (Hopke et al. 1980; Tokahoglu and Kartal 2006; Ahmad and Ishiga 2006). Moreover, dust composition and accumulation is controlled

by several factors such as weather, traffic density, industrial activity, and proximity of soil (Al-Rajhi et al. 1996). In this context, this paper provides additional insights into the magnetic properties and HM contents of the roadside material.

SAMPLING AND LABORATORY TECHNIQUES

Dust samples were collected from (i) the rubber plants of the Kalanki–Tripureshwar–Babarmahal road (Fig. 1a) and (ii) Maitighar–Babarmahal area (Fig. 1b) in February 2002. The dust deposited on large and concave-up leaves of young rubber plants, tens of cm to 1 m high, growing at roadsides (directly at the sides of footpaths or a few metres away in the green belt of Ring Road). Their accumulation preceded the suspension of street dust by turbulence (such as wind or vehicular movement) within a maximum period of ca. 4 months after the summer monsoon. Sediment samples (RD) were collected from a 0.5 to 2 m^2 area near the edge of the road. The sites RD1 to RD3 belong to a secondary but well-paved and well-maintained road frequented mainly by vehicles from administrative institutions (i.e., Ministries, Oil Corporation etc.). In contrast, the sites RD5 to RD7 belong to a moderately maintained and dusty secondary road. The sites RD4 and RD8 to RD10 are located on the main road with heavy traffic.

The road sediment samples (RD) were first dried at 75 °C for 24 hours and then separated into bulk samples (particle diameter <2 mm) and size fractions of 0.2–0.63 mm (coarse), 0.063–0.2 mm (medium), and <0.063 mm (fine), using analytical

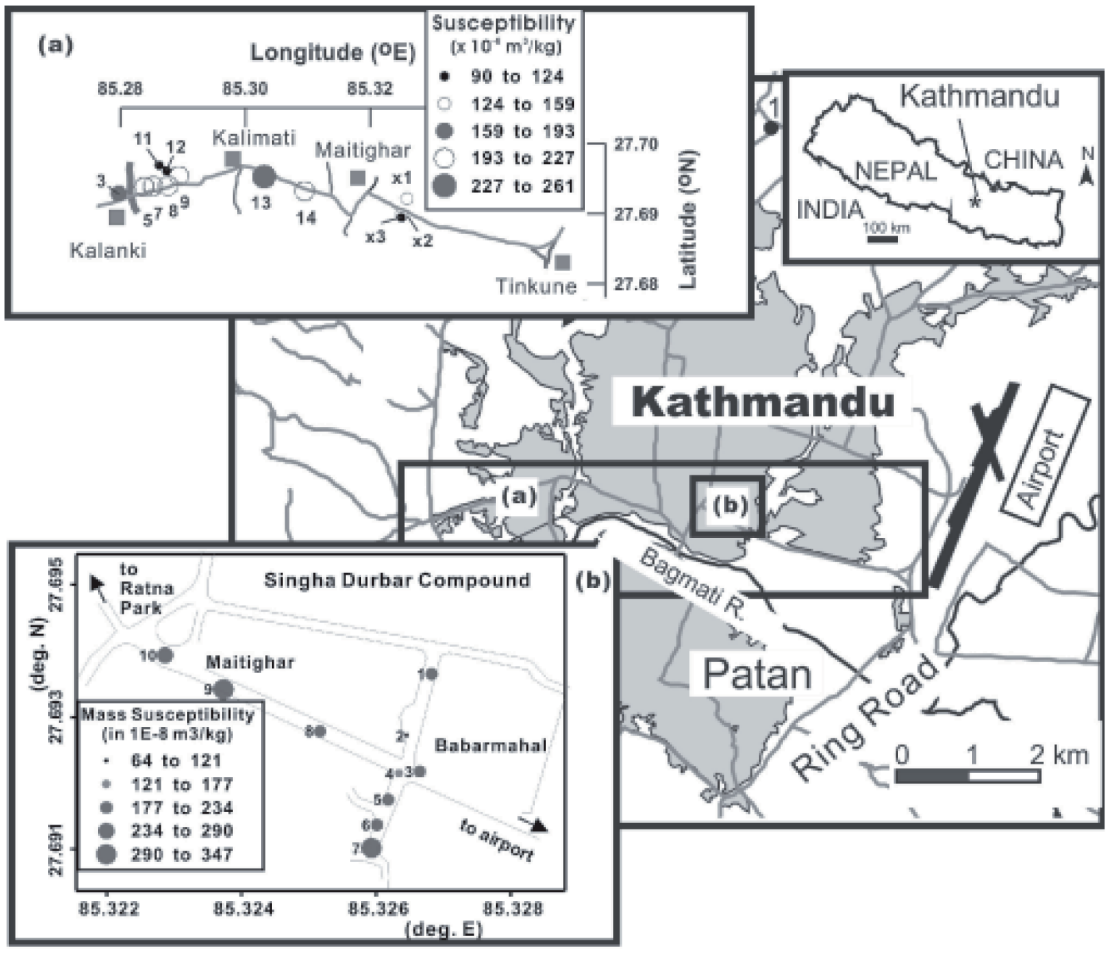

Fig. 1: Sketch map of the Kathmandu city after Shrestha and Pradhan (2000), showing the main urban area (shaded) and the areas sampled for street dust. (a) Locations of leaf-dust samples, mainly along the Kalanki–Tinkune Road (points 3-14, representing DS3–DS14, and X1–X3) and at Basundhara, Ring Road (Point 1). These are shown by symbols (solid and open circles) with size proportional to the magnitude of the low-field mass-specific magnetic susceptibility (χ_{lf}). (b) Locations of road dust samples in the Maitighar–Babarmahal area. The size of the location symbols is proportional to the magnitudes of magnetic susceptibility (χ), as given in the accompanying legend.

sieves. The grain size analysis (Fig. 2) of several leaf-dust (DS) samples by a laser diffraction analyser (Malvern Master Sizer Micro) revealed them to be rather fine with their median particle size ca. 30 μm and ca. 80% (by volume) of particles falling into the clay fraction (<.063 mm). The lognormal distribution of grain size for DS13 reveals that the predominant mode (with 89% of grain size) satisfies a Gaussian curve defined by a median of 35.5 μm and a logarithmic dispersion parameter $\log_{10}$(DP) of 0.28 μm (Kruiver et al. 2001).

For the measurement of magnetic susceptibility and remanence, the samples (also fractions, in case of RD) were transferred to standard containers (cylinders with 2.54-cm diameter and 10-cc volume). The susceptibility was measured on AGICO KLY-2 Kappabridge with an operating frequency of 920 Hz and sensitivity of 4×10^{-8} SI, and normalised by the sample mass to obtain the mass-specific susceptibility (χ). A Bartington MS2B dual-frequency sensor was used to measure the susceptibility magnitudes in a low frequency (0.47 kHz) χ_{lf} and a high frequency (4.7 kHz) χ_{hf}; the frequency-dependent susceptibility (χ_{fd}) was then calculated as $(\chi_{lf} - \chi_{hf})/\chi_{lf} \times 100\%$. The measurement of isothermal remanence (IRM), anhysteretic remanent magnetisation (ARM), and variation of susceptibility with temperature (-194 to 0 °C and 40 to 700 °C) were made using the standard procedure (Gautam et al. 2004). Magnetic grains were separated from the samples using a hand magnet and then were subjected to scanning electron microscopic and X-ray analyses. Chemical analysis for contents of HM (Cd, Cu, Co, Cr, Mn, Ni, Pb, Zn and Fe) was carried out using a Perkin-Elmer M1100 atomic absorption spectrophotometer on 13 DS samples and 21 RD samples (7 each from coarse, intermediate, and fine fractions) digested by aqua regia in a Kjeldatherm system (at 140 °C, for 2 hours) following Gautam et al. (2005b).

RESULTS OF LEAF-DUST ANALYSIS

Susceptibility and artificial remanence data

The value of χ for 14 samples ranged from 0.9×10^{-6} to 2.6×10^{-6} m^3/kg (Figs. 1 and 3a). The sites located at secondary roads or at a greater distance from the major road yielded distinctly lower values (i.e., $<1.5 \times 10^{-6}$ m^3/kg). The value of χ_{fd} was <4.4% and showed an inverse relationship with χ_{lf} except for Sample 13 (Fig. 3a).

The IRM analysis of 5 samples revealed two components differing in magnetic hardness. For Sample DS1, representative of the whole set, the soft component was contributed by low coercivity phases (median acquisition field $B_{1/2}$ = 48 mT, logarithmic dispersion parameter corresponding to 1-standard deviation DP = 0.33), while the hard component of high coercivity phase had $B_{1/2}$ of 631 mT

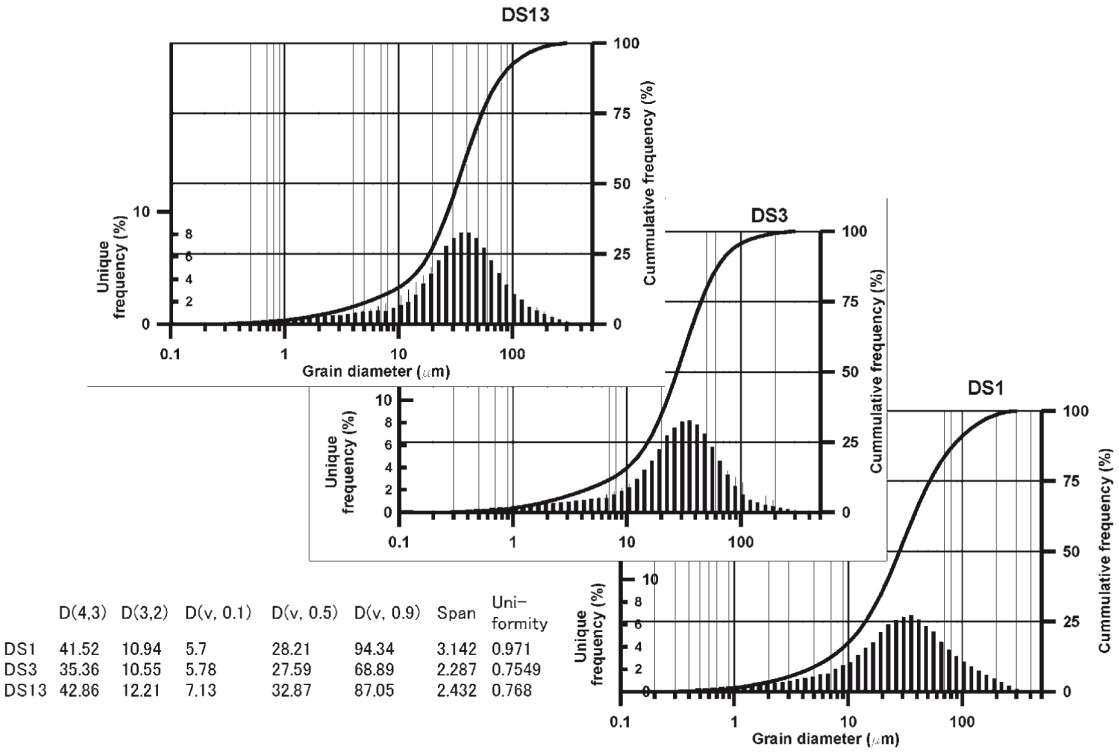

	D(4,3)	D(3,2)	D(v, 0.1)	D(v, 0.5)	D(v, 0.9)	Span	Uni-formity
DS1	41.52	10.94	5.7	28.21	94.34	3.142	0.971
DS3	35.36	10.55	5.78	27.59	68.89	2.287	0.7549
DS13	42.86	12.21	7.13	32.87	87.05	2.432	0.768

Fig. 2: Results of grain-size analyses of representative leaf-dust samples. Note a rather narrow median grain size range of 28–33 μm and a high uniformity coefficient (0.75).

and DP of 0.25 (Fig. 3b). The soft component is dominant with 85–91% of the total IRM ($IRM_{2.5T}$ or SIRM). Its estimate is practically identical (within ± 1%) to the $IRM_{0.3T}/IRM_{2.5T}$ ratio (Fig. 3c). Both SIRM and soft component exhibit an excellent linear correlation ($R^2 = 0.993$) to χ_{lf}. The best-fit line gives a slope or $SIRM/\chi_{lf}$ ratio of 11004 A/m, a value which is very close to 10,000 A/m reported for magnetite having the effective grain size of 5 μm (Thompson and Oldfield 1986, p. 31) implying that a relatively coarse magnetite-like phase contributes to most of the observed magnetic signal (Fig. 3c).

The remanence coercivity during DC backfield demagnetisation ranged between 37 and 40 mT for all samples except for DS13 (34 mT). The observed highest contribution of soft component, relatively lower coercivity of remanence, and χ_{lf} > 4% for Sample DS13 indicate the presence of some ultrafine (<0.03 μm) superparamagnetic grains of ferrimagnets (for magnetite, <0.04 μm at room temperature: Dunlop and Özdemir 1997; Muxworthy et al. 2002). Such ultrafine ferromagnetic particles (<100 nm or finer than PM10) are considered inhalable, deep into the unciliated and alveolar sections of the lungs, and are of serious health concern (Matzka and Maher 1999). The ARM magnitudes for 3 samples (DS3, DS13, X3) with widely differing susceptibilities also varied linearly with χ_{lf}. The SIRM/ARM ratio ranged between 76 and 92. The median destructive field of ARM (MDF_{ARM} = the peak demagnetising field that corresponds to the decay of half of the ARM magnitude) was ca. 21 mT pointing to identical magnetic stability for all samples.

Thermal variation of the magnetic susceptibility

The high-temperature susceptibility versus temperature curves illustrated in Fig. 4a, reveal: (i) a low-amplitude susceptibility rise and fall between ca. 265–360 °C with a maximum at ca. 285 °C. (This feature reappears upon second heating though with a lesser amplitude.); (ii) another much more remarkable and asymmetric susceptibility rise and fall between ca. 455–590 °C with a maximum at ca. 520 °C. Feature (i) is interpreted as characteristic of maghemite-like phase (Gautam et al. 2004). For feature (ii), a Curie temperature of ca. 578 °C marking the initiation of the linear relationship between the susceptibility and temperature (Fig. 4b) as a marker of transition from ferromagnetic to paramagnetic behaviour (Petrovsky and Kapička 2006) and the low-

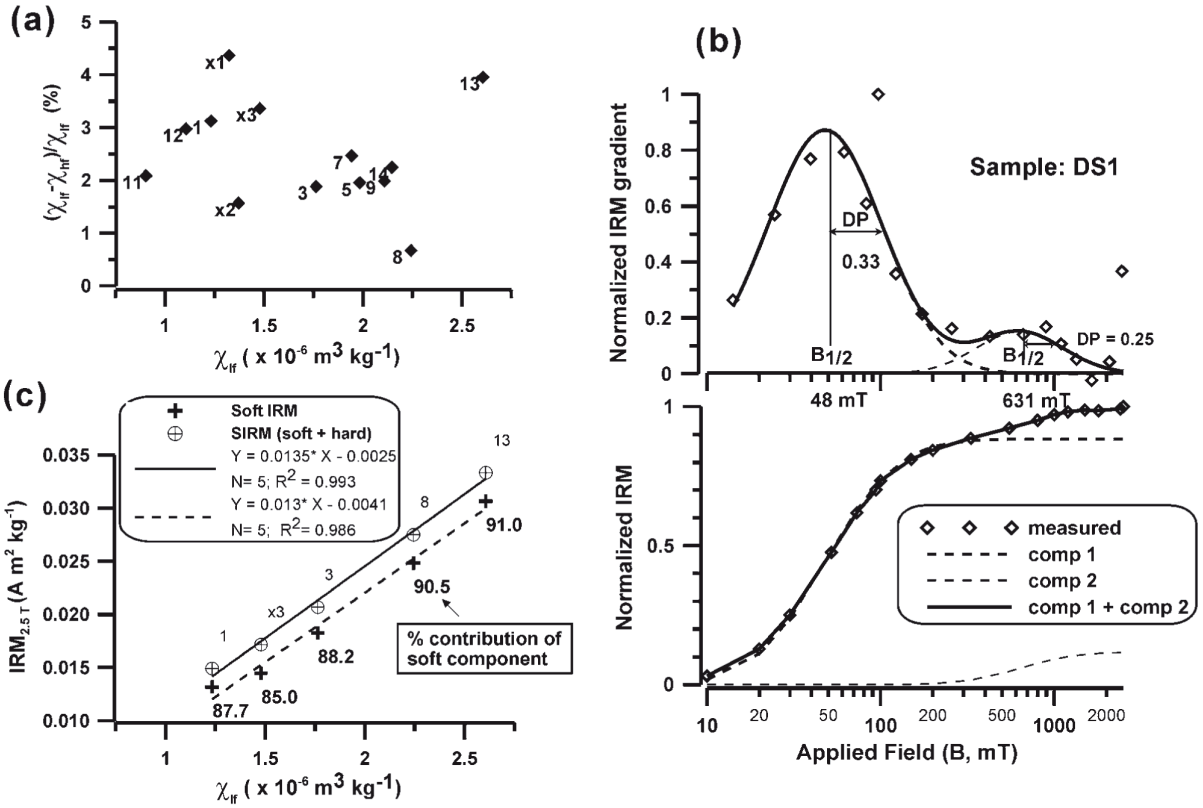

Fig. 3: Susceptibility and isothermal remanent magnetization (IRM) data for the leaf-dust samples: (a) percent frequency dependence of magnetic susceptibility; (b) results of IRM component analysis for a representative sample; and, (c) IRM vs. magnetic susceptibility.

temperature transitions (Fig. 4c) confirm the presence of pure magnetite.

Microscopic and chemical characterisation of magnetic constituents in the leaf dust

The magnetic particles in the magnetic extracts of leaf-dust samples can be morphologically grouped into 3 types: (i) euhedral to anhedral crystalline grains, (ii) solitary spherical grains exhibiting orange peel and (or) framboidal textures, and (iii) agglomerates formed apparently by welding of subspherical grains, which occasionally show the presence of holes or cavities in them (Fig. 5). As shown in Table 1, the apparent longer dimension of type (i) grains has a range of 7.5–49.5 μm. In contrast, a much smaller range of 3.6–22.0 μm characterises the diameter of grains of type (ii) and individual grains constituting type (iii). The spherical grains contain up to 77 wt% of iron and corresponding 23 wt% of oxygen (Table 1). The octahedral crystals, typical of magnetite, yield up to 74 wt % of iron. Agglomerates contain Ca, S, and Cl. Significantly lower values of Fe in many non-spherical grains, especially when accompanied by Mg, Al, Si, Ti, etc in significant amounts, may arise from the contamination of the analysed spots by background silicate material.

Heavy metals in leaf dust and their relationship with magnetic susceptibility (χ)

The contents of HM, presented together with χ, yield the following: Fe (1.88–2.20 wt%), Mn (329–467 mg/kg), Zn (155–302 mg/kg), Pb (22–86 mg/kg), Cu (38–76 mg/kg), Cr (22–32 mg/kg), Ni (17–26 mg/kg), Co (1–9 mg/kg) and Cd (< 1 mg/kg). The values of χ, Zn, Cu, and Pb are remarkably variable and are strongly correlated (Table 2 and Fig. 6). Despite the low variability, Cr and Ni contents also show an excellent correlation ($R^2 = 0.98$).

RESULTS OF ROAD SEDIMENT ANALYSIS

Susceptibility and artificial remanence data

For bulk samples of road sediment, χ_{lf} had a range of 0.64×10^{-6}–3.47×10^{-6} m^3/kg. The average value of χ_{lf} was 2.28×10^{-6} m^3/kg whereas the minimum value was observed in Sample RD2. The average value of χ_{lf} in the fine, medium, and coarse fractions was respectively 121%, 115%, and 68% of the total value for the bulk sample. The value of χ_{fd} for bulk samples and fractions was below 1.8%, being too low to judge the presence of detectable amount of ultrafine particles. The value of χ_{lf} was practically insignificant for the fine and medium fractions in half of the collected samples. The anomalously low value of χ_{lf} for Sample RD2 probably resulted due to cleaning, as it was located close to the entrance of several public institutions. The SIRM magnitudes showed a behaviour similar to that of χ, with Sample RD2 having the lowest concentration of magnetic material. The relative concentration of magnetic minerals at various sites is proportional to the average of fine and medium fractions. The ARM magnitude, an indicator of the concentrations of a

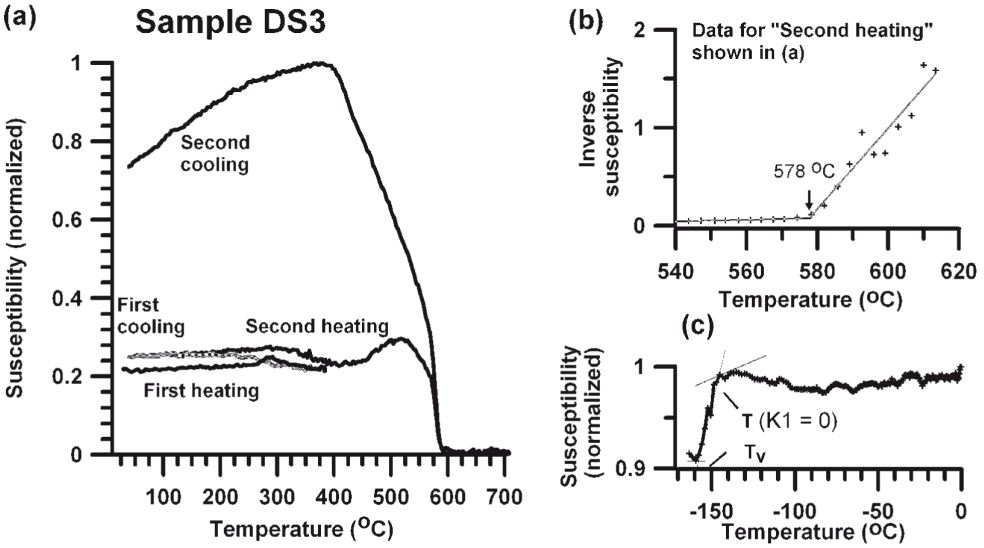

Fig. 4: Variation of susceptibility with temperature. (a) Heating–cooling cycles in high temperature range. (b) Plot of inverse susceptibility vs. temperature data obtained during the second heating between 540 and 620 °C to find the transition from ferromagnetic to paramagnetic behaviour by fitting lines to data segments. The transition at 578 °C corresponds to the Curie point of magnetite. (c) The low-temperature run showing the Verwey transition (Tv) and the zero point of crystalline anisotropy constant T(K_1=0) further supports the presence of the magnetite-like phase as a dominant magnetic constituent.

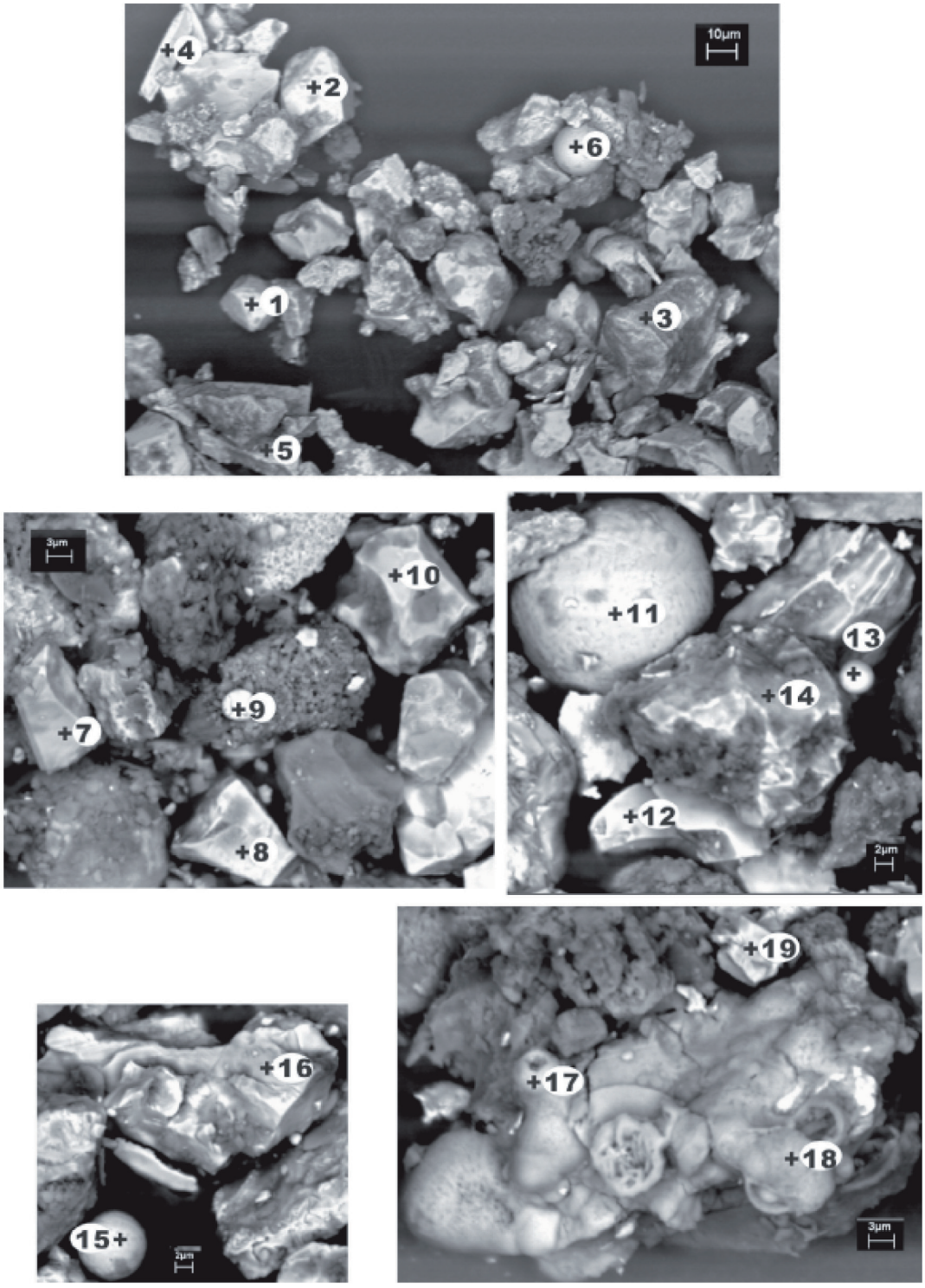

Fig. 5: Magnetic grains observed by scanning electron microscopy from a magnetic extract from a single sample (DS3) of leaf dust. The numbered grains were analysed by energy dispersive X-ray techniques and their chemistry is shown in Table 1). There are two distinct types of grains – spherules of anthropogenic origin (grains 6, 9, 11-13, 15 and 17-18; shaded columns in Table 1) and non-spherical, euhedral to subhedral grains of probably lithogenic origin.

Table 1: Energy dispersive X-ray analytical data (wt %) on magnetic mineral grains constituting the dust sample from site DS3

Grain no.[a]	1	2	3	4	5	**6**	7	8	**9**	10	**11**	**12**	**13**	14	**15**	16	**17**	**18**	19
d (micron)	19.3	33.6	27.7	32.2	49.5	**18.0**	16.6	12.5	**3.9**	17.3	**22.0**	**14.2**	**3.6**	25.2	**7.3**	10.8	**4.6**	**7.6**	7.5
Element																			
Fe	73.98	69.37	71.46	76.56	75.21	**75.86**	41.68	58.47	**73.93**	77.01	**75.8**	**73.4**	**72.66**	69.13	**76.9**	75.22	**56.02**	**66.69**	67.65
Na								0.26									**1.03**		
Mg		0.18	0.15					0.24						0.33			**0.39**		
Al	0.41	1.83	0.76	0.14	0.53	**0.4**	0.24	4.11	**0.08**	0.24	**0.61**	**0.28**	**0.84**	1.06	**0.22**	0.74	**1.65**	**1.14**	1.57
Si	0.63	2.53	1.65	0.13	0.83	**0.24**	0.54	4.78	**0.3**	0.23	**0.63**	**0.88**	**1.59**	2.25	**0.29**	0.86	**4.55**	**1.54**	2.17
K		0.48	0.31		0.16			1.02						0.37			**0.46**		0.37
Ti						**0.69**		1.88											
Ca	0.18	0.34	1.01		0.21		0.29	0.76	**0.53**			**0.41**	**1.08**	0.58			**3.48**	**1.6**	1.09
Cr		0.38		0.66				0.27	**0.21**										
Mo			0.7						**0.33**										
Co	0.68																		
Br																			
Tb	1.38								**1.68**			**2.25**		2.12					2.95
Mn									**0.47**										
S							17.32										**2.71**	**1.9**	
P																		**0.36**	
Po							1.02												
Cl								0.2									**0.88**	**0.94**	
O	22.74	24.9	23.95	22.51	23.07	**22.82**	38.9	28	**22.46**	22.53	**23**	**22.8**	**23.82**	24.16	**22.6**	23.18	**28.84**	**25.82**	24.2
Total	100	100	99.99	100	100.01	**100**	99.99	99.99	**99.99**	100	**100**	**100**	**99.99**	100	**100**	100	**100**	**99.99**	100

[a] Locations of analysed point numbers are given in Fig.4. Numbers in bold correspond to grains of definitely anthropogenic origin.

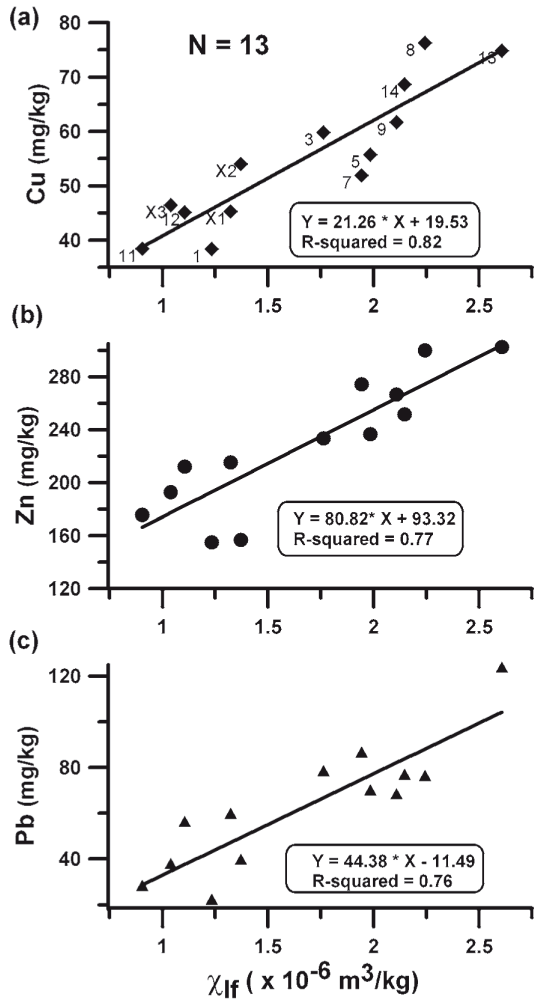

Fig. 6: Relationship between magnetic susceptibility (χ) and the contents of Zn, Cu, and Pb in leaf-dust samples. The linear-regression lines and the equations describing them are also given along with the correlation coefficient (R^2).

stable single domain (and a fine pseudo-single domain) ferromagnetic component, varied inversely with the grain size of the fractions. RD5–RD7 bulk samples contain a relatively high proportion of the soft coercivity material residing in the coarser fraction (≥ 0.63 mm).

The value MDF_{ARM} for the fine fraction of fine sediment samples was 18.0–23.3 mT. The coercivities of remanence (B_{cr}), based on DC back-field IRM destruction, for fine, medium, and coarse fractions were 28.4–31.8 mT, 28.9–33.5 mT, and 28.8–34.5 mT, respectively. RD2 was found to have relative enhancement of magnetic susceptibility, IRM, and ARM, indicating that this site indeed is enriched in finer particles with a higher concentration of a magnetic phase showing soft coercivity. In contrast, RD7 shows the presence of a relatively higher amount of high-coercivity material, as shown by IRM analysis for relative contribution of the soft and hard coercivity phases.

Heavy metal (HM) contents and their relation to magnetic susceptibility

The HM contents in road sediment decreased with the size of analysed fractions. In comparison with the coarse fraction, the medium and fine fractions are enriched in HM by 200% and 225% respectively. Such a variability is partially illustrated in Pb, Zn, and Fe contents versus χ_{lf} plots (Fig. 7). The HM contents in fine fractions decrease in the following order: Fe (1.37–1.82 wt%), Mn (245–375 mg/kg), Zn (92–161 mg/kg), Cu (31–75 mg/kg), Pb (24–55 mg/kg), Cr (11–23 mg/kg), Ni (13–18 mg/kg), Co (3–6 mg/kg), and Cd (<1 mg/kg). It is noteworthy that only Cu content is significantly linearly related with χ (Fig. 8). Concerning the mutual relationships (not illustrated in this paper), among the heavy metals, Fe and Mn showed an excellent correlation with each other and a good correlation with Cr. Also, a negative correlation was found between Cu and Cr contents. These data imply that the use of magnetic susceptibility as a heavy metal proxy is limited only to Cu as far as the road sediment is concerned.

INTERPRETATION AND DISCUSSION

The susceptibilities of the bulk samples of leaf dust (χ = 0.9–2.6 × 10^{-6} m^3/kg) and road sediment (0.64–3.47 x 10^{-6} m^3/kg) show a significant overlap. Also, the susceptibility range observed in the street dust is smaller than that exhibited by the urban and suburban soils (3.5–637.5 x 10^{-8} m^3/kg; Gautam et al. 2005a) in Kathmandu. However, even the weakest samples are at least an order of magnitude stronger than the most magnetic natural black clay or silt sediments in the Northern part of the Kathmandu valley (average χ = 8.5 x 10^{-8} m^3/kg: see Gautam et al. 2001). The magnetic extracts of the roadside material such as leaf dust from rubber trees (this study) and dust from the leaves growing at 2.0–2.5 m heights (Gautam et al. 2004, 2005a) contain magnetic grains derived from geogenic and anthropogenic processes. The geogenic minerals exhibit euhedral to anhedral crystals with a long dimension commonly >10 μm, whereas the anthropogenic phase is represented by spherules of commonly 2–20 μm in diameter as well as agglomerates that resemble clusters of welded spherules with the long dimensions reaching over 100 μm. Energy dispersive X-ray data on most grains (of both lithogenic and anthropogenic origin) contain commonly 73–77 wt% of Fe indicative of magnetite composition. The presence of magnetite-like and haematite-like phases is suggested by IRM data, whereas the presence of pure magnetite-like phase and maghemite-like phase is inferred from thermal behaviour of susceptibility. Brick

Table 2: Correlation matrix for magnetic susceptibility (χ_{lf}) and heavy metal contents in leaf-dust samples (N = 13)

	MS	Fe	Mn	Zn	Cu	Pb	Cr	Ni	Co
MS	1.00								
Fe	0.15 (0.625)	1.00							
Mn	0.47 (0.109)	0.48 (0.101)	1.00						
Zn	**0.88 (0.000)**	0.27 (0.371)	**0.66 (0.014)**	1.00					
Cu	**0.91 (0.000)**	0.05 (0.882)	0.40 (0.170)	**0.82 (0.001)**	1.00				
Pb	**0.87 (0.000)**	0.2 (0.523)	**0.58 (.036)**	**0.90 (.000)**	**0.79 (0.001)**	1.00			
Cr	0.24 (0.432)	-0.06 (0.841)	0.03 (0.920)	0.15 (0.624)	0.06 (0.854)	0.15 (0.618)	1.00		
Ni	0.40 (0.175)	-0.04 (0.901)	0.07 (0.809)	0.27 (0.381)	0.21 (0.499)	0.28 (0.351)	**0.98 (0.000)**	1.00	
Co	-0.28 (0.357)	0.14 (0.651)	-0.41 (0.161)	-0.35 (0.243)	-0.21 (0.500)	-0.17 (0.576)	-0.26 (0.392)	-0.32 (0.293)	1.00

For each pair, the Pearson's product-moment correlation r is given with the level of significance p (in brackets). Correlations significant at p < .050 are shown in boldface.

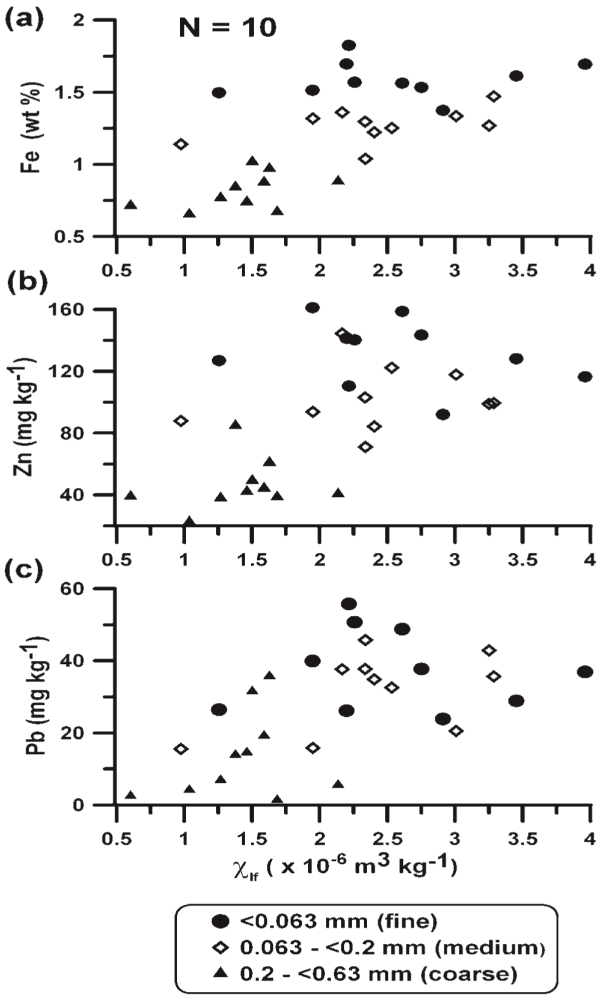

Fig. 7: Variations of the contents of selected heavy metals with magnetic susceptibility in different grain size fractions of the road dust.

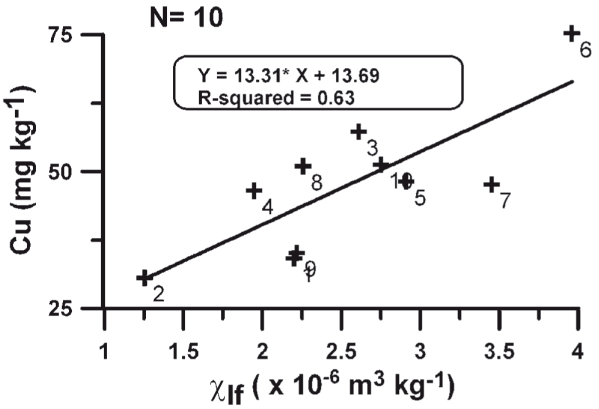

Fig. 8: Relationship between χ_{lf} and the Cu content in fine fraction of road sediment

particles known to contain maghemite-like phase along with very soft coercivity magnetite, as well as the soot from the tailpipe of vehicles and cement characterised by the abundance of magnetite-like phases contribute at least partly to the magnetic material in the street dust (Gautam et al. 2005a).

In road sediments, the concentration of Fe diminishes with decreasing grain size. For the urban elements (Zn, Cu and Pb; De Miguel et al. 1997), however, the concentrations in fine and medium fractions often overlap. Therefore, it seems logical to use the fraction finer than <0.2 mm for HM content characterisation in road sediments. The leaf dust was 1.5 to 2 times more enriched in HM than the road dust. Unlike the leaf dust showing a good to excellent (R^2 = 0.76–0.82) linear relationship of susceptibility with Zn, Cu and Pb, the road sediment susceptibility correlated reasonably well (R^2 = 0.63) only with Cu content (Fig. 8). We note that this observation is in contrast with the findings from the Dhaka city, where the analyses of street dust from the industrial areas with a medium traffic density, commercial areas with a high traffic density, and residential areas with a low traffic density were correlated with elevated concentrations of Pb,

Zn, Cu, Ni, and Cr (Ahmad and Ishiga 2006). The elevated concentrations of Pb and Zn were mostly attributed to automobiles, whereas that of others (i.e., Cu, Ni and Cr) to the combined effects of urbanisation, industrialisation, and vehicular movement. Considering the present study, however, the use of magnetic susceptibility of road sediments to predict metal enrichment or the quantification of pollution may be limited. Due to the site-dependent variation in dust input from multiple factors (natural, biological etc.) controlling the deposition and removal, road sediment samples are suitable mainly for judging the site-specific level and nature of the metallic contamination.

CONCLUSIONS

The samples of leaf dust from <1 m height may be equated to those recovered from passive roadside samplers installed at a waist height. Hence, the integration of these data with those of dust from tree leaves (from a relatively larger height of ca. 2–2.5 m) can better reveal the spatial variation of heavy metal pollution in urban road corridors.

Magnetic susceptibility and isothermal remanence measured in vertical soil profiles in urban and suburban areas serve as the proxy of cumulative pollution load index (PLI) based on heavy metal contents resulting from the long-term (from years to decades) accumulation of contaminants. In contrast, the magnetic susceptibility of the dust accumulated in leaves growing at a height of decimetre to several metre and the magnetic material contained in it reflect the effect of anthropogenic pollution over shorter time-scales (several months to a particular season). This method represents an effective magnetic biomonitoring technique aimed at periodic (seasonal or half-yearly) screening of the vehicular pollution. Likewise, in situ susceptibility screening is suited for rapid and cost-effective environmental screening of the level of contamination of road corridors or other urban locales, such as parks close to roads with heavy traffic or areas in the vicinity of industries.

ACKNOWLEDGEMENTS

This study was initiated under a collaborative research programme between the University of Tuebingen, Germany, and Tribhuvan University, Nepal, under a Georg Forster Research Fellowship granted to PG by the Alexander-von-Humboldt Foundation. Further work was done at Hokkaido University, Japan, under a 21st century COE Programme for the Neo-Science of Natural History and a JSPS Grant-in-aid for Scientific Research (*kakenhi kiban C*: No. 17540427).

REFERENCES

Ahmad, F. and Ishiga, H. 2006, Trace metal concentrations in street dusts of Dhaka city, Bangladesh. Atm. Environment, v. 40, pp. 3835–3844.

Al-Rajhi, M. A., Al-Shayeb, S. M., Seaward, M. R. D., and Edwards, H. G. M, 1996, Particle size effect for metal pollution analysis of atmospherically deposited dust. Atm. Environment, v. 30(1), pp. 145–153.

De Miguel, E, Llamas, J. F., Chacón, E., Berg, T., Larssen, S., Royset, O., and Vadset, M., 1997, Origin and patterns of distribution of trace elements in street dust: unleaded petrol and urban lead. Atm. Environment, v. 31(17), pp. 2733–2740.

Dunlop, D. and Özdemir, O., 1997, Rock magnetism – fundamentals and frontiers. Cambridge University Press, Cambridge.

Faiz, A., Ale, B. B. and Nagarkoti, R. K., 2006, The role of inspection and maintenance in controlling vehicle emissions in Kathmandu Valley, Nepal. Atm. Environment, v. 40, pp. 3835–3844.

Gautam P., Blaha, U., and Appel, E., 2005a, Magnetic susceptibility of dust-loaded leaves as a proxy of traffic-related heavy metal pollution in Kathmandu city, Nepal. Atm. Environment, v. 39, pp. 2201–2211.

Gautam, P., Blaha, U., and Appel, E., 2005b, Integration of magnetism and heavy metal chemistry of soils to quantify the environmental pollution in Kathmandu, Nepal. The Island Arc, v. 14, pp. 424–435.

Gautam, P., Blaha, U., Appel, E., and Neupane, G., 2004, Environmental magnetic approach towards the quantification of pollution in Kathmandu urban area, Nepal. Phys. and Chem. of the Earth, v. 29, pp. 973–984.

Gautam, P., Hosoi, A., Sakai, T., and Arita, K., 2001, Magneto-stratigraphic evidence for the occurrence of pre-Brunhes (>780 kyr) sediments in the northwestern part of the Kathmandu Valley, Nepal. Jour. Nepal Geol. Soc., v. 25, pp. 99–109.

Hopke, P. K., Lamb, R. E., and Natusch, D. F. S., 1980, Multielemental characterization of urban roadway dust. Env. Sci. and Tech., v. 14, pp.164–172.

Kruiver, P. K., Dekkers, M. J., and Heslop, D., 2001, Quantification of magnetic coercivity components by the analysis of acquisition curves of isothermal remanent magnetization. Earth Planet. Sci. Lett., v. 189, pp. 269–276.

Matzka, J. and Maher, B. A., 1999, Magnetic biomonitoring of roadside tree leaves: identification of spatial and temporal variations in vehicle-derived particulates. Atm. Environment, v. 33, pp. 4565–4569.

Muxworthy, A. R., Schmidbauer, E., and Petersen, N., 2002, Magnetic properties and Mössbauer spectra of urban atmospheric particulate matter: a case study from Munich, Germany. Geophys. Jour. Int. v. 150, pp. 558–570.

Petrovsky, E. and Kapička, A. 2006, On determination of the Curie point from thermomagnetic curves. Jour. Geophys. Res. 111 (B12S27), doi:10.1029/2006JB004507.

Sharma, T., Rainey, R. C., Neumann, C. M., Shrestha, I. L., Shahi, K. B., Shakya, A., and Khatri, S., 2002, Roadside particulate levels at 30 locations in the Kathmandu Valley, Nepal. Int. J. Environment and Pollution, v. 17(4), pp. 293–305.

Shrestha, B. and Pradhan, S., 2000, Kathmandu Valley GIS database. ICIMOD, Kathmandu.

Thompson, R. and Oldfield, F., 1986, *Environmental Magnetism.* Allen & Unwin, London.

Tokahoglu, S. and Kartal, S., 2006, Multivariate analysis of the data and speciation of heavy metals in street dust samples from the Organized Industrial District in Kayseri (Turkey). Atm. Environment, v. 40, pp. 2797–2805.

4

Magnetic response to atmospheric heavy metal pollution recorded by dust-loaded leaves in Shougang industrial area, western Beijing

Chinese Science Bulletin

ARTICLES

Magnetic response to atmospheric heavy metal pollution recorded by dust-loaded leaves in Shougang industrial area, western Beijing

HU ShouYun[1,5†], DUAN XueMei[1,2], SHEN MingJie[3], U BLAHA[4], W ROESLER[4], YAN HaiTao[1,2,4], E APPEL[4] & V HOFFMANN[4]

[1] State Key Laboratory of Lake Science and Environment, Nanjing Institute of Geography and Limnology, Chinese Academy of Sciences, Nanjing 210008, China;
[2] Graduate University of Chinese Academy of Sciences, Beijing 100049, China;
[3] Department of Geography, East China Normal University, Shanghai 200062, China;
[4] Institute for Geosciences, University of Tübingen, 72076 Tübingen, Germany;
[5] Department of Geography, Shanghai Normal University, Shanghai 200234, China

Fifty-five evergreen tree's leaves growing less than one year were collected from Shougang industrial area in western suburb of Beijing, including steel plants and its ambient residential areas, recreational parks and farmlands. Rock magnetic properties and heavy metal contents were studied. The results show that the magnetic properties of leaf samples are predominated by low-coercivity magnetite, and both the concentration and grain size of magnetite particles gradually decreased with the distance from the main pollution source increases. Moreover, there is a significant linear relationship between magnetic parameters (the low-field magnetic susceptibility, saturation isothermal remanent magnetization and anhysteretic remanent magnetization) and heavy metals contents (Fe, Pb, V, Cr and Zn) ($0.73 \leqslant R \leqslant 0.88$). Hence, the magnetic parameters of leaves can serve as a proxy for quick detecting of the recent atmospheric metallic pollution.

Shougang industrial area, tree leaves, magnetic parameters, heavy metal contents

GEOPHYSICS

In the last few years, rapid development in industry has caused serious impacts to air quality due to the discharge of exhaust gases and dusts derived from combustion processes. Especially, atmospheric heavy metal pollution still is a major problem for the urban environment, as well as the economical and social development[1].The greatest health impacts may come from the fine-grain particulate material with sizes less than 10 μm, which can be inhaled deeply into the alveolar sections of the lungs, injuring the lung's function, and causing diseases, such as pneumonia of the respiratory system, even threatening human life[2]. Therefore, it is of significance both in science and in practice to learn and monitor air pollution in urban and industrial areas.

There are different objects and methods used for studying atmospheric heavy metal pollution. The use of high volume active air samplers equipped with filters is very common, yet expensive and time-consuming. Additionally, filters appear to be inefficient collectors for the smallest particles. Establishing a dense grid of atmospheric dust filters for particle investigations is a rather time consuming and costly work, and it is very difficult to apply on a large scale[3]. Collecting street dust is less expensive. Street dust, however, will likely contain larger particles, which is not airborne and poses little health risk[4–6]. Soils as a pollution receptor reflect

Received September 6, 2007; accepted January 2, 2008
doi: 10.1007/s11434-008-0140-9
†Corresponding author (email: hu_shouyun@hotmail.com)
Supported by the National Natural Science Foundation of China (Grant Nos. 40374021, 40674033, 40172102) and DFG project (AP 34/21)

a relatively long pollution history (accumulating within years, decades, and even longer time); in addition, the signal of the geological background is highly variable in a large areas and the urban soil is strongly influenced by anthropogenic input. All this creates difficulties in sampling. Thus, it is a challenge to select new scientific research targets, and to search for new working methods for investigating atmospheric heavy metals pollution efficiently and economically.

In the last few years, magnetic monitoring of tree leaves has been used as a target for studying air pollution, which is one of the new developments of environmental magnetism. Several magnetic studies on tree leaves[7−14] have shown that there is some certain correlation between regional air quality and magnetic properties of tree leaves along traffic lines and in industrial areas, and magnetic variation can reflect the changes of the current atmosphere quality. Thus, it can be taken as a proxy during pollution study. Leaves have many advantages in monitoring atmospheric heavy metal pollution. First, leaves have a large surface area per unit weight and a certain long lifespan. Its wax layer can directly absorb and keep dust, suspended particles and non-volatile organic compounds. Especially, it can easily capture the particulates less than 10 μm, which then can transfer to the inner layer from epidermis by diffusion; second, the magnetic particles absorbed from the roots and soils can be neglected compared to those come from leaf wax layers. So, the biological background of tree leaves is very low. Furthermore, leaves are widely distributed and available, and therefore, are convenient for high density sampling and can provide a high-resolution map of air pollution in urban areas[15,16].

In this article, biomonitoring of air pollution around Steel Group has been conducted based on the magnetic properties of evergreen tree leaves which offer a good coverage of both steel work and its ambient areas, including residential areas, recreational parks and some farmland in the western suburbs of Beijing. The aim of this work is to find out the relationship between magnetic properties and heavy metals in the studied areas, and to test the validity of the method for quantifying the environmental pollution state, and finally to provide and improve a new, fast and effective method for heavy metal pollution assessment.

1 Material and methods

1.1 Location of sampling area

Shougang Groups are located in the Shijingshan industrial area, including a series of branch steel factories, heating and power plants and other companies. The site is about 17 km west of the Tian An Men Square away and has caused serious impacts to air quality of Beijing (due to the waste discharges from all kinds of production equipments with high energy consumption, high water consumption and high discharges. The topography of Beijing area is variable. In the western and north-western parts there are dotted hills with relatively higher elevation, whereas, the city centre and eastern areas are a plain basin. The exhaust gas from steel production is further aggravated because of the topography in Beijing. Moreover, the wind direction shows an obviously seasonal variation: north and north-west winds are prevalent during the winter half year, whereas the south wind is prevalent in the summer half year. Owing to the topography and climatic condition, the pollutants derived from Shougang industrial area will be released to most parts of Haidian District and city center areas even to Chaoyang District (east of Beijing), especially when the west wind is prevalent. The studied region covers a large area limited by the Yongding River in the west and south, the west Fifth Ring in the east and west, and Badachu and Fahai Temple in the north), covering Shougang industrial area and its ambient residential areas, the recreational parks and the farmland in western suburb.

1.2 Sampling methods

Samples were taken at intervals of 1—2 km to ensure a systematic investigation integrated with a GIS-database. It was necessary to sample three different species of trees: *Sabina chinensis*, *Pinus bungeana* and *Chanaecyparis obtusa*, in order to ensure wide and homogeneous sampling coverage within the studied area. These evergreen trees were selected because of the long- term accumulation of heavy metal in leaves during the whole year. To minimize weather effects on accumulation and abrasion, the leaves were taken in clear days (April in 2004) and at least 2 weeks after rainfall. To further avoid climatic effects and to increase sample efficiency, two sampling teams operating by cars made it possible to take all the samples within two days. At each location a composite sample was collected to reduce the local

s of leaf canopy structure and resulting bias due to sure direction. Composite samples contain leaves different directions around the same tree and only ess than one-year old tree leaves or newest twig n on the branch were collected. Each sample was from the outer canopy at a convenient sampling t of 1.5 m above the ground to minimize pollutants ng from the ground. In addition, to avoid in- ollution during sampling, new one-off gloves were for each sampling procedure. Samples were imme- y put into pocket-sized sealable plastic bags and ing drying at 40℃ in the lab before measure- s.

Analysis methods

agnetic measurements were conducted on leaf ma- directly, except for the measurement of tempera- lependent susceptibility, where the dusts dropped leaves after drying at 40℃ were used. Mass mag- susceptibility (χ) was measured using a KLY-3S abridge. Laboratory-induced anhysteretic remanent etization (ARM) was measured using a 2G-719 alternating magnetometer with imparted 100mT alternating fields (AF) and a 50 μT direct current bias field parallel to the AF. IRM was generated IMPM9 pulse magnetometer. IRM acquired in a of 1.5 T is regarded as saturation IRM (SIRM). S is defined as the ratio of IRM at a backfield of 0.3T s SIRM. All magnetic measurements of ARM and were carried out on a 2G-755 R SQUID magne- er. Temperature dependent susceptibilities were ured with a KLY-3S Kappabridge with an attached high-temperature furnace in argon atmosphere, gh temperature cycles from room temperature to and back to room temperature (the interval of erature reading 2℃, heating rate: 8—10℃/min). low-temperature dependent susceptibilities, the les were cooled down to −196℃ by liquid nitrogen, emperature cycles from −196℃ to room tempera- were recorded. All magnetic measurements were ucted in the paleomagnetism lab of the University bingen in Germany.

r elemental analysis: unwashed leaf samples were at 40℃ and dissolved using $HClO_4$ + HNO_3 + HCl. concentrations of Fe, Pb, Cr, V and Zn were de- ned by inductively coupled plasma-mass spec- try (ICP-AES). Accuracy is within 5% for all ele- ments. Elemental analyses were conducted at Nanjing Institute of Geography and Limnology, Chinese Academy of Sciences.

2 Results and analysis

2.1 Temperature-dependent susceptibility for representative samples

Temperature-dependent magnetic properties can be used to identify the type of magnetic minerals based on their Curie-point[17,18]. High-temperature susceptibility analyses were conducted on samples 303 and 314 (collected from the residential area and the recreational park) and samples 315, 482, 468 and 484 (collected from the Shougang industrial area, and the last two taken from an iron foundry). As shown in Figure 1, temperature-dependent susceptibility of sample 303 slowly increased between 0—400℃ and slightly decreased between 400—540℃, then dropped abruptly at about 540℃, and finally decreased to the baseline at around 580℃, indicating that magnetite is main magnetic carrier. Its cooling cycle is almost reversible. Temperature-dependent susceptibilities of sample 314 rapidly decreased between 100—200℃ during heating, revealing significant paramagnetic contribution[19]. It then gradually decreased above 200℃, and abruptly dropped at about 550℃, and reached the baseline at around 580℃, again clearly indicating the presence of magnetite[20]. During the cooling cycle, the susceptibility dramatically increased at about 580℃, obviously much higher than that in heating cycles, showing that new magnetite with high susceptibility was formed during the cooling cycle. During heating, the susceptibilities of all other samples (315, 482, 468, and 484) dramatically decreased at about 580℃, indicating the Curie point of magnetite. In the cooling cycle, like for sample 314, susceptibilities rapidly increased at about 580℃, much higher than those during the heating cycles.

Figure 2 shows low-temperature- dependent susceptibilities of six representative samples. The Verwey transition at about −150℃ clearly demonstrates the existence of magnetite in all samples[21], supporting the same conclusion as by high-temperature dependent susceptibility cycles in Figure 1.

2.2 ARM acquisition and its AF demagnetization curves for representative samples

The crossover point of ARM acquisition and its AF de-

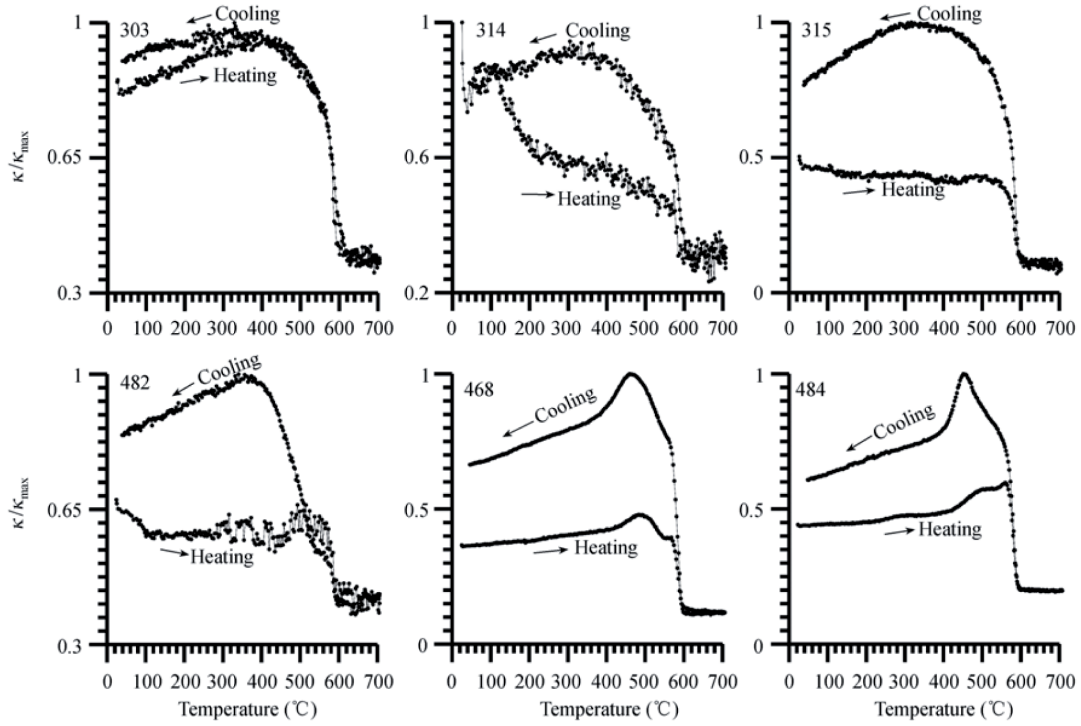

Figure 1 High-temperature-dependence of the low-field magnetic susceptibility of representative samples.

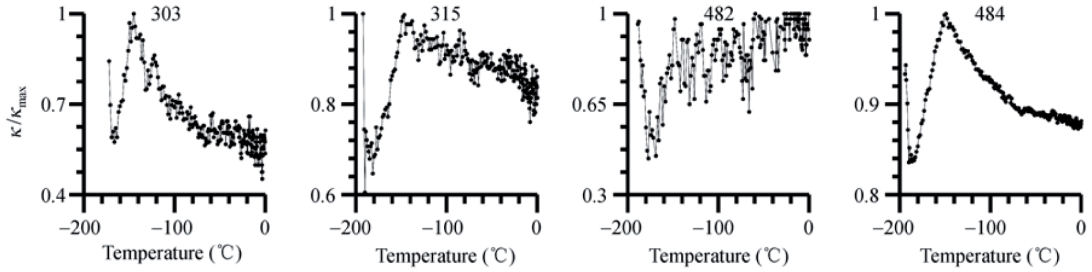

Figure 2 Low-temperature-dependence of the low-field magnetic susceptibility of representative samples.

magnetization curves can indicate the coercive force of magnetic minerals[22]. As shown in Figure 3, the cross-over points of ARM acquisition and its demagnetization curves for six representative leaf samples range among 25—30 mT, suggesting that low coercive force magnetite is the major carrier within the samples.

Figure 4 shows a significant correlation between low frequency χ_{lf} and SIRM (R = 0.96), which demonstrates a predominant contribution of ferrimagnetic minerals rather than from paramagnetic, or superparamagnetic minerals. Such a linear relationship between χ and SIRM also reveals that the changes of magnetization mainly reflect changes of concentration rather than grain sizes of magnetic particles.

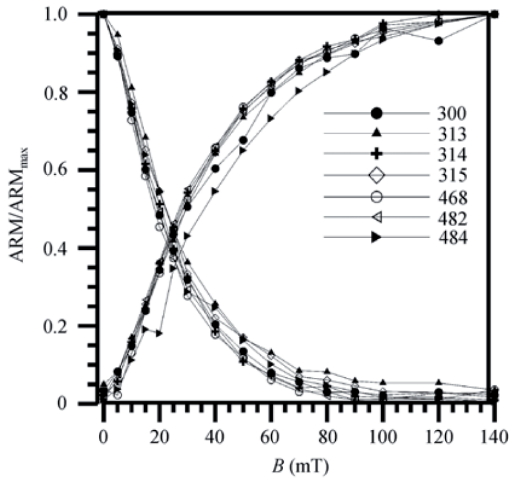

Figure 3 ARM acquisition and its back-field demagnetization curves.

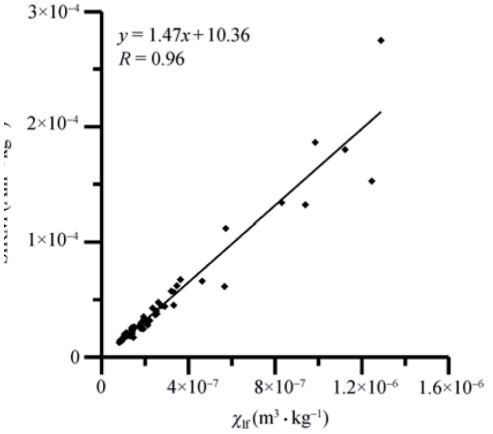

4 Linear regression analysis between susceptibility (χ_{lf}) and on isothermal remanent magnetization (SIRM).

Distribution of magnetic parameters for leaf les in Shougang industrial area

1 gives the minimum, maximum, mean value, and ard deviation of magnetic parameters such as χ, , SIRM, S ratio, ARM/χ, ARM/SIRM and SIRM/χ 5 leave samples. Although direct comparison of the agnetic background for the 3 different tree species ot been conducted, the average susceptibility of the af samples from all 3 different tree species col- l from the agricultural region in the eastern suburb eijing (between County Tong and Town Yanjiao, e it is relatively less or not polluted) is 11.3×10^{-8} $^{-1}$ (minimum value and maximum value: 5.1×10^{-8} $^{-1}$ and 17.6×10^{-8} $m^3\ kg^{-1}$ respectively, standard tion: 3.4×10^{-8} $m^3\ kg^{-1}$), i.e., in the same range as usceptibility of local fluvio-lacustrine sediments. e, it is obvious that such a low magnetic back- ıd of leaves has no (or little) effect on the heavy study in the Shougang industrial area. In the gang industrial area, the magnetic properties of s are dominated by magnetic particles mixed with heavy metals released by industry. Meanwhile, similar studies also revealed that the biomagnetic ground is less important. Hanesch et al.[8] studied two different tree species in one same street, and found that the difference between the two species is not larger than the difference between different samples taken from one tree or even one branch of a tree (but, the relative differences between samples taken from one tree can be up to 10%). Gautam et al.[9] also neglected the difference among the tree species when they studied the traffic-related heavy metal pollution in Kathmandu city using the magnetic properties of dust loaded leaves. χ and SIRM can be used for generally estimating the relative contribution from ferrimagnetic minerals, which is dependent on both the type of ferrimagnetic minerals and the grain-size of the magnetic particles[17,18]. Figure 5(a) displays a contour plot of susceptibility for leaves in Shougang industrial area. Relatively higher susceptibility values appear in a rather long and narrow area around Shougang industrial area. Within Figure 5(a), sample 208 was taken in an iron foundry; sample 216 from the third steel making plant; sample 193 from east entrance of Shougang Groups; sample 195 from a truck company of Shougang Groups; and sample 235 from waste coal ash dumps. The highest susceptibility value (128.79×10^{-8} $m^3\ kg^{-1}$) is observed in the iron foundry. Relatively lower susceptibility values (around 8—15×10^{-8} $m^3\ kg^{-1}$) are found in ambient areas of Shougang industrial area, including area $1^{\#}$ (including Fahai Temple, Beijing University of Technology, and the Park Badachu), area $2^{\#}$ (residential area and green parks located in prevailing wind direction of industrial area), and area $3^{\#}$ (less polluted area situated in the western suburb), where the lowest susceptibility value, (8.1×10^{-8} $m^3\ kg^{-1}$), is observed. Such relatively lower susceptibility is in the same order as the average susceptibility of 35 leaf samples collected from the eastern suburb as mentioned above. Thus, this value can be considered as the natural magnetic background of the tree leaves in this area. Figure 5(c) shows the contour plot of SIRM for leaves in Shougang industrial area. Its spatial distribution pattern is similar to that of χ (Figure 5(a)). Meanwhile, there is a strong correlation between SIRM and χ (Figure 4),

1 Statistics of magnetic parameters (n = 55)

	χ (10^{-8} $m^3\ kg^{-1}$)	SIRM (10^{-6} $Am^2\ kg^{-1}$)	ARM (10^{-6} $Am^2\ kg^{-1}$)	S ratio	SIRM/χ (KA/m)	ARM/χ (10^2A/m)	ARM/SIRM
ım value	8.10	1272.36	17.10	0.88	10.86	1.12	0.007
ım value	128.79	27510.82	244.57	0.98	21.36	2.69	0.015
value	30.25	4887.91	54.91	0.92	16.07	2.01	0.013
rd deviation	29.93	45.81	45.81	0.01	2.09	0.33	0.001

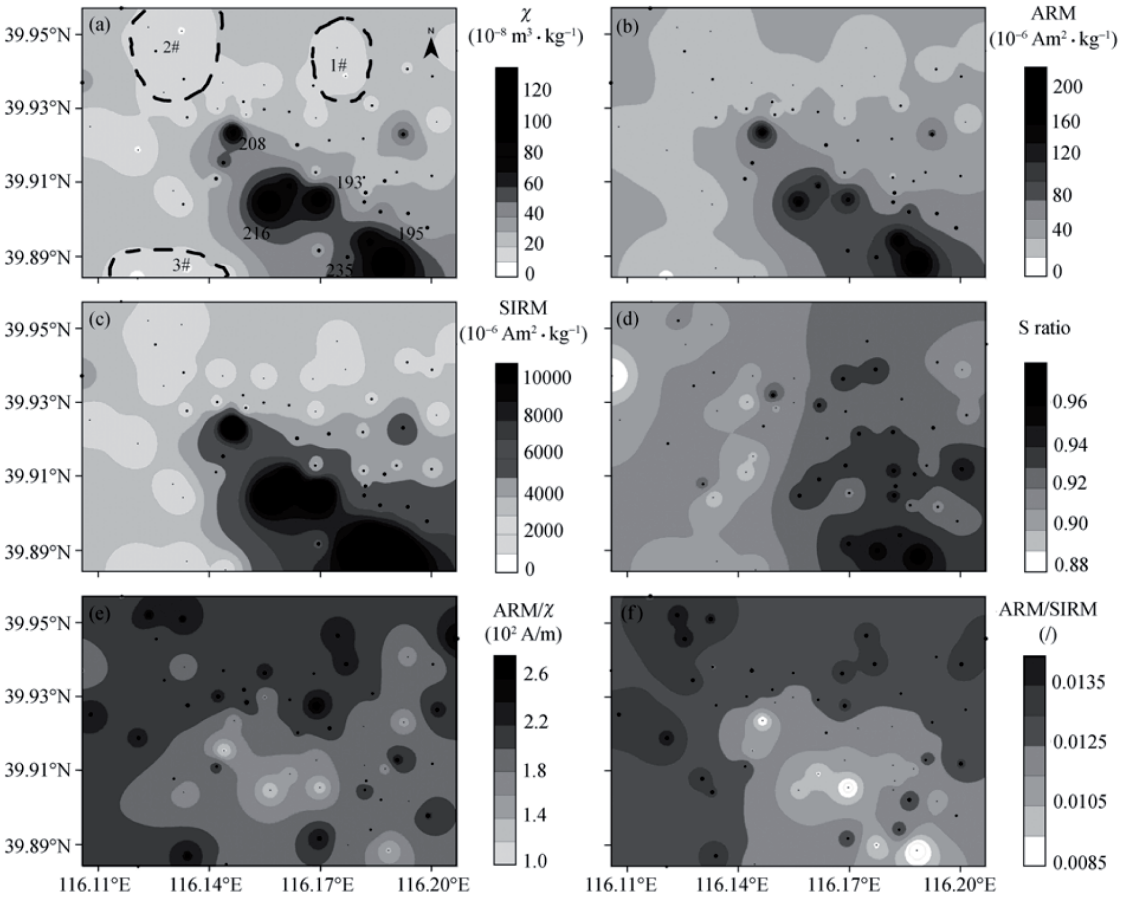

Figure 5 Contour maps of magnetic parameters (the areas defined by dashed lines are #1, #2 and #3 areas mentioned in the text; the closed circles are sampling sites).

which further confirms that ferrimagnetic minerals are the predominant magnetic carrier in the samples[23,24]. The leaf itself is diamagnetic and weakly magnetic in less industrialized areas, which might lead to a relative high measurement error. However, the isothermal remanent magnetization (IRM) is acquired under artificial fields applied in lab. Thus, it might intensify anthropogenic pollution signals, and yield better results in comparison with low susceptibility. In the studied area, SIRM and χ have the same spatial distribution patterns with an excellent correlation between them (R = 0.96). The two parameters can, therefore, be assumed as representative of the amount of ferrimagnetic particles. Furthermore, in this study, the susceptibility for leaves is normalized by its mass. We suppose that the susceptibility of dust accumulated on a leaf per volume can represent that of the whole leaf and there is a good liner relationship between its susceptibility per volume and per mass. As shown in Figure 5, the spatial distribution of susceptibility looks reasonable. Hence, the above-mentioned hypothesis is tenable. Of course, the best way should be only to collect all dust accumulated on leaf rather than a leaf itself. But it is very difficult to do so in practice, especially when studying a large area with a high resolution sampling procedure. Until now, measurements were conducted only on whole-leaf sample rather than the dust dropped from the leaf reported in many other studies too[7−14].

The ARM is dependent on both type of magnetic minerals and their grainsizes, and is most sensitive to the presence of single domain (SD) magnetic particles[25]. In this study, the spatial distribution pattern of ARM is similar to χ (Figure 5(b)), which may testify that ARM is controlled mainly by concentration of ferrimagnetic minerals rather than by their grainsizes[10].

The S ratio indicates the relative contribution of

nagnetic and antiferrimagnetic minerals[25]. As n in Table 1, the S ratio values ranging from 0.88)8, with a mean value of 0.92, indicates the pre- nance of ferrimagnetic components[26,27]. Higher S s are found in Shougang industrial area and its n parts (Figure 5(d)), interpreted as higher concen- n of ferrimagnetic minerals. Besides, it is worth to out that the average value of SIRM/χ is 16.07 , close to those reported by Moreno et al.[12] and t al.[28]. Such a value is normally related to multi- in (MD) magnetite contained within industrial fly ery common. The corresponding average values of I/χ are 14 kA/m[12] and 12—16 kA/m[28], while the ial magnetic fields applied to acquire SIRM were and 1 T respectively.

e ARM/χ ratio depends on the composition and the size of the magnetic particles. When the magnetic alogy is homogeneous, ARM/χ and ARM/SIRM indicates the variation of the grainsize of the mag- minerals. In general, both lower ARM/χ and ARM/ I indicate coarse grains of magnetite, whilst higher indicate fine grains, especially SD grains[24,29]. As n in Figure 5e and f, in the vicinity of heavily pol- Shougang industrial area, both lower ARM/χ and /SIRM hint towards predominant coarse magnetic les, while in its ambient areas, both higher ARM/χ RM/SIRM indicate fine ones.

mmarizing, magnetic concentration is relatively r, and ferrimagnetic grains are coarser in and y pollution sources (Shougang industrial area); concentration is lower and grains are finer at far ice from the pollution source. Therefore, for the ants the transportation mode results in higher con- ation of magnetic particles with coarser grainsize in ly polluted areas, but decreasing in concentration ncreasing in grainsize as the pollutants transport onger distance.

Heavy metal contents of leaf samples

own in Table 2, there is a big difference between inimum and the maximum value of the tested ele- s. The maximum value is as around three times as inimum. The minimum value is very close to the ge value of 18 leaf samples collected from the ag- ural region in the eastern suburb (as mentioned between Tong County and Yanjiao Town). The ge content of Fe, Pb, Cr, V and Zn are 732.92, 4.52,

Table 2 Statistics of heavy metal contents (n = 24)

(mg/kg)	Fe	Pb	Cr	V	Zn
Minimum value	631.11	4.39	1.26	1.01	19.97
Maximum value	2253.91	11.56	4.26	3.37	45.96
Mean value	1113.47	7.30	2.00	1.63	28.00
Standard deviation	448.0	2.03	0.74	0.54	6.66

1.45, 1.27 and 21.09 mg/kg respectively in the eastern suburb. The minimum value of heavy metal contents can be considered as the background in the studied area. Hence, the big difference between the minimum and the maximum value of the elements in leaves may reflect anthropogenic inputs. Shougang industrial area is a very complex pollution source, with coking, power generating, sintering, iron making and steel making plants where coking plants and power plants are the major sources releasing magnetic minerals during dry distillation and combustion of coals. Some results[30,31] showed that the average content of Pb in the coal in China is about 19.96 mg/kg. Pb contained in the coal and petroleum will convert to low fusing point chloride during the burning process, and is then released into the atmosphere. Some authors found that the toxic element V originates from fossil fuel combustion and exhibits a gradually increasing trend around the industrial areas[32,33]. Furthermore, Lindstrom[34] also observed that the Cr content was obviously higher than that around smelt and metal processing plants, and was enriched remarkably in moss nearby. Pb and Zn can be directly released into the atmosphere through vehicle's transportation of raw material and products in/around Shougang industrial area[35]. The above-mentioned reasons can explain why big differences between the elements exist.

3 Discussions

In order to judge how close the variables (magnetic parameters and heavy metals) are related to each other, a tree diagram (Figure 6) is constructed (variables are standardized, then processed with SPSS software). The abscissa represents the interval between the variables within the figure; the shorter the distance the higher the correlation. As shown in Figure 6, the average distance between elements (Fe, Pb, Cr, V and Zn) and magnetic concentration parameters (χ, ARM and SIRM) is smaller than 5, which suggests that there is a strong correlation between them, also confirmed by the correlation coefficients in Table 2. All the correlation coefficients be-

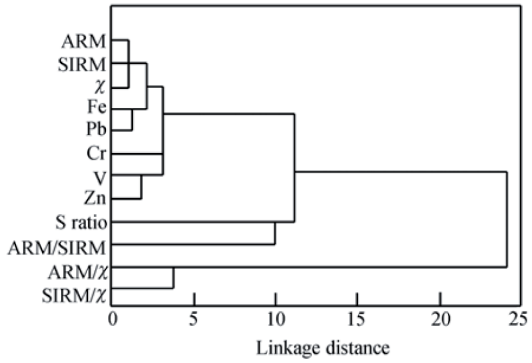

Figure 6 Tree diagram derived from cluster analysis of magnetic parameters and heavy metals.

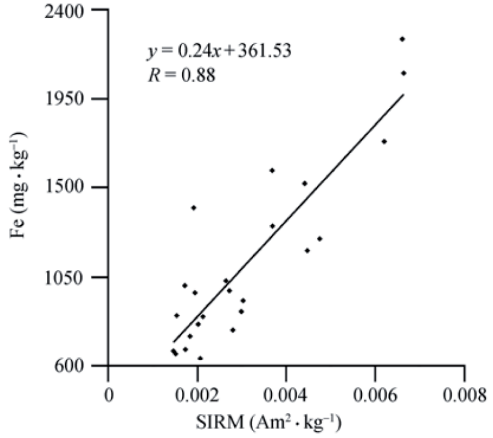

Figure 7 Linear regression analysis between SIRM and total iron content.

tween magnetic parameters (χ, ARM and SIRM) and elements (Fe, Pb, Cr, V and Zn) are greater than 0.73, reflecting that the magnetic mineral and elements originate from the same pollution source. However, the above-mentioned elements are relatively less correlated with magnetic parameters indicating relative mineral composition ratios (S ratio, ARM/SIRM, ARM/χ and SIRM/χ).

Many authors have emphasized the correlation between the magnetic minerals and heavy metals on dust in suspension. Hansen et al.[36] observed that Fe, Pb, V, Cr, Zn and Ni contained in fly ash from coal combustion in industrial production are mostly related to with magnetic minerals, and found that Fe, O, Si and Zn are strongly correlated with magnetic spheres derived from steel work. Lauf et al.[37] observed there existed a correlation between the magnetic spheres and heavy metals in dust derived from coal combustion and mentioned that magnetic spheres were converted from pyrite during coal combustion. In Shougang industrial area, being a very complex pollution sources, the magnetic particles, derived mostly from combustion and smelting procedures, may remain in air for some time, but most of them finally deposit on the leaves around the pollution sources. Both magnetic minerals and heavy metals deriving from the same source is the main reason for the significant correlation between them. An excellent linear correlation (R = 0.88) between the SIRM and the total iron content can be found in Figure 7. For zero magnetization the calculated regression line intercepts the y-axis at an iron content of 361.53 mg/kg, which is ascribed to biogenic iron[7]. It is suggested that biogenic iron is diamagnetic. A close correlation of SIRM and Fe content shows that non-destructive, time-efficient environmental magnetism of leaf can perfectly preserve the magnetic properties for a long time. Furthermore, there is a strong linear correlation ($0.73 \leqslant R \leqslant 0.88$) between magnetic concentration parameters (χ, ARM and SIRM) and heavy metals (Fe, Pb, V, Cr and Zn) in Table 3. Despite the dependence of magnetic parameters and heavy metal contents on a variety of spatial and temporal factors, the excellent linear correlation between them suggests the former can serve as an effective proxy for heavy metal pollution. Hence, a susceptibility-based biomonitoring technique is recommended as an economic and fast tool for assessment of environment pollution in urban areas like Beijing. The regression equations between low frequency susceptibility (χ_{lf}) and heavy metal content are established in Figure 8. Hence, we can roughly estimate the selected heavy metal content by rapid, sensitive magnetic mapping on tree leaves in industrial area by the help of integrated data processing in lab.

Table 3 Correlation matrix (R) for magnetic parameters and heavy metal contents (n = 24)

	Fe	Pb	Cr	V	Zn
χ	0.88	0.84	0.82	0.79	0.78
SIRM	0.88	0.82	0.75	0.73	0.80
ARM	0.87	0.85	0.77	0.74	0.78
S ratio	0.34	0.35	0.33	0.15	0.38
ARM/χ	0.49	0.48	0.50	0.43	0.32
ARM/SIRM	0.48	0.56	0.39	0.36	0.27
SIRM/χ	0.25	0.18	0.18	0.32	0.19

It is worth to be pointed out that a variety of spatial and temporal factors will affect the dust disposition and the amount of accumulation on leaves, such as human

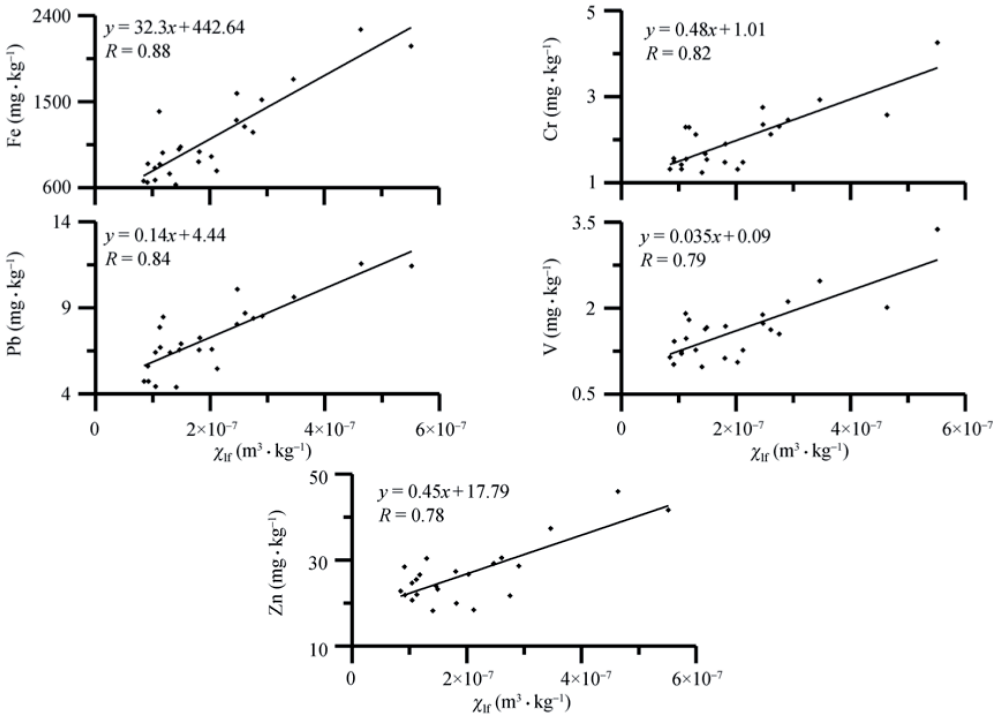

Figure 8 Linear regression analysis between susceptibility (χ_{lf}) and element contents (Fe, Pb, V, Cr and Zn) (n = 24).

activities, efficiency of disposition, leaf canopy structure, exposure direction, precipitation, wind direction, wind speed etc. Hence, magnetic measurement in terms of anthropogenic and lithogenic origin identified by a regional experimental model of the relationship between magnetic properties and heavy metals will help to outline the spatial and temporal extent of atmospheric pollution in industrial areas. Besides monitoring, we see an urgent need for characterization and quantification of the particles in different environmental systems (atmosphere, soil, vegetation, water, etc.) using rapid and cost-effective techniques, such as combined environmental, magnetic and analytical chemical methods.

4 Conclusions

(1) The main magnetic mineral carried by the dust-loaded leaf sample is low-coercivity magnetite. Its concentration and grainsize are higher in a relative long and narrow area centering in the Shougang Groups, and gradually decrease as distance from the pollution source increases;

(2) There is an evident correlation ($0.73 \leqslant R \leqslant 0.88$) between the magnetic parameters (χ, ARM and SIRM) and elements (Fe, Pb, Cr, V and Zn), demonstrating that magnetism can serve as a good proxy for heavy metal pollution. Rapid, sensitive magnetic mapping of tree leaves integrated with data processing can help to build a regional experimental model of the relationship between magnetic properties and heavy metals for assessment of atmospheric pollution in urban areas like Beijing;

(3) For monitoring heavy metal pollution, leaf has many advantages, such as widely spread, easily available and the low background. It is convenient to provide a high density of sampling points and building high-resolution maps of air pollution. Hence, susceptibility-based bio-monitoring technique is recommended as an economic and rapid tool for assessment of environment pollution in urban areas like Beijing.

We are grateful to three anonymous reviewers for their stimulating comments.

1 Ping C. Status and Comprehensive control countermeasures of urban air pollution in China. Environ Sci Manage (in Chinese), 2006, 31(1): 18－21

2 Pope C A, Thun M J, Namboodiri M M, et al. Particulate air pollution as a predictor of mortality in a prospective study of US adults. Am J Resp Crit Care Med, 1995, 151: 669－674

3 Muxworthy A R, Schmidbauer E, Petersen N. Magnetic properties and Mossbauer spectra of urban atmospheric particulate matter: a case study from Munich, Germany. Geophys J Int, 2002, 150: 558－570[doi]

4 Simonich S T, Hites R A. Organic pollutant accumulation in vegetation. Environ. Sci Technol, 1995, 29: 2905－2913[doi]

5 Rautio P, Huttunen S, Lamppu J. Element concentrations in Scots pine needles on radial transects across a subarctic area. Water, Air, Soil Pollut, 1998, 102: 389－405[doi]

6 Steinnes E, Lukina N, Nikonov V, et al. A gradient study of 34 elements in the vicinity of a copper-nickel smelter in the Kola peninsula, Environ Monit Assess, 60, 71－88

7 Urbat M, Lehndorff E, Schwark L. Biomonitoring of air quality in the Cologne conurbation using pine needles as a passive sampler—Part I: magnetic properties. Atmos Environ, 2004, 38: 3781－3792[doi]

8 Hanesch M, Scholger R, Rey D. Mapping dust distribution around an industrial site by measuring magnetic parameters of tree leaves. Atmos Environ, 2003, 37: 5125－5133[doi]

9 Gautama P, Blaha U, Appel E. Magnetic susceptibility of dust-loaded leaves as a proxy of traffic-related heavy metal pollution in Kathmandu city, Nepal. Atmos Environ, 2005, 39: 2201－2211[doi]

10 Zhang C X, Huang B C, Li Z Y, et al. Magnetic properties of high-road-side pine tree leaves in Beijing and their environmental significance. Chin Sci Bull, 2006, 51(12): 1459－1468[doi]

11 Matzka J, Maher B A. Magnetic biomonitoring of roadside tree leaves: identification of spatial and temporal variations in vehicle-derived particulates. Atmos Environ, 1999, 33: 4565－4569

12 Moreno E, Sagnotti L, Dinarès-Turell J, et al. Biomonitoring of traffic air pollution in Rome using magnetic properties of tree leaves. Atmos Environ, 2003, 37: 2967－2977[doi]

13 Maher B A, Moore C, Matzkac J. Spatial variation in vehicle-derived metal pollution identified by magnetic and elemental analysis of roadside tree leaves. Atmos Environ, 2007, [doi]

14 McIntosh G, Gómez-Paccard M, Osete M L. The magnetic properties of particles deposited on Platanus x hispanica leaves in Madrid, Spain, and their temporal and spatial variations. Sci Total Environ. 2007, 382: 135－146[doi]

15 Alfani A, Baldantoni D, Maisto G, et al. Temporal and spatial variation in C, N, S and trace element contents in the leaves of Quercus ilex within the urban area of Naples. Environ Pollut, 2000, 109: 119－129[doi]

16 Monaci F, Moni F, Lanciotti E, et al. Biomonitoring of airborne metals in urban environments, new tracers of vehicle emission, in place of lead. Environ Pollut, 2000, 107: 321－327[doi]

17 Tian L L, Zhu R X, Pan YX. Rock-magnetic properties of Hannuoba basalt in ZhangBei section. Chin J Geophys. 2002, 45(6): 832－838.

18 Ju Y T, Wang S H, Zhang P, et al. Mineral magnetic properties of polluted topsoils: a case study in Sanming city, Fujian province, southeast China. Chin J Geophys, 2004, 47 (2): 282－288

19 Dunlop D J, Ozdemir Ozden. Rock Magnetism: Fundamentals and Frontiers. Cambridge UK: Cambridge University Press, 1997. 76－79

20 Hu, S Y, Goddu S R, Appel E, et al. Palaeoclimatic changes over the past 1 million years derived from lacustrine sediments of Heqing basin (Yunnan, China), Quat Inter, 2005, 136:123－129[doi]

21 King J G, Williams W. Low-temperature magnetic properties of magnetite. J Geophys Res, 2000, 105: 16427－16436[doi]

22 Maher B A. Characterization of soil by mineral magnetic measurements. Phys Earth Planet Inter, 1986, 42: 76－92[doi]

23 Verosub K L, Roberts A P. Environmental magnetism: past, present, and future. Geophys Res, 1995, 100 (B2): 2175－2192[doi]

24 Oldfield F. Environmental magnetism——A personal perspective. Quat Sci Rev, 1991, 10:73－85[doi]

25 Sun Z M, Hu S Y, Ma X H. A rock magnetic study of recent lake sediments and its palaeoenvironmental implication. Chin J Geophys (in Chinese), 1996, 39(2): 178－187

26 Robinson S G. The late Pleistocene palaeoclimatic record of North Atlantic deep-sea sediments revealed by mineral-magnetic measurements. Phys Earth Planet Inter, 1986, 42: 22－47 [doi]

27 Thompson R, Oldfield F. Environmental Magnetism. London: Allen & Unwin, 1986

28 Shu J, Dearing J A, Morse A P, et al. Magnetic properties of daily sampled total suspended particulates in Shanghai. Environ Sci Technol, 2000, 34: 2393－2400[doi]

29 Yu L Z, Xu Y, Zhang W G. Magnetic measurement on lake sediment and its environmental application. Prog Geophys (in Chinese), 1995, 10(1): 11－22

30 Liao Z J. The Pollution and Transform of Trace Heavy Metals in Environment (in Chinese). Beijing: Science Press. 1989, 253－260

31 Ren D Y, Xu D W, Zhang J Y et al. Distribution of Associated Elements in Coals from Shenbei Coalfield. J Chin Univ Min Technol (in Chinese), 1999, 28 (1): 5－8

32 Moskalyk R R, Alfantazi A M. Processing of vanadium: a review. Miner Eng, 2003, 16: 793－805[doi]

33 Seiler H G, Sigel A, Sigel H. Handbook on Metal in Clinical and Analytical chemistry. New York: Marcel Decker, 1994. 217－226

34 Lindstrom M. Urban land use influences on heavy metal fluxes and surface sediment concentrations of small lakes. Water Air Soil Pollut, 2001, 126: 363－383[doi]

35 Nicholson F A, Smith S R, Alloway B J, et al. An inventory of heavy metals inputs to agricultural soils in England and Wales. Sci Total Environ, 2003, 311: 205－219[doi]

36 Hansen L D, Silberman D, Fisher G L. Crystalline components of stack-collected size-fractionated coal fly ash. Environ Sci Technol, 1981, 15: 1057－1062[doi]

37 Lauf R J, Harris L A, Rawiston S S. Pyriteframboids as the source of magnetic spheres in fly ash. Environ Sci Technol, 1982, 16: 218－220[doi]

5

A magnetic study of a polluted soil profile at the Shijingshan industrial area, western Beijing, China

CHINESE JOURNAL OF GEOPHYSICS Vol.49, No.6, 2006, pp: 1524~1532

A MAGNETIC STUDY OF A POLLUTED SOIL PROFILE AT THE SHIJINGSHAN INDUSTRIAL AREA, WESTERN BEIJING, CHINA

SHEN Ming-Jie[1,2] HU Shou-Yun[1] U. Blaha[3] YAN Hai-Tao[1,2] W. Rösler[3] V. Hoffmann[3]

1 *Nanjing Institute of Geography and Limnology, Chinese Academy of Sciences, Nanjing* 210008, *China*

2 *Graduate School of the Chinese Academy of Sciences, Beijing* 100049, *China*

3 *Institute of Geosciences, University of Tuebingen,* 72076 *Tuebingen, Germany*

Abstract A soil profile of 74 cm length was sampled in the hillside close to Beijing Muslim's cemetery, which is located in the Yingshan Forest Park near the Shijingshan industrial area. Coal-fired power plants, a steel mill, and a cement factory are located close to the sampling site. Gray-black pollutants can be found within the uppermost part of the soil. Magnetic measurements, grain size and geochemical analysis, as well as multivariate statistics were performed. Magnetic proxies show similar trends compared to heavy metal elements with higher concentrations at the top and lower concentrations in the lower part. The anthropogenic dust input from industrial activity is the predominant cause for strong magnetic signals in the uppermost soil horizon (0∼3 cm). The main magnetic component is magnetite contained in the grain size fractions of 4∼16μm and 16∼32μm. These pollutants are observed up to about 10 cm depth. Below 10 cm, there is little pollution in soil with lowest concentration of magnetic minerals and heavy metals comparable to natural background values. Multivariate statistics and fuzzy C-means cluster analysis show positive correlation of χ, ARM, SIRM and Mn, Cu, Fe, Pb, Zn, Al, Sr. Based on the results, it can be concluded that magnetic parameters can be used as a sensitive indicator for screening heavy metal pollution.

Key words Soil profile, Industrial pollution, Magnetic parameter, Heavy metal, Multivariate statistics

1 INTRODUCTION

Anthropogenic pollution can seriously affect ecological environment and human health. With the development of modern industry, iron and steel production, metal smelters, and coal-fired power plants are important functions in our society, but they also produce considerable amounts of pollutants including toxic heavy metals, which badly pollute ambient soil environment by accumulating, enriching and migrating in soil[1,2]. Previous studies have shown that they also contain magnetic particles going with heavy metals bringing on the soil pollution, so it is possible to use magnetic methods to study the industrial pollution[3,4].

Traditional environmental screening or monitoring relies on chemical analyses by well-established and accurate laboratory techniques (AAS, ICP-MS etc.) mostly based on point sampling[5,6]. Unfortunately, these methods are time consuming and costly. It is a challenge for the scientific community to develop and improve fast and cost-efficient screening methods for soil monitoring, which can be combined with existing standard chemical methods in order to optimize the entire screening and monitoring strategy. Comparing to traditional chemical methods, magnetic method is relatively simple, rapid, sensitive, non-destructive and low-cost, so it has been widely applied in domestic and international studies with the relationship between magnetic parameters and heavy metals[7~10]. The particulate pollution sources such as iron and steel works, power plants and cement works also contribute to soil contamination. They are normally characterized by an enhanced magnetization and magnetic susceptibility, which are roughly proportional to the concentration of the strongly magnetic Fe-oxides[11~14]. Therefore it is most important to understand the industrial pollution, particularly the magnetic mechanism of heavy metal pollution and clarify the relationship between magnetic parameters and soil pollution using environmental magnetic approaches.

In this paper, a detailed characterization of a soil profile at Shijingshan industrial area, western Beijing

city was obtained. With the aim of better understanding the relationship between magnetic properties and their links to heavy metals, an integrated approach, combining magnetic, geochemical, grain size analyses and multivariate statistics methods were carried out for screening the contaminated soils and vertical migration of pollutants with depth.

2 MATERIALS AND METHODS

Shijingshan industrial area is located in Western Beijing, to the west of the Fifth Ring Road and east of the Yongding River valley and includes iron and steel mills of Shou Gang Group, power plants, cement and chemical factories. The sampling site is located in the hillside of Beijing Muslim's Cemetery, which is in the west of the Yingshan Forest Park, to the south-west of Yongding river valley nearby the industrial area (Fig. 1). 12 short soil profiles of 40 ~ 50 cm length were obtained there using the soil corer. Gray-black pollutants can be directly observed by eye within the uppermost soil, while in the lower part, the soil color becomes brown and lighter. All the profiles were measured onsite with the Soil Magnetic Susceptibility Meter SM-400 (made by MAGPROX group), which yielded almost the same results (Fig. 2). Therefore in this paper as a representative example, the profile BJ904S of 76 cm is selected and sampled by the small shovel. Sub-samples for magnetic, grain size and geochemical analyses were taken into the sealed plastic bags at an interval of 0.5 cm for the topmost 16 cm, at an interval of 1 cm for 16~26 cm, 2 cm for 26~40 cm, and 4 cm below.

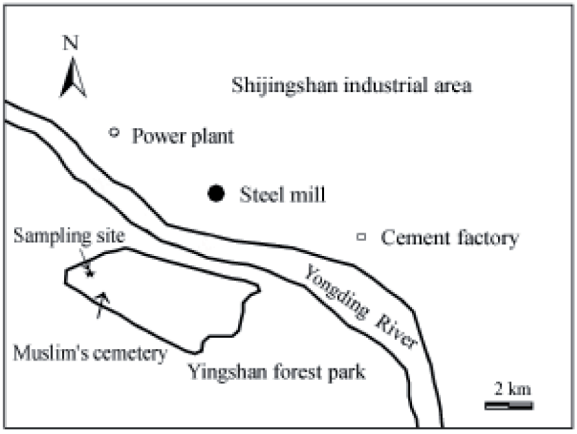

Fig. 1 Map showing geographical location of the studied area

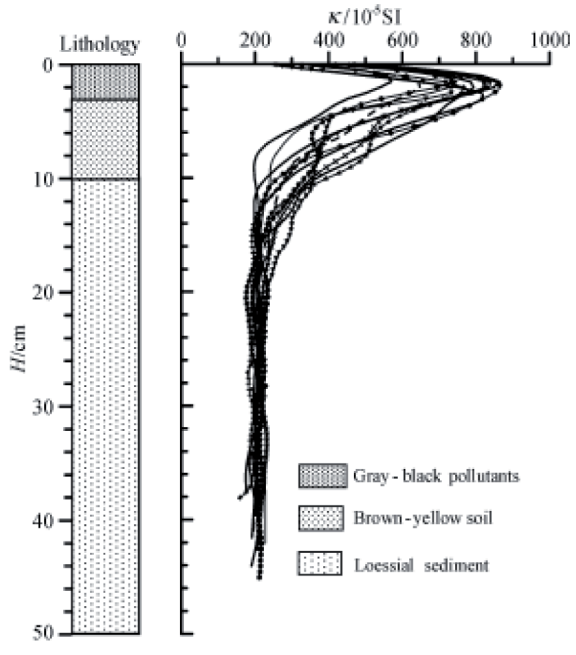

Fig. 2 Lithostratigraphy and 12 magnetic susceptibility κ curves along with depth H of the soil profile

Magnetic samples were put into cubic plastic boxes with a size of 2 cm×2 cm×2 cm. Bulk-specific magnetic susceptibility (κ) was measured using the AGICO KLY-3 Kappabridge in the geophysical laboratory of Earth Science Department, Nanjing University. Anhysteretic Remanent Magnetization (ARM) was acquired at an AF field of 100 mT with a bias field of 50 μT using a Molspin AF demagnetizer. Saturation Isothermal Remanent Magnetization (SIRM) was acquired in a DC-field of 1 T using a Molspin pulse magnetizer. S-ratio was calculated as the absolute value of the IRM remaining after exposure to a reversed field of 300 mT divided by the SIRM. All these remanent magnetization measurements were measured using a Molspin spinner magnetometer. The mass-specific magnetic susceptibility (χ), ARM, SIRM by mass normalization and other ratio parameters were calculated on the basis of these values.

After drying in 55°C and rinsing within 100-mesh size-sieve, element contents of Al, Fe, Mn, Cu, Zn, Pb and Sr were analyzed using a LEEMAN LABS PROFILE ICPAES treated by NO_3-HF-$HClO_4$ in a Berghof MWS-3 microwave digester. Grain size analysis was performed with a Mastersizer2000 laser grain size analyzer.

All these measurements mentioned above except κ were carried out at Nanjing Institute of Geography and Limnology, Chinese Academy of Sciences. Thermomagnetic curves (κ-T) on soil samples were measured using a CS-3 temperature unit attached to a KLY-3 Kappabridge in the Paleomagnetic Laboratory of Tuebingen University, Germany. It was performed from room temperature up to 700°C.

3 RESULTS AND ANALYSIS

3.1 Magnetic Results

Magnetic parameters of soil profile can reflect the characters of magnetic minerals along with depth. Magnetic susceptibility (χ) and SIRM are usually regarded as approximate estimates of ferro(i)magnets content (i.e. magnetite) in the sample, and S_ratio reflects the relative proportion of ferro(i)magnets to the imperfect antiferromagnets (i.e. hematite and goethite). It decreases gradually with increasing contribution of imperfect antiferromagnets[15,16]. As shown in Fig. 3, χ, ARM and SIRM fluctuate in the same trend towards the depth with a pronounced χ peak at around 3 cm. Above this borderline, values of χ are very high (average $950.58\times10^{-8}m^3\cdot kg^{-1}$) within the gray-black samples, and they decrease gradually from 3 cm to 10 cm (average $516.14\times10^{-8}m^3\cdot kg^{-1}$) within soil of brown-yellow color. Values of χ are quite stable and relatively low and reduced to the average $136.56\times10^{-8}m^3\cdot kg^{-1}$ with much lighter color below 10 cm, which means that the concentration of ferromagnetic particles generally decreases with depth. S_ratio is relatively stable and higher than 0.90 in the whole soil profile, which indicates the collected samples are overwhelmingly predominant by ferro(i)magnetic minerals, while the contribution of a few imperfect antiferromagnetic components is also observed.

ARM/χ, ARM/SIRM, SIRM/χ ratios have been widely accepted to be indicators of grain size of magnetite[17,18]. Since ARM is sensitive to grain size of ferro(i)magnetic minerals, especially to single domain (SD) grains and smaller magnetite grains have higher ability to acquire remanence, in especial the ARM, smaller magnetite particles can generally yield higher ARM/χ and ARM/SIRM ratios. Whereas lower ratios of ARM/χ and ARM/SIRM could point to coarse ferro(i)magnetic grains, such as PSD or MD particles. The values of SIRM/χ can provide information about the kinds of magnetic minerals. It shows a scatter distribution with non-linearity if many kinds of magnetic minerals are contained, whereas it shows linear figure if only one mineral existing or being predominated even their particle sizes would change[19].

Our results from Fig. 3 show that ARM/χ and ARM/SIRM values for soil samples collected in the uppermost 10 cm of the profile are relatively low, which indicates the coarse particle-size (PSD or MD) is primary components. It is related to concentrated pollutants discharged from steel mill and power plant in the industrial area and represents the characteristic of industrial pollution with distinct high χ and MD grains, which accords with the previous magnetic study on pollution[20,21]. Whereas the ARM/χ and ARM/SIRM values are stable and generally below 10 cm, implying the average grain size state of coarse particle is dominant. It may be affected by the pedogenesis of soils in this low mountain area, and the grain size of the magnetic minerals in soils is originally coarse and stable for the nature cause. The values of ARM/SIRM are really linear with a few fluctuations, it seems many magnetic minerals existing but only one mineral predominated.

3.2 Grain Size Analysis

The grain size of soil and sediments can influence the components and element contents of the minerals as well as reflect of the energy of transit medium and the changes of sediment environment, but also affect their magnetic characteristics[17,22]. Fig. 3 shows the variation of grain size fractions with depth. The content of clay fraction ($< 4\mu$m) of the 85% samples is less than 10%, while the silt fraction content ($4 \sim 64\mu$m) ranges from 58% to 68%. In more detail, fine silt ($4\sim16\mu$ m) is 10.3% of average, medium silt ($16\sim32\mu$ m) 13.5%, and coarse silt ($32\sim64\mu$m) 38.6%. The sand fraction ($> 64\mu$m) content ranges from 30% to 40%. This clearly shows that

coarse silt is the predominant fraction of silt, and the clay fraction changes less with depth. Comparing to the curves of magnetic parameters, it is found that fine silt and medium silt show a similar trend with χ, ARM and SIRM, but differ greatly with coarse silt.

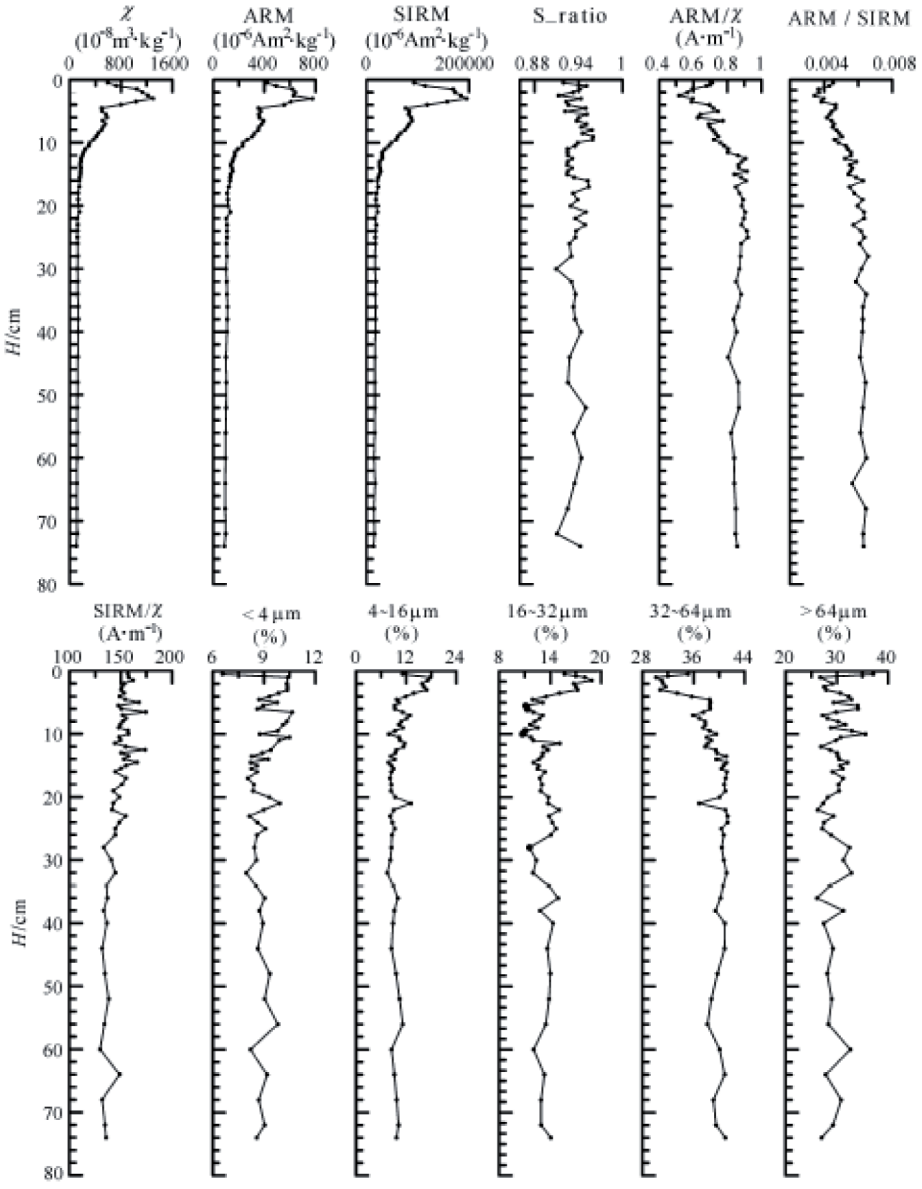

Fig. 3 Vertical variations of magnetic parameters and grain size of the soil profile

3.3 Heavy Metal Analysis

The heavy metals in soil usually come from bedrock and biology relics in natural status and their contents are relatively low, which will not result in any harm to human beings and to the ecosystem. But anthropogenic influence perhaps is another important cause for the heavy metal pollution in soils. Because the industrial process makes it possible for a great deal accumulating and a significant increase of heavy metals in soil through transformations in hydrospheric and atmospheric system. They also adsorb with organics, humus and colloids and enter the sediment process. So the vertical distribution of heavy metal contents of the soil profile is an important record for the pollution history.

The contents of Cu, Fe, Pb, Mn, Zn, Al and Sr have similar distribution pattern. Above 3cm the concentration is relatively high with a peak occurring at 3 cm (Fig. 4). Then it decreases gradually between 3~10 cm, and it is followed by the stable and low values corresponding to the background below 10 cm[23]. From this point of view it also reflects that the input of pollutants enhances the accumulation of heavy metals in the upper part.

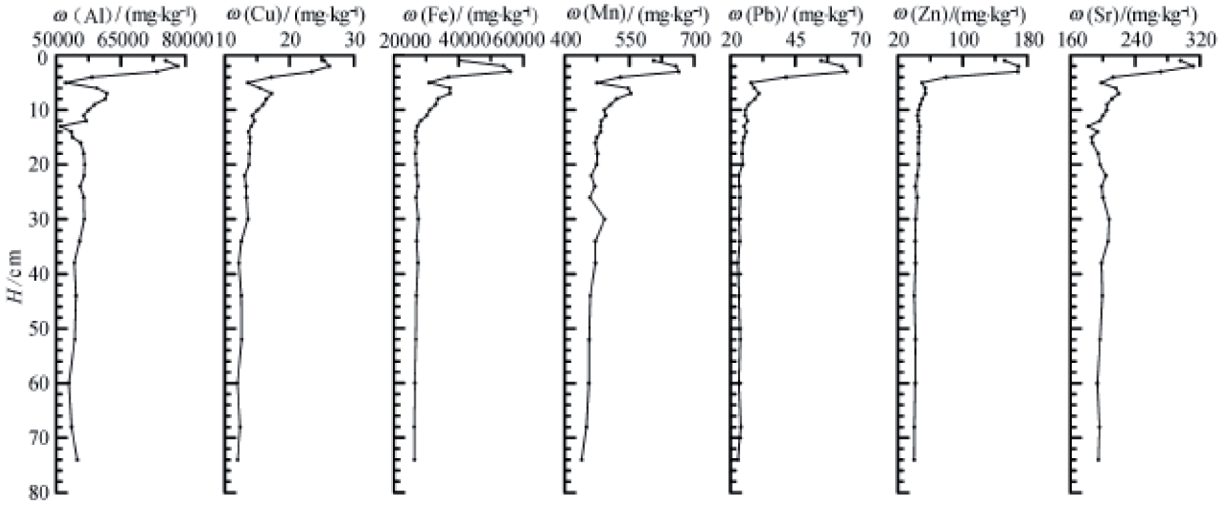

Fig. 4 Vertical variations of heavy metal contents ω of the soil profile

3.4 Thermomagnetic Analysis

Thermomagnetic analysis can show the changes of magnetic phases by heating and it is widely used in identifying the magnetic minerals and provides useful information about soil pollution[24]. For a better understanding of the magnetic properties of soil, thermomagnetic runs ($\kappa - T$) were conducted on bulk samples from depths of 3.0, 7.5, 44.0 cm, respectively (Fig. 5a). The soil sample taken at 3 cm depth shows the predominance of a well-expressed magnetite phase with a Curie point of 580°C. A second phase can be determined at around 470°C. The two phases are also preserved in the cooling curve. Another two samples also show Curie points of

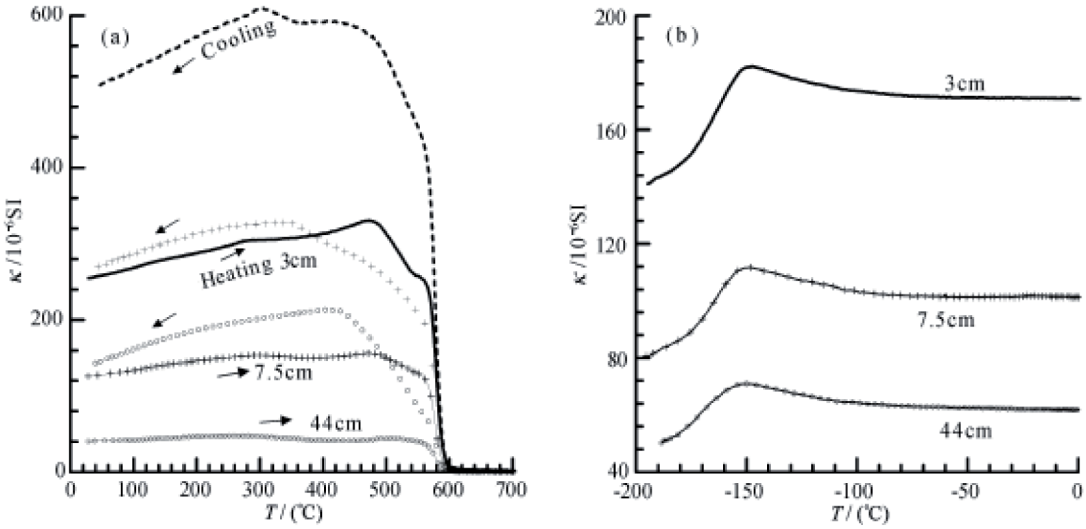

Fig. 5 Thermomagnetic runs ($\kappa - T$) for the raw soil samples

(a) High-temperature curves, solid line represents heating, dashed line represents cooling; (b) Low-temperature curves.

580°C, indicating the presence of initial magnetite in soil. However their concentration is distinct at different depths from the original κ value in Fig. 5. It shows the sample at 7.5 cm has the same magnetic components, but its concentration generally decreases. This decrease in concentration could be explained as migration of pollutants from the top. So the concentration of magnetite is relatively much lower in the profile bottom.

Data from low-temperature experiments (Fig. 5b) from all the samples show a well-defined Verwey transition at about −150°C, also pointing to the presence of magnetite[25~27].

4 DISCUSSION

To synthetically discuss the magnetic parameters and their links to heavy metals contents and samples grain size and to better reveal distribution and vertical migration of pollutants in soil profile, multivariate statistics were conducted on the magnetic, grain size and element parameters of the soil samples.

4.1 Index Linkage Analysis

It is difficult to judge the results from a huge data set with many parameter indexes in a general research. Index cluster can visually predigest the whole data processing and acquire the substantial relationship among all the variables. It can offer the numbers of categories according to the actual require from the researcher, obtain compositions of sub-clusters, and detect the relationship of each other[28]. 19 measured and calculated parameters were standardized and clustered using SPSS software (Fig. 6). The horizontal axis of the tree diagram represents the linkage distance (calculated by Euclidean distance). If the distance of two parameters is closer, their correlation will be higher. It is shown all the parameters can be gathered in one group based on several combinations. χ, ARM, SIRM and Fe, Mn indexes can cluster the same group at first stage. Their distance is the closest (<5) and also closer to other heavy metal elements (< 10), indicating that those magnetic concentration parameters have significant correlation with heavy metal contents, and also showing the same sources and the homogeneous geochemistry characteristic. Furthermore, correlation analysis also proves the prominent correlativity between magnetic parameters and heavy metal contents (Table 1). Therefore, those magnetic parameters can be used as proxies of heavy metal distribution. Heavy metals may have a close linkage with specific iron oxides and combine with iron oxides by adsorption and deposition[29]. And ferromanganese oxide is the main existing form for the heavy metal of non-residue state, which controls the geochemistry circulation of other metals to a great degree. So the abnormity of magnetism and heavy metal contents in the topsoil is not due to the pedogenesis or lithogenesis but the industrial pollution. The pollutants have many coarse particle-size ferromagnetic minerals enriching with heavy metals and dominate the magnetic properties of soils. Consequently magnetic measurements can be widely used to locate the pollution sources, define the pollution regions, trace the transportation and so on.

Table 1 also shows these magnetic parameters have obviously positive relationships with the fractions of 4~16μm and 16~32μm, but have negative correlation with 32~64μm fraction, which interprets ferro(i)magnets are mainly contained in these fractions. As shown above ARM/χ and ARM/SIRM have negative correlation with the fractions of 4~16μm and 16~32μm, but have significant positive correlation with 32~64μm fraction.

On the other hand, linkage distance between ratio parameters (S_ratio, ARM/χ, SIRM/χ, and ARM/SIRM), which can indicate grain size or the type of magnetic phases, and magnetic concentration parameters (χ, ARM, SIRM), is relatively far due to the indirect linkage between the particle size of magnetic

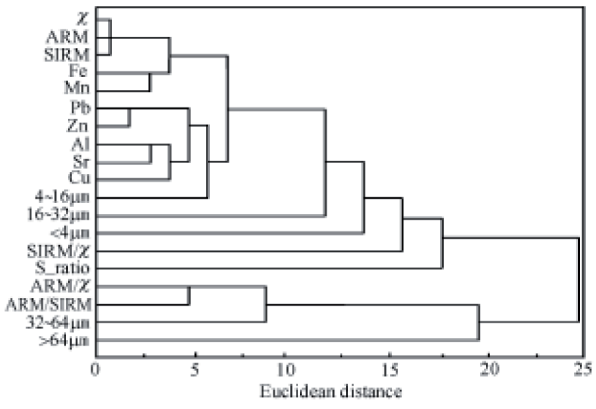

Fig. 6 Tree diagram of 19 parameters of the soil profile

particles and its type and concentration. The same trend is observed for the distance between ratio parameters and heavy metal contents.

Table 1 Correlation coefficient of magnetic parameters, grain size and heavy metals of the soil profile

	χ	ARM	SIRM	ARM/χ	ARM/SIRM	SIRM/χ
$< 4\mu$m	0.466**	0.484**	0.471**	–0.472**	–0.474**	0.251
$4 \sim 16\mu$m	0.827**	0.815**	0.827**	–0.728**	–0.662**	–0.233**
$16 \sim 32\mu$m	0.511**	0.467**	0.512**	–0.330**	–0.268**	0.043
$32 \sim 64\mu$m	–0.907**	–0.903**	–0.908**	0.833**	0.775**	–0.302**
$> 64\mu$m	–0.013	0.019	–0.016	–0.102	–0.129	–0.101
Al	0.844**	0.816**	0.844**	–0.772**	–0.724**	0.327**
Cu	0.893**	0.881**	0.897**	–0.804**	–0.806**	0.468**
Fe	0.976**	0.951**	0.973**	–0.899**	–0.841**	0.375**
Mn	0.943**	0.923**	0.942**	–0.870**	–0.845**	0.432
Pb	0.935**	0.914**	0.934**	–0.800**	–0.759**	0.365**
Zn	0.831**	0.798**	0.833**	–0.768**	–0.696**	0.281**
Sr	0.885	0.856**	0.885**	–0.745**	–0.745**	–0.700**

Note: sample number for statistic $n = 29$; significance level** $\alpha < 0.01$.

4.2 Fuzzy C-means Cluster Analysis

Fuzzy C-means cluster analysis (FCM) can divide the samples into different clusters according to their membership probability (probability belonging to a cluster). One can try to divide into different numbers of clusters to find a reasonable result[30]. FCM with the 10 parameters (χ, ARM, S_ratio, ARM/χ, SIRM/χ, $4 \sim 16\mu$m, Cu, Fe, Pb and Zn) was carried out to distinguish different intervals in the profile and to understand the vertical distribution and migration of pollutants. The values were first standardized by subtracting their means and dividing by their standard deviations, and cluster results are shown in Fig. 7 for three clusters cases. The profile is clearly divided into three parts at 3 cm and 10 cm depth. The upper part (0~3cm) obviously belongs to the cluster 1 with the membership (average value >90%) representing the strong magnetism of soils and high concentration of Cu, Fe, Pb and Zn. Between 3 and 10 cm is the separa- ting cluster 2 with the membership (60%~90%), indicating a transition zone and intermediate characteristic from top to bottom. The lower part (below 10 cm) is of cluster 3, and its significance given by membership probabilities is also 60%~90%. The values of χ, ARM and S_ratio as well as the heavy metal contents become very low, indicating the low values of their nature background and little influence from anthropogenic impacts.

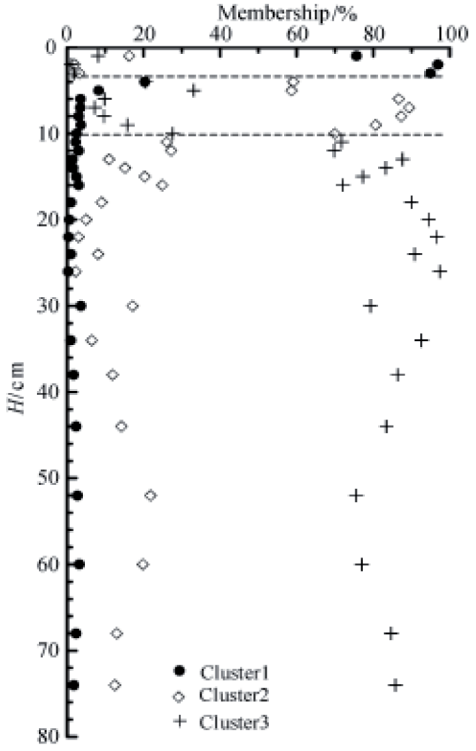

Fig. 7 Results of fuzzy C-means cluster analysis

From FCM, we can find an obvious difference among the upper, middle and lower part. The difference is mainly caused by the content of metal and magnetic phases. The pollutants from industrial process carrying

abundant metallic phases (including ferro(i)magnetic phases) increase the contents of metals and magnetic particles vastly on the topsoil. In addition, the soil texture is very loose, its metallic particles could cumulate and migrate in the upper part where the contents of metals and magnetic minerals are maximum and also could migrate downward easily in the soil profile. We think that the lower part is not polluted by anthropogenic pollution according to the magnetite and element contents.

5 CONCLUSIONS

Combining the information of magnetic parameters, grain size distribution, geochemical analysis, and multivariate statistics, the main conclusions can be summarized as follows:

The soil profile can be divided into three parts. The uppermost 3 cm represent the pollution-rich layer with a high concentration of ferromagnetic phases and metallic elements due to ambient industrial pollution. Enrichment of magnetic phases and heavy metals is found at 3 cm. Anthropogenic pollutants are the major material, and MD magnetite in the fractions of 4∼16μm and 16∼32μm is the dominant ferro(i)magnetic material. The middle part (3∼10 cm) is a pollution migration layer with gradually decreasing contents as an intermedial transition zone. The lower part (below 10 cm) is a natural background layer with the lowest concentration of magnetic minerals and heavy metals, representing the pedogenic or geogenic signal with little anthropogenic pollution.

Index clusters and linkage analysis reveal strong correlations between χ, ARM, SIRM and Mn, Cu, Fe, Pb, Zn, Al, Sr. Magnetic concentration parameters can be used as one kind of proxy for pollution investigation, it can be concluded it is a fast, sensitive, low-cost and high-efficient indicator for screening heavy metal pollution.

Fuzzy C-means cluster analysis can clearly divide the soil profile into different intervals and help to distinguish their characteristics. It can characterize the accumulation depth of pollutants i.e., enrichment, migration and background and reveal the process of pollution in the soil profile and improve identification of the unpolluted background and depth of migration.

ACKNOWLEDGMENTS

This work was supported by the National Natural Science Foundation of China (40374021, 40172102), the Key Project of National Basic Research Development Plan (2002CB412300) and German Research Foundation (AP 34/21).

We are grateful to Zhu Y X for conducting geochemical analyses. We also highly appreciate the help of the Institute of Geosciences, University of Tuebingen, Germany for providing their rock magnetic laboratory facilities.

REFERENCES

[1] Urszula K, Che F I, Malcolm E S, et al. Composition and element solubility of magnetic and non-magnetic fly ash fractions. *Environmental Pollution*, 2003, **123**: 255∼266

[2] Stanislav V V, Christina G V, Ali I K, et al. Phase-mineral and chemical composition of composite samples from feed coals, bottom ashes and fly ashes at the Soma power station, Turkey. *International Journal of Coal Geology*, 2005, **61**: 35∼63

[3] Petrovsky E, Kapicka A, Jordanova N, et al. Low-field magnetic susceptibility: a proxy method of estimating increased pollution of different environment systems. *Environmental Geology*, 2000, **39**(3-4): 312∼318

[4] Veneva L, Hoffmann V, Jordanova D, et al. Rock magnetic, mineralogical and micro-structural characterization of fly ashes from Bulgarian power plants and the nearby anthropogenic soils. *Physics and Chemistry of the Earth*, 2004, **29**: 1011∼1023

[5] Wang Y P, Pei T, Cheng H X, et al. Research on the distribution characters of heavy metals in column profile of soil within B city. *Bulletin of Mineralogy, Petrology and Geochemistry* (in Chinese), 2003, **22**(2): 144∼148

[6] Zhang M K, Ke Z X. Heavy metals, phosphorus and some other elements in urban soils of Hangzhou city, China. *Pedosphere*, 2004, **14**(2): 27∼36

[7] Desenfant F, Petrovsky E, Rochette P, et al. Magnetic signature of industrial pollution of stream sediments and correlation with heavy metals: Case study from South France. *Water, Air, and Soil Pollution*, 2004, **152**: 279∼312

[8] Lecoanet H, Leveque F, Ambrosi J P, et al. Combination of magnetic parameters: An efficient way to discriminate soil-contamination sources (south France). *Environmental Pollution*, 2003, **122**: 229∼234

[9] Strzyszcz Z, Magiera T. Magnetic susceptibility and heavy metal contamination in soils of Southern Poland. *Physics and Chemistry of the Earth*, 1998, **23**: 1127∼1131

[10] Dekkers M J. Environmental magnetism: an introduction. *Geologie en Mijnbouw*, 1997, **76**: 163∼182

[11] Kapicka A, Petrovsky E, Ustjak S, et al. Proxy mapping of fly-ash pollution of soils around a coal-burning power plant: A case study in the Czech Republic. *Geochemical Exploration*, 1999, **66**: 291∼297

[12] Kapicka A, Jordanova N, Petrovsky E, et al. Magnetic stability of power-plant fly ash in different soil solutions. *Physics and Chemistry of the Earth*, 2000, **25**: 431∼436

[13] Kapicka A, Jordanova N, Petrovsky E, et al. Effect of different soil conditions on magnetic parameters of power-plant fly ashes. *Journal of Applied Geophysics*, 2001, **48**: 93∼102

[14] Peter C, Thompson R, Harrison A, et al. Low temperature magnetic characterization of fire ash residues. *Physics and Chemistry of the Earth*, 2002, **27**: 1355∼1361

[15] Maher B A. Characterization of soil by mineral magnetic measurements. *Physics of the Earth and Planetary Interiors*, 1986, **42**: 76∼91

[16] Kenneth L, Veerosub, Andrew P R. Environmental magnetism: past, present, and future. *Journal of Geophysical Research*, 1995, **100**: 2175∼2192

[17] Oldfield F, Yu L Z. The influence of particle size variations on the magnetic properties of sediments from the north-eastern Irish Sea. *Sedimentology*, 1994, **41**: 1093∼1108

[18] Oldfield F. Toward the discrimination of fine-grained ferrimagnets by magnetic measurements in lake and near shore marine sediments. *Journal of Geophysical Research*, 1994, **99**: 9045∼9050

[19] Sun Z M, Hu S Y. A rock-magnetic study of recent lake sediments and its palaeo-environmental implication. *Chinese J. Geophys.* (in Chinese), 1996, **39**(2): 178∼187

[20] Hunt A. The application of mineral magnetic methods to atmospheric aerosol discrimination. *Physics of the Earth and Planetary Interiors*, 1986, **42**: 10∼21

[21] Hu S Y, Deng C L, Appel E, et al. Environmental magnetic studies of lacustrine sediments. *Chinese Science Bulletin*, 2002, **47**(7): 613∼616

[22] Zheng H, Oldfield F, Yu L Z. The magnetic properties of particle-sized samples from the Luo Chuan loess section: evidence for pedogensis. *Physics of the Earth and Planetary Interiors*, 1991, **68**: 250∼258

[23] Chen T B, Zheng Y M, Chen H, et al. Background concentrations of soil heavy metals in Beijing. *Environmental Science*, 2004, **25**(1): 117∼122

[24] Ju Y T, Wang S H, Zhang Q P, et al. Mineral magnetic properties of polluted top soils: A case study in Sanming city, Fujian province, south east China. *Chinese J. Geophys.* (in Chinese), 2004, **47**(2): 282∼288

[25] Verwey E J, Haa Yman P W, Romeijn F C. Physical properties and cation arrangement of oxides with spinal structures. *J. Chemical Physical*, 1947, **15**: 181∼189

[26] Özdemir ö, Dunlop D J, Moskowitz B M. The effect of oxidation on the Verwey transition in magnetite. *Geophys. Res. Lett.*, 1993, **20**: 1671∼1674

[27] Dunlop D J, Özdemir ö. Rock Magnetism. London: Cambrige University Press, 1997. 50∼52

[28] Hong N. SPSS for Windows Statistic Product and Service Solving Project (in Chinese). Beijing: Tsinghua University Press, 2003. 300∼311

[29] Thompson R, Oldfield F. Environmental Magnetism. London: Allen & Unwin Press, 1986. 34∼36

[30] Knab M, Appel E, Hoffmann V. Separation of the anthropogenic portion of heavy metal contents along a highway by means of magnetic susceptibility and fuzzy c-means cluster analysis. *European Journal of Environmental & Engineering Geophysics*, 2001, **6**: 125∼140

6

Magnetic susceptibility of dust-loaded leaves as a proxy of traffic-related heavy metal pollution in Kathmandu city, Nepal

Available online at www.sciencedirect.com
SCIENCE DIRECT®
Atmospheric Environment 39 (2005) 2201–2211
ATMOSPHERIC ENVIRONMENT
www.elsevier.com/locate/atmosenv

Magnetic susceptibility of dust-loaded leaves as a proxy of traffic-related heavy metal pollution in Kathmandu city, Nepal

Pitambar Gautam[a,*], Ulrich Blaha[b], Erwin Appel[b]

[a]*COE for Neo-Science of Natural History, Graduate School of Science, Hokkaido University, N10 W8, Sapporo 060-0810, Japan*
[b]*Institute of Geosciences, University of Tübingen, 72076 Tübingen, Germany*

Received 22 September 2004; received in revised form 24 December 2004; accepted 6 January 2005

Abstract

Dust-loaded tree leaves from Kathmandu have been analyzed for magnetic susceptibility (χ) and heavy metal (HM) contents. For 221 samples of leaves of cypress (mainly *Cupressus corneyana*), silky oak (*Grevillea robusta*) and bottlebrush (*Callistemon lanceolatus*), χ has a range of $(0.01–54)\times10^{-8}\,m^3\,kg^{-1}$ with a median of about $10.0\times10^{-8}\,m^3\,kg^{-1}$. Trees situated close to the busy road intersections, near the main bus station and sectors of roads with steep slope yield elevated susceptibility.

Chemical analysis of 20 samples of varying susceptibility by atomic absorption spectrometry yields the following maximum HM contents: Fe (1.3 wt%), Mn (281.9 ppm), Zn (195.2 ppm), Cu (41.5 ppm), Pb (38.4 ppm), Ni (8.1 ppm), Cr (6.4 ppm), Co (4.1 ppm) and Cd (1.2 ppm). The logarithmic susceptibility on dry mass basis (χ_d) shows significant linear relationship with HM contents: Pearson's correlation coefficient $r>0.8$ with Zn, Fe, Cr; $r>0.7$ with Mn, Cu; $r>0.6$ with Pb, Ni. Magnetic phases are of soft (magnetite/maghemite) and hard (hematite) coercivities. Microscopy of magnetic extracts reveals spherules (mostly of 2–20μm diameter) originated from vehicle exhausts through the combustion process as well as crystalline grains of lithogenic origin.

The dust accumulation in leaves took place mainly after monsoon (beginning of October 2001) till the sampling period (first half of February 2002). Despite the dependence of susceptibility and HM contents on a variety of spatial and temporal factors (amount of particulate matter (PM), efficiency of deposition/removal of PM by wind, precipitation, birds etc.), a significant correlation of susceptibility to HM implies that the former serves as an effective proxy of metallic pollution. Hence, susceptibility-based bio-monitoring technique is recommended as an economic and rapid tool for assessment of environmental pollution in urban areas like Kathmandu.

Keywords: Magnetic bio-monitoring; Dust loadings; Urban pollution; Environmental magnetism; Magnetic spherules

1. Introduction

Roadsides in urban area are commonly polluted by particulate matter (PM) derived mostly from traffic: motor vehicle emissions, abrasion of tyres, brake linings as well as road surface, cycling of dust in suspension due to vehicular movement, dispersion of construction material, etc. (Petrovsky and Ellwood, 1999; Gautam et al., 2004b). After its initial release into the atmosphere, PM may remain in air for some time, but most of it ultimately gets deposited along the narrow roadside corridor forming an integral part of the road dust,

*Corresponding author. Fax: +81 11 706 2986.
E-mail addresses: p-gautam@nature.sci.hokudai.ac.jp, pgautam2000@yahoo.com (P. Gautam).

1352-2310/$ - see front matter © 2005 Elsevier Ltd. All rights reserved.
doi:10.1016/j.atmosenv.2005.01.006

roadside soil, vegetation and drainage system. Hence, any material in and close to the road corridor serves as an archive of elevated concentrations of trace metals and their compounds. Knowledge on the nature of the metallic particles is important along with the concentration and size distributions, which are dictated by the nature of emissions, the rates of wet and dry deposition, nature and intensity of atmospheric phenomena as well as chemical transformations (e.g. Fang et al., 2004).

The content of airborne PM may be expressed in terms of total mass of suspended particles (TSP). However, the mass of particles with aerodynamic diameters below 10 μm (PM_{10}) per unit volume has been in common use since its monitoring started in the US in 1987 (Samet et al., 2000). The inhalability of PM_{10}-sized particles deep into the respiratory system causing adverse health effects, the higher rate of incidence of health problems with decrease in the particle size, association of the levels of fine PM in air with enhancement in morbidity and mortality rates and reduction in visibility etc. led to efforts to classify PM to even smaller size levels such as $PM_{2.5}$ and PM_1 (e.g. Samet et al., 2000; Palmgren et al., 2003).

The problem of vehicular pollution is relatively more severe in cities, like Kathmandu, in developing countries because of inadequate technical, economic as well as legislative provisions. High traffic density compared to the size and length of roads, predominance of old vehicles prone to high emission levels, poor quality of fuel and lubricants, late introduction of emission control standards and weaknesses in enforcing them and lack of fundamental database on emissions are the real problems. According to KEVA (2003), the annual average PM_{10} concentration in Kathmandu city in 2002–2003 was estimated at 198 $\mu g/m^3$ with a $PM_{2.5}$ to PM_{10} ratio of 0.64 implying a high contribution from combustion sources. Several recent changes, e.g. introduction of unleaded gasoline in 1999, closure of the Himal cement factory in 2000, increasing tendency in replacement of the Bull's trench-type kilns by new kilns with reduced emissions for brick production, use of kerosene and gas for cooking instead of biomass, have led to reduce pollution in Kathmandu. Because of a three-fold increase in the number of vehicles during the last decade, however, traffic emission has significantly increased and the vehicles are the number one source of pollution (KEVA, 2003).

Recent awareness to the rise in cases with respiratory diseases (e.g. chronic obstructive pulmonary disease, asthma) etc. led the Nepalese government to initiate programs to monitor PM and formulate the national ambient air quality standards in terms of a few parameters (TSP, PM_{10}, $PM_{2.5}$, CO, NO_2, SO_2 and benzene) (NESS, 2001; KEVA, 2003; MOPE Nepal, 2004). Besides monitoring, we see an urgent need for characterization and quantification of the particles in differing environmental systems (atmosphere, soil, vegetation, water etc.) using rapid and cost-effective techniques, such as combined environmental, magnetic and analytical chemical methods, similar to those applied in European countries (Petrovsky and Ellwood, 1999; Hoffmann et al., 1999; Hanesch and Scholger, 2002; Muxworthy et al., 2002).

This study is a part of the ongoing magnetic and geochemical investigations of urban material (soil, road dust and tree-leaves) to address the problems of environmental degradation of the Kathmandu valley subjected to accelerated urbanization (population overpressure by ca. 1.5 million people) and environmental stress (increasing traffic, industries, etc.) (Gautam et al., 2004b). Studies related to the use of magnetic properties of tree leaves are not new. For example, effective use of susceptibility of conifer needles as pollution proxy was established in Germany by Schädlich et al. (1995) for an industrial region affected by fly ash deposition and by Knab et al. (2003) in an apparently clean area of Black Forest. Matzka and Maher (1999) found the isothermal remanent magnetization (IRM) imparted to leaves of birch (Betula pendule) in urban and suburban area, around the city of Norwich (UK), useful as a proxy of traffic pollution. Suitability of both susceptibility and IRM of dust-loaded leaves of deciduous trees (Platanus sp. and *Quercus ilex*) for mapping vehicular traffic emissions in the city of Rome in Italy was described by Moreno et al. (2003). Similarly, Hanesch et al. (2003) demonstrated the potential of susceptibility and IRM to susceptibility ratio of maple tree leaves in and around an Austrian industrial site in Leoben for monitoring short-term (up to several months) dust deposition. Though the effectiveness of these methods is established, there exist no standards for the sampling material and study parameters.

This paper deals with the first magnetic bio-monitoring study, in Kathmandu, based on three types of trees, represented by cypress, silky oak, and bottlebrush, which collectively offer a good coverage in both urban and suburban areas. We describe the magnetic susceptibility of the tree leaves, the contents of heavy metals (HM: Cd, Cu, Co, Cr, Fe, Mn, Ni, Pb, Zn), and the susceptibility vs. HM relationship to characterize and quantify the environmental pollution.

2. Research methodology

2.1. Sampling

Leaves with dust loadings were sampled along road corridors as well as recreational parks in both urban and suburban areas in February 2002. Samples came from the following routes and areas (Fig. 1): (i) the western

half of the Ring Road; (ii) inner roads between Kalanki and Koteshwar; (iii) the arterial roads leading to Kirtipur and Dakshinkali; and (iv) around the Ratna Park and Rani Pokhari, in the core urban areas.

A total of 221 trees represented by cypress (mainly *Cupressus corneyana*) found commonly along the inner city roads and gardens, silky oak (*Grevillea robusta*) that is abundant along the Ring Road, the bottlebrush (*Callistemon lanceolatus*) that fills large gaps between the former two species) (Figs. 1 and 2, Table 1). In the case of cypress, only the young tender leaves were taken. Whenever possible, sampling was confined to branches, facing road, at a height of 2–2.5m above ground. Samples were put in pocket-sized sealable plastic bags, of known susceptibility, and allowed to dry at room temperature, before measuring them in the laboratory.

2.2. Susceptibility measurement, IRM acquisition and microscopy

Volume magnetic susceptibility was measured on the AGICO KLY-2 Kappabridge, with an operating frequency of 920 Hz and sensitivity of 4×10^{-8} SI. For intra-species and inter-species comparisons, it was then normalized by the sample mass to obtain the mass-specific susceptibility (χ).

A small amount of dust-loaded leaf sample was inserted into a 10 cc volume polyethylene cylinder, fixed with nonmagnetic cement slurry, solidified, and then subjected to IRM acquisition up to a maximum of 2.5 T, using pulse fields at 18–20 steps generated by a Magnetic Measurements pulse magnetizer. The acquired IRM moment was measured by a Molspin spinner magnetometer.

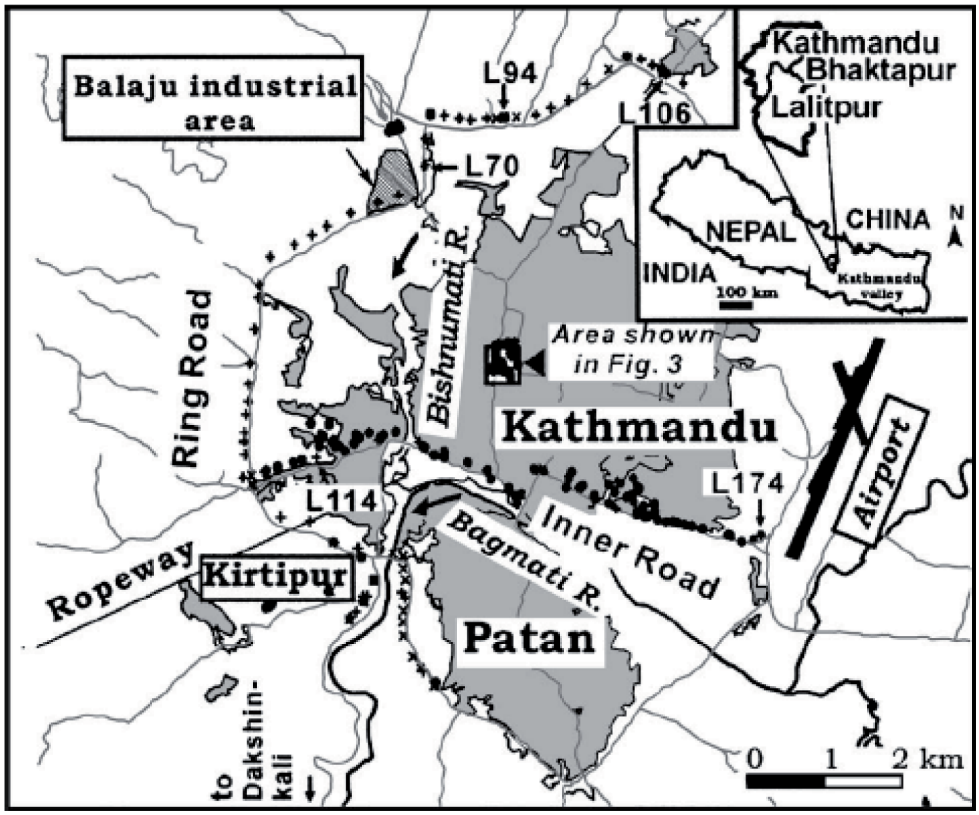

Fig. 1. Sketch maps showing the locations of trees sampled for the dust-loaded leaves. Location of the three districts of Kathmandu valley is indicated in the index map in upper right corner of the map. The greater Kathmandu urban area comprising Kathmandu and Patan cities is shown by light shading. The light and dark lines indicate the major road network and major rivers marking district boundaries. The Ratna Park area at the heart of the Kathmandu city investigated in more detail (Fig. 3) is marked. Symbols (plus, multiplication and dot) stand for the location of sampled trees (silky oak, bottlebrush, cypress) and susceptibility variation in them along two major profiles is shown in Fig. 2. Samples from 5 sites labelled as L70, L94, L106, L114 and L174 used to describe magnetic minerals and chemistry in Figs. 4 and 5 are indicated by arrows. The background map was modified from Shrestha and Pradhan (2000).

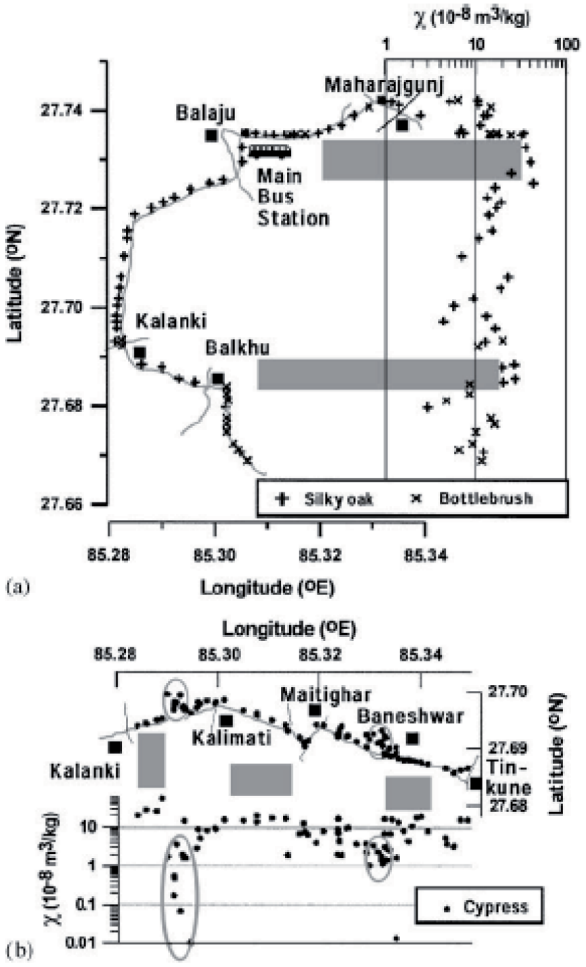

Fig. 2. Magnetic susceptibility (χ) of the dust-loaded leaves from trees, sampled along the two major road profiles. For the Ring Road profile (Fig. 2a, left side), a χ vs. latitude plot is given. For the inner road profile (Fig. 2b, upper part), between Kalanki and Tinkune, a χ vs. longitude plot better reflects the variation. The shaped rectangles, in both profiles, mark sectors showing consistently high χ. In contrast, the points included within ovals mark the relatively low χ which can be explained in terms of the distance of the sites from the road axis.

Magnetic extracts of some samples separated by using a hand magnet were observed under a scanning electron microscope (Leo SEM 1450VP) after coating with carbon. Major element composition of selective grains was measured with an Oxford INCA EDS 200 micro-analysis system linked to SEM, the details of which are given in Gautam et al. (2004b).

2.3. Chemical analysis

Twenty samples of dust-loaded leaves with varying χ were oven dried at 75 °C for 48 h, then ashed at 500 °C for 2 h and about 0.5 g of ash was digested for metals by 5 ml aqua regia (conc. HCl to HNO_3 ratio of 2:1) in a Kjeldatherm system (at 140 °C, 2 h). A Perkin-Elmer M1100 atomic absorption spectrophotometer of the Department of Geography, University of Tübingen was used to analyze the pseudo-total contents of Cd, Cu, Co, Cr, Fe, Mn, Ni, Pb, Zn using a standard procedure (Ure, 1995).

In order to compare the measured quantities, both susceptibility and HM contents were recalculated on oven-dried mass basis. This involved, (i) subtraction of the susceptibility contribution of the water content from χ to obtain χ_d following Walden et al. (1999), and (ii) reduction of the HM contents measured for ash to the oven-dried sample taking into account the mass lost upon ashing.

3. Magnetic properties and heavy metal chemistry

3.1. Magnetic susceptibility

A brief summary on χ of all dust-loaded leaf samples according to type of trees is given in Table 1. Cypress offers the maximum range (χ_{max}–χ_{min}) followed by silky oak and bottlebrush. It has the lowest median and spread as indicated by the interquartile range. Silky oak and bottlebrush have median values close to each other but the former has a larger spread. Although direct

Table 1
Magnetic susceptibility data by dust-loaded leaves by tree types

Tree type	No. of samples	MS (10^{-8} m^3kg^{-1})					
		Min.	Quartiles			Range (Max–Min)	Interquartile range (Q3–Q1)
			Q1 (25%)	Median (50%)	Q3 (75%)		
Himalayan cypress	142	0.01	2.23	5.27	10	53.97	7.77
Silky oak	55	2.75	7.55	13.08	18.83	40.33	11.28
Bottlebrush	24	1.12	7.12	10.31	15.31	23.49	8.19

comparison may not be well justified, the median values suggest that the dust-loaded leaves may be as strong as the fine-grained black clay/silt sediments, constituting the Kathmandu valley fluvio-lacustrine sediments, which yield $(5.8–11.2)\times10^{-8}\,m^3\,kg^{-1}$ and a mean of $8.2\times10^{-8}\,m^3\,kg^{-1}$ (Gautam, unpublished data).

Two major road profiles shown in Fig. 2 reveal remarkable regularities in the susceptibility distribution. The Ring Road profile (Fig. 2a) exhibits a smooth susceptibility variation irrespective of the tree type (silky oak or bottlebrush) and the presence of anomalous zones, of distinctly high χ ($>20\times10^{-8}\,m^3\,kg^{-1}$), accompanied by flanks characterized by moderate χ ($10–15\times10^{-8}\,m^3\,kg^{-1}$). Two wide anomalous zones correspond to the areas around the main bus station and a rather long road sector, situated between Balkhu and Kalanki, where the TATA trucks spewing up black smokes are commonly parked along the roadsides. In the Kalanki–Tinkune profile, for which only data for cypress are shown (Fig. 2b). χ has a much wider range that can be explained by its inverse relationship with the distance of sampled trees from the major road axis. The two clusters of trees, located at appreciable distances from the road, to the West of Kalimati and near Baneshwar have correspondingly low susceptibilities ($0.01–5\times10^{-8}\,m^3\,kg^{-1}$). The highest values observed near Kalanki correspond to the road sector with relatively steep slopes. In general, the average susceptibility along the inner road is lower than along the Ring Road, which might be explained in terms of a larger volume of traffic as well as the probably a higher dust trapping potential of the silky oak and bottle brush than the cypress.

Along roadsides in the city core area, high χ occurs close to the road junctions (e.g. near the clock tower, Fig. 3). Increase in χ is observed while moving toward roads from recreational parks (Fig. 3). Moderate values characterize trees in open spaces, which are prone to dust supply from nearby roads or exposed grounds. This is shown by a profile across the Ratna Park, where most trees in the row form a wind barrier as well as an effective trap for dust coming in from the adjacent open ground (Fig. 3).

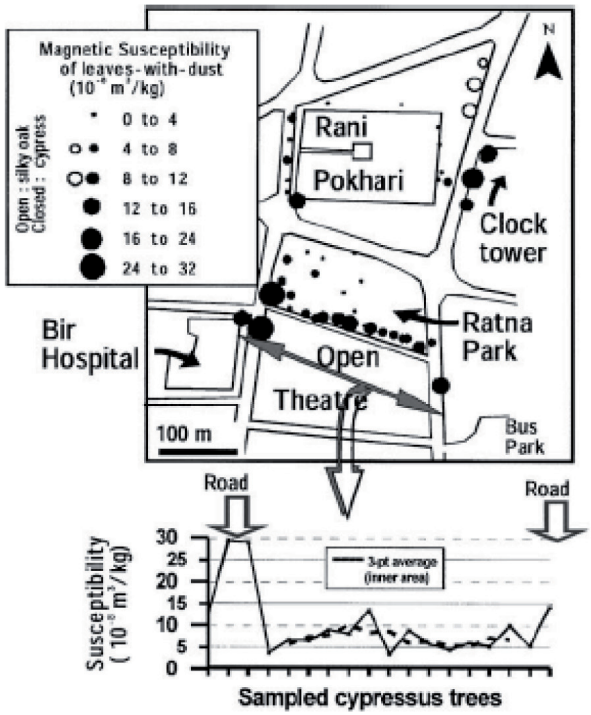

Fig. 3. Magnetic susceptibility of the dust-loaded leaves around the Ratna Park–Rani Pokhari, in the core urban area. The rows of trees along a foot trail in between the Ratna Park and the open-air theatre has been shown in map as well as profile. The size of the symbols (filled circles: cypress; open circles: silky oak) is proportional to the susceptibility magnitude as shown in the class legend. Elevated values occur near the road intersections. Within the Ratna Park area, trees located in the innermost parts possess the lowest χ.

3.2. Magneto-mineralogical characterization

3.2.1. IRM characteristics

In several specimens sampled from different localities, the IRM acquired at 0.1 and 0.3 T is about 70% and 85–90% of the total magnitude acquired at 2.5 T, respectively (Fig. 4a). It means that soft magnetic minerals (magnetite and probably maghemite) contribute significantly (Fig. 4b,c). Judging from 10% to 20% of IRM acquired within 0.3 and 2.5 T, a high content of a harder magnetic phase is confirmed. Most likely the hard phase is hematite. It probably comes from the bricks which are known to contribute significantly to the susceptibility of urban soils (Gautam et al., 2004b).

3.2.2. Scanning electron microscopy (SEM) images

Microscopy of magnetic extracts from the dust contained in tree leaves reveals basically two morphologies of grains (Fig. 5): firstly, euhedral to anhedral crystalline grains mostly derived from rock sources and secondly, spherical grains. The isolated spherical grains exhibit orange peel and/or framboidal textures (Fig. 5a,c). Agglomerates exhibit welded (to clusters) textures (Fig. 5b). The diameter of isolated spherules is typically 2–20 μm. However, the linear dimension may exceed 100 μm for agglomerates (Fig. 5c). In terms of chemistry (Table 2), the isolated grains have the following typical composition: Fe (76–77 wt%) and O (22–23 wt%), irrespective of the grain geometry. For the spots within the agglomerated grain, the contents of Fe and O are 70–71 and >24 wt% (points 7, 8 in Fig. 5b and Table 2). Spherules contain traces of Co and Tb, whereas the agglomerate contains S and Cl. The lower

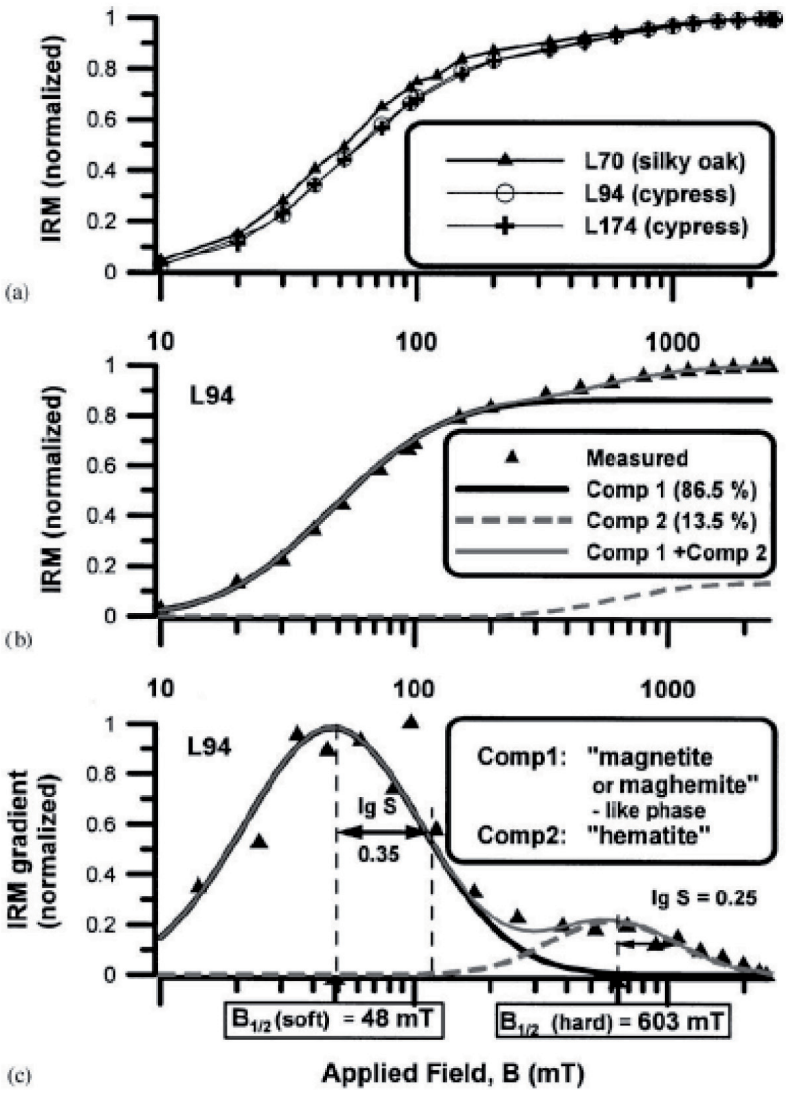

Fig. 4. Isothermal remanent magnetization (IRM) data for the dust-loaded leaves. (a) IRM acquisition curves for three samples (see Fig. 1, for locations), exhibiting remarkably similar shapes. (b, c) Results of component modelling for a sample, following Kruiver et al. (2001). The IRM magnitude and its gradient along with the modelled median acquisition field ($B_{1/2}$) values, indicated by arrows, as contributing to the curves and the respective logarithmic standard deviations (lgS), are shown.

values of Fe as well as the presence of Mg, Al, Si, Ti, etc. in some analyses (1, 5, 6 in Fig. 5 and Table 2) may be the result of contamination of the analyzed spots by background silicate material. In general, the chemical composition of the isolated grains is close to that of pure magnetite.

3.3. Heavy metal chemistry and their correlation with susceptibility

The ranges of metal contents measured for a set of 20 samples are as follows: 0.08–1.33 wt% of Fe, 18.3–281.9 ppm of Mn, 15.9–195.2 ppm of Zn, 4.7–41.5 ppm of Cu, 1.8–38.4 ppm of Pb, 0.6–8.1 ppm of Ni, and 1.7–6.4 ppm of Cr. The exceptionally high contents of Cr (76.8 ppm), Ni (48.8 ppm) and Pb (46.1 ppm) for sample L114 are considered to be outliers and not included in these ranges. The maximum contents of Co and Cd were 4.1 and 1.2 ppm, respectively. Contents of Co and Cd were below 1.0 ppm in 12 and 17 samples, respectively, being mostly around the analytical detection limit. Hence, Co and Cd contents are not discussed.

It is evident from the correlation matrix in Table 3 that the logarithmic χ_d has a significant linear relationship with metal contents: Pearson's correlation

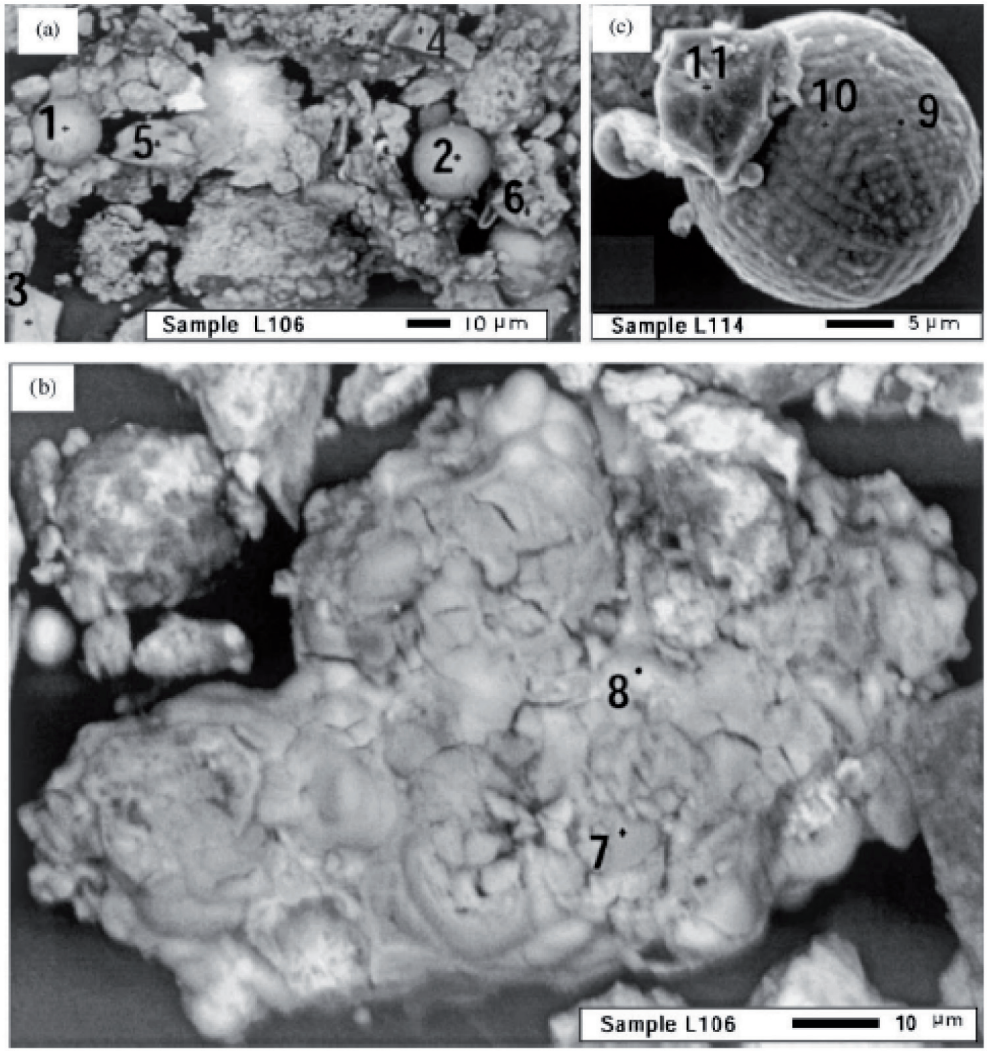

Fig. 5. Back-scattered images of the magnetic grains observed in magnetic extracts of the leaf-dust. The sample locations are given in Fig. 1. The magnetic material can be classified roughly into two groups: (i) isolated relatively fine spherules and agglomerates formed by aggregation or welding of smaller spherules, of anthropogenic origin, and (ii) euhedral to subhedral grains of lithogenic origin. Note the relatively large magnetic spherule with distinct orange-peel structure indicative of combustion. Numbered symbols (+) are spots of energy-dispersive X-ray analyses, data for which are given in Table 2.

coefficient $r>0.8$ with, Zn, Fe, Cr; $r>0.7$ with Mn, Cu; and $r>0.6$ with Pb, Ni. Among metals themselves, Fe exhibits a very strong correlation ($r>0.85$) with Mn, Zn and Cr. Similarly, Zn, Cu and Pb are strongly related among themselves with $r=0.83-0.87$.

In order to judge how closely the variables (metal contents and susceptibility), are related to each other, a tree diagram is constructed using the single linkage distance ratio method (Fig. 6a). This interpretation is not unique but a reasonable description of the observed dataset. According to the diagram, the metals Fe, Zn and Cr form a close cluster as do Mn and Cu. Further, these two groups are closer to each other than with χ_d. Pb is relatively farther from all variables, while Ni is farthest from all.

The linear relationship between a set of 3 urban elements (Cu, Pb and Zn, known to originate from vehicular pollution; e.g. de Miguel et al., 1997) and Fe with logarithmic χ_d is detailed in Fig. 6b. There are clearly two groups which show varying goodness of fit (r^2) but striking similarities in variation of contents with respect to susceptibility within each group are evident.

Table 2
Energy-dispersive X-ray analytical data (wt. %) on magnetic grains constituting the dust in leaves

Points[a]	L106								L114		
	Spherules		Nonspherical grains				Agglomerate		Spherules		Nonsph. gr.
Elements	1	2	3	4	5	6	7	8	9	10	11
Fe	**69.77**	**76.98**	**76.24**	**77.44**	**74.75**	**72.77**	**70.12**	**70.88**	**77.24**	**76.69**	**77.44**
Mg	0.63	—	—	—	—	0.40	—	—	—	—	—
Al	0.97	—	0.35	0.10	0.41	0.41	—	0.33	—	—	—
Si	1.39	0.22	0.46	0.09	0.62	0.58	0.73	0.72	0.29	0.23	0.09
K	0.46	—	—	—	—	0.24	—	0.32	—	—	—
Ti	0.92	—	—	—	—	—	—	—	—	—	—
Ca	—	—	0.20	—	0.87	0.86	1.35	1.01	—	—	—
Co	—	—	—	—	—	—	—	—	—	0.67	—
Tb	2.00	—	—	—	—	—	—	—	—	—	—
Mn	—	—	—	—	—	0.62	0.83	0.60	—	—	—
S	—	—	—	—	0.21	—	1.91	1.44	—	—	—
P	—	—	—	—	—	0.61	—	—	—	—	—
Br	—	0.50	—	—	—	—	—	—	—	—	0.17
Cl	—	—	—	—	—	—	0.49	0.45	—	—	—
O	**23.86**	**22.30**	**22.75**	**22.37**	**23.15**	**23.50**	**24.57**	**24.23**	**22.46**	**22.41**	**22.29**
Total	100.00	100.00	100.00	100.00	100.01	99.99	100.00	99.98	99.99	100.00	99.99

[a]The analyzed points corresponding to these numbers are given in Fig. 5.

Table 3
Correlation matrix for magnetic susceptibility and heavy metal contents ($N = 20$)

	lg (MS)	Fe	Mn	Zn	Cu	Pb	Ni	Cr
lg (MS)	1.00							
Fe	0.84 (0.000)	1.00						
Mn	0.76 (0.000)	0.91 (0.000)	1.00					
Zn	0.86 (0.000)	0.92 (0.000)	0.83 (0.000)	1.00				
Cu	0.74 (0.000)	0.86 (0.000)	0.92 (0.000)	0.87 (0.000)	1.00			
Pb	0.64 (0.002)	0.78 (0.000)	0.76 (0.000)	0.85 (0.000)	0.83 (0.000)	1.00		
Ni	0.60 (0.006)	0.57 (0.012)	0.53 (0.021)	0.67 (0.002)	0.61 (0.006)	0.68 (0.001)	1.00	
Cr	0.80 (0.000)	0.94 (0.000)	0.79 (0.000)	0.95 (0.000)	0.79 (0.000)	0.72 (0.001)	0.66 (0.002)	1.00

For each pair, the Pearson's product–moment correlation r is given with the level of significance p (in brackets).

4. Discussion and conclusions

The highest range of χ (Table 1) of the dust-loaded leaves of cypress trees, which are ubiquitous along the inner roads and recreational parks in Kathmandu, makes them suitable for magnetic bio-monitoring along profiles and also over selected areas. As the silky oak and bottlebrush yield comparable susceptibilities as shown by the Ring Road profile (Fig. 2a), the preference of one over the other will depend on the availability of the concerned trees. It is notable, however, that all three species offer reasonable contrasts in susceptibility that has significant correlation to the HM contents, especially the urban elements like Cu, Pb and Zn.

The observed maximum contents of urban elements in dust-loaded leaves (Zn: 195.2 ppm; Cu: 41.5 ppm; Pb: 38.4 ppm) are enhanced by 232%, 122% and 240% with respect to the local background contents (Zn: 84 ppm, Cu: 34 ppm, Pb: 16 ppm) for a soil profile at an urban background site in Kirtipur (Gautam et al., 2004a). Their magnitudes are, however, low compared to the maximum contents for Bagmati river sediments (Zn: 277.0 ppm, Cu: 63.6 ppm, and Pb: 173.3 ppm) obtained by similar type of analysis (Devkota, 2001). Although direct comparisons of the metal contents in soils, river sediments and leaves are problematic due to many factors (e.g., differences in timescales, depositional/removal processes and the differences in areas averaged by the samples), they show that temporary

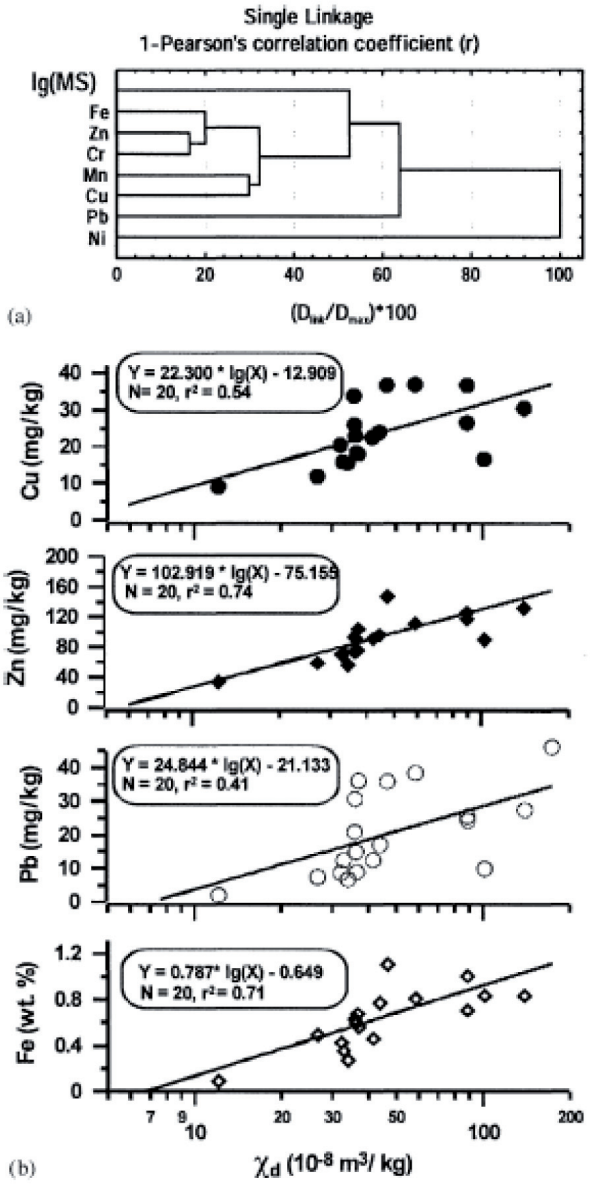

Fig. 6. (a) A tree diagram, derived from cluster analysis, depicting the correlation between HM contents and susceptibility based on single linkage distance. (b) Linear regression analysis between selected heavy metals and magnetic susceptibility and the regression equations for estimating metal contents from the magnetic susceptibility (χ_d). The coefficient determination (r^2) gives the goodness of fit of the regression line.

accumulations of PM in roadside tree leaves may give rise to very high levels of metal contents.

The magnetic spherules are attributed to anthropogenic input, arising from any type of combustion related to vehicles as shown also by dust samples taken from the road surface or the rubber plant leaves at <0.5 m height (Gautam et al., 2004b). Palmgren et al. (2003) found that the tailpipe emissions give rise to fine and ultrafine particles with modal aerodynamic diameters of 0.1–2 and 0.03–0.1 μm, respectively, whereas abrasion-related particles yield rather coarse modes (>2 μm). According to Matzka and Maher (1999), the grain size was found to lie between 0.3 and 3 μm interpreted in favor of derivation of such fine particles from vehicle exhaust rather than friction wear or resuspended road dust. Despite the relatively large predominant size (2–20 μm) of spherules observed in this study, we attribute them to the tailpipe emissions as they occur along the roadside trees which are far away from industrial sources. Possibility of generation of large-sized particles through combustion in vehicles is also supported by recent findings of: (i) large-sized magnetite (up to 8 μm diameter) formed by burning FeS_2 containing fossil fuel (Flanders, 1999); and (ii) a significant amount of 7–50-μm (with a maximum of 300 μm)-sized spherules in road dust from Visakhapatnam in India (Goddu et al., 2004). Most of the euhedral to subhedral grains yielding magnetite-like mineralogy are attributed to lithogenic origin (Gautam et al., 2004b).

The dust accumulation on tree leaves took place mostly after post-monsoon (beginning of October 2001) until the sampling period (first half of February 2002). The measured quantities depend on the degree of pollution governed by a variety of time- and space-dependent factors: amount of particles of anthropogenic and lithogenic origin; efficiency of deposition of particles in leaves as a function of the distance from road (Matzka and Maher, 1999), height and areal coverage of leaves; intensity of precipitation; intensity and direction of wind; degree of disturbance by living beings such as humans, animals and birds, etc. Lack of adequate knowledge on all these factors makes the interpretation of minute susceptibility variations difficult. In such cases, it may be sometimes more realistic to judge the variations in qualitative terms by grouping into susceptibility classes as shown in Fig. 3. A significant linear relationship between the HM contents and susceptibility proves that the latter serves as an effective proxy of the metallic pollution (especially by Pb, Cu and Zn originating mainly from vehicular sources).

Occurrence of relatively higher metal contents in sides of trees proximal to roads than in the distal sides, and the ability of trees to draw dust and hence reduce particulate concentrations at respirable heights may be a positive feature (e.g., Matzka and Maher, 1999). This is indeed true for trees along sides of highways with spacious lawns and houses located reasonably away from the roads. However, in urban areas like Kathmandu with narrow roadsides, with human activity occurring in proximity of roads, the capability of trees to collect and hold harmful PM, on a temporary basis, may have adverse health effects on the residents.

In conclusion, magnetic susceptibility measurements of leaves are effective in identifying pollution hot spots with marked input of magnetic materials derived from anthropogenic traffic-related pollution. Because of the good correlation of susceptibility with the heavy metals related to urbanization, the former serves as a proxy for metallic pollution. Therefore, use of susceptibility-based bio-monitoring technique should be considered for temporal (short-term, mostly up to several months) and spatial assessment of pollution in cities, like Kathmandu, where traffic-related problems are ever increasing. With proper calibration of susceptibility with metal contents for the most characteristic tree-type available, this method can be used for a detailed monitoring of anomalously polluted areas.

Acknowledgements

PG acknowledges a Forster Research Fellowship by Alexander von Humboldt Foundation and the 21st Century COE Program for Neo-Science of Natural History. We thank Rolf Beck (University of Tübingen) for expert advice during chemical analyses and Sabita Poudel (Tribhuvan University) for assisting us with the identification of tree types.

References

De Miguel, E., Llamas, J.F., Chacón, E., Berg, T., Larssen, S., Røyset, O., Vadset, M., 1997. Origin and patterns of distribution of trace elements in street dust: unleaded petrol and urban lead. Atmospheric Environment 31 (17), 2733–2740.

Devkota, D., 2001. Total and extractable (mobilizable and mobile) heavy metals in the Bagmati river sediment of Kathmandu, Nepal. A Journal of the Environment 6 (7), 34–51.

Fang, G.-C., Chag, C.-N., Wu, Y.-S., Chen, M.-H., Ho, T.-T., Huang, S.-H., 2004. A study of metallic elements at suburban and industrial regions in central Taiwan during 2002–2003. Atmospheric Research 70, 131–142.

Flanders, P.J., 1999. Identifying a fly ash at a distance from fossil fuel power stations. Environmental Science and Technology 33, 528–532.

Gautam, P., Blaha, U., Appel, E., 2004a. Integration of magnetic properties and heavy metal chemistry to quantify environmental pollution in urban soils, Kathmandu, Nepal. Himalayan Journal of Sciences 2 (4), 140–141.

Gautam, P., Blaha, U., Appel, E., Neupane, G., 2004b. Environmental magnetic approach towards the quantification of pollution in Kathmandu urban area, Nepal. Physics and Chemistry of the Earth 29 (13,14), 973–984.

Goddu, S.R., Appel, E., Jordanova, D., Wehland, R., 2004. Magnetic properties of road dust from Visakhapatnam (India)—relationship to industrial pollution and road traffic. Physics and Chemistry of the Earth 29 (13,14), 985–995.

Hanesch, M., Scholger, R., 2002. Mapping of heavy metal loadings in soils by means of magnetic susceptibility measurements. Environmental Geology 42, 857–870.

Hanesch, M., Scholger, R., Rey, D., 2003. Mapping dust distribution around an industrial site by measuring magnetic parameters of tree leaves. Atmospheric Environment 37, 5125–5133.

Hoffmann, V., Knab, M., Appel, E., 1999. Magnetic susceptibility mapping of roadside pollution. Journal of Geochemical Exploration 66, 313–326.

KEVA, 2003. Health impacts of Kathmandu's air pollution. Report submitted to Kathmandu Electrical Vehicle Alliance (KEVA) by Clean Energy Nepal and Environmental and Public Health Organization, Kathmandu, 87pp. (unpubl.)

Knab, M., Appel, E., Hoffmann, V., 2003. The anthropogenic dust load of coniferous tree needles in the Black Forest area, SW Germany: an approach using magnetic susceptibility (MS). In: Abstracts, XXIII General Assembly of the International Union of Geodesy and Geophysics, Sapporo, GAI.02/01A/A16-007. A.261.

Kruiver, P.K., Dekkers, M.J., Heslop, D., 2001. Quantification of magnetic coercivity components by the analysis of acquisition curves of isothermal remanent magnetization. Earth and Planetary Science Letters 189, 269–276.

Matzka, J., Maher, B.A., 1999. Magnetic biomonitoring of roadside tree leaves: identification of spatial and temporal variations in vehicle-derived particulates. Atmospheric Environment 33, 4565–4569.

MOPE Nepal, 2004. http://www.mope.gov.np/environment/air.php and http://mope.gov.np/mopepollution/.

Moreno, E., Sagnotti, L., Winkler, A., Dinarès-Turell, J., Cascella, A., 2003. Air pollution survey in Rome using magnetic properties of tree leaves. Geophysical Research Abstracts, vol. 5, 02551, European Geophysical Society.

Muxworthy, A.R., Schmidbauer, E., Petersen, N., 2002. Magnetic properties and Mössbauer spectra of urban atmospheric particulate matter: a case study from Munich, Germany. Geophysical Journal International 150, 558–570.

NESS, 2001. Air Quality Database of Nepal (special issue). Nepal Environmental and Scientific Services Co., Kathmandu.

Palmgren, R., Wåhlin, P., Kildesø, J., Afshari, A., Fogh, C.L., 2003. Characterization of particle emissions from the driving car fleet and the contribution to ambient and indoor particle concentrations. Physics and Chemistry of the Earth 28, 327–334.

Petrovsky, E., Ellwood, B.B., 1999. Magnetic monitoring of pollution of air, land and waters. In: Maher, B.A., Thompson, R. (Eds.), Quaternary Climates, Environments and Magnetism. Cambridge University Press, Cambridge, pp. 279–322.

Samet, J.M., Francesca, D., Curriero, F.C., Coursac, I., Zeger, L. Scott, 2000. Fine particulate air pollution and mortality in 20 US cities, 1987–1994. New England Journal of Medicine 343, 1742–1749.

Schädlich, G., Weissflog, L., Schuurmann, G., 1995. Magnetic susceptibility in conifer needles as indicator of fly ash deposition. Fresenius Environmental Bulletin 4 (1), 7–12.

Shrestha, B., Pradhan, S., 2000. Kathmandu Valley GIS Database. ICIMOD, Kathmandu.

Ure, A.M., 1995. Methods of analysis for heavy metals in soils. In: Alloway, B.J. (Ed.), Heavy Metals in Soils, second ed. Blackie Academic & Professional, London, pp. 59–100.

Walden, J., Oldfield, F., Smith, J.P. (Eds.), 1999. Environmental Magnetism: A Practical Guide. Technical Guide Series, No. 6. Quaternary Research Association, London, pp. 250.

7

Integration of magnetism and heavy metal chemistry of soils to quantify the environmental pollution in Kathmandu, Nepal

The Island Arc (2005) 14, 424–435

Thematic Article

Integration of magnetism and heavy metal chemistry of soils to quantify the environmental pollution in Kathmandu, Nepal

PITAMBAR GAUTAM,[1,*] ULRICH BLAHA[2] AND ERWIN APPEL[2]

[1]*COE for Neo-science of Natural History, Graduate School of Science, Hokkaido University, N10 W8, Sapporo 060-0810, Japan (email: p-gautam@nature.sci.hokudai.ac.jp) and* [2]*Institute of Geosciences, University of Tübingen, Sigwartstrasse 10, D-72076 Tübingen, Germany*

Abstract Soil profiles of the Kathmandu urban area exhibit significant variations in magnetic susceptibility (χ) and saturation isothermal remanence (SIRM), which can be used to discriminate environmental pollution. Magnetic susceptibility can be used to delineate soil intervals by depth into normal ($< 10^{-7}$ m^3/kg), moderately enhanced (10^{-7}–$< 10^{-6}$ m^3/kg) and highly enhanced ($\geq 10^{-6}$ m^3/kg). Soils far from roads and industrial sites commonly fall into the 'normal' category. Close to a road corridor, soils at depths of several centimeters have the highest χ, which remains high within the upper 20 cm interval, and decreases with depth through 'moderately magnetic' to 'normal' at approximately 30–40 cm. Soils in the upper parts of profiles in urban recreational parks have moderate χ. Soil SIRM has three components of distinct median acquisition fields ($B_{1/2}$): soft (30–50 mT, magnetite-like phase), intermediate (120–180 mT, probably maghemite or soft coercivity hematite) and hard (550–600 mT, hematite). Close to the daylight surface, SIRM is dominated by a soft component, implying that urban pollution results in enrichment by a magnetite-like phase. Atomic absorption spectrometry of soils from several profiles for heavy metals reveals remarkable variability (ratio of maximum to minimum contents) of Cu (16.3), Zn (14.8) and Pb (9.3). At Rani Pokhari, several metals are well correlated with χ, as shown by a linear relationship between the logarithmic values. At Ratna Park, however, both χ and SIRM show significant positive correlation with Zn, Pb and Cu, but poor and even negative correlation with Fe (Mn), Cr, Ni and Co. Such differences result from a variety of geogenic, pedogenic, biogenic and man-made factors, which vary in time and space. Nevertheless, for soil profiles affected by pollution (basically traffic-related), χ exhibits a significant linear relationship with a pollution index based on the contents of some urban elements (Cu, Pb, Zn), and therefore it serves as an effective parameter for quantifying the urban pollution.

Key words: environmental pollution, heavy metals, isothermal remanence, Kathmandu, magnetic susceptibility, soil magnetism.

INTRODUCTION

The Kathmandu Valley is situated within the Lesser Himalaya and is filled by fluvial and lacustrine sediments of Plio-Pleistocene age, derived from the north and northeast and surrounding metasedimentary terrains (Yoshida & Gautam 1988). The present state of the environment of the Kathmandu Valley has been deteriorating as a result of various causative factors such as the traffic pollution dominant in the urban area, industrial activities, including the cement factory, emissions from the traditional brick kilns scattered throughout the valley, biomass burning, etc. (Devkota 2001; Malinovsky 2001; Sharma *et al.* 2002). Hence, recognition of the major sources and types of pollution, estimation of the share of each source, quantification of the degree of pollution, and monitoring are essential in order to reveal the spatial and temporal differences in pollution levels.

*Correspondence.

Received 28 December 2004; accepted for publication 29 August 2005.

Following the effectiveness of the integration of chemistry and magnetic properties in studies of the degree of pollution of the air, water, vegetation and land systems (Petrovsky & Ellwood 1999; Knab *et al.* 2001; Hanesch & Scholger 2002), these properties have already been applied by the authors of the present study to successfully characterize and quantify the degree of pollution in the Kathmandu urban area (Gautam *et al.* 2004, 2005). The variables measured in this respect are the various rockmagnetic properties (mass-specific magnetic susceptibility, χ; isothermal remanent magnetization, IRM; χ *vs* temperature characteristics) of a variety of materials (dust-loaded leaves of roadside trees, road dust and soils from the surface, as well as vertical sections of up to several meters), and the contents of heavy metals (HM) in them.

In the present paper, χ, IRM and its components, the contents of HM (Cd, Cu, Co, Cr, Fe, Mn, Ni, Pb, Zn) and their relationship to χ and IRM in urban and suburban soils are described in order to quantify the pollution levels. Emphasis is given to the use of magnetic parameters as stand-alone properties to characterize pollution and also as the effective proxy of contamination using an index that combines the contents of Cu, Pb, Zn, which represent the urban elements (De Miguel *et al.* 1997). Soil samples were collected from the following areas (Fig. 1): (i) the suburban background site in Kirtipur; (ii) the recreational areas and parks (Ratna Park, Rani Pokhari and exhibition ground) situated in the core urban areas; and (iii) the recreational park area in Balaju, which is close to an industrial area.

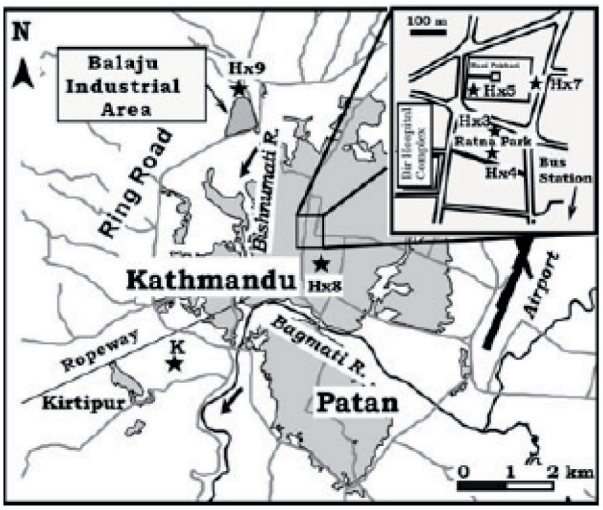

Fig. 1 Schematic map of the urban area (shaded) and its surroundings in Kathmandu City in Nepal. Several soil coring sites (K, suburban area near Kirtipur; Hx3–5 & Hx7–8, core urban area; Hx9, close to the industrial area in Balaju), which are the objects of investigation for magnetic properties and heavy metal chemistry, are indicated by stars. Background map after Shrestha and Pradhan (2000).

RESEARCH METHODOLOGY

The samples used in the present study were collected during a field magnetic susceptibility survey in Kathmandu in February 2002. Soils were taken either as cores of 3.5-cm diameter (obtained by vertically inserting a 30-cm-long hollow pipe into the ground) or as samples in 2.54-cm diameter (10 cc in volume) non-magnetic containers obtained from walls of pits dug *in situ*.

MEASUREMENTS OF MAGNETIC PROPERTIES

Standard (cylindrical with 2.54-cm diameter and 10-cc volume) samples were measured for susceptibility using an AGICO KLY-2 Kappabridge, with an operating frequency of 920 Hz and sensitivity of 4×10^{-8} SI, and normalized by the sample mass to obtain χ.

Isothermal remanent magnetization acquisition up to a maximum of 2.5 T, using pulse fields at 18–20 steps generated by a Magnetic Measurements pulse magnetizer, was carried out on standard samples. The IRM moment acquired was measured by a Molspin spinner magnetometer. The IRM curves were analyzed using cumulative log-normal Gaussian decomposition techniques to discriminate the contribution of magnetic materials with differing coercivity spectra (Kruiver *et al.* 2001).

Variation of susceptibility with temperature (40–700°C) was recorded for soil, rock or cement specimens (approximately 0.25 cm^3) using an AGICO KLY-3 Kappabridge, which operates at 875 Hz and has a sensitivity of 3×10^{-8} SI, with an attached CS-3 furnace. Experiments were conducted in air and the measurement interval was 2.5°C with a heating rate of 10°C/min.

CHEMICAL ANALYSIS

For chemical analysis, 37 samples from various depth levels, chosen to represent the susceptibility variation along each selected soil profile, were taken from six soil profiles. The samples were oven-dried at 75°C for 48 h, homogenized and quartered, and then approximately 1.8 g of each

was digested by 8 mL aqua regia (solution of 37% extra pure HCl and 65% extra pure HNO_3 mixed in a ratio of 2 : 1) in a Kjeldatherm system (at 140°C, 2 h). The solution was filtered and diluted by distilled water to get 250 mL of solution in a graduated flask. A Perkin-Elmer M1100 atomic absorption spectrophotometer from the Department of Geography, University of Tübingen, was used to determine the contents of Cd, Cu, Co, Cr, Mn, Ni, Pb, Zn and Fe using standard laboratory procedure.

MAGNETIC PROPERTIES AND APPLICATION FOR SOIL PROFILE ZONATION

ISOTHERMAL REMANENT MAGNETIZATION CHARACTERISTICS

Isothermal remanent magnetization acquisition curves measured for representative soils from the background, as well as urban areas and other possible constituents of urban soils (soot from diesel engine tailpipes, cements and brick fragments embedded into soils), are presented in Figure 2. They exhibit complex shapes caused by the contributions from a number of components of differing magnetic coercivity. The difference in contribution of the soft coercivity components in group 1 (soot and cement specimens), group 2 (soils) and group 3 (brick fragments) is clearly shown by the acquisition of 95–100%, 80–85% and 65–70% of the total remanence at 0.3 T, respectively.

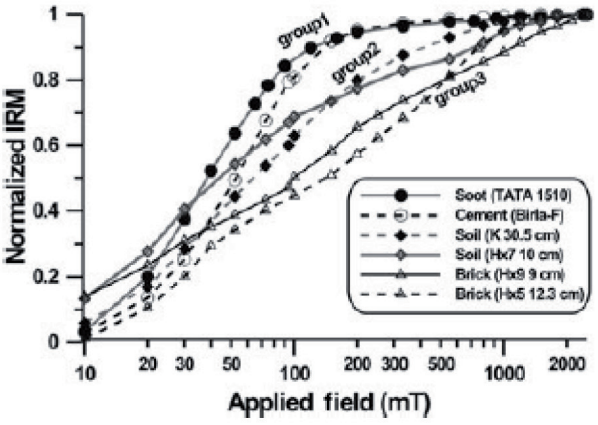

Fig. 2 Isothermal remanent magnetization (IRM) curves for representative samples showing three distinct appearances: group 1, sample of a cement (Birla Faizal, manufactured in India), used currently for construction of structures and the soot material (TATA 1510) extracted from the tailpipe of a Tata truck run on a diesel fuel; group 2, soils from Kirtipur (K) regarded as the urban background in pollution studies and urban center (Hx7); and group 3, brick particles from urban soils (Hx5, Hx9) at various depths.

Modeling data for three specimens, one from each group, performed on IRM gradient data following Kruiver *et al.* (2001) are shown in Figure 3. In general, three components are evident: soft (median acquisition field [$B_{1/2}$] = 30–50 mT), intermediate ($B_{1/2}$ = 125–185 mT) and hard ($B_{1/2}$ = 560–580 mT), which are inferred to represent a magnetite-like phase, a maghemite-like phase (or possibly a soft coercivity hematite) and a hematite phase, respectively. Inference of a maghemite-like phase for the intermediate coercivity is based on the close link of this phase to the 340–350°C decomposition temperatures seen in thermal variation of susceptibility discussed in Gautam *et al.*

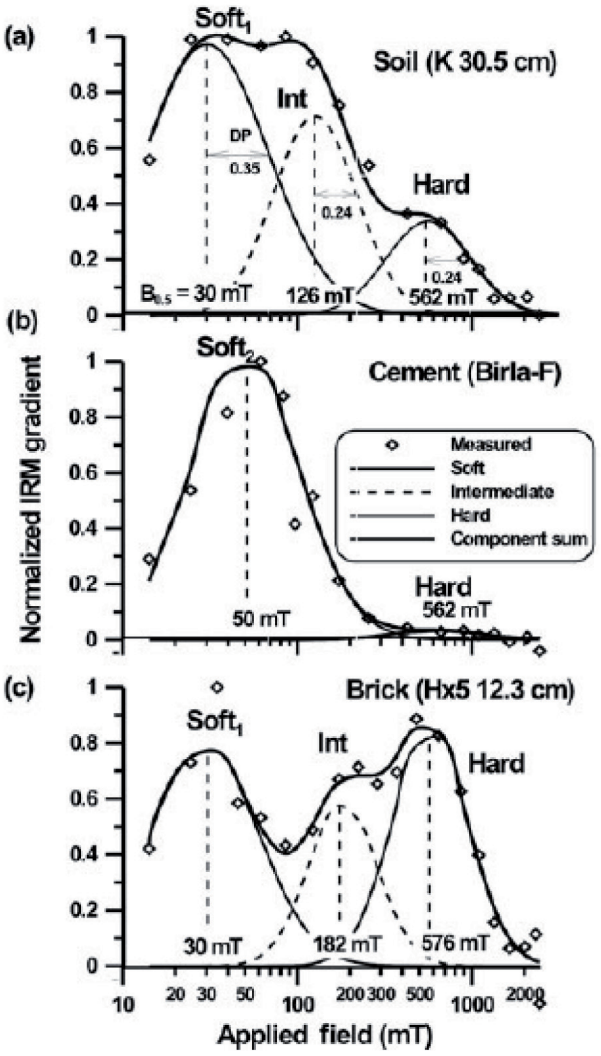

Fig. 3 Isothermal remanent magnetization gradient analysis to discriminate the magnetic components differing in coercivity spectra. Following Kruiver *et al.* (2001), each component modeled can be characterized uniquely by two parameters: a median acquisition field ($B_{1/2}$) and a dispersion parameter (DP), both of which are illustrated for components contributing to the soil.

(2004). Alternatively, an interpretation of the intermediate coercivity phase in terms of a soft hematite is in line with the widely observed coercivity range (28–769 mT) found in the published literature (Peters & Dekkers 2003; Fig. 3; Table 1). The magnetite-like phase found in soil and brick fragments has lower coercivity than that in the soot or cement material.

THERMAL VARIATION OF MAGNETIC SUSCEPTIBILITY

The heating curves for high-susceptibility soils (Hx3, Hx8), brick and cement specimens exhibit differing behavior (Fig. 4a,b). In broad terms, the urban soils exhibit the following characteristic features (Fig. 4a), indicative of two magnetic phases: (i) a gradual, although not regular, increase of susceptibility between room temperature to approximately 260–280°C, attaining an enhancement peak (e_1); (ii) subsequent gradual decrease of susceptibility culminating at a minimum (d_1) within approximately 400–420°C; (iii) further rapid increase of susceptibility resulting in a maximum enhancement peak (e_2) at approximately 510–530°C; and (iv) a subsequent near complete susceptibility drop by approximately 580–600°C (d_2). The cooling curves (not shown here) for these soil samples showed a significant rise in susceptibility (the maximum susceptibility peaks were two- to fivefold higher than the susceptibility measured before initial heating) and partial recovery of all the characteristic features. Analogous to previous work on soil from Kathmandu (Gautam *et al.* 2004; Fig. 9), paleosols from China (Liu *et al.* 2005) and partially oxidized magnetite (Kosterov 2002), features (i) and (ii) may arise from gradual unblocking of fine-grained single-domain particles or annealing of some defects and/or internal stresses in magnetic particles and partial conversion of maghemite to magnetite and/or even hematite, respectively. In contrast, features (iii) and (iv) in the high-temperature range are inferred to be a result of a magnetite-like phase, which in its pure form would have yielded a Curie temperature of 580°C (Dunlop & Özdemir 1997). The susceptibility enhancement (e_2) probably results in part from the neoformation of magnetite during heating (Liu *et al.* 2005).

In contrast, the brick and cement specimens are characterized by continued susceptibility enhancement (e) between room temperature and approximately 400–420°C and a subsequent rapid drop (d) by approximately 560–580°C, indicating that a high-temperature magnetic phase predominates the magnetic mineralogy (Fig. 4b).

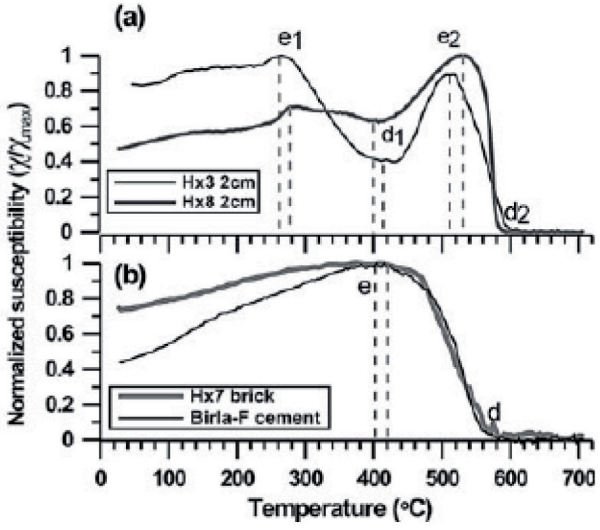

Fig. 4 Thermal variation of magnetic susceptibility (χ) for urban soils (Hx3, Hx8), brick particle in soil (Hx7) and cement (Birla Faizal). Note the presence of at least two distinct magnetic phases in soil samples (a), as opposed to single phase in the brick and cement samples (b). Cross-hatched areas are placed against the temperature ranges within which the characteristic susceptibility enhancement peaks (e, e_1, e_2) and drops (d, d_1, d_2) occur.

MAGNETIC ZONATION OF VERTICAL SOIL PROFILES USING SUSCEPTIBILITY AND ISOTHERMAL REMANENT MAGNETIZATION DATA

The presence of significant lateral and vertical magnetic susceptibility variations in the background sites as well as in urban areas of the Kathmandu Valley, and application of susceptibility for mapping was described by Gautam *et al.* (2004). Here, χ and IRM magnitudes are analyzed together with the percentage contribution of the components of differing coercivity spectra for vertical zonation of the urban soil profiles. Because of the ease, rapidity and low cost of measurements, χ alone is recommended for zonation using its magnitudes differing by factors of 10 (i.e. normal, $< 10^{-7}$ m^3/kg; moderately enhanced, 10^{-7}–$< 10^{-6}$ m^3/kg; and highly enhanced, $\geq 10^{-6}$ m^3/kg). In addition, information on the relative contribution of IRM components is useful in discerning the nature of magnetic minerals or phases that may be attributed to anthropogenic, geogenic/lithogenic and pedogenic sources. Discrimination of the soil intervals is illustrated for two profiles in Figure 5. In urban soil profiles, the relative contribution of the soft IRM component, commonly present in the magnetite-like phase, decreases with depth, as does the degree of metallic pollution caused by

Table 1 Magnetic parameters and heavy metal contents of soil samples from Kathmandu

Site	Depth (cm)	Magnetic parameters: χ (10^{-9} m³/kg)	SIRM (10^{-6} A m²/kg)	SIRM/χ[†] (10^{3} A/m)	Heavy metal contents (pseudo-total analysis, AAS[‡]): Fe (%)	Mn (mg/kg)	Zn (mg/kg)	Cu (mg/kg)	Pb (mg/kg)	Cr (mg/kg)	Ni (mg/kg)	Co (mg/kg)	Cd (mg/kg)
K, paddy field, Kirtipur													
	2.5	93.8	238.0	2.5	3.4	441.6	85.5	35.4	19.4	34.0	33.5	12.8	−0.5
	5.1	92.0	265.6	2.9	3.2	409.3	84.6	35.4	19.2	33.5	32.9	13.8	−0.1
	10.2	120.2	1116.8	9.3	3.4	520.9	84.3	35.2	19.6	34.8	36.5	13.5	0.1
	15.2	116.4	290.9	2.5	3.6	495.3	88.4	35.5	21.5	34.3	36.7	13.9	0.1
	25.4	124.4	570.5	4.6	3.6	644.0	86.5	36.2	20.3	35.8	37.2	15.2	0.3
	30.5	105.4	184.7	1.8	3.4	501.2	90.9	37.8	20.4	35.7	34.3	13.3	−0.1
	35.6	143.6	228.6	1.6	3.2	497.5	84.7	34.4	15.7	33.8	35.1	13.0	0.1
	52.1	139.4	163.9	1.2	3.4	379.8	89.2	35.9	18.0	35.4	33.3	11.0	−0.3
	64.8	118.8	549.6	4.6	3.7	757.2	85.2	34.5	18.4	36.9	37.4	12.8	−0.6
	69.9	107.8	288.3	2.7	3.7	631.8	91.7	37.6	20.7	37.5	36.2	12.9	−0.6
Hx3, Ratna Park, approximately 5 m off road													
	2.0	473.3	6745.2	14.3	1.5	266.8	131.5	43.7	37.1	20.7	13.9	3.5	0.5
	8.0	538.9	7450.5	13.8	2.0	324.2	154.0	51.7	44.2	27.5	17.8	7.9	0.6
	12.0	538.8	7918.5	14.7	2.1	336.6	131.8	50.0	43.9	27.1	19.4	7.6	0.2
	18.0	513.2	7124.5	13.9	2.3	481.1	118.5	51.4	43.7	29.1	19.4	8.9	−0.2
	26.0	216.6	2738.9	12.6	2.4	312.3	70.6	35.6	22.8	29.1	20.9	10.6	−0.1
	43.0	96.8	493.3	5.1	3.0	357.8	78.4	35.5	20.5	42.7	38.1	12.6	−0.2
	53.0	113.1	1084.3	9.6	1.8	307.5	60.9	31.8	15.5	22.5	15.9	8.2	−0.1
Hx7, Rani Pokhari (eastern side), behind Saraswati Sadan													
	2.0	1808.7	39738.2	22.0	2.0	233.9	123.5	30.8	20.4	18.5	9.6	5.6	0.0
	5.0	6374.6	80102.0	12.6	3.2	289.7	636.6	32.3	31.5	21.1	11.8	5.5	−0.6
	10.0	1506.7	40979.1	27.2	1.8	269.6	121.3	29.5	23.0	21.2	10.8	5.3	−0.2
	15.0	822.8	13287.3	16.1	1.6	215.2	90.6	25.0	21.1	20.2	10.9	5.6	−0.4
	21.0	717.8	11195.8	15.6	1.6	250.5	61.0	20.9	17.0	18.2	9.1	6.5	−0.4
	28.3	348.1	4469.5	12.8	1.5	188.2	61.1	21.1	17.3	18.8	7.7	6.7	−0.7
Hx8, exhibition ground													
	2.0	3585.8	95673.8	26.7	3.9	490.8	184.2	165.5	70.9	29.5	15.1	10.9	−1.3
	12.0	467.1	11993.2	25.7	1.6	232.2	126.0	128.5	57.1	21.7	12.7	6.9	0.1
	16.0	102.9	2980.2	29.0	1.8	379.4	142.1	162.7	64.4	22.4	15.1	11.1	0.2
	22.0	159.3	3032.0	19.0	2.5	494.1	192.1	225.7	93.2	30.2	20.1	10.9	0.2
	28.0	88.6	1453.2	16.4	1.4	197.1	89.4	133.1	40.3	19.6	13.0	8.9	−0.2
	37.0	78.2	1674.7	21.4	1.4	153.1	82.8	156.8	35.9	20.4	11.7	8.7	0.3
	43.0	46.6	112.1	2.4	2.6	400.1	70.1	165.8	30.0	33.1	26.3	12.3	−0.2
	55.0	34.9	82.5	2.4	2.0	463.5	67.1	98.4	37.2	27.2	22.1	11.8	0.0
Hx9, Balaju Park, close to industrial area													
	2.0	112.5	1231.4	10.9	2.0	263.0	107.4	35.8	25.4	25.0	18.0	9.8	0.1
	6.0	212.7	2575.0	12.1	1.6	234.6	104.2	31.6	18.4	22.2	12.3	6.3	−0.1
	14.0	118.5	1108.1	9.4	1.9	260.9	101.7	34.6	25.1	24.0	15.2	9.4	−0.3
	25.0	69.2	407.7	5.9	1.7	211.3	60.7	23.7	11.4	21.5	14.9	9.9	0.3
	38.0	36.0	162.5	4.5	1.2	140.6	42.9	13.9	0.7	15.4	9.4	7.0	0.4
	49.0	51.9	191.1	3.7	1.9	192.1	56.5	24.2	10.0	22.1	17.3	8.1	0.3

AAS, atomic absorption spectrometry; χ, mass-specific magnetic susceptibility; SIRM, saturation isothermal remanence at 2.5 T.
[†] Cd content in most samples is below detection limit and imprecise (e.g. negative); [‡] very low (< 5 kA/m) SIRM/χ for K and the lower parts of Hx8, Hx9 point to large paramagnetic contribution.

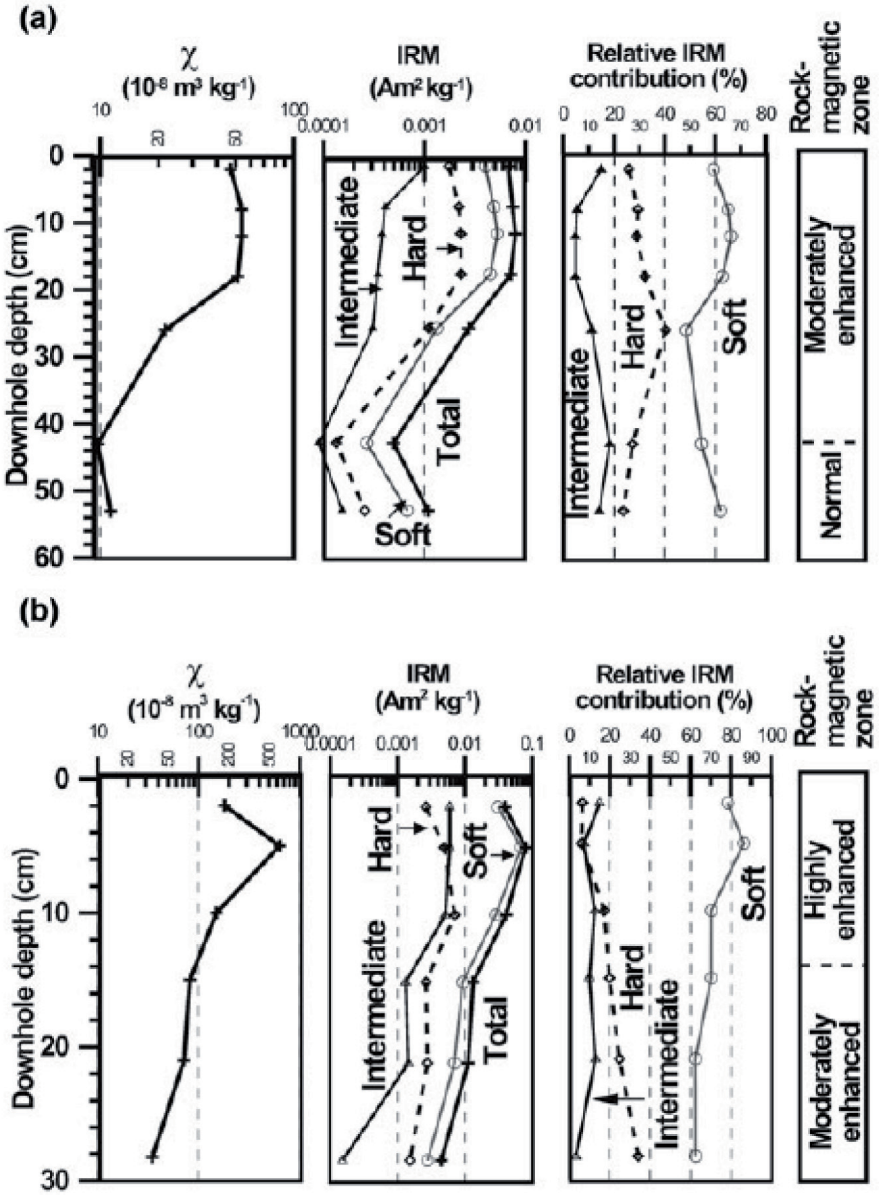

Fig. 5 Use of magnetic susceptibility (χ) and isothermal remanent magnetization (IRM) data for zonation and magnetic qualification of urban soils. Zonation is based on the magnitudes of χ (normal, $< 10^{-7}$ m³/kg; moderately enhanced, $10^{-7} - < 10^{-6}$ m³/kg; highly enhanced, $\geq 10^{-6}$ m³/kg), whereas the quality can be judged by the relative contribution of the IRM components of varying coercivity. (a) Hx3, Ratna Park, north side; (b) Hx7, Rani Pokhari.

anthropogenic factors (also described later). Gautam *et al.* (2004) described the derived nature of the soils, at least in the upper parts of the soil profiles, in the studied sites within the urban recreational parks and the systematic decrease of the in situ magnetic susceptibility with distance from road edges. Hence, the relative contribution of the anthropogenic or industrial sources to the susceptibility enhancement in the uppermost parts of soils is interpreted to be much higher than that arising from pedogenic processes leading to the formation of magnetic minerals. Analysis of the susceptibility profiles in an urban setting in Kathmandu suggests that 'normal' soil, in terms of the susceptibility enhancement attributable to the effect of pollution, commonly occurs below a depth of 30 cm (Fig. 3).

RELATIONSHIP BETWEEN HEAVY METAL CONTENTS AND MAGNETIC PROPERTIES

HEAVY METAL CONTENTS IN SOILS

Data on the HM contents and magnetic parameters (χ, SIRM and SIRM/χ ratio) for discrete specimens collected from five vertical soil profiles (K, background site in Kirtipur; Hx3, Hx7, Hx8 and Hx9, from soils affected by urbanization) are presented in Table 1. As χ shows generally a strong grain-size dependency in samples with a complex

assemblage of magnetic minerals, its magnitude alone may not be attributable to absolute enrichment of iron-bearing materials. However, in case of the dominant contribution of magnetite (or maghemite) to susceptibility, as is the case in the upper parts of the urban soil profiles considered, the use of χ as a measure for the concentration of magnetic particles is theoretically justified (Heider *et al.* 1996). The interparametric ratio SIRM/χ varies with grain size and concentration as well as mineralogy, and is therefore not easy to interpret even in the case of predominant magnetite/maghemite mineralogy. However, very low values of this ratio and SIRM are thought to reflect a large paramagnetic contribution with a negligible concentration of soft coercivity phases, such as magnetite/maghemite (Table 1). Site K has the least variability of the magnetic properties, as well the content of each heavy metal, whereas the opposite can be said for site Hx8. The Cd contents are quite low (< 0.6 mg/kg) and are below the detection limit in the majority of samples.

For relative interpretation, the HM data measured are listed together with the average contents found in the Earth's crust, uncontaminated soils and the sediments sampled from the Bagmati River in Kathmandu (Table 2). As the HM contamination in the soils considered is of anthropogenic nature, the possible sources for various elements are also summarized. Because of the obvious differences in magnitudes as well as variability of HM contents, the soils from Kirtipur and the urban soils from other sites have been considered separately.

The average values, or at least the values at the lower end for the Kirtipur site, are very close to the average contents for the uncontaminated soils, with some exceptions for Zn and Ni characterized by clearly high values (Table 2). Both atmospheric deposition and agricultural practices might be the sources of these slightly elevated values for Zn and Ni. Nevertheless, the Kirtipur site can be regarded as the urban background site in terms of HM contents. Likewise, the lowest values commonly observed at greater depths (mostly below 30 cm) in the urban soils are similar to the average values in uncontaminated soils and may be regarded as local backgrounds. The contents of Pb and Zn in soils are generally lower than those in the Bagmati River sediments (Devkota 2001), whereas the opposite is true for Cu.

Figure 6 gives an insight into the elemental variations with depth in the urban soil profiles. The soil along Hx3 has no distinct layering; it is basically silty soil with the presence of a relatively higher portion of sand in 12–22-cm and 33–43-cm intervals, as well as the occasional presence of clasts of bricks. The soil in Hx7 is also undifferentiated garden soil with predominantly silt-sized particles. For profile Hx3, we see that elements Cu, Pb and Zn behave differently from the others (Fe, Cr, Mn, Ni). The elements in these two groups vary coherently, with very good internal correlation. A common feature for both profiles is the abrupt decay of contents of HM, especially of Cu, Pb and Zn, approaching close to the local background levels at or below a depth of approximately 25 cm.

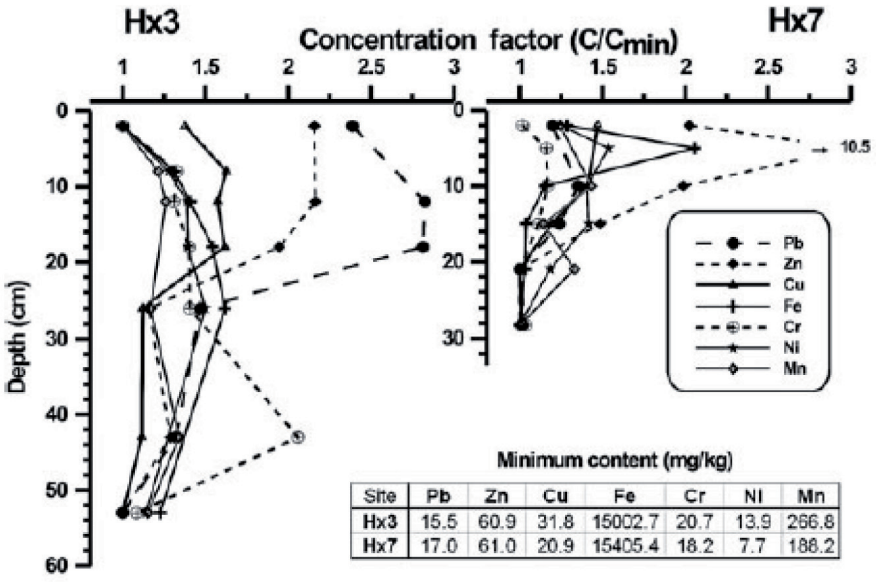

Minimum content (mg/kg)

Site	Pb	Zn	Cu	Fe	Cr	Ni	Mn
Hx3	15.5	60.9	31.8	15002.7	20.7	13.9	266.8
Hx7	17.0	61.0	20.9	15405.4	18.2	7.7	188.2

Fig. 6 Down-hole variation of normalized heavy metal contents along two vertical soil profiles (Hx3, left, from Ratna park; Hx7, right, from Rani Pokhari, eastern side) situated in the urban center. Note that some urban elements show maximum concentration within 10–20 cm leading to a remarkable decrease by approximately 25 cm.

Table 2 Comparison of heavy metal contents in soils in the Earth's crust, uncontaminated soils around the world, and soils and sediments from Kathmandu

Element	Importance[†‡]	Average content (mg/kg)[†]		Principal sources of metal contamination in urban/suburban soils[‡]	Heavy metal contents (mg/kg) for Kathmandu		
		Earth's crust	Un-contaminated soils		Paddy field, Kirtipur ($n = 10$)[§]	Urban soils ($n = 27$)	Bagmati River sediments ($n = 12$)[¶]
Cd	No essential biological function; toxic at all levels	0.1	0.53	Atmospheric deposition; incineration of plastic containers and batteries; sewage sludge application to land; burning of fossil fuels	< 0.3	< 0.6	0.08–0.33
Co	Essential for microorganisms and ruminant animals	20	10–15	Application of Co salts or Co-treated phosphate fertilizers to topsoils	13.2 (11.0–15.2)	3.5–12.6	n.a.
Cr	Essential for animals	100	40	Atmospheric deposition (production of ferrochromes, refractory bricks and steel, coal combustion, forest fires); disposal of fly ash; sewage sludge; wear of Cr-containing asbestos brake linings; application of fertilizers (phosphates), limestones and manures	35.2 (33.5–37.5)	15.4–42.7	n.a.
Cu	Essential for animals and plants	50	30	Application of fungicides, fertilizers, livestock manures; sewage sludge, fossil fuel combustion	35.8 (34.4–37.8)	13.9–225.7	10.6–63.6
Mn	Essential for animals, microorganisms and higher plants	950	20–500	Application of Mn (normally in the form of $MnSO_4$, MnO or as an addition to macronutrient fertilizers) to soils	527.9 (379.8–757.2)	140.6–494.1	n.a.

Table 2 *Continued*

Element	Importance[†‡]	Average content (mg/kg)[†] Earth's crust	Un-contaminated soils	Principal sources of metal contamination in urban/ suburban soils[†]	Heavy metal contents (mg/kg) for Kathmandu Paddy field, Kirtipur ($n=10$)[§]	Urban soils ($n=27$)	Bagmati River sediments ($n=12$)[¶]
Ni	Essential for animals, some microorganisms and higher plants	80	23	Atmospheric deposition (burning of fuel and residual oils, forest fires); diesel exhaust; application of fertilizers (phosphates), limestones and manures; sewage sludge	35.3 (32.9–37.4)	7.7–38.1	n.a.
Pb	No essential biological function; poisonous for mammals	14	17	Application of manures and sewage sludge; vehicle exhausts; pesticides; atmospheric deposition (vehicle fumes); abraded tire material, coal, plastics and rubber factories, insecticides, car batteries, old paint etc.	19.3 (15.7–21.5)	10.0–93.2	40.0–173.3
Zn	Essential for humans, animals and higher plants	75	50	Atmospheric deposition (the burning of coal and fossil fuels), the smelting of non-ferrous metals, sewage sludge, agrochemicals (mineral and organic fertilizers, soil amendments, pesticides, etc.	87.1 (84.3–91.7)	42.9–636.6	60.3–277.0

[†] Alloway (1995) – compiled from several papers in the edited volume; [‡] all elements but Cd and Pb are micronutrients that are essential (i.e. they are required for normal growth and their deficiency may lead to abnormality) to certain levels, but their excessive contents, however, are toxic and poisonous; [§] for site K, characterized by least variability of chemical contents, the mean values are accompanied by the min–max range within the brackets; [¶] Devkota (2001).

n.a., not available.

HEAVY METAL CONTENTS *VS* MAGNETIC SUSCEPTIBILITY

Of the metals considered, Cu, Pb and Zn are found to correlate well with susceptibility. This is exemplified by the Pb *vs* χ plot (Fig. 7). It is evident that Pb has good correlation with χ for each profile, but a relationship that differs by locality obviously because of differences in the types of soils (Hanesch & Scholger 2005). For example, Hx3 and Hx9 together fit into a line that passes through the mean value for the rather tightly clustered values for profile K. For profile Hx8, the data points are more scattered but a positive correlation still holds true.

MAGNETIC PROPERTIES *VS* POLLUTION LOAD INDEX

Joint analysis of the soil profiles reveals that the contents of the urban elements (Cu, Pb and Zn) correlate among themselves and also with χ. In order to facilitate rapid characterization of the soil section in terms of metallic contamination, it was proposed that the contents of the three elements should be combined into a single index called the Tomlinson pollution load index (PLI; Angulo 1996; Chan *et al.* 2001; Fig. 8). This index is calculated as the geometric mean of the concentration factors (CF_i; i = 1 to n) of several metals, where CF_i of the i^{th} metal represents the ratio of the content of that metal (C_i) in the sample analyzed to its content at a background site (C_b) unaffected by pollution as follows:

$$PLI = \sqrt[3]{(CF_{Cu} \times CF_{Pb} \times CF_{Zn})}, \text{where } CF_{i(i=Cu,Pb or Zn)} = C_i / C_b \quad (1)$$

It represents the number of times by which the concentration of the urban elements in soil at a particular horizon exceeds the background. In this paper, C_b has been replaced by the minimum value ($C_{i\,min}$) generally observed at depths virtually untouched by urban pollution. The index allows comparison of several profiles and judgment on the relative degree of metallic contamination and accordingly the degree of urban pollution. It is obvious from Figure 8 that the PLI variation correlates very well with susceptibility as well as SIRM magnitudes.

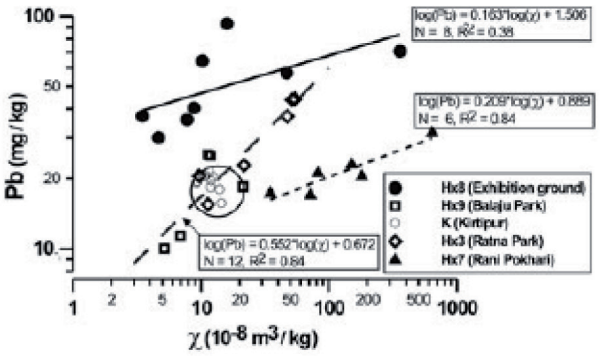

Fig. 7 Relationship between the contents of Pb in all soil samples against the mass-specific susceptibility. The least variability of both parameters characterizes the urban background site of Kirtipur (data points shown within the circle), whereas for other sites a reasonably linear, although variable, dependence between the logarithmic values can be noted.

DISCUSSION AND CONCLUSIONS

Results of recent research on particulate matter (PM10 – mass of particles with aerodynamic diam-

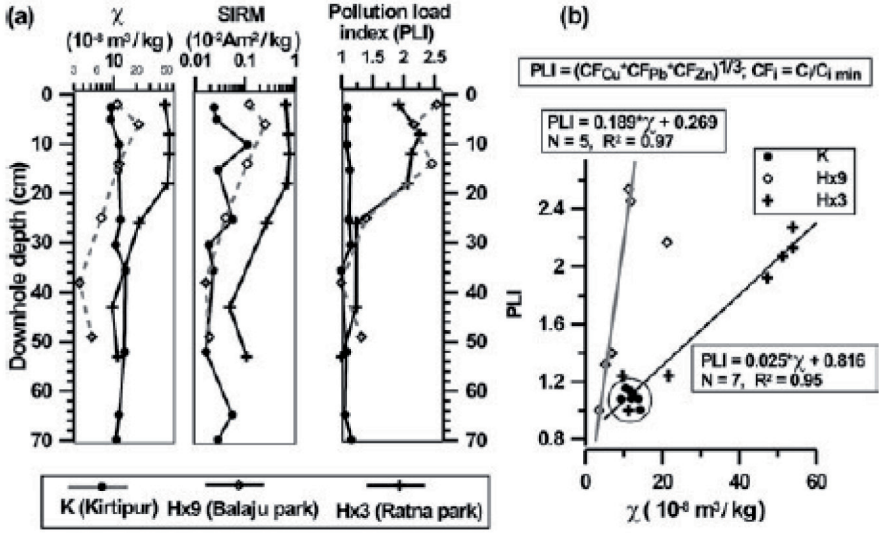

Fig. 8 (a) Comparison of the magnetic properties (χ, magnetic susceptibility; SIRM, saturation isothermal remanence) and the pollution load index (PLI) based on the concentration factors (CF) of 'urban elements' in three sites belonging to suburban (K), industrial (Hx9) and core urban (Hx3) areas (see Fig. 1). (b) Cross-plot showing significant (coefficient of determination, $R^2 \geq 0.95$) linear correlation, although site-dependent, between PLI and χ, justifying the use of the latter as a proxy of the pollution load.

eters less than 10 μm per unit volume), river sediments, dust-loaded leaves from roadsides, road dust and soil samples allow us to qualify and quantify urban pollution. Sharma *et al.* (2002) described high values (1150–3837 μg/m^3) of the hourly mean PM10 levels, at a height of 1.5 m at 30 busy urban locations in the Kathmandu Valley in 1999, and related them basically to the vehicular traffic (vehicle emissions and suspension of dust as a result of vehicle movement). Devkota (2001) found significant variations in Cd, Cu, Pb and Zn among the sediment samples of the Bagmati River (Table 2), along which the HM contents increase after entering the main urban area when tributaries carrying city wastes meet the trunk river. These facts relate the elevated input of metals into the river to urbanization. Gautam *et al.* (2005) studied the HM content in the dust-loaded leaves from trees at Kathmandu roadsides with varying levels of traffic movement, and found the following ranges: Fe (0.08–1.30 wt%), Mn (18.3–281.9 p.p.m.), Zn (15.9–195.2 p.p.m.), Cu (4.7–41.5 p.p.m.), Pb (1.8–38.4 p.p.m.), Ni (0.6–8.1 p.p.m.), Cr (1.7–6.4 p.p.m.), Co (up to 4.1 p.p.m.) and Cd (up to 1.2 p.p.m.). One of the notable features of the leaf data was a significantly positive linear correlation of logarithmic χ with most of the HM and a high degree of mutual correlation, with a coefficient of determination (R^2) of 0.69–0.77 among Cu, Pb and Zn, implying that both the magnetically soft minerals of anthropogenic origin and the urban elements arise predominantly from traffic pollution. In yet another pilot study (Gautam, unpubl. data, 2004), the fine fraction (<0.063 mm) constituting the dust from the road surface in the Babarmahal area of Kathmandu was found to have much higher HM contents, as follows: Fe (1.4–1.8 wt%), Mn (244.9–374.9 p.p.m.), Zn (92.1–161.2 p.p.m.), Cu (30.6–75.2 p.p.m.), Pb (23.9–55.8 p.p.m.), Ni (12.8–18.2 p.p.m.), Cr (10.7–23.4 p.p.m.), Co (2.6–6.1 p.p.m.) and Cd (up to 1.0 p.p.m.), for which the contribution from the traffic-related source was obvious.

Joint analysis of χ, SIRM and HM contents in the soil profiles from Kathmandu presented above reveals that each of these quantities has a wide range of variation and could be a potential pollution indicator. For the soils studied, Cu, Pb and Zn consistently correlate to χ as well as the SIRM magnitudes. Analogous to the results from leaves and road dust, these elevated HM contents can be associated with the degree of urbanization and traffic movement (motor vehicle emissions; abrasion of tires, brake linings and the road surface; cycling of dust in suspension as a result of vehicular movement) as has been found in other studies (e.g. Wong 1996; De Miguel *et al.* 1997).

In the case of Kathmandu soils or similar situations, the use of magnetic susceptibility is recommended as widely as possible, for the sake of ease and rapidity and the low-cost of the measurements, for both lateral and vertical zonation. As the quality of magnetic material will differ according to the soil type, the proximity to roads, the proximity to various point sources of pollution, the rate of dry and wet atmospheric deposition etc., additional information can be acquired through analysis of IRM acquisition curves. The correlation of χ with PLI (based on Cu, Pb and Zn contents) is excellent at a local level (Fig. 8b), implying that susceptibility actually serves as an effective proxy of urban pollution. For effective use of susceptibility as a proxy of the degree of pollution in soils through the use of a PLI and its translation to the metallic levels in a new urban area, however, it is desirable to have a reference database that includes information on soil types, parent material, background susceptibility, the background contents of each metal in areas differing in geological/pedological conditions, and knowledge of the possible sources of contamination.

ACKNOWLEDGEMENTS

The authors are grateful to Prakash C. Adhikari, Tribhuvan University, and the Environmental Unit of the Kathmandu Municipality for support during field work. P Gautam gratefully acknowledges a Georg Forster postdoctoral fellowship from the Alexander von Humboldt Foundation, Germany, and also the postdoctoral researcher position under the 21st Century COE for Neo-Science of Natural History (project leader: Hisatake Okada) at Hokkaido University. Advice on chemical analysis by Rolf K. Beck and critical remarks on the manuscript by M. Torii and R. Scholger are very much appreciated.

REFERENCES

ALLOWAY B. J. (ed.) 1995. *Heavy Metals in Soils.* Blackie Academic & Professional, London.

ANGULO E. 1996. The Tomlinson pollution load index applied to heavy metal 'mussel-watch' data: A useful index to assess coastal pollution. *Science of the Total Environment* 187, 19–56.

CHAN L. S., NG S. L., DAVIS A. M., YIM W. W. S. & YEUNG C. H. 2001. Magnetic properties and heavy-metal contents of contaminated seabed sediments of Penny's Bay, Hong Kong. *Marine Pollution Bulletin* 42, 569–83.

DE MIGUEL E., LLAMAS J. F., CHACÓN E. *et al.* 1997. Origin and patterns of distribution of trace elements in street dust: Unleaded petrol and urban lead. *Atmospheric Environment* 31, 2733–40.

DEVKOTA D. 2001. Total and extractable (mobilizable and mobile) heavy metals in the Bagmati river sediment of Kathmandu, Nepal. *A Journal of the Environment* 6, 34–51.

DUNLOP D. J. & ÖZDEMIR O. 1997. *Rock Magnetism: Fundamentals and Frontiers*. Cambridge University Press, Cambridge.

GAUTAM P., BLAHA U. & APPEL E. 2005. Magnetic susceptibility of dust-loaded leaves as a proxy of traffic-related heavy metal pollution in Kathmandu city, Nepal. *Atmospheric Environment* 39, 2201–11.

GAUTAM P., BLAHA U., APPEL E. & NEUPANE G. 2004. Environmental magnetic approach towards the quantification of pollution in Kathmandu urban area, Nepal. *Physics and Chemistry of the Earth* 29, 973–84.

HANESCH M. & SCHOLGER R. 2002. Mapping of heavy metal loadings in soils by means of magnetic susceptibility measurements. *Environmental Geology* 42, 857–70.

HANESCH M. & SCHOLGER R. 2005. The influence of soil type on the magnetic susceptibility measured throughout soil profiles. *Geophysical Journal International* 161, 50–56.

HEIDER F., ZITZELSBERGER A. & FABIAN K. 1996. Magnetic susceptibility and remanent coercive force in grown magnetite crystals from 0.1 μm to 6 mm. *Physics of the Earth and Planetary Interiors* 93, 239–56.

KNAB M., APPEL E. & HOFFMANN V. 2001. Separation of the anthropogenic portion of heavy metal contents along a highway by means of magnetic susceptibility and fuzzy c-means cluster analysis. *European Journal of Environmental and Engineering Geophysics* 6, 125–40.

KOSTEROV A. 2002. Low-temperature magnetic hysteresis properties of partially oxidized magnetite. *Geophysical Journal International* 149, 796–804.

KRUIVER P. K., DEKKERS M. J. & HESLOP D. 2001. Quantification of magnetic coercivity components by the analysis of acquisition curves of isothermal remanent magnetization. *Earth and Planetary Science Letters* 189, 269–76.

LIU Q. S., DENG C. L., YU Y. J. *et al.* 2005. Temperature dependence of magnetic susceptibility in an argon environment: Implications for pedogenesis of Chinese loess/paleosols. *Geophysical Journal International* 161, 102–12.

MALINOVSKY M. 2001. Air quality management in Kathmandu Valley. *A Journal of the Environment* 6, 50–57.

PETERS C. & DEKKERS M. J. 2003. Selected room temperature magnetic parameters as a function of mineralogy, concentration and grain size. *Physics and Chemistry of the Earth* 28, 659–67.

PETROVSKY E. & ELLWOOD B. B. 1999. Magnetic monitoring of pollution of air, land and waters. *In* Maher B. A. & Thompson R. (eds). *Quaternary Climates, Environments and Magnetism*, pp. 279–322. Cambridge University Press, Cambridge.

SHARMA T., RAINEY R. C., NEUMANN C. M. *et al.* 2002. Roadside particulate levels at 30 locations in the Kathmandu Valley, Nepal. *International Journal of Environment and Pollution* 17, 293–305.

SHRESTHA B. & PRADHAN S. 2000. *Kathmandu Valley GIS Database*. ICIMOD, Kathmandu.

WONG J. W. C. 1996. Heavy metal contents in vegetables and market garden soils in Hong Kong. *Environmental Technology* 17, 407–14.

YOSHIDA M. & GAUTAM P. 1988. Magnetostratigraphy of Plio-Pleistocene lacustrine deposits in the Kathmandu Valley, central Nepal. *Proceedings of the Indian National Science Academy* 3, 410–17.

8

Environmental magnetic approach towards the quantification of pollution in Kathmandu urban area, Nepal

Available online at www.sciencedirect.com
SCIENCE DIRECT®
Physics and Chemistry of the Earth 29 (2004) 973–984
PHYSICS and CHEMISTRY of the EARTH
www.elsevier.com/locate/pce

Environmental magnetic approach towards the quantification of pollution in Kathmandu urban area, Nepal

Pitambar Gautam [a,c,*], Ulrich Blaha [b], Erwin Appel [b], Ghanashyam Neupane [c]

[a] COE Office for Neo-Science of Natural History, N222 Faculty of Science, Hokkaido University N10 W8, Sapporo 060-0810, Japan
[b] Institute of Geosciences, University of Tübingen, 72076 Tübingen, Germany
[c] Central Department of Geology, Tribhuvan University, Kirtipur, Kathmandu, Nepal

Received 27 June 2003; received in revised form 16 January 2004; accepted 12 February 2004

Abstract

The Kathmandu Valley is a bowl-shaped intermontane basin, which occupies an area of 583 km^2 in the heart of the Himalayas, with its floor at ≈1400 m and the surrounding mountains attaining a height of 2000–2800 m. It is inhabited by ≈1.5 million people, concentrated mostly in three cities, Kathmandu, Patan and Bhaktapur. Due to rapid but uncontrolled urbanisation and factors such as traffic movement, emissions from brick-kilns, cement factories, waste disposal and biomass burning, environmental pollution has been constantly increasing; adversely affecting land, water, air and biological systems.

In order to quantify the degree of environmental pollution using magnetic methods, magnetic susceptibility of soils, sediments and roadside materials, in and outside the Kathmandu urban area has been measured. In areas far from roads or industry, median magnetic susceptibility is between 3 and 35×10^{-5} SI, similar to that observed in the valley-filling clastic sediments and hence consistent with geologic or pedogenic origin. In traverses of in situ susceptibility across roads, a 5-m wide zone situated on either side of the asphalt-paved road exhibits an enhancement zone with maximum susceptibility of $240–850\times10^{-5}$ SI occurring 0.5–2.5 m from the road edge. In urban recreational areas, magnetic susceptibility varies within a broad range (3 to $>100\times10^{-5}$ SI) with lowest values occurring ≈50 m from surrounding roads, in areas least disturbed by human activity. A systematic increase in susceptibility towards the roads or industrial sites is observed. Within urban areas, in the vicinity of heavy traffic or industrial sites, the upper 30–50 cm of soil profiles exhibit frequent enhancement in susceptibility, of one or two orders of magnitude, higher than those expected from geologic input. Such enhancement is attributed to input from anthropogenic or industrial sources. Magneto-mineralogical analyses and scanning electron microscopy on magnetic extracts, grain size fractions or bulk samples of road dust and soils, suggest lithogenic magnetite-like minerals and anthropogenic magnetic spherules to be the dominant contributors to the magnetic susceptibility signal.

As the soils, sediments and roadside material exhibit significant susceptibility contrasts, which are most effective in identifying traffic-related pollution "hotspots", it is highly desirable that the potential of susceptibility maps of the entire area affected by urbanisation, be fully explored to assess the status of environmental degradation.

Keywords: Environmental pollution; Kathmandu; Magnetic susceptibility; Environmental magnetism; Magnetic spherules

1. Introduction

Environmental magnetic methods based on the study of variations in magnetic susceptibility and rock magnetic parameters have been successfully used over

* Corresponding author. Address: COE Office for Neo-Science of Natural History, N222 Faculty of Science, Hokkaido University N10 W8, Sapporo 060-0810, Japan. Fax: +81 11 706 2986.
E-mail addresses: p-gautam@nature.sci.hokudai.ac.jp, pgautam2000@yahoo.com (P. Gautam).

1474-7065/$ - see front matter © 2004 Elsevier Ltd. All rights reserved.
doi:10.1016/j.pce.2004.02.001

several decades to characterise and quantify the degree of pollution of air, water, vegetation and land systems (Petrovsky and Ellwood, 1999). The effective use of these methods in studying the urban pollution has been shown by more recent studies (e.g., Hoffmann et al., 1999; Matzka and Maher, 1999; Shu et al., 2000; Knab et al., 2001; Hanesch and Scholger, 2002; Muxworthy et al., 2002). These prompted us to undertake joint magnetic and geochemical investigations of urban materials (soil, road dust and tree-leaves) to address the environmental pollution of Kathmandu city, that has been subjected to environmental stress, due to population overpressure and related urbanisation. The factors responsible for the pollution are uncontrolled traffic movement and related vehicular pollution, emissions from the Himal cement factory (existing until 2000), brick-kilns, other industrial activities and biomass burning (Shrestha and Pradhan, 2000; Devkota, 2001; Malinovsky, 2001; NESS, 2001; Shrestha and Raut, 2002).

The Kathmandu Valley is situated within the Lesser Himalaya and is filled by fluvial and lacustrine sediments, of Plio-Pleistocene age, derived from the north and north-east and surrounding metasedimentary terrains (Yoshida and Gautam, 1988; Sakai et al., 2002). The high concentration of atmospheric particulate matter is of serious concern in Kathmandu Valley. The high amount of atmospheric dust partly arises from the fact that the bowl-shaped valley (with its height of up to 1500 m) is an effective trap for dust material reworked from the heavily cultivated land. In 1999–2000, the 24-h averages of particulate matter less than 10 μm in size (PM_{10}) and total suspended particulate (TSP) ranges were 49–495 $\mu g/m^3$ and 61–572 $\mu g/m^3$, respectively. Also a direct relationship between the atmospheric particulate matter concentration and the degree of urbanisation was seen (NESS, 2001). According to an inventory in 2001, the total annual PM_{10} and TSP loads in Kathmandu Valley amounted to 7580 and 19,885 t, respectively, with 67% of the PM_{10} load believed to arise from vehicular emissions (Shrestha and Raut, 2002).

Recent studies point out that emission from the brick-kilns alone contributes to a quarter of the PM_{10} concentration in the Kathmandu Valley (Raut, 2003). About 90% of the brick-kilns operating in Kathmandu Valley are of the so-called Bull's trench type (an arch-less version of the Hoffmann kiln designed by W. Bull, a British engineer, toward the end of the 19th century). Though these kilns have advantages of low cost of construction and comparatively low specific energy consumption (1.2–1.75 MJ kg^{-1}) they produce a high amount of smoke as the fuel used is any combustible material or a combination of coal, lignite, peat, firewood, saw dust or agricultural waste (such as rice husks).

Detailed are the results of magnetic susceptibility measurements aimed at defining a mapping strategy of the whole Kathmandu urban area (Fig. 1). We conducted a preliminary in situ soil susceptibility survey as follows:

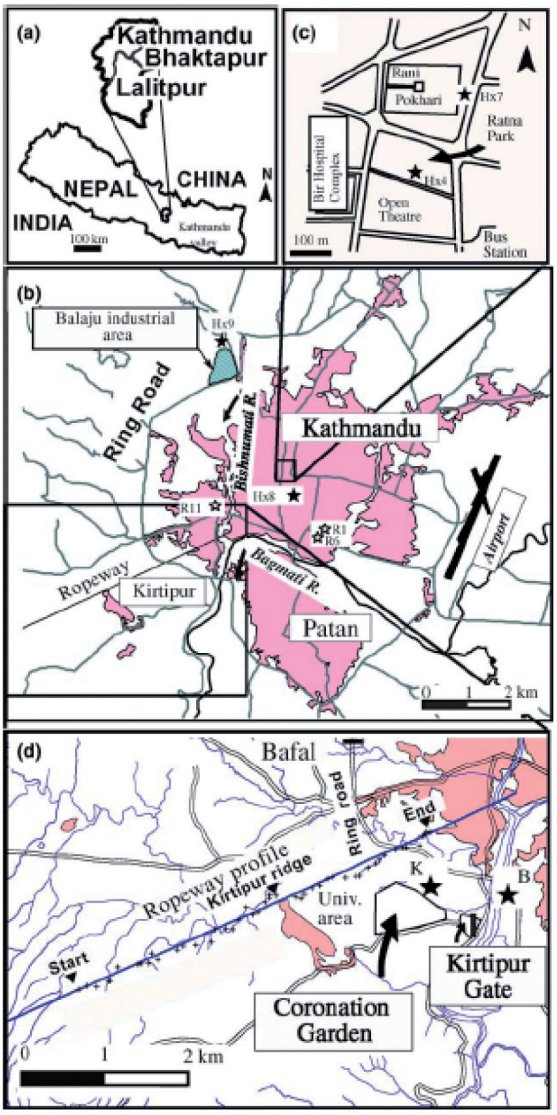

Fig. 1. Sketch maps showing the sites of the pilot environmental magnetic study. (a) Index map showing the three districts of Kathmandu Valley. (b) The greater Kathmandu urban area comprising Kathmandu and Patan cities (light shade). The light and dark lines indicate the major road network and major rivers marking district boundaries. (c) and (d) The Ratna Park area at the heart of the Kathmandu city and Kirtipur area investigated in more detail. Filled stars: sites of vertical soil profiles. $H \times n$ are urban area sites and K = Kirtipur and B = Balkhu are background sites. Open stars: locations of selected road dust samples (Rn).

(i) Profiling along relatively long traverses encompassing both urban as well as peripheral parts. Short profiles across roads of varying categories, combined with meter-scale vertical soil sections.

(ii) Mapping of areas 0.02–0.6 km^2, located within both seemingly unpolluted areas, far away from the urban areas, as well as the recreational parks in the vicinity of urban and industrial areas that are susceptible to pollution. Besides susceptibility, magneto-mineralogical, microscopic and chemical composition of magnetic minerals, are also described, to characterise the urban material.

2. Research methodology

Measurements of the low-field magnetic susceptibility of the top-soil or ground (hereafter called in situ susceptibility) were conducted at discrete points along profiles (lateral or vertical), or over selected areas, using either a Bartington Ltd. MS2D or MS2F meter or a pocket susceptibility WSLA meter made by Aerogeophysical Survey of China. The MS2D and MS2F loop sensors operate at frequencies of 958 and 580 Hz, respectively, and their average diameters are 185 and 15.5 mm, respectively (Dearing, 1999). For MS2D, 95% of the susceptibility signal comes from the upper 80 mm of the subsurface and the integrated volume corresponds to 4300 cm^3 (Lecoanet et al., 1999). The detection depth of the MS2F sensor is about 15 mm from the tip of the sensor. The sensitivity of both the MS2D and MS2F probes is about 2×10^{-6} SI. The WSLA probe, with a diameter of 34 mm and sensitivity of 1×10^{-5} SI, has a larger detection depth compared to MS2F.

Cores of 3.5 cm diameter (obtained by vertically inserting a 30-cm long hollow pipe into the ground) and 2.54 cm diameter (10 cc in volume) were sampled in the field. In the laboratory, the former were measured on a Bartington MS2C meter, with operating frequency of 565 Hz, internal sensor diameter of 40 mm, and sensitivity of 2×10^{-6} SI, for volume susceptibility (hereafter called susceptibility or k). The susceptibility of the latter was measured on the AGICO KLY-2 Kappabridge, with an operating frequency of 920 Hz and sensitivity of 4×10^{-8} SI, and normalised by the sample mass to obtain the mass-specific susceptibility (hereafter called mass susceptibility or χ).

Samples of road dust were collected from a 2 m^2 area at the rim of the road using a nylon brush and plastic container. Large particles (such as stones, brick pieces and other detrital material) and organic matter were removed at the spot. In the laboratory, the samples were dried at 75 °C for 24 h. The dried samples were then separated using analytical sieves into a bulk sample (particle diameter <2 mm) and size fractions of 0.2–0.63 mm (coarse), 0.063–0.2 mm (medium) and <0.063 mm (fine).

The variation of susceptibility with temperature (−194 to 0 and 40–700 °C) was recorded for small specimens (≈0.25 cm^3) of soil and road dust using the AGICO KLY-3 Kappabridge (operates at 875 Hz and has a sensitivity of 3×10^{-8} SI), with an attached CS-3 furnace. Experiments were conducted in air and the measurement interval was 2.5 °C with a heating rate of 10 °C/min.

The characteristic temperatures related to Curie points or mineral phase decomposition, inversion or transition are estimated in different ways.

(a) Determination of Curie/Neel temperatures from thermomagnetic curves using the method of tangents (Moskowitz, 1981) and second derivatives (Tauxe, 1998), which have been traditionally used also for susceptibility curves.
(b) Detection of the temperature at which the inverse susceptibility starts to change linearly with temperature, following the Curie–Weiss law applicable for paramagnetic material (Petrovský and Kapička, 2003). The temperature marking the beginning of the paramagnetic behaviour, in this method, also marks the end of the spontaneous ferromagnetic behaviour and serves as a marker for the Curie or Neel temperature. Exact determination of the relatively short linearity range (generally <100 °C) by using strict numerical criteria for linearity was difficult because of a quasi-periodic high frequency noise superposed on a weak signal. Therefore, the starting point of the linear sector is estimated by judging the line-fit by eye.

Samples of 10 cc volume were subjected to isothermal remanent magnetisation (IRM) acquisition up to a maximum magnetic field of 2.5 T, using pulse fields at 18–20 steps generated by a magnetic measurements pulse magnetiser. The acquired IRM moment was measured by a Molspin spinner magnetometer. The IRM curves were

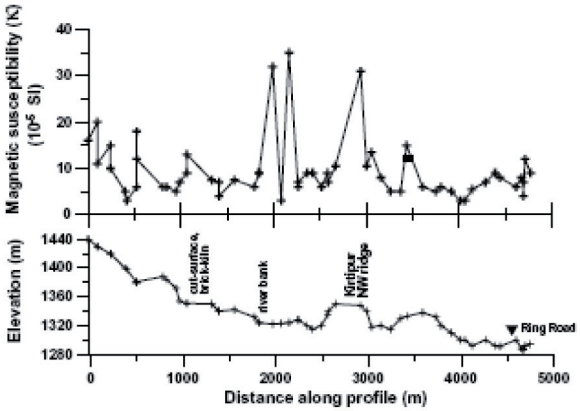

Fig. 2. The magnetic susceptibility profile parallel to the ropeway between Machhegaon and Kuleshwar (Fig. 1d). Susceptibility in excess of 30×10^{-5} SI seems to arise from periodic baking of the soil due to firing (sites near 2000 m, at the river terrace and at the edge of cultivated areas) or debris from construction materials, mainly fired brick pieces (e.g. at the Kirtipur ridge).

analysed using cumulative log-normal Gaussian decomposition techniques to discriminate the contribution of magnetic materials with differing coercivity spectra (Kruiver et al., 2001).

Magnetic extracts from some samples were isolated using a hand magnet. These extracts were coated with carbon and observed using a scanning electron microscope (SEM), model Leo SEM 1450VP. Major element composition of selective grains was measured with an Oxford INCA EDS 200 microanalysis system linked to the SEM and run at an accelerating voltage of 15 kV, a beam current of 250 pA and counting time of 60 s per element. Quantification is based on the internal default standard calibration using the strobe peak function and the XPP correction model (Pouchou and Pichoir, 1991). Results were normalised by preset O-stoichiometry (total iron Fe^{2+} as FeO_{tot}, Al as Al_2O_3, Si as SiO_2 and Co as CoO).

3. Magnetic susceptibility data

3.1. Lateral profiling

A greater than 4-km long in situ susceptibility profile approaching the ring road from outskirts in Machhegaon is shown in Fig. 2. The median in situ susceptibility along the profile varies between 3×10^{-5} and 60.5×10^{-5} SI with a log-normal mode of 8.3×10^{-5} SI. Most values lie within $2–20\times10^{-5}$ SI, which is typical for the fluvio-lacustrine sediments constituting the study

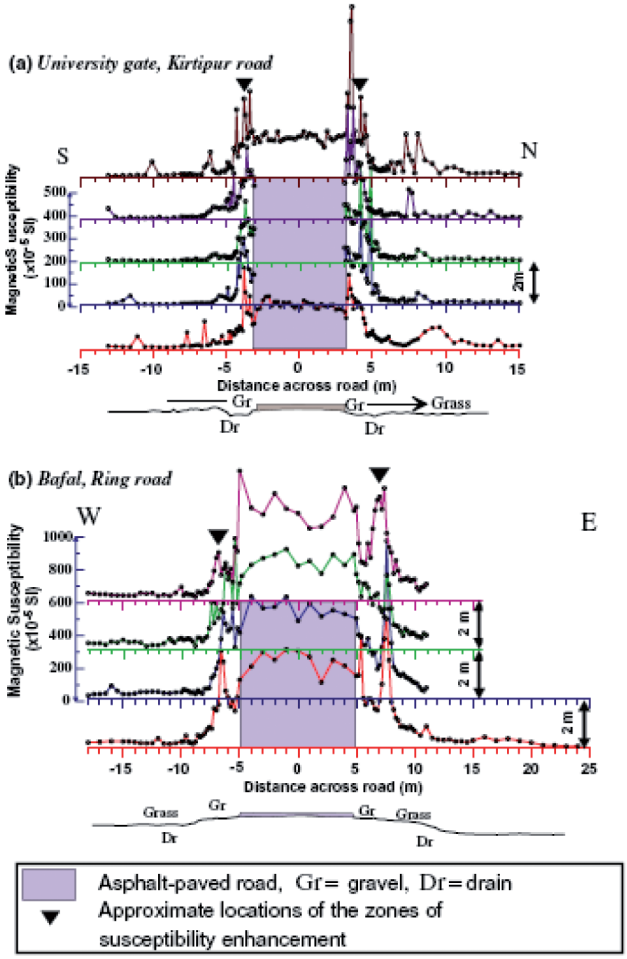

Fig. 3. In situ magnetic susceptibility traverses across urban roads at Kirtipur (measured on 9 August 1999 using susceptibility meter Bartington MS2 D-sensor) and the Ring Road at Bafal (measured on 27 May 2001 using susceptibility meter WSLA, AGS China). The locations are indicated as short bars in Fig. 1d. The 28 km long and 10m wide 'ring road' (Fig. 1d) is a major urban road encircling most of the Kathmandu urban area and has the highest traffic flow in the city. The Kirtipur Road, just 6.2 m wide, passing through the University Campus and connecting Kathmandu with the satellite town of Kirtipur has a much lower traffic volume. All susceptibility profiles at 2 m spacing.

area. Within the first 500 m of the profile, located close to active brick-kilns, in situ susceptibility is in excess of 10×10^{-5} SI and seems to correlate to topography with larger values on higher ground. Sometimes, large local variations of in situ susceptibility were observed in dry agricultural fields which are lacking in irrigation. These variations may arise due to differences in the effect of biomass burning, fertiliser usage or natural soil variability.

In situ susceptibility variations across roads differing in width and traffic density are illustrated in Fig. 3. Compared to the peripheries of the city, these variations are much more pronounced along road traverses closer to or in the urban area. A relatively high in situ susceptibility characterises the asphalt-paved portion of any road corridor. However, higher in situ susceptibility values reaching 850×10^{-5} SI, at distances 0.5–2.5 m away from the paved road edge are observed. Decay of in situ susceptibility to the background value of $\approx10\times10^{-5}$ SI occurs within about 5 m of the road edge. The decay of the in situ susceptibility anomalies away from the

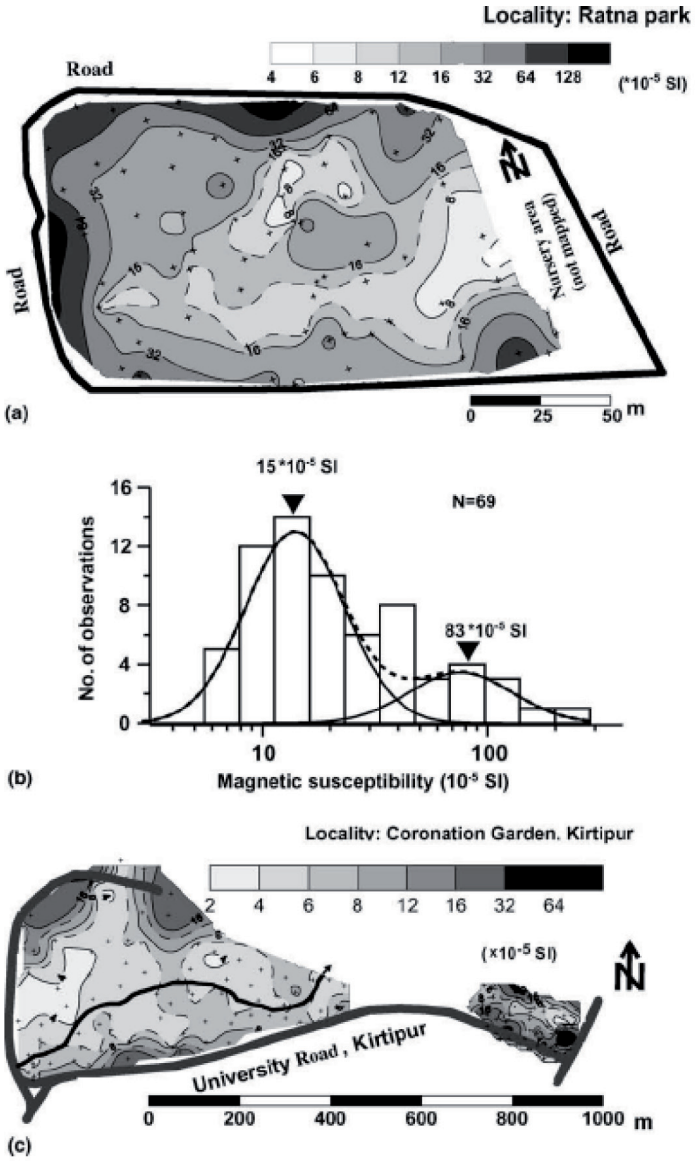

Fig. 4. Results of detailed magnetic susceptibility mapping. (a) Contour map of susceptibility in Ratna Park, centre of the urban area, (+) indicates measurement points, (b) Histogram of susceptibility values for Ratna Park and its interpretation in terms of a bimodal log-normal distribution. (c) Contour map of susceptibility in the Coronation Garden and University Campus (Kirtipur suburban area).

road is generally monotonous and exponential with respect to the distance. In addition, there is asymmetry in the anomalies with respect to the road axis, as the anomalous zone opposite to the prevailing wind direction is wider and more intense in traverses such as at Bafal (Fig. 3b), where the wind blows from WSW. These characteristics are similar to in situ susceptibility studies for the Tübingen area (Hoffmann et al., 1999) and can be attributed to the traffic pollution producing vehicular engine emissions, dust from the braking system, and abrasion of the asphalt. For some road profiles in Tübingen, a positive correlation of the lateral and vertical (down to a depth of 1 m) variations of susceptibility with contents of heavy metals (Cd, Cu, Zn, and Pb attributable to automotive sources) in soil samples has been established (Hoffmann et al., 1999; Knab et al., 2001). We infer that the localised, narrow and linear configuration of in situ susceptibility enhancement par-

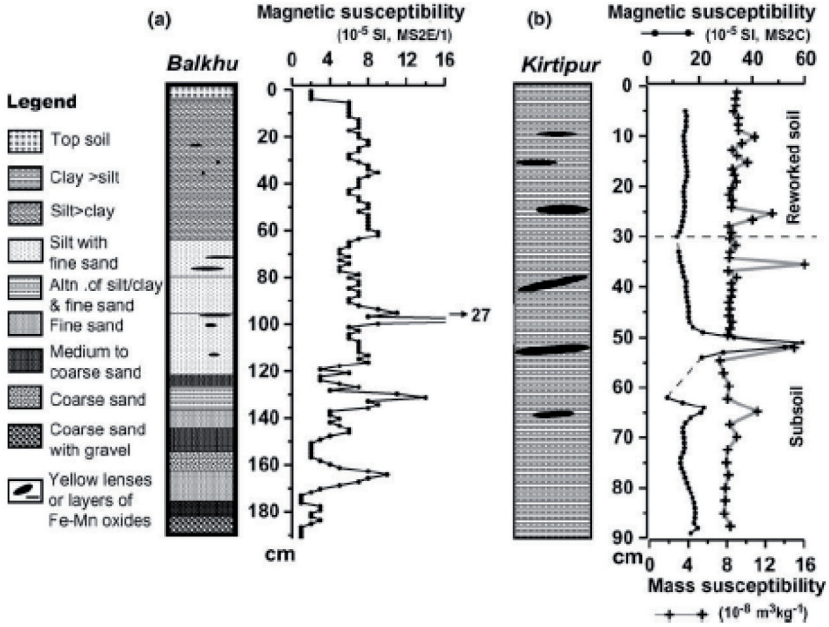

Fig. 5. Magnetic susceptibility variation along vertical profiles, of soils and sediments, from background areas at Balkhu and Kirtipur (sites B and K in Fig. 1d.). For site K, both volume (k) and mass-specific (χ) susceptibilities are shown to demonstrate that significant anomalies are identified irrespective of the sample size and susceptibility meters employed. In situ susceptibility measured with MS2F for Balkhu and MS2C (k) and KLY-2 (χ) for Kirtipur.

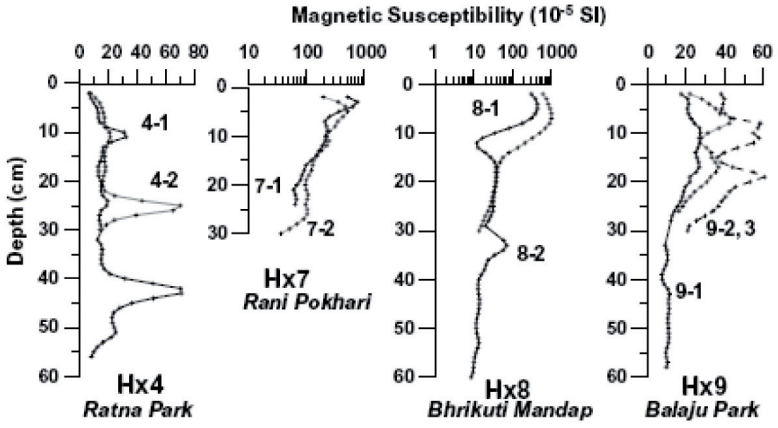

Fig. 6. Magnetic susceptibility variation along vertical sediment and soil profiles in the urban area. Profiles $H\times4$, $H\times7$, $H\times8$ are from the centre of Kathmandu city whereas $H\times9$ is from Balaju Park situated adjacent to the industrial area (Fig. 1b, cross-hatched). Data on duplicate or triplicate cores (each 35 mm in diameter) sampled very close to each other are shown using differing line styles.

allel to the road alignment, results from the deposition of traffic-related particles. These particles accumulate in the close vicinity of the road immediately after discharge into the environment as described by Petrovsky and Ellwood (1999).

3.2. Mapping

Within the urban area, relatively small areas, of 0.02–0.6 km^2, and recreational parks, which were seemingly less polluted, were mapped in detail. In order to demonstrate the in situ susceptibility variation, we present data from Ratna Park, situated at the city centre, and Kirtipur Park situated ≈1 km away from the ring road and outside the urban area with heavy traffic.

Within Ratna Park, median susceptibility lies between 3 and 155×10^{-5} SI. The lowest values occur more than 50 m from roads and a systematic increase of susceptibility towards the roads is observed (Fig. 4a). The susceptibility data from Ratna Park show a multimodal distribution (Fig. 4b). A bimodal logarithmic distribution yields modes of 15×10^{-5} SI (the local background) and 83×10^{-5} SI that is biased by anthropogenic input of magnetic material related to vehicular emission (Fig. 4b).

In Kirtipur Park area, in situ susceptibility varies from 2 to greater than 100×10^{-5} SI (Fig. 4c). Here again, areas lying more than 100 m from road or built-up areas surrounding the park have a low susceptibility of $2–8\times10^{-5}$ SI. The rapid increase in susceptibility is observed approaching roads, built-up areas or sites with construction material debris.

3.3. Soil and sediment vertical profiles

3.3.1. Background areas

A 2-m soil profile from Balkhu, downstream from the bridge at the ring road is shown in Fig. 5a (site B in Fig. 1d). The fluvial sediment sequence, of Pleistocene age (Yoshida and Gautam, 1988), has no signs of present-day environmental pollution and soil development. The in situ susceptibility has a range of $2–27\times10^{-5}$ SI showing an approximate inverse relationship with the grain size. Thin yellowish layers (up to 2 cm thick) rich in Fe–Mn oxides or hydroxides give rise to locally high susceptibilities within distinct lithologic layers, e.g. at 97 and 131 cm (Fig. 5a). This profile serves as a guide to the lithogenic background susceptibility in the Kathmandu basin.

The susceptibility profile at a paddy field site (K in Fig. 1d) in Kirtipur, close to the Tribhuvan University Campus, with a silty clay soil is shown in Fig. 5b. Though it has no layered structure, light gray and dark gray domains caused by varying silt to clay ratio and moisture content was seen. The upper ≈30 cm of the soil is manually reworked at least twice a year prior to cultivation of rice and other crops (such as potato, mustard and wheat). Measurements on long cores yield susceptibility value of less than 20×10^{-5} SI except at several levels, characterised by yellowish grey lenses showing values up to 60×10^{-5} SI (Fig. 5b). Values of mass susceptibility based on short diameter cores, sampled separately from the same profile, yield more consistent values. Anomalies caused by thin individual layers or lenses are clearly recognised in both volume and mass susceptibility data (Fig. 5b).

3.3.2. Recreational park sites close to urban and industrial areas

The soil profiles shown in Fig. 6 are dominated by silt or sand, occasionally containing gravel, rock fragments and pieces of baked and unbaked brick (the most common traditional construction material in Kathmandu). Most of the soil material seems to have

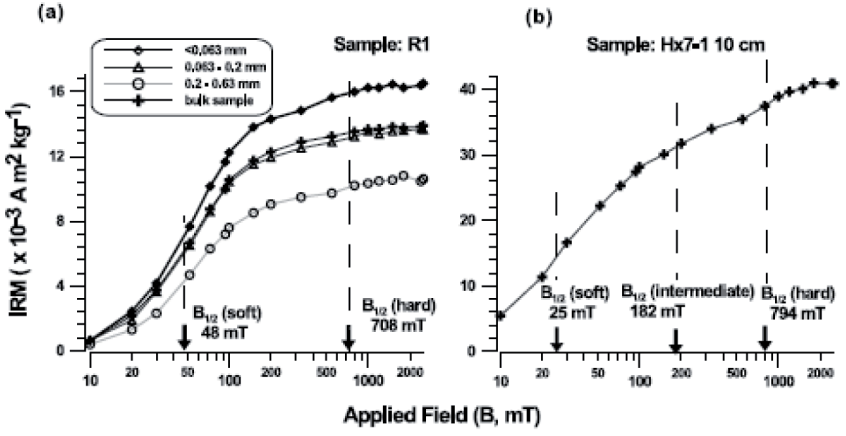

Fig. 7. Isothermal remanent magnetisation curves for the road dust sample (a) and urban soil sample (b). The respective median acquisition field ($B_{1/2}$) values modelled, indicated by arrows, as contributing to the curves were determined using Kruiver et al. (2001).

been transported from elsewhere or reworked during landscaping and gardening (before or during the 1960's, prior to the commencement of industry or heavy traffic), such that no natural layered soil profile is seen. In most sites, the upper 30–50 cm interval exhibits frequent enhancement of susceptibility, 10–100 times larger than those expected from natural soils. The thin and erratic susceptibility highs correspond mostly to localised brick fragments. Broader susceptibility highs, such as that above 10 cm in $H\times8$ (Fig. 6), are believed to result from material related to vehicular pollution or industry-related activities.

4. Magnetic mineralogy

4.1. Isothermal remanent magnetisation acquisition

The IRM acquisition curves for road dusts of bulk samples and its different-sized fractions (Fig. 7) are best modelled in terms of two components. A soft coercivity fraction with $B_{1/2}$ of 48 mT and a hard coercivity fraction with $B_{1/2}$ of 708 mT. They correspond to magnetite-like and hematite-like phases respectively. The former contributes to 88–93% of the SIRM. The IRM curve for the urban soil (Fig. 7b) is best modelled by three coerciv-

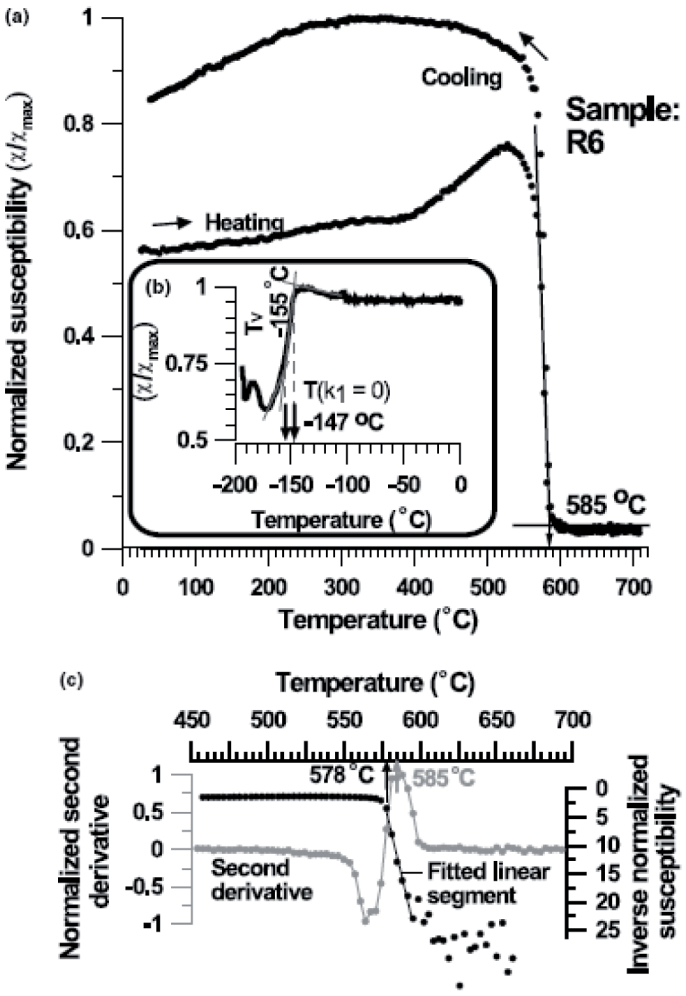

Fig. 8. Thermal variation of the normalised low-field magnetic susceptibility for a typical road dust sample: (a) heating–cooling cycle above room temperature; (b) warming from −194 to 0 °C, and; (c) the inverse normalised susceptibility curve and second derivative of the normalised susceptibility near the magnetite Curie point, both calculated from the heating curve shown in (a). The beginning of the linear segment in inverse susceptibility curve (at about 578 °C) and low-temperature transitions (the observed Verwey transition, T_v, at about −155 °C and the zero point of crystalline anisotropy constant $T(k_1=0)$ at about −147 °C) point magnetite as the dominant magnetic phase. The characteristic temperatures determined by methods based on tangent fitting and maxima of second derivative (see text) are in fact higher than the actual Curie temperature of magnetite and so are not useful for characterising the magnetic minerals.

ity components; a soft dominant phase with $B_{1/2}$ of 25 mT, an intermediate with $B_{1/2}$ of 182 mT and a hard with $B_{1/2}$ of 794 mT. Their model contribution to the SIRM is 70%, 13% and 17%, respectively. The soft and hard components probably correspond to the magnetite-like and hematite-like phases noted for the road dust.

4.2. Thermal variation of the magnetic susceptibility

In the heating curves for a typical road dust sample (Fig. 8), the following features are observed.

(i) A susceptibility high occurring below ≈360–370 °C.
(ii) A susceptibility rise above 400 °C leading to a peak at about 540 °C.
(iii) A rapid susceptibility drop, at high temperature, which is estimated by both the tangent method and second-derivative method at 585 °C. However, the well-defined linear segment in the calculated inverse susceptibility- temperature curve shows this drop to start at 575–580 °C.
(iv) Irreversible susceptibility behaviour upon cooling showing the presence of a single characteristic temperature equivalent to that in (iii).

The IRM data indicate a magnetite-like phase, as does the initiation of paramagnetic behaviour at 575–580 °C interpreted to correspond to the Curie temperature of 578 °C for pure magnetite (Dunlop and Ozdemir, 1997). Further support for magnetite comes from the Verwey transition observed at −155 °C during the low-temperature warming (Fig. 8c). The susceptibility enhancement between 400 and 540 °C (Fig. 8a) is the Hopkinson effect related to a magnetite-like phase (Dunlop and Ozdemir, 1997).

Similar features are observed also in the curve for soil sample $H\times7$ (Fig. 9). The soil samples behave somewhat differently than the road dust in terms of the characteristic temperatures, with irreversible susceptibility upon recycling below 450 °C (Fig. 9a). Despite noise, there is a well-defined linear segment in the inverse susceptibility-temperature curve starting at 340–350 °C (Fig. 9a). This is interpreted as decomposition

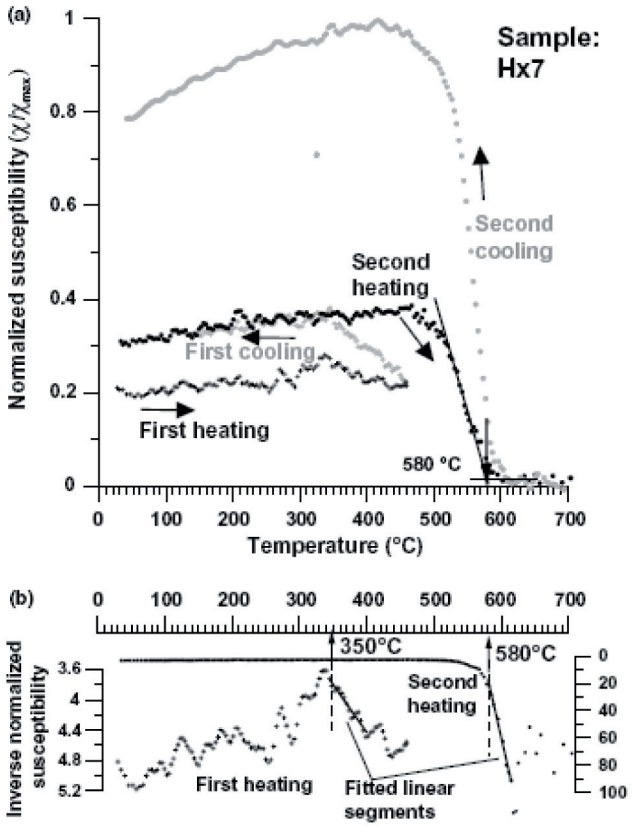

Fig. 9. (a) Thermal variation of low-field magnetic susceptibility for urban soil sample ($H\times7$, from 10 cm depth). (b) Plots of the inverse susceptibility data derived from the first heating and second heating curves in (a). Two mineral phases of differing Curie and decomposition temperatures of about 580 and 350 °C are evident.

of maghemite, present initially or produced upon heating. Such mineralogical interpretation of this low-temperature rise in soil and road dust susceptibility is consistent with the experimental data of Kosterov (2002). In temperatures above 450 °C, a Curie temperature of 580 °C is shown by the inverse susceptibility-temperature data, as well as the two tangents estimate (Fig. 9b). Hence, magnetite is the major ferrimagnetic constituent in the soil samples.

Analysis of susceptibility-temperature runs and IRM acquisition curves (not shown here) obtained from some brick pieces, points to a close link between the phase with 340–350 °C decomposition temperatures and the intermediate-coercivity phase with $B_{1/2}$ of 182 mT. These features are inferred to be diagnostic of a maghemite-like phase, which is responsible for the unstable susceptibility behaviour upon heating. The maghemite formation might be explained in terms of the rather low temperatures achieved during the preparation of bricks in the kilns, such that formation of stable magnetic phases such as magnetite and hematite was not complete (Jordanova et al., 2001).

4.3. Microscopic and chemical characterisation of magnetic constituents

Microscopy of the magnetic extract from the road dust reveals basically two morphologies of grains (Fig. 10). Firstly, euhedral to anhedral crystalline grains derived from rock sources and secondly spherical grains. These two types are respectively related to lithogenic and anthropogenic inputs, with the latter formed by combustion processes. Spherules of diameter 2–40 μm, were abundant in the dust from road surface as well as from road-side tree-leaves, but absent in the soil samples from sites distant from roads (the results from leaves and soils are not detailed here). Therefore, the most likely source of these spherules is the road traffic. These spherules are inferred to be produced in exhausts of vehicles, as shown in the Tübingen study, although some of the larger particles, with diameter of tens of microns, may be too large to be explained in this way (Knab et al., 2001). Judging from the iron content, the lithogenic grains with content of FeO_{tot} of about 96.6 wt.% (or 75.1 wt.% of Fe) in average are practically indistinguishable from the spherules (Table 1).

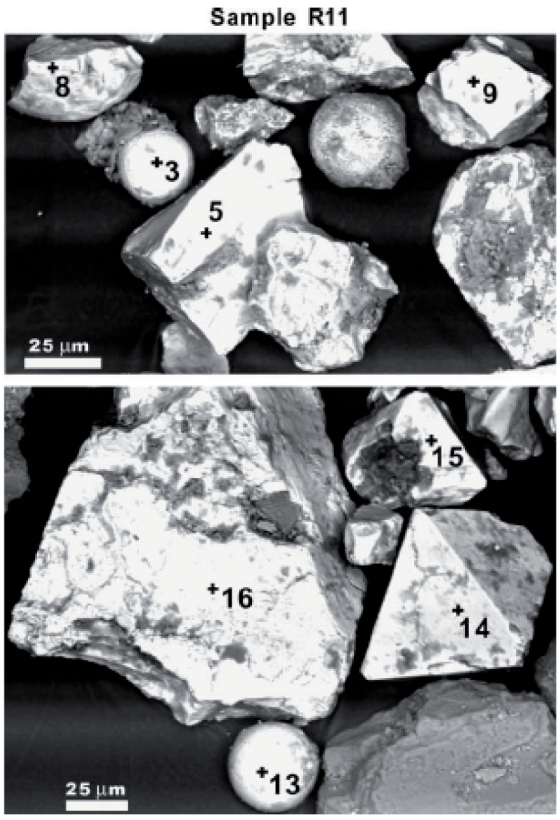

Fig. 10. Magnetic grains observed by scanning electron microscopy from a magnetic extract from road dust (sample R11). The numbered grains were analysed by energy dispersive X-ray techniques and their chemistry is shown in Table 1). There are two distinct types of grains; spherules of anthropogenic origin (grains 3 and 13) and non-spherical, euhedral to subhedral grains of lithogenic origin (grains 5, 8, 9, 14–16).

Table 1
Energy dispersive X-ray analytical data (wt.%) on magnetic mineral grains constituting the road dust

Grain no.[a]	Anthropogenic grains		Lithogenic grains					
	3	13	5	8	9	14	15	16
Element								
Fe	74.85	75.48	76.63	73.25	73.82	75.90	75.33	75.67
Al	0.68	0.59	0.30	1.04	1.02	0.31	0.44	0.59
Si	0.76	0.84	0.40	1.23	1.09	0.83	1.05	0.72
Co	0.64			0.92	0.62			
O	23.08	23.10	22.67	23.56	23.46	22.96	23.17	23.02
Total	100.01	100.01	100.00	100.00	100.01	100.00	99.99	100.00

[a] Locations of analysed points corresponding to these numbers are given in Fig. 10.

5. Discussion and conclusions

Magnetic susceptibility measurements on ground and soils in the urban and suburban areas of the Kathmandu Valley, reflect the effect of pollution related to vehicular emissions as well as ubiquitous and irregular distribution of construction materials in the soils. Microscopy reveals both lithogenic magnetic grains and anthropogenic magnetic spherules of which the latter are derived from vehicular emission (Knab et al., 2001). The presence of lithogenic magnetite is clearly shown by octahedral and rounded to angular magnetic grains. The predominance of minerals with a Curie temperature of 575–580 °C in both road dust and soils points to magnetite as both lithogenic mineral grains and spherules of anthropogenic origin. The magnetic spherules and lithogenic grains are practically indistinguishable in terms of FeO_{tot} wt.%. Elevated top-soil susceptibilities in the suburban and peripheral parts seem to be due to the emissions from the brick-kilns. Based on these findings, it is suggested that a soil magnetic susceptibility map covering the whole Kathmandu urban area and its peripheries could be prepared and used for rapid identification of pollution "hotspots" that can be further detailed by additional rock-magnetic as well as other non-magnetic environmental studies. Judging from the possibilities of these measurements as providing both non-destructive and rapid application, the magnetic susceptibility technique deserves inclusion into the environmental screening and monitoring system of the Kathmandu urban area.

Acknowledgments

The laboratory work was accomplished at the University of Tübingen during a Georg Forster Research Fellowship granted to PG by Alexander-von-Humboldt Foundation, Germany. The Environmental Unit of the Kathmandu Metropolitan City as well as the Central Department of Geology supported execution of the field-work. Suggestions from reviewers Ken Kodama, John Smith, Colin Booth and the guest editor Mark W. Hounslow were helpful in revising the original manuscript.

References

Dearing, J., 1999. Environmental Magnetic Susceptibility. Using the Bartington MS2 System, second ed. Chi Publishing, England, p. 54.

Devkota, D., 2001. Total and extractable (mobilizable and mobile) heavy metals in the Bagmati river sediment of Kathmandu, Nepal. A Journal of the Environment 6 (7), 34–51.

Dunlop, D.J., Ozdemir, Ö., 1997. Rock Magnetism: Fundamentals and Frontiers. Cambridge University Press, Cambridge, p. 573.

Hoffmann, V., Knab, M., Appel, E., 1999. Magnetic susceptibility mapping of roadside pollution. Journal of Geochemical Exploration 66, 313–326.

Hanesch, M., Scholger, R., 2002. Mapping of heavy metal loadings in soils by means of magnetic susceptibility measurements. Environmental Geology 42, 857–870.

Jordanova, N., Petrovsky, E., Kovacheva, M., Jordanova, D., 2001. Factors determining magnetic enhancement of burnt clay from archaeological sites. Journal of Archaeological Science 28, 1137–1148.

Knab, M., Appel, E., Hoffmann, V., 2001. Separation of the anthropogenic portion of heavy metal contents along a highway by means of magnetic susceptibility and fuzzy c-means cluster analysis. European Journal of Environment and Engineering Geophysics 6, 125–140.

Kosterov, A., 2002. Low-temperature magnetic hysteresis properties of partially oxidized magnetite. Geophysical Journal International 149, 796–804.

Kruiver, P.K., Dekkers, M.J., Heslop, D., 2001. Quantification of magnetic coercivity components by the analysis of acquisition curves of isothermal remanent magnetization. Earth and Planetary Science Letters 189, 269–276.

Lecoanet, H., Leveque, F., Seguna, S., 1999. Magnetic susceptibility in environmental applications: comparison of field probes. Physics of the Earth and Planetary Interiors 115, 191–204.

Malinovsky, M., 2001. Air quality management in Kathmandu Valley. A Journal of the Environment 6 (7), 50–57.

Matzka, J., Maher, B.A., 1999. Magnetic biomonitoring of roadside tree leaves: identification of spatial and temporal variations in vehicle-derived particulates. Atmospheric Environment 33, 4565–4569.

Moskowitz, B.M., 1981. Methods for estimating Curie temperatures of titanomagnetites from experimental Js-T data. Earth Planetary Science and Letters 53, 84–88.

Muxworthy, A.R., Schmidbauer, E., Petersen, N., 2002. Magnetic properties and Mössbauer spectra of urban atmospheric particulate matter: a case study from Munich, Germany. Geophysics Journal International 150, 558–570.

NESS, 2001. Air quality database of Nepal. Nepal Environmental and Scientific Services Co., special issue, Kathmandu.

Petrovsky, E., Ellwood, B.B., 1999. Magnetic monitoring of pollution of air, land and waters. In: Maher, B.A., Thompson, R. (Eds.), Quaternary Climates, Environments and Magnetism. Cambridge University Press, Cambridge, pp. 279–322.

Petrovský, E., Kapička, A., 2003. Temperature dependence of magnetic susceptibility and determination of Curie (Neel) temperature: are we correct? In: Abstracts, XXII General Assembly of the International Union of Geodesy and Geophysics, Sapporo, A.265.

Pouchou, J.L., Pichoir, F., 1991. Quantitative analysis of homogenous or stratified microvolumes applying the model PAP. In: Heinrich, K.F.J., Newbury, D.E. (Eds.), Electron Probe Quantification. Plenum, New York, pp. 31–75.

Raut, A.K., 2003. Brick kilns in Kathmandu Valley: current status, environmental impacts and future options. Himalayan Journal of Sciences 1 (1), 59–61.

Sakai, H., Fujii, R., Kuwahara, Y., 2002. Changes in the depositional system of the paleo-Kathmandu lake caused by uplift of the Nepal lesser Himalayas. Journal of Asian Earth Science 20, 267–276.

Shrestha, B., Pradhan, S., 2000. Kathmandu Valley GIS Database. ICIMOD, Kathmandu.

Shrestha, R.M., Raut, A.K., 2002. Air quality management in Kathmandu. In: Proceedings of the Symposium of Better Air Quality in Asian and Pacific Rim Cities (BAQ 2002), Hong Convention and Exhibition Center, Hong Kong, pp. 1–6.

Shu, J., Dearing, J.A., Morse, A.P., Yu, L., Li, C., 2000. Magnetic properties of daily sampled total suspended particulates in

Shanghai. Environmental Science and Technology 34, 2393–2400.

Tauxe, L., 1998. Paleomagnetic Principles and Practice. Kluwer Academic Publishers, Dordrecht.

Yoshida, M., Gautam, P., 1988. Magnetostratigraphy of Plio-Pleistocene lacustrine deposits in the Kathmandu Valley, central Nepal. Proceedings of Indian National Science Academy 3, 410–417.